UNDERSTANDING POROSITY FORMATION AND PREVENTION WHEN WELDING TITANIUM ALLOYS WITH 1 μm WAVELENGTH LASER BEAMS

A thesis submitted to The University of Manchester for the degree of

Doctor of Engineering

in the Faculty of Engineering and Physical Sciences

2011

JONATHAN EDWARD BLACKBURN

SCHOOL OF MECHANICAL, AERSOSPACE AND CIVIL ENGINEERING

List of Contents

Final word count: 78,239

List of Tables

List of Figures

List of Symbols

c	Speed of light
c_p	Specific heat
d	Workpiece thickness
d_α	Absorption depth
g	Gravitational acceleration constant
$g_{e,i,0,n}$	Electron, ion, atom and state n degeneracy factor
h	Planck's constant
k	Component of the refractive index
k_b	Boltzmann constant
k_c	Thermal conductivity
k_{cs}	Thermal conductivity of the solid phase
k_d	Thermal diffusivity
k_{ds}	Thermal diffusivity of the solid phase
m	Complex index of refraction
m_e	Electron mass
m_g	Particle mass
$n_{e,g,i,0}$	Electron, particle, ion and atom density
p_{abl}	Ablation pressure
p_b	Boundary condition constant
p_g	Hydrostatic pressure
p_h	Hydrodynamic pressure
p_v	Vapour pressure
p_γ	Surface tension
r	Radius
r_p	Radius of plume particles
t	Time
$t_{m,v}$	Time required to reach $T_{m,v}$

u_g	Particle velocity
v	Frequency of electromagnetic radiation
v_{cf}	Collision frequency between different species
v_p	Plasma frequency
w	Beam waist radius of a non-Gaussian laser beam
w_0	Beam waist radius of a Gaussian laser beam
z	Depth
A	Absorption coefficient
A_{nm}	Atomic transition probability between states n and m
D	Laser beam diameter at focussing lens
E_i	Ionisation energy
E_n	Energy level of state n
E_v	Vaporisation energy
F	Focal length of focussing lens
I	Intensity
I_{nm}	Spectral intensity associated with transition between states n and m
I_0	Axial intensity
L	Latent heat of fusion
M^2	Value of beam quality
N	Total density of a given state
N_p	Density of particles in plume
P	Laser power
P_e	Péclet number
P_r	Prandtl number
$Q_{ABS,EXT,SCA}$	Absorption, extinction, scattering efficiencies
R	Beam radius
R_e	Reynolds number
R_f	Reflectivity
R_k	Keyhole radius
R_{km}	Function of keyhole radius and melt pool radius
$R_{1,2}$	Radii of keyhole curvature
T_e	Electron temperature
$T_{m,v}$	Melting, vaporisation temperature
T_0	Ambient temperature
V	Welding speed

V_b	Terminal velocity as a result of buoyant forces
X	Melt pool depth
$Z(T_e)$	Partition function
Z_f	Depth of focus
$\emptyset$	Angle of incidence
α	Gas ionisation fraction
α_{ea}	Electron neutral atom absorption coefficient
α_{ei}	Electron ion absorption coefficient
α_{ib}	Inverse Bremsstrahlung absorption coefficient
γ	Surface tension coefficient of molten material
ε	Value relating to the material properties and wavelength
θ	Half angle divergence
$\mu_{f,g}$	Dynamic viscosity of the fluid and gas.
λ	Wavelength
λ_{nm}	Wavelength of spectral line associated with photonic emission during transition between states n and m
ρ	Density
Θ	Polar angle of melt pool speed

List of Abbreviations

ANSI	American National Standards Institute
ATIG	Activated Tungsten Inert Gas
AWS	American Welding Society
BSI	British Standards Institution
BPP	Beam Parameter Product
BS	British Standard
BWRA	British Welding Research Association
CFD	Computational Fluid Dynamics
CMOS	Complementary Metal-Oxide Semiconductor
CRP	Core Research Programme
EDX	Energy-Dispersive X-Ray
EngD	Engineering Doctorate
EPSRC	Engineering and Physical Sciences Research Council
FEG	Field Emission Gun
FKW	Front Keyhole Wall
FZ	Fusion Zone
GSP	Group Sponsored Project
HAZ	Heat-Affected-Zone
ISO	International Standards Organisation
JIP	Joint Industry Project
JWRI	Joining and Welding Research Institute (at Osaka University)
KTIG	Keyhole mode Tungsten Inert Gas
LTE	Local Thermodynamic Equilibrium
MPI	Mean Pixel Intensity
NA	Numerical Aperture
NTIS	National Technical Information Service
PAW	Plasma Arc Welding
RGB	Red Green Blue

RKW	Rear Keyhole Wall
SCP	Single Client Project
SEM	Scanning Electron Microscopy
SM	Single Mode
SSFSW	Stationary Shoulder Friction Stir Welding
TEM	Transverse Electromagnetic Mode
TIG	Tungsten Inert Gas
TRL	Technology Readiness Level
TWI	The Welding Institute
YAG	Yttrium-Aluminium-Garnet

Abstract

The University of Manchester
Jonathan Edward Blackburn
Doctor of Engineering
Understanding Porosity Formation and Prevention when Welding Titanium Alloys with 1μm Wavelength Laser Beams
January 2011

Keyhole laser welding is a joining technology characterised by the high focussed power density applied to the workpiece, facilitating deep penetration at high processing speeds. High aspect-ratio welds produced using this process invariably have narrow heat-affected-zones and minimal thermal distortion compared with traditional arc welding processes. Furthermore, the ability to process out of vacuum and the easy robotic manipulation of fibre optically delivered 1μm wavelength laser beams, allow keyhole laser welding to process geometrically complex components. The widespread uptake of keyhole laser welding for the production of titanium alloy components in the aerospace industry has been limited by the stringent weld quality requirements. Producing welds with levels of subsurface weld metal porosity content meeting the required weld quality criteria has been the primary obstacle.

Here, three techniques for controlling the levels of weld metal porosity when welding titanium alloys with Nd:YAG rod lasers have been developed. Characterisation of the welding processes using high speed photography and optical spectroscopy, have allowed an original scientific understanding of the effects these methods have on the keyhole, melt pool and vapour plume behaviour. Combining this with a thorough assessment of the weld qualities produced, has enabled the effects of these process behaviours on the formation of weld metal porosity to be determined.

It was found that with the correct process parameters a directed gas jet and a dual focus laser welding condition can both be used to reduce the occurrence of keyhole collapse during Nd:YAG laser welding. The directed gas jet prevents the formation of a beam attenuating vapour plume and interacts with the molten metal to produce a stable welding condition, whereas the dual focus laser welding condition reduces fluctuations in the process due to an enlarged keyhole. When applied, both techniques reduced the occurrence of porosity in the weld metal of full penetration butt welds produced in titanium alloys. A modulated Nd:YAG laser output, with the correct waveform and modulation frequency, also reduced the occurrence of porosity in the weld metal compared with welds produced with a continuous-wave output. This was a result of an oscillating wave being set-up in the melt pool which manipulated the keyhole geometry and prevented instabilities in the process being established.

In addition, the potential for welding titanium alloys to the required weld quality criteria with state-of-the-art Yb-fibre lasers has been assessed. It was found that the high power densities of suitably focussed laser beams with excellent beam quality, were capable of producing low-porosity full penetration butt welds in titanium alloys without the techniques required for laser beams with a lower beam quality.

These new techniques for keyhole laser welding of titanium alloys will encourage the uptake of keyhole laser welding for producing near-net-shape high-performance aerospace components. The advantages offered by this joining technology include high productivity, low heat input and easy robotic automation.

Declaration

No portion of the work referred to in the thesis has been submitted in support of an application for another degree or qualification of this or any other university or other institute of learning.

Copyright Statement

Acknowledgements

The research presented in this thesis has only been possible as a result of funding from the Engineering and Physical Sciences Research Council, and sponsorship from TWI Ltd. These organisations are gratefully recognised. I would like to acknowledge my supervisors, Paul Hilton and Lin Li, who successfully applied for the project's funding in the first instance, and have entertained and provided guidance on my ideas from the outset of the project.

The research has greatly benefited from discussions with all my colleagues in the Lasers and Sheet Processes Section at TWI Ltd, past and present, and in the Laser Processing Research Centre at The University of Manchester. To name a few, but not so many as to make the list redundant, Chris Allen, Steve Shi and Ali Khan. Several colleagues on the Engineering Doctorate programme at The University of Manchester for excellent 'academic' discussions, particularly Imdadul Hoque.

My brothers, Gavin and Richard, and all my friends and family for helping me remember that there are things in life other than research. Kym is especially acknowledged for continuously providing support throughout the duration of this research. Finally, my parents, Steve and Yvonne, for their encouragement of all things I undertake, and having confidence in the majority of them...

Publications

Portions of the research reported here have been presented in the following publications:

Blackburn, J., Allen, C., Hilton, P. & Li, L. (2009) 'Statistical analysis of low porosity laser welding of TI alloys using a directed gas jet', *Proc. ICALEO 2009, Orlando (USA)*, 172-181.

Blackburn, J., Hilton, P., Allen, C. & Li, L. (2010) 'Comparison of high power Yb-fibre and Nd:YAG lasers when welding TI-6AL-4V', *Proc. PICALO 2010, Wuhan (China)*, paper 404.

Blackburn, J.E., Allen, C.M., Hilton, P.A., Li, L., Hoque, M.I. & Khan, A.H. (2010) 'Modulated Nd:YAG laser welding of Ti-6Al-4V', *Sci. and Technol. of Weld. and Joining,15(5), 433-439.*

Blackburn, J.E., Allen, C.M., Hilton, P.A. & Li, L. (2010) 'Dual focus Nd:YAG laser welding of titanium alloys', *Proc. of MATADOR conference, Manchester (England)*, 279-282.

Blackburn, J., Allen, C., Hilton P. & Li, L. (2010) 'Nd:YAG laser welding of titanium alloys using a directed gas jet', *J. Laser Appl.*, 22(2), 71-78.

Blackburn, J.E., Allen, C.M., Hilton, P.A. & Li, L. (2011) 'Dual focus Nd:YAG laser welding of titanium alloys: effect on porosity formation', *Lasers in Engineering*, under review.

Blackburn, J.E., Hilton, P.A. Allen, C.M., Khan, A. & Li, L. (2011) 'Welding Ti-6Al-4V with excellent beam quality 1μm wavelength laser sources', under embargo.

Preface

This thesis is the culmination of four years doctoral research which has focussed on keyhole laser welding of titanium alloys. The research has been predominantly performed at TWI Ltd, the operating arm of The Welding Institute (TWI), based in Abington, Cambridge. Experimental research was also performed at The University of Manchester, Manchester, and at the Fraunhofer Institut für Werkstoff- und Strahltechnik (IWS), Dresden.

The author completed a Post-Graduate Diploma in Management Sciences from Manchester Business School during the doctoral research period. Prior to performing the above laser materials processing research, the author obtained a MEng (hons) in Mechanical Engineering/USA from Lancaster University in July 2005, which incorporated an academic year spent at Iowa State University of Science and Technology.

Chapter 1

Introduction

1.1 Growth of the Laser Materials Processing Industry

The term 'laser' is an acronym for 'Light Amplification by Stimulated Emission of Radiation' and refers to the method for producing electromagnetic radiation by the stimulated emission process. Ordinarily, the emitted light has a wavelength between the infra-red and ultraviolet frequencies of the electromagnetic spectrum. The term was formulated by Gordon Gould and first published in 1959 [Gould, 1959] in a paper at the Ann Arbor conference of Optical Pumping. Subsequently, Maiman [1960] reported the first successful stimulated emission of electromagnetic radiation in the journal Nature. Maiman [1960] utilised a flash-lamp to pump a ruby crystal, and observed stimulated emissions at wavelengths of 692.9 and 694.3 nm. Previous research performed by Einstein [1916], Ladenburg [1928], Schawlow and Townes [1958], Javan [1959], and several others formed the basis for the theoretical and practical knowledge required to produce these stimulated emissions. In the same decade as the first successful demonstration of stimulated emission, numerous other laser sources were developed which utilised active mediums other than the ruby crystal. These included the gallium-arsenic (GaAs) semiconductor laser [Hall et al, 1962], the neodymium:yttrium-aluminium-garnet (Nd:YAG) laser [Geusic et al, 1964] and the carbon dioxide (CO_2) laser [Patel, 1964].

In contrast with the light emitted from all other light sources, the electromagnetic radiation emitted from laser sources (commonly known as a laser beam or laser light) is; highly monochromatic - the spectrum of emitted light has a narrow spectral linewidth, which is determined by the bandwidth of the gain medium and the number of longitudinal modes available in the resonator; highly coherent; and, of very low divergence. Published works by researchers such as Schwarz and DeMaria [1962], and Bahun and Eng-Quist [1962] quickly

reported the potential for utilising the laser beam for materials processing applications, including; cutting, drilling, surfacing and welding processes. The characteristics of laser light allow it to be narrowly focussed, resulting in a power density suitable for the aforementioned materials processing applications. Focussed beams of light from modern laser sources have sufficient power density to initiate melting and vaporisation of metallic workpieces, thereby enabling conduction limited and keyhole laser welding to be performed.

During the fifty years that have elapsed since the demonstration of the first laser source, the laser materials processing industry has been firmly established through the adoption of laser technology to improve quality and/or productivity in numerous industry sectors. Market figures for 2008 [Belforte, 2010] show that $6.1 Billion of revenue was generated by the sale of laser systems for materials processing world-wide. Approximately 12%, by units, of the laser systems sold were for macro welding applications [Belforte, 2009].

1.2 Titanium Usage in Aerospace Applications

Among the commonly utilised metallic materials in the aerospace industry are titanium and its alloys, as their mechanical properties are particularly suitable for the service requirements of both airframe and aeroengine applications. Titanium alloys are already employed in applications which require corrosion resistance, weight or space savings, fatigue resistance, or when the capability to operate within a large temperature differential is required. The production of many of these titanium alloy components by traditional manufacturing methods, i.e. casting or forging and/or machining, is ordinarily the preferred method. High quality titanium alloy components can be produced with these manufacturing techniques, although the finished components may have buy-to-fly ratios (the mass of material prior to machining compared with the mass of the finished component) which are economically unattractive, in comparison with aluminium alloys and structural steels. It has been reported that for structural aerospace components the ratio may be 10:1 [Threadgill et al, 2008]. Welding processes offer the potential to manufacture near-net-shape components, which may require post weld machining, that will have significantly lower buy-to-fly ratios and hence reduce material wastage and overall component cost.

1.3 Keyhole Laser Welding

Keyhole laser welding is a non-contact joining process characterised by its high focussed energy density, which is capable of producing high aspect ratio welds (weld width:weld depth) in many metallic materials. It can be performed at atmospheric pressure and with a

relatively low heat input, compared with inert gas arc welding processes. The current generation of solid-state laser sources (Nd:YAG, Yb-fibre, and Yb:YAG disc lasers) emit laser light with a wavelength of ~1 μm, which can be delivered through optical fibres up to 50 m in length (depending upon the required beam quality). Consequently, the process may be easily automated using robotic manipulators, providing extensive flexibility in terms of part size and shape when compared with 10 μm wavelength laser, electron beam and friction welding systems. Table 1-1 details the key characteristics of keyhole laser welding, the reasons the characteristic occurs, and the industrial advantage this gives to the process adopter.

Table 1-1. Characteristics of the keyhole laser welding process [Duley 1999, p.7; Steen 1998, p.151].

Charact-eristic	**Reasons why characteristic occurs**	**Industrial significance/advantage**
High processing speed	- laser beam can be narrowly focussed - very high power laser sources available - efficient coupling of energy into workpiece	- high productivity, potential for cost savings - possibility for longer weld seams, increasing component stiffness
Low heat input	- laser beam can be narrowly focussed - high intensity heat source making high processing speeds possible.	- high aspect ratio (width:depth) welds - narrow heat-affected-zone (HAZ) - minimal thermal distortion - possibility for simpler clamping
Flexible process	- can operate at atmospheric pressure - non-contact process - autogeneous process or with filler material - fibre optic delivery of laser beam (wavelength dependent) - easy robotic automation	- few/no component size limitations - complex welding geometries possible - variety of joint configurations possible (butt, lap, t-butt etc)
Repeatability	- easy robotic automation - excellent equipment reliability - laser beam is not affected by magnetic fields	- accurate reliable welding process

Despite the potential advantages for utilising keyhole laser welding as a manufacturing technique for near-net-shape welding of titanium alloy components, if the welding process is

to be adopted the produced welds must be of an acceptable quality. Of particular concern when laser welding with 1 μm wavelength laser beams is the formation of porosity in the weld metal, which would reduce the fatigue resistance of the welded joint [Lindh and Peshak, 1969]. Relatively little research has been published concerning porosity formation and prevention in laser welded titanium alloys, when compared with aluminium alloys and stainless steels. As a result, this project was established to bridge this knowledge gap.

1.4 Aim and Objectives

The research presented in this thesis represents a joint project undertaken by The University of Manchester and TWI Ltd, the operating arm of The Welding Institute (TWI). The research has been funded by the Engineering and Physical Sciences Research Council (EPSRC) by grant number C537750 and the Industrial Member companies of TWI. The research has been supervised by Paul Hilton, Technology Fellow for Laser Materials Processing at TWI Ltd, and Lin Li, Head of the Laser Processing Research Centre at The University of Manchester.

The aim of this research project was to *establish an understanding of the formation of weld metal porosity when keyhole laser welding titanium alloys with 1 μm wavelength laser sources and develop techniques which could prevent its formation*.

Five specific objectives were identified from studies of the background literature to achieve this aim. For completeness, the objectives are detailed below, but the reasons why these objectives were chosen are discussed at the end of the Literature Review (where the objectives are repeated).

a. *To determine whether an accurately positioned jet of inert gas directed at the laser-material interaction point can be used for reducing weld metal porosity when welding titanium alloys relevant to the aerospace industry with an Nd:YAG laser. Furthermore, determine the influence of key process parameters on the resultant weld quality and the dynamic behaviour of the welding process.*
b. *To determine whether a modulated laser power can be used for reducing weld metal porosity when welding titanium alloys relevant to the aerospace industry with an Nd:YAG laser. Furthermore, determine the influence of key process parameters on the resultant weld quality and the dynamic behaviour of the welding process.*
c. *To determine whether a dual focus laser beam can be used for reducing weld metal porosity when welding titanium alloys relevant to the aerospace industry with an Nd:YAG laser. Furthermore, determine the influence of key process parameters on the resultant weld quality and the dynamic behaviour of the welding process.*

d. *Establish the weld qualities possible when keyhole laser welding titanium alloys relevant to the aerospace industry with excellent beam quality 1 μm wavelength laser sources.*
e. *Compare the potential benefits for adopting keyhole laser welding as a production process for titanium aerospace components with the competing manufacturing processes.*

1.5 The Engineering Doctorate Degree

The Engineering Doctorate (EngD) is a postgraduate degree that is more industrially focussed than a traditional PhD. It is offered by numerous universities in the United Kingdom, with each university establishing one, or more, EngD Academic Centres with a particular research theme. The research theme for the EngD centre at The University of Manchester connected with this research is "Engineering for Manufacture". Research projects are devised in collaboration with sponsor organisations and a Research Engineer is recruited for each project. The EngD programme at The University of Manchester is a four year full-time programme which, in addition to a doctoral level research project of the same standard as a PhD, incorporates taught courses and professional development.

1.5.1 The Research Project

The research project is of the same scientific and technological standard as a traditional PhD, with the chosen topic of research related to an area of strategic importance to the sponsoring company. Three quarters of the four year programme is devoted to the research project, with the Research Engineer taking at least two technical courses to support the research. Similarly to a PhD, the EngD requires the submission of a thesis which is examined by *viva voce*. In addition to examination of the original scientific and technical contributions, the thesis is also examined on its commercial implications.

1.5.2 The Taught Element

For the EngD at The University of Manchester the taught courses constituted a Postgraduate Diploma in Management Science, administered by Manchester Business School. Eight examined modules were taken in the first two years of the degree, which equated to 120 credits or 1200 hr of study. The eight modules covered Production Systems; Industrial Relations; Managerial Economics; Individuals, Groups and Organisations; Total Quality Management; Logistics and Supply; Management Accounting; and, Marketing Management. The topics are pertinent to the EngD, enabling the Research Engineer to understand

connections between the research project; its commercial drivers and factors which may impede the successful commercial deployment of the project's outcome; and, the commercial environment in which their industrial sponsors operate.

1.5.3 Professional Development

The EngD is a professional doctorate and, as a consequence, it incorporates courses and workshops to aid the professional development of the Research Engineer. Courses and workshops cover communication skills; negotiation skills; understanding the management role; effective project management techniques; time management techniques; industrial law; presentation skills and writing skills. Together with the research project and the taught courses, the EngD programme at The University of Manchester is accredited by the Institute of Mechanical Engineers and the Institute of Engineering and Technology, allowing progression of the Research Engineer to Chartered status by the end of the degree.

1.6 Thesis Structure

This thesis differs from traditional doctoral theses in that it has been submitted in an alternative format. The body of research performed is presented in four parts, each in the style of a peer reviewed journal paper. These papers have been prepared for, submitted to, accepted for publication, or published in a peer reviewed journal. Preceding each journal paper the information regarding the stage of publication is given. The primary author of each paper is the author of this thesis. However, to avoid uncertainty, the specific contribution of the co-authors is also detailed before each paper. In addition, portions of the literature review have been accepted for publication in the academic textbook 'Welding and Joining of Aerospace Materials' (Ed. Professor Mahesh Chatevurdi).

The primary rationale for submitting the thesis in this format is related to the commercial aspects of the Engineering Doctorate programme. As stated above, the research performed has been performed in collaboration with TWI. It has been decided that the publication of the results from this thesis will strengthen the reputation of TWI in the laser welding industry. The motives related to increasing the reputation of the authors of these papers in the laser materials processing industry are also noted.

Nevertheless, the structure of this thesis bears a resemblance to that of a traditional doctoral thesis. Proceeding this introductory chapter, the Literature Review is given, which is presented in two parts. The first part, Chapter 2, gives a brief overview of laser welding, highlights the potential defects which may arise when keyhole laser welding titanium alloys,

and details the weld quality criteria which must be met if keyhole laser welding is to be utilised by the aerospace industry. It is established in Chapter 2 that the formation of porosity in the weld metal as a result of keyhole instabilities is of primary concern. The second part of the Literature Review, Chapter 3, therefore concentrates on the forces which determine the stability of the keyhole and the mechanisms by which these can be perturbed. Potential solutions for reducing weld metal porosity as a result of controlling the process dynamics are discussed. The majority of the published experimental research has focussed on metals other than titanium alloys, but it is nevertheless valuable and is included. Concluding the Literature Review are the specific objectives of this project, which were determined from the knowledge gaps identified in the Literature Review and the aspirations of TWI Ltd.

Following the Literature Review are six chapters detailing the experimental work performed and the analysis and discussion of the results; four of these being peer reviewed journal papers. Chapter 4 describes the materials, equipment and experimental procedures used during this project. Chapter 5 details the results of research performed using a directed jet of argon to control the keyhole laser welding process. Chapter 6 covers the results of research performed with a modulated laser power output. In Chapter 7, the results of research performed with a dual focus laser beam configuration are presented, analysed and discussed. The details of research performed with excellent beam quality 1 μm wavelength laser sources are presented in Chapter 8. Chapters 5-8 contain individual discussions of results. Chapter 9 presents and discusses a small number of further results used to analyse the origin of porosity when keyhole laser welding titanium alloys with 1 μm wavelength laser beams.

The commercial aspects and implications of this research are detailed in Chapter 10 and Chapter 11. Finally, the Conclusions of this research and Recommendations for the Future are given in Chapter 12.

Part I

Literature Review

Chapter 2: Literature Review; Part I: An Overview of Laser Welding Titanium Alloys for Aerospace Applications

Chapter 3: Literature Review; Part II: Keyhole Behaviour, and the Formation and Prevention of Porosity

Chapter 2

Literature Review; Part I: An Overview of Laser Welding Titanium Alloys for Aerospace Applications

2.1 Introduction

Potentially, this thesis may be accessed by persons unfamiliar with laser materials processing but who have a specific interest in the joining of titanium and its alloys. Consequently, this Literature Review initially provides a brief overview of the interaction between light and metallic materials and how the absorption of the electromagnetic radiation may be used for conduction limited laser welding and keyhole laser welding. Significantly more attention is paid to the keyhole laser welding process, since the process offers certain key advantages pertinent to the aerospace industry compared with conduction limited laser welding. The weldability of titanium alloys by the keyhole laser welding process is discussed, in terms of the weld microstructure and potential weld defects. Of particular concern when keyhole laser welding is the formation of porosity in the weld metal, which decreases the fatigue life of the welded joint. The potential sources of weld metal porosity when keyhole laser welding are then detailed.

Uptake of the keyhole laser welding process in the aerospace industry is dependent upon the process being able to produce welds of a quality suitable for their intended application. Therefore, the international welding standards relevant to laser welding are compared with a

company specific standard in order to give an overview of the weld quality criteria that must be adhered to for certain aerospace applications. Finally, the potential weld performance when utilising the current generation of solid-state lasers is reviewed.

The majority of literature for this review was identified by performing regular Boolean logic searches across the following scientific and engineering academic databases; Compendex, Inspec, Scopus, NTIS and Weldasearch. Literature was also identified through citations in published research.

2.2 Laser Light and its Interaction with Metallic Materials

2.2.1 Key Characteristics of Laser Light

Laser light has a number of key characteristics, it is highly monochromatic, has a low beam divergence and is highly coherent, which are conducive to utilising it as a materials processing tool. The design, manufacture and integration of the gain medium, population inversion pump and optical resonator will all determine the properties of the emitted electromagnetic radiation (laser light). When deciding on a laser source for a particular materials processing application the emission wavelength, temporal and spatial operating modes, available output power and beam quality are among the key factors that should be considered. In addition, the chosen optics used to guide the laser light to the workpiece will determine critical parameters such as the beam waist and the depth of focus.

The light emitted from the majority of laser sources is highly monochromatic, in that the total spectrum of the light has a very narrow spectral linewidth. The exact spectrum is dependent upon the bandwidth available in the gain medium and the longitudinal modes present in the optical resonator. Laser sources which operate in the continuous-wave mode are capable of generating a constant power to the workpiece, although this may be modulated and/or ramped up/down if required so long as it does not exceed the maximum rated output power of the laser source. Conversely, pulsed laser sources are capable of generating very high peak powers for a short duration, either through Q-switching or pulsed pumping.

The standing longitudinal electromagnetic waves established in the optical resonator may be separated by varying angles - related to the design of the resonator. Constructive and destructive interference between these longitudinal standing waves give rise to the formation of an electromagnetic radiation field pattern transverse to the longitudinal waves. This is referred to as the transverse electromagnetic mode (TEM_{mn}, where the integers m and n indicate the number of zero fields in a particular direction) structure of the laser beam, which

determines the intensity distributions perpendicular to the direction of the laser beam propagation. A complete description of the potential TEM modes is outside the scope of this chapter. Nevertheless, it can be summarised that laser beams with a higher TEM mode are more difficult to focus than a laser beam with a lower TEM mode [Steen 1998, p. 82]. The TEM_{00} mode, or fundamental mode, is the simplest mode, and its intensity distribution, I, as a function of radius, r, from the central axis can be theoretically described by a Gaussian function [Ready 1997, p. 41].

$$I(r) = I_0 exp^{\frac{-2r^2}{w_0{}^2}} \tag{2-1}$$

where I_0 is the axial intensity of the laser beam, and w_0 is radius of the beam waist.

A Gaussian beam radius is usually defined as the radius where its intensity is $1/e^2$ of the axial irradiance. The beam waist is the point in the propagation direction where the laser beam diameter converges to a minimum, and the radius at this point is referred to as w_0. For a Gaussian laser beam propagating in free space the beam radius will converge to a minimum, the beam waist, before diverging. The angle at which the laser beam diverges is termed the beam divergence angle, 2θ. The half-angle divergence, θ, is shown in Figure 2-1. Knowing the half-angle divergence, the beam waist of a Gaussian laser beam can be calculated according to Equation 2-2 [Ready 1997, p. 38].

$$\theta = \frac{\lambda}{\pi w_0} \tag{2-2}$$

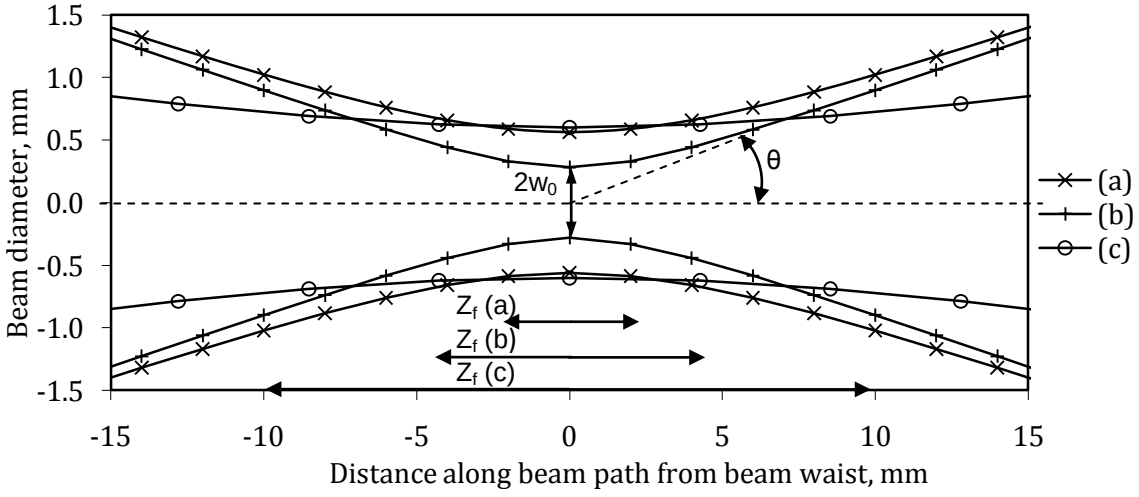

Figure 2-1. Two dimensional profiles of three different laser beams of ~1 μm wavelength (a) BPP = 12 mm.mrad, 300 mm focal length focussing lens (b) BPP = 6 mm.mrad, 300 mm focal length focussing lens (c) BPP = 6 mm.mrad, 640 mm focal length focussing lens.

The product of the beam waist and the half-angle divergence is a constant and known as the beam parameter product (BPP), stated in mm.mrad. Therefore, the BPP of a Gaussian laser beam will be λ/π, which is the theoretical optimum. However, the emitted outputs of actual laser sources are not truly Gaussian, although single-mode Yb-fibre and Yb:YAG disc lasers are very near, and are characterised by measures of their beam quality. Perhaps the most commonly used measure of beam quality is the M^2 value of the laser beam, which compares the BPP of an actual laser beam to that of a Gaussian laser beam of identical wavelength. The M^2 value of a laser beam is its BPP divided by λ/π [International Standards Organisation, 2005]. For laser sources emitting beams of approximately 1 μm wavelength, the BPP is often utilised as a measure of beam quality. Nonetheless, both these beam quality values can be utilised to approximate the propagation of actual laser beams with an expansion of Gaussian beam analysis. Equation 2-3 [Steen 1998, p.85] can be utilised to calculate the beam waist radius, *w*, of a real laser beam.

$$w = \frac{4M^2\lambda F}{\pi R} \tag{2-3}$$

where F is the focussing lens focal length, and R is radius of the beam at the focussing lens.

The above equation indicates that laser beams with a smaller value of M^2, or BPP, can be focussed into smaller diameter spots than those with higher M^2 or BPP values. Another important factor when determining the characteristics of a laser beam used for a particular materials processing application is its depth of focus, Z_f. The depth of focus is equal to the distance travelled in either direction from the beam waist over which the intensity remains about the same, which corresponds to approximately a 5% increase in the beam diameter. Materials processing applications that utilise laser beams with a long depth of focus are less susceptible to shifts in the focal plane position. Equation 2-4 [Havrilla 2002, p.16] details the calculation of the depth of focus for a 5% increase in beam diameter.

$$Z_f = \frac{w^2}{\lambda M^2} \tag{2-4}$$

Figure 2-1 details the profiles of three different laser beams, all of ~1 μm wavelength. It illustrates that laser beams with lower BPPs may be focussed into smaller beam waists using the same optical system, thereby maintaining an acceptable stand-off distance. Conversely, a laser beam with a lower BPP may be focussed into a similar beam waist to that produced with a laser beam of higher BPP but have a greater depth of focus and an increased stand-off distance.

2.2.2 Absorption by the Solid Phase

Light incident on the surface of a thick opaque metal, may be absorbed provided that the metal has a quantised energy level (electronic, atomic or molecular), e.g. $E_3 - E_2$, which matches that of the incident electromagnetic radiation, according to Equation 2-5 [Ready 1997, p.2].

$$E_3 - E_2 = h\nu = \frac{hc}{\lambda} \tag{2-5}$$

where λ is the wavelength of the incident electromagnetic radiation, ν is its corresponding frequency, h is Planck's constant, and c is the speed of light.

Absorption of the laser light is therefore dependent upon the substrate properties as well as the characteristics of the incident laser light. Figure 2-2 details the reflectivity of aluminium, iron, nickel and titanium for a normal angle of incidence (at normal angles of incidence absorption is independent of polarisation) and at room temperature, over a range of wavelengths. For the metals shown in Figure 2-2, there is a considerable difference in their reflectivity between wavelengths of ~1 μm (as produced by Nd:YAG rod, Yb:YAG disc and Yb-fibre laser sources) and ~10 μm (as produced by CO_2 laser sources).

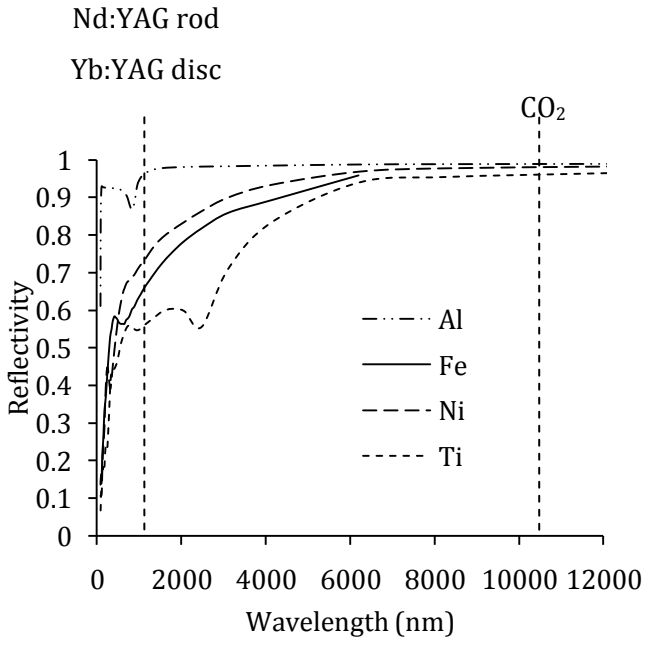

Figure 2-2. Reflectivity of aluminium, iron, nickel and titanium for a normal angle of incidence and at room temperature, over a range of wavelengths. Values from Lide [1997].

The value of reflectivity, R_f, used in this chapter may fall within a range of 0 to 1, where 1 indicates that all the incident electromagnetic radiation is reflected. For opaque materials

with a smooth surface Equation 2-6 [Steen 1998, p.67] can be used to calculate the reflectivity.

$$R_f = 1 - A \tag{2-6}$$

where A is the absorptivity or absorption coefficient.

The absorption of the incident laser radiation is also dependent upon its angle of incidence with the metal's surface and the light's polarisation. Figure 2-3 details the effect of the angle of incidence, ϕ, on the absorption of the substrate for aluminium and titanium at wavelengths of 1 and 10 μm. The maximum absorption of parallel polarised light by a metal occurs at the Brewster angle, which is wavelength and material dependent. This may be significant in terms of weld penetration [Sato et al, 1996] and weld quality [Gräf et al, 2010] when welding with laser sources whose output is polarised in a certain direction, such as CO_2 lasers. The laser light emitted from the majority of modern multi-mode solid-state laser sources, such as Yb-fibre and Yb:YAG disc lasers, is randomly polarized.

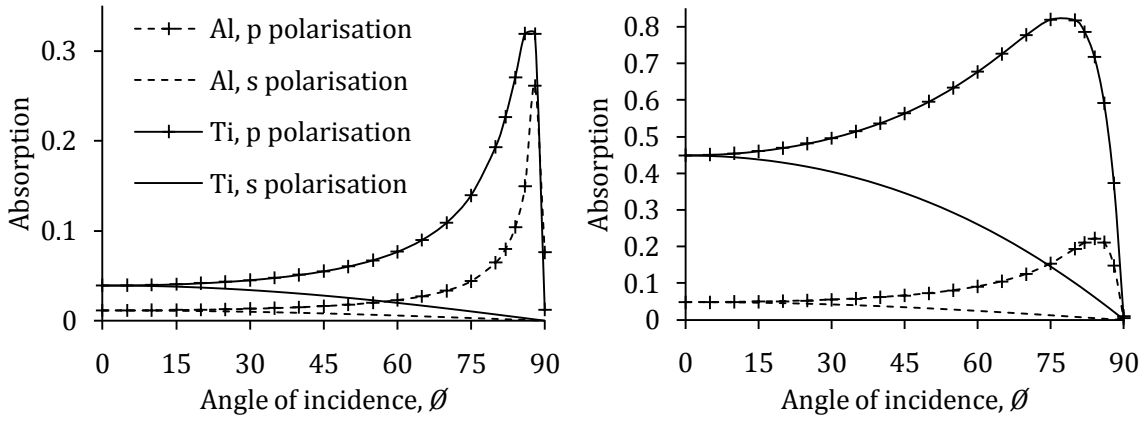

Figure 2-3. Absorption coefficients of aluminium and titanium at room temperature for parallel (p) and perpendicular (s) polarisation as a function of the angle of incidence, Ø and for (a) 10 μm wavelength, and (b) 1 μm wavelength. Note different y-axis scales. Values from Lide [1997].

The proportion of electromagnetic radiation absorbed by the substrate will change during the interaction time since the absorption is also dependent upon the temperature, as shown for a laser of 10.6 μm wavelength in Figure 2-4 for aluminium, copper and tin. As the temperature of the solid metal rises there is a steady increase in absorptivity. Subsequently, the absorptivity rises appreciably at the materials melting point. In keyhole laser welding, the absorption of the incident electromagnetic radiation will increase extensively either through

multiple Fresnel absorptions at the keyhole walls, or through inverse Bremsstrahlung absorption.

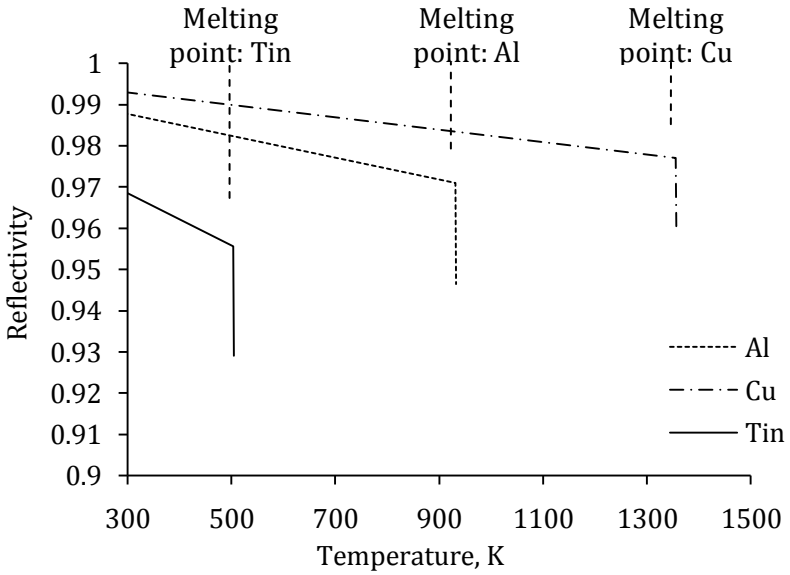

Figure 2-4. Change in reflectivity of aluminium, copper and tin during interaction with a 10.6 μm laser at a normal angle of incidence as a function of temperature. Values from Brückner et al [1989, 1991].

Equation 2-7 indicates the depth of absorption, d_α, over which the absorbed intensity reduces by $1/e^2$. The absorption depth of metals is typically less than the wavelength of the incident electromagnetic radiation, since the k value of the refractive index is greater than 1, and therefore the laser beam can be initially treated as a surface heat source for metallic substrates [Duley 1999, p.68].

$$d_\alpha = \frac{\lambda}{4\pi k} \tag{2-7}$$

2.2.3 Conduction and Melting

At very low values of applied laser intensity, there will be insufficient energy deposited at the surface of the substrate for a phase transition from solid to liquid to take place. The rate at which this thermal energy diffuses through the substrate is characterised by the material's thermal diffusivity, k_d; a property which is related to the thermal conductivity, k_c, the specific heat, c_p, and the density, ρ, of the material. If the intensity of the laser radiation incident on the substrate is increased sufficiently ($\sim 10^2$ Wmm^{-2} for most metals), surface melting will begin to occur, and a pool of molten material will form. The depth of the melt pool, X, can be

approximated by Equation 2-8 [Cohen, 1967] under the assumption that the thermal conductivity and diffusivity in the solid and liquid phases are nominally identical.

$$X(t) \approx \frac{0.16P(t-t_m)}{\rho L} \tag{2-8}$$

where t is the time the laser radiation is applied for, t_m is the time required to reach the melting temperature, T_m, at the surface of the workpiece, P is the absorbed laser power density, and L is the latent heat of fusion.

The time taken to for the surface of the substrate to reach its melting temperature can be approximated by Equation 2-9 [Cohen, 1967].

$$t_m = \frac{\pi {k_{cs}}^2 {T_m}^2}{4K_{ds}I^2} \tag{2-9}$$

where k_{cs} and k_{ds} are the thermal conductivity and thermal diffusivity of the solid phase.

2.2.4 Vaporisation

Vaporisation of metallic substrates can occur at applied intensities as low as 10^2 Wmm^{-2} if the interaction time is sufficient. However, applied laser intensities exceeding 10^4 Wmm^{-2} are often used to achieve vaporisation of the surface for materials processing applications such as keyhole laser welding, laser cutting and laser drilling. Equation 2-10 [Ready 1997, p.322] can be utilised to estimate the time taken, t_v, to reach the vaporisation temperature, T_v, of the substrate.

$$t_v = \frac{\pi k_c \rho c_p (T_v - T_0)^2}{4P^2} \tag{2-10}$$

where T_0 is the ambient temperature.

This initial vaporisation of the substrate creates a depression in the molten pool, through the recoil pressure exerted by the vapour, thereby forcing the molten metal to the peripheries of the interaction area. It is a critical stage in the formation of a vapour cavity in the substrate, as it leads to a significant reduction in reflectivity. Efficient coupling of the laser beam into the substrate is then achieved either through multiple Fresnel absorptions by the molten material (for 1 μm wavelength laser sources). For wavelengths of the order of 10 μm, the absorption method is more complex. Absorption of the incident laser energy by free-free electrons (inverse Bremsstrahlung absorption) is possible at this wavelength, as is Fresnel absorption. The proportion absorbed by each mechanism is a function of the welding

parameters [Solana and Negro, 1997]. Inverse Bremsstrahlung absorption can be neglected for 1 μm wavelength. Figure 2-5 details the formation of a vapour cavity through a series of co-axial high speed images taken when a laser beam emitted from an Nd:YAG rod laser was incident on a plate of Ti-6Al-4V.

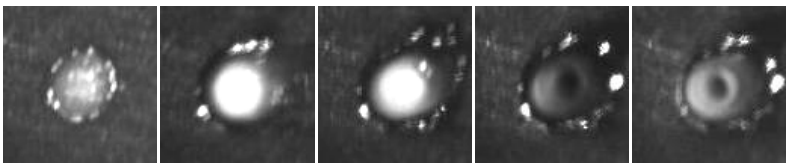

(a) (b) (c) (d) (e)

Figure 2-5. Formation of a vapour cavity in Ti-6Al-4V using an Nd:YAG rod laser, (a) surface melting, (b) - (c) vaporisation of the substrate occurs, molten metal is pushed to the peripheries and absorption of the laser beam significantly increases, and (d) – (e) this leads to the formation of a high aspect ratio vapour cavity.

2.2.5 Plasma Formation

Above, it was discussed that the formation of a keyhole in a substrate with a laser beam is dependent on the vaporisation of the substrate. For laser beams of ~10 μm wavelength the metallic vapour may become ionised and the radiation is efficiently absorbed via the inverse Bremsstrahlung absorption process. The proportion of incident radiation absorbed by the plasma, a gas which is constituted of both electrons and ions, depends upon the ratio of the electron, n_e, and ion density, n_i, to the density of the vapour atoms, n_o. This can be calculated by Equation 2-11 [Mitchener and Kruger 1973, p.43], if the gas is assumed to be in local thermodynamic equilibrium (LTE).

$$\frac{n_e n_i}{n_0} = \left(\frac{g_i g_e}{g_0}\right) \frac{(2\pi m_e k_b T_e)^{\frac{3}{2}}}{h^3} \exp^{\left(\frac{E_i}{k_b T_e}\right)} \qquad (2\text{-}11)$$

where, k_b is the Boltzmann constant, m_e is the electron mass, E_i is the ionisation energy of the gas, $g_{e,i,0}$ are the degeneracy factors of the electrons, ions and neutral atoms respectively, and T_e is the electron temperature.

It is possible that a plasma may form above the keyhole and attenuate the incident laser radiation, either through inverse Bremsstrahlung absorption or defocussing as a result of a gradient electron density, and lead to a reduction in depth of the keyhole [Poueyo-Verwaerde et a, 1993]. For laser beams of ~1 μm wavelength, inverse Bremsstrahlung absorption of the laser beam is not a concern. However, it has been shown that when welding with an Nd:YAG

rod laser the beam can be attenuated and defocussed by a vapour plume of nano-scale particles [Greses, 2003], causing a reduction in penetration depth or keyhole instabilities.

2.3 Laser Welding Fundamentals

The absorption of laser light by a metallic substrate and the conduction of the resultant thermal energy leading to possible phase changes in the substrate were detailed in the previous Section. These potential phase changes can be utilised to distinguish between the two fundamental modes of laser welding; (i) conduction limited, and (ii) keyhole. Only solid-liquid and liquid-solid phase changes occur when laser welding in the conduction limited mode, whereas during keyhole laser welding a portion of the substrate is vaporised and hence the gaseous phase is also present. Furthermore, as discussed above, there is the potential for plasma to be present when keyhole laser welding. Laser welding can be utilised to weld a number of metallic materials, including; carbon steels, stainless steels, nickel alloys, aluminium alloys, magnesium alloys, titanium alloys and copper. Certain combinations of dissimilar metals may also be joined by keyhole laser welding, with the rapid cooling rates allowing segregation and grain growth to be reduced.

This chapter is primarily concerned with keyhole laser welding, since, if the process is optimised, it is more advantageous to laser weld typical grades and thicknesses of metallic aerospace materials in the keyhole mode than in the conduction limited mode. Principally, this is a result of the lower heat-input and increased processing speeds possible when keyhole laser welding.

2.3.1 Conduction Limited Laser Welding

Conduction limited laser welding involves only the solid and liquid phases of the substrate and consequently the energy from the incident laser radiation is only absorbed by the surface of the substrate. Subsequently, this thermal energy is transferred from the surface into the bulk of the substrate via thermal conduction. Melting occurs when the applied intensity is sufficient and a weld is made when the molten material solidifies. When conduction limited laser welding, the resultant penetration depth is heavily influenced by the Marangoni forces, or forces due to a surface tension gradient. Conduction limited laser welding can be used to produce spot or seam (either through overlapping spots or a continuous process) welds.

Since the process relies solely on conduction, the weld depths possible are limited by the thermal conductivity of the substrate. A power density of approximately 10^2 – 10^4 Wmm^{-2} is ordinarily sufficient for conduction limited welding to be performed. The resulting fusion

zone has a hemispherical weld profile, with a width exceeding the depth by a factor of ~2, shown in Figure 2-6. A significantly larger HAZ (shown in Figure 2-6) compared with welds made using keyhole laser welding also occurs.

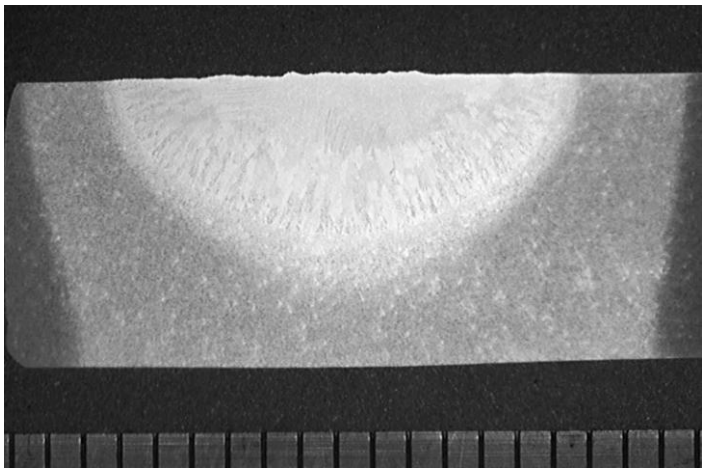

Figure 2-6. Conduction limited laser autogeneous melt run in 8 mm thickness 2024 aluminium alloy, produced with the laser beam emitted from an Nd:YAG rod laser source (scale in mm). Courtesy of TWI Ltd.

Table 1-1 summarises the characteristics and subsequent advantages of utilising keyhole laser welding in an industrial environment. The advantages associated with the flexibility and repeatability of the process are also valid for conduction limited laser welding. However, the heat inputted to the workpiece when operating in the conduction regime, is significantly higher than when operating in the keyhole regime. Furthermore, processing speeds are significantly lower for a given material and thickness. In comparison with keyhole laser welding, conduction limited laser welding is an inherently stable process. As will be discussed in the subsequent Section, defects arising from instabilities in the vapour cavity, such as porosity, are not formed in conduction limited laser welds. High integrity welds with few, or no, defects can therefore be more easily produced when conduction limited laser welding.

For conduction limited spot welds, Equation 2-8 can be utilised to approximate the depth of penetration. This equation is subject to certain boundary conditions so that only parameters which cause melting are chosen. It has been reported [Williams et al, 2001] that fully penetrating welds in aluminium alloy (2000 series) at least 6.35 mm in thickness can be produced by conduction limited laser welding if the focussed intensity is optimised such that the surface temperature of the melt pool is just below the vaporisation temperature.

Accurate control of the melt pool temperature, and hence the heat input, is required to ensure the penetration depth remains constant and no penetration spiking occurs. Figure 2-2 and

Figure 2-3 show that the absorption of the laser beam by a particular substrate is dependent upon the wavelength of the beam and its angle of incidence with the workpiece. A result of this is that laser beams of wavelengths ≤ 1 μm are more suited to conduction limited welding of metallic substrates, since they are more readily absorbed, than longer wavelength laser beams. Operation at an angle of incidence equal to the Brewster angle of a particular laser-beam material combination will further increase absorption of the beam by the substrate. It is also known that the proportion of the incident laser light absorbed is a function of the temperature of the substrate (see Figure 2-4). An accurate knowledge of the temperature-absorptivity relationship, as well as the temperature dependent values of thermal conductivity and effective viscosity would allow an approximate heat input to be calculated [De and Debroy, 2006]. Furthermore, it is critical that the temperature of the substrate does not exceed its vaporisation temperature, as this would result in a significant increase in absorption of incident laser light and the formation of a vapour cavity. However, in practice, temperature-absorptivity relationships are not known and it is not feasible to determine them. Real time monitoring and feedback of the melt pool temperature is a possible approach to controlling penetration depth when conduction limited laser welding [Bardin et al, 2005].

2.3.2 Keyhole Laser Welding

Keyhole laser welding (also referred to as deep penetration laser welding) is similar in concept to electron beam welding, in that a vapour cavity is formed in the substrate and subsequently traversed across it. A liquid sheath surrounds the vapour cavity, or keyhole, which is in turn surrounded by the solid substrate. The keyhole is primarily maintained by the ablation pressure and the pressure of the vapour within it. A portion of this vapour is ejected from the keyhole and therefore, a steady-state cannot be achieved with a stationary keyhole as ultimately it will fully penetrate the substrate and the vaporised material that is ejected cannot be replenished to sustain the vapour pressure. However, a quasi steady-state can be considered for a moving keyhole. As the keyhole is traversed through the substrate, the sheath of molten material surrounding it is continuously transported from the region in front of the keyhole to the trailing melt pool.

The dominant transportation process is the flow of molten material around the keyhole, although a proportion of the molten material is vaporised and transported across the keyhole maintaining the vapour pressure and potentially producing a quasi steady-state. Thermal conduction in the direction of travel ensures the continuous replenishment of the molten material. Figure 2-7 shows the formation of the keyhole laser welding process in C-Mn steel, and a schematic of the keyhole and molten pool geometries.

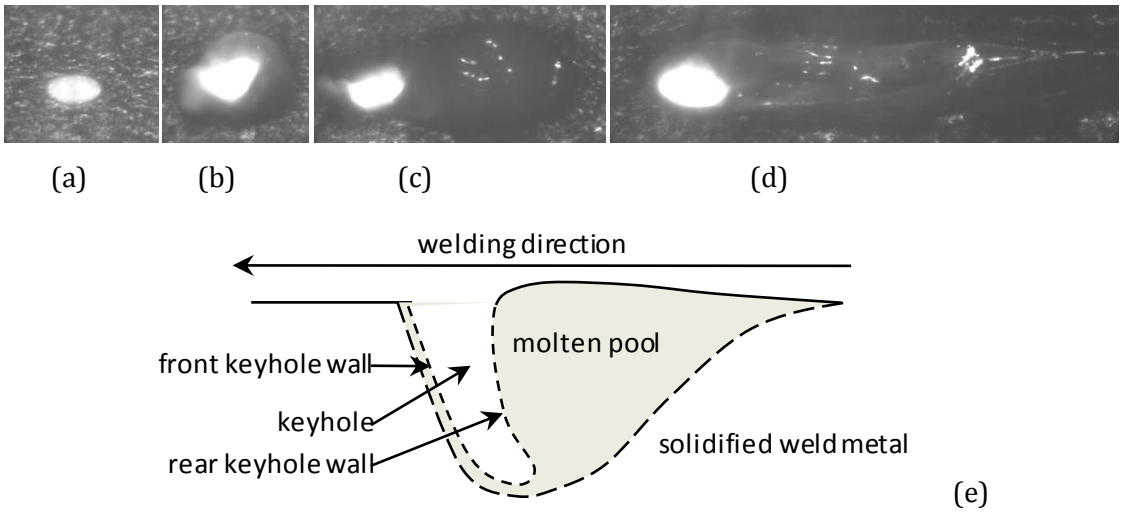

Figure 2-7. Formation of keyhole laser welding process in C-Mn steel, (a) surface melting, (b) vaporisation of substrates occurs, (c) keyhole traverses across the workpiece and melt pool begins to form, and (d) the melt pool length increases and stabilises; (e) schematic of the side view of a keyhole.

The keyhole is not cylindrical in shape and has a characteristic curve to it which is determined by the absorption mechanism, travel speed and thermal conductivity of the substrate. Analogous to conduction limited laser welding, keyhole laser welding can be utilised for either spot or seam welding. Typically, a continuous process is employed to maximise the potential advantages of the process, although pulsed laser sources are particularly suited to spot welding applications. Characteristic profiles of keyhole laser welds produced in Ti-6Al-4V with a 1 μm wavelength laser source are shown in Figure 2-8.

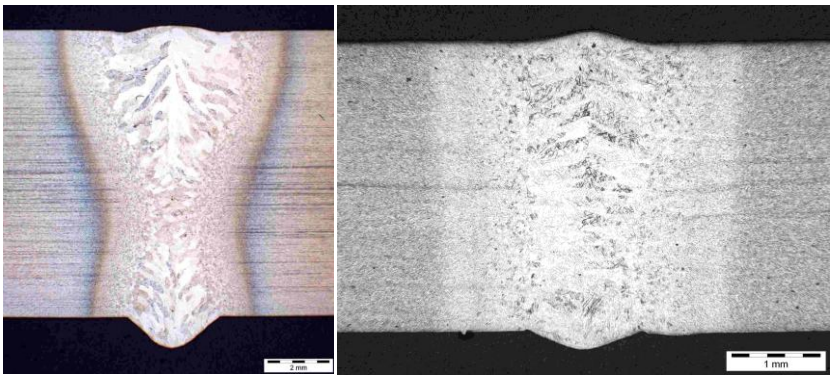

Figure 2-8. Profiles of keyhole laser welds produced in Ti-6Al-4V, (a) 9.3 mm thickness, and (b) 3.2 mm thickness. Note: different scales. Courtesy TWI Ltd.

Table 1-1 summarises the characteristics and subsequent advantages of utilising keyhole laser welding in an industrial environment. Disadvantages associated with keyhole laser welding include:

1. Equipment cost – the initial cost of high power laser sources can be high compared with arc welding equipment. This is ordinarily offset by an increase in productivity. Recent advances in solid-state laser technology are driving down initial costs, as well as increasing wall plug efficiency.
2. Safety – absorption of laser radiation by the skin, and in particular the retinal hazard region, is of great concern. The exact safety measures are dependent on wavelength and power. BS EN 60825-1:2007 or ANSI Z136.1-2007 should be referred to for exact safety requirements.
3. Joint fit-up requirements – narrowly focussed laser beams may stray from the required joint line through workpiece misalignment or thermal distortion. This tolerance can be increased by using hybrid laser-arc welding, or a seam tracking system.

Power intensities of $\sim 10^4$ Wmm^{-2} and above are ordinarily sufficient for a keyhole to be initiated in the substrate, although vaporisation is possible at lower power densities if the values of welding speed and thermal conductivity of the substrate are conducive. Equation 2-12 [Qin et al, 2007] can be utilised to approximate the critical power required for keyhole laser welding with a Gaussian beam, as a function of welding speed, V.

$$P = \rho\pi(2k_d V)^{\frac{1}{2}} w_0^{\frac{3}{2}} E_v \tag{2-12}$$

where E_v is the energy required to vaporise the material.

This relationship should be treated as an approximation only, since it is known from empirical evidence that oscillations in the keyhole behaviour may occur even with a constant set of parameters [Arata et al, 1984] making a quasi steady-state particularly difficult to achieve. Variations in the keyhole and melt pool behaviour may lead to certain weld defects, such as intermittent penetration and weld metal porosity. Consequently, the formation and subsequent dynamic behaviour of a keyhole has been the subject of intense theoretical and practical investigations (e.g. Arata et al, 1984; Kaplan, 1994; Dowden et al, 1995; Matsunawa et al, 1998; and Fabbro and Chouf, 2000). Thorough details of the keyhole and melt pool dynamics is particularly extensive and challenging, and the published investigations of the aforementioned researchers should be referred to for an excellent understanding of this area. Fundamentally, the transient behaviour of the keyhole is dependent upon the forces acting to maintain it, and those tending to close it. Duley [1999, p.83] summarised that, the forces maintaining the keyhole are the evaporative and radiative pressures, whilst those acting to

close it are the hydrostatic and hydrodynamic pressures of the surrounding molten material and its surface tension.

Optimisation of the process parameters is critical if high quality welds are to be produced with the keyhole laser welding process. Table 2-1 specifies the critical process parameters that should be considered when keyhole laser welding, either autogenously or with filler material. A significantly more extensive list can be found in BS EN ISO 15609-4:2009 '*Specification and qualification of welding procedures for metallic materials, Welding procedure specification*, *Laser beam welding'.* Further process parameters will emerge if more complicated processes are chosen, such as hybrid laser-arc welding and dual focus keyhole laser welding.

Table 2-1. Potential process parameters for keyhole laser welding [Duley 1999, p.28; Steen 1998, p.156]

Type	Parameters	
Laser source/focussed beam	wavelength	polarisation
	power	welding speed
	focussed spot size	focal plane position
	beam quality	depth of focus
	stand-off distance	pulse energy (pulsed laser)
	pulse time (pulsed laser)	pulse shape (pulsed laser)
	pulse frequency (pulsed laser)	waveform (modulated output)
	frequency (modulated output)	duty cycle (modulated output)
Workpiece	surface preparation	shielding gas type
	joint geometry	shielding gas arrangements
	jigging/fixturing	
Filler material	chemical composition	feed rate
	type (wire or powder)	
	gauge/diameter	
	position with respect to welding process	

2.4 Laser Weldability of Titanium Alloys

Titanium weld metallurgy is controlled by the transformation from the close-packed-hexagonal structure (α phase) into the body-centred-cubic crystalline structure (β phase)

which occurs at the β transus temperature (882°C). The allotropic transformation is reversible, and the transus temperature can be manipulated with the alloying of α (e.g. aluminum, carbon, nitrogen and oxygen) and/or β (e.g. chromium, copper, iron and molybdenum) phase stabilisers, whereby;

- the addition of β phase stabilisers decrease the β transus temperature such that the β phase can be retained as the weld cools to ambient temperature; and,
- the addition of α phase stabilisers increases the β transus temperature, promoting the formation of the α phase.

The majority of titanium alloys are considered readily weldable, often determined by the ductility and toughness of the as-welded zone, by fusion welding processes. Ordinarily, the higher strength alloys are more difficult to weld as a result of [Lütjering and Williams 2007, p.105];

- the alloys forming microstructures of poor toughness and low ductility; and,
- containing eutectoid alloying elements, e.g. chromium and iron, which may cause liquation cracking.

During fusion welding, the temperature of the fusion zone, and also a portion of the heat affected zone, is above the β transus temperature and consequently may exhibit β transformed microstructures and properties. The microstructure of fusion welds in titanium alloys is ordinarily martensitic, which, in comparison with martensite formed in stainless steels, has a higher toughness and a decreased susceptibility to cracking [Yunlian et al, 2000]. Cooling rates above $410°Cs^{-1}$ are necessary to achieve a completely martensitic structure in Ti-6Al-4V [Ahmed and Rack, 1998]. These cooling rates are easily obtainable when keyhole laser welding and the weld metal will undergo a particularly fast thermal cycle compared with inert gas arc welding, consequently producing a finer martensitic microstructure which will have a smaller content of alloying elements [Costa et al, 2007; Yunlian et al, 2000]. The required cooling rates to obtain a martensitic structure will be different for all grades of titanium. For commercially pure titanium a similar trend to the above Ti-6Al-4V microstructure has been reported [Li et al, 2009] – increased cooling rates lead to an increased content of fine-grained acicular α' present in the fusion zone.

Despite the high cooling rates promoting a fine grained martensitic structure in keyhole laser welding of titanium alloys, the potential still exists for a number of defects to occur, including; weld bead embrittlement, cracking, geometrical defects in the profile, and weld metal porosity.

2.4.1 Embrittlement

Titanium has an elevated affinity for light elements (such as hydrogen, nitrogen and oxygen) at temperatures exceeding 500°C, which may result in embrittlement of the weld metal if they are absorbed. The discoloration of the weld metal can be utilised as an indicator of the shielding adequacy, whereby the weld metal follows the colour sequence [American Welding Society, 2001]; silver (indicating no discoloration), light straw, dark straw, bronze, brown, violet, green, blue, gray and white (indicating heavy discoloration and embrittlement). This discoloration is directly related to the degree of weld metal embrittlement and hardness of the weld metal.

The effects of oxygen contamination (0.001 to 10%) in argon shielding gas was studied by Li et al [2005] when laser welding commercially pure titanium. At increased oxygen contents the weld bead discoloration followed the sequence outlined in AWS D17.1, and which also corresponded to a change in the surface hardness. Table 2-2 details the hardness data reported by Li et al [2005]. However, it is imperative that the weld bead discoloration not be utilised as an inspection tool for shielding adequacy, as the discoloration sequence will repeat as the oxidation thickness increases [Talkington et al, 2000].

Table 2-2. Surface colour and hardness of Nd:YAG laser welds made in 0.5 mm thickness commercially pure titanium sheets with varied oxygen content in the argon shielding gas [Li et al, 2005].

Oxygen content, %	Surface colour	Hardness, Hv
0	Silver	242±11
0.15	Straw	246±16
0.5	Dark straw	247±13
1.5	Dark straw/purple	254±20
2.0	Dark	282±18
3.0	Purple/blue	295±16
5.0	Blue	323±15
10.0	Blue	373±20

To avoid embrittlement titanium alloys are ordinarily shielded with a high-purity inert gas when they are keyhole laser welded. For reasons related to its ionisation energy and the formation of a beam attenuating plasma (see Section 3.5), helium is utilised when welding with a 10 μm wavelength focussed laser beam, whereas argon is used when welding with a 1

μm wavelength focussed laser beam. The shielding gas is often delivered through a trailing shield which covers the weld face, and through an efflux channel covering the weld root. At sufficiently slow welding speeds, the shielding gas may be delivered through a co-axial or lateral nozzle. This approach is often employed when laser welding titanium alloys with a pulsed laser source.

2.4.2 Cracking

Titanium alloys are, in general, not considered susceptible to solidification cracking since they contain low concentrations of impurities. However, research has suggested [Inoue and Ogawa, 1995] that titanium alloys may be vulnerable to solidification cracking if they are incorrectly restrained during welding. It is likely that the degree of vulnerability is related to the amount of back diffusion of solute-elements in the solid [Inoue and Ogawa, 1995]. Of more concern when welding titanium alloys is contamination cracking, which may occur if the weld metal is exposed to light elements at temperatures exceeding 500°C or iron particles during welding. When absorbed, the light elements, such as hydrogen, nitrogen and oxygen, will migrate to interstitial sites and may cause cracking as a result of the welding stresses. Particularly high levels of these elements are required in the welding atmosphere, for example; 3000 ppm oxygen in the weld metal may cause transverse cracking [Donachie 2000, p.88]. As previously, the presence of light elements in the vicinity of the welding process and cooling weld bead may be reduced by utilising an effective trailing shield and a high-purity inert shielding gas with a low dew point. Particles of iron on the workpiece may be dissolved into the melt pool and, potentially, cause embrittlement of the weld metal [Donachie 2000, p.88]. An appropriate materials preparation and handling procedure will minimise the risk of iron particle contamination.

2.4.3 Geometrical Weld Profile Defects

Geometrical defects in the weld profile, such as undercut and concavity at the weld face or root, are particularly undesirable for components subject to dynamic loading. The defects may act as stress concentrators and subsequently be initiation sites for fatigue cracks. Fundamentally, the defects can either be attributed to the laser welding process or to the joint configuration/restraint. For instance, joint misalignment, where the laser beam wanders from the joint line resulting in a portion of the weld seam not being welded, is an example of a defect which is not related to the welding process. It may occur when the laser beam is not correctly aligned with the joint line or when the component is not correctly clamped allowing movement of the joint during welding. Consequently, this defect is more commonly observed

in keyhole laser welding as the finely focussed beams are more susceptible to missing the joint line than in conduction limited laser welding. Incorrect joint configuration/restraint, errors in gap fit up, or inadequate machining of the abutting edges may lead to other geometrical defects in the weld profile, specifically [Duley 1999, p.202]; burn through, drop out, or a loss of penetration.

The above defects can be eliminated through the adoption of adequate weld clamping and workpiece preparation. Geometrical weld profile defects associated with the laser welding process, such as humping, undercut and concavity, may occur as a consequence of incorrect welding parameters. Often, a balance of process parameters is found to achieve the required weld penetration and minimise weld profile defects. Figure 2-9 [Hilton et al, 2007] details the terminology adopted in this project for defining the weld profile's geometry and defects.

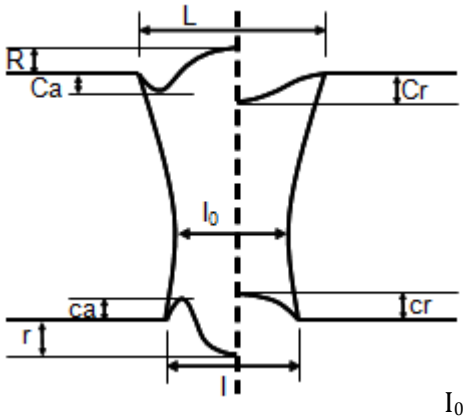

Ca = Face undercut
ca = Root undercut
Cr = Face concavity
cr = Root concavity
r = Excess penetration
R = Excess weld metal
L = Face weld width
I = Root weld width
I_0 = Minimum weld width

Figure 2-9. Potential weld profile defects and terminology [Hilton et al, 2007].

Humping, which is not shown in Figure 2-9, refers to the formation of ellipsoidal swellings in the top bead of a weld. The swellings are severely undercut and are separated by an elongated concavity along the weld face. Humping is ordinarily observed when particularly high welding speeds and laser powers are adopted. For example, humping was observed at speeds above 20 $mmin^{-1}$, when using a 4 kW laser power focussed into a 600 µm beam diameter, for welding of 3 mm thickness 304L stainless steel [Fabbro et al, 2007].

Defects in the weld profile which cannot be eliminated through alteration of process parameters may be removed by further processing and/or machining. Filler material, either powder or wire, may be added during the process, or a low-power cosmetic pass utilised to re-shape the top bead. Workpieces which are thicker at the joint could be used, which would allow post-weld machining to eliminate the defects without having an undersized weld.

2.4.4 Weld Metal Porosity

It has been reported [Matsunawa et al, 2001] that weld metal porosity can easily form when keyhole laser welding. This is a concern for high-performance components that are in cyclic loading, as the pores will reduce its fatigue resistance. Figure 2-10, reproduced from Lindh and Peshak [1969], indicates the significant decrease in fatigue life of Ti-6Al-4V welds containing weld metal porosity compared with defect free welds. Porosity is of primary concern for components whose weld profiles are dressed (to remove geometrical defects in the weld profile, etc), as pores will break the surface, act as stress concentrators and further reduce the fatigue resistance of the weld, as indicated in Figure 2-10.

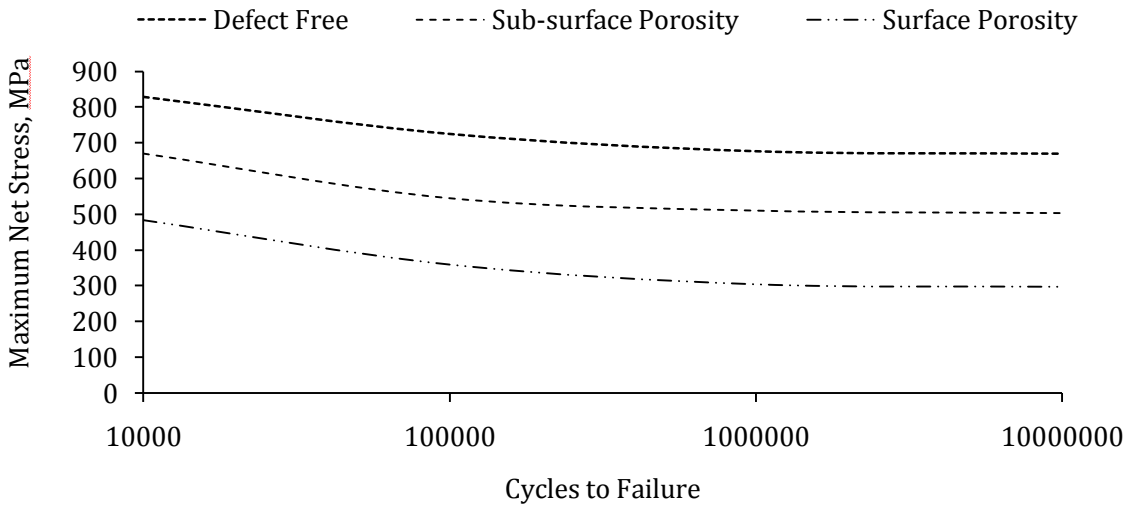

Figure 2-10. Fatigue behaviour of welds in Ti-6Al-4V, showing the effect of surface and subsurface weld metal porosity in comparison with defect free welds. Reproduced from Lindh and Peshak [1969].

A significant amount of research has been performed into the causes of porosity when laser welding metallic materials, although only a small proportion of this concerns the formation of porosity when processing titanium alloys. The majority of the reported fundamental investigations have been performed on aluminium alloys and ferrous metals. Potential sources of porosity when laser welding titanium alloys are from:

- The presence of excessive hydrogen in the melt pool, which is rejected upon solidification and subsequently trapped in the solidifying melt pool.
- Instabilities in the welding process, leading to the entrapment of shielding gases and/or metal vapour.

2.4.4.1 Hydrogen Porosity

Figure 2-11 details the solubility of hydrogen in titanium as a function of temperature, reproduced from Lakomski and Kalinyuk [1963]. The overall trend of this relationship is an increasing solubility with a decreasing temperature. Ordinarily, this would not result in the rejection of hydrogen from the solidifying melt pool and the formation of porosity. However, at the solidification temperature there is a significant drop in hydrogen solubility, which may lead to weld metal porosity.

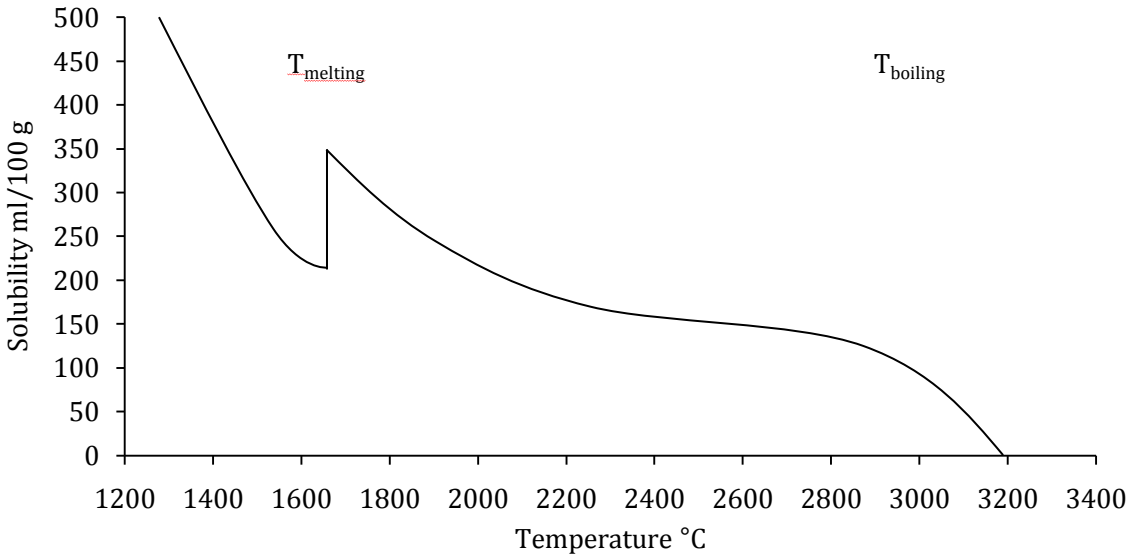

Figure 2-11. The solubility of hydrogen in titanium as a function of temperature. Reproduced from Lakomski and Kalinyuk [1963].

Figure 2-11 indicates that hydrogen will be rejected if the content is greater than ~210 ml/100g (280 ppm), which may result in the formation of hydrogen bubbles and subsequently porosity. The hydrogen content of modern titanium alloys is generally <280 ppm and therefore will not pose a problem on its own. However, other potential sources of hydrogen exist when laser welding titanium, which will, if not properly addressed, contribute towards the total amount of hydrogen in the melt pool. Specifically, these other potential sources of hydrogen may be from;

- the hygroscopic titanium oxide layer present on the workpiece surfaces;
- shielding gas(es);
- welding consumable(s); and,
- workpiece preparation.

Titanium oxide will form on the surface of titanium alloys if sufficient levels of oxygen are present in the media surrounding it. This self-healing oxide layer gives titanium its excellent corrosion resistance to different types of aggressive media. However, the oxide layer has a hygroscopic behaviour and will consequently adsorb moisture from the atmosphere under ambient conditions. Removal of the hydrated layers prior to welding is critical in minimising the potential hydrogen content of the melt pool. Consequently, the effectiveness of the method used to remove the hydrated layer and other surface contaminants (for example, oil, dirt, and grease) may have a large influence on the formation of weld metal porosity.

Mechanical cleaning methods, such as scratch brushing and abrasive cleaning, are often utilised because they are relatively straight forward processes compared with chemical pickling. Mueller et al [2006] produced welds with small amounts of weld metal porosity when laser welding 6.35 mm thickness Ti-6Al-4V if the joint was cleaned with a stainless steel brush prior to welding. It should be noted there is a slight risk of iron pick up with stainless steel brushes, and titanium brushes should be used for critical applications [Smith et al, 1999]. Autogeneous melt runs and butt welds with very low levels of porosity were also produced in titanium alloys up to 9.3 mm in thickness by Hilton et al [2007]. In this work the surfaces were cleaned with an abrasive pad and acetone degreased prior to welding, and abutting joint edges of butt were also dry machined. However, it should be noted that, in both of the above publications [Mueller et al, 2006; Hilton et al, 2007], a directed gas jet was also used to achieve the low levels of weld metal porosity (see Sub-section 3.6.2).

Chemical pickling of titanium alloys prior to welding is usually performed with an aqueous solution of hydrofluoric and nitric acid [Smith et al, 1999]. In comparison with mechanical cleaning methods, a more uniform surface finish is possible and there is less dependency on the operator. A comparison of different pickling solutions was performed by Gong et al [2003], who concluded that 10%HF-30%HNO_3-60%H_20 was the most suitable formula for removing the oxide layer of the titanium alloy BT20. The other formulas tested were 3%HF-30%HNO_2-67%H_20 and 5%HF-30%HNO_3-65%H_20.

Welding should be performed as soon as possible after removal of the hydrated layers since the oxide layer will continue to adsorb moisture. No critical time period for significant hydration has been established, and will depend on the local temperature and humidity. For practical purposes, welding within the same 24 hr period as the workpiece preparation should minimise porosity [Mitchel, 1965; Hughes, 1989]. Gong et al [2003] reported that the timing of material preparation had an effect on the porosity levels observed.

It is difficult to directly compare the effectiveness of the different surface preparation techniques from the above, since there are a number of other process variables that must be accounted for. Furthermore, in most of the work, other techniques have been utilised to control the laser welding process and reduce other sources of weld metal porosity. Nevertheless, it can be concluded that the type of material preparation utilised may have an effect on the weld metal porosity that is caused as a result of hydrogen rejection by the melt pool upon solidification. It appears from the published research summarised above that mechanical cleaning with an abrasive pad, scratch brushing with a stainless steel or titanium brush, and chemical pickling with an appropriate aqueous solution of hydrofluoric and nitric acid are all appropriate methods of removing hydrated layers. The time between welding and workpiece preparation should be minimised. Pre-weld degreasing should also be performed with an appropriate vapour or liquid degreasing method, and the time between workpiece preparation and welding should be kept to a minimum.

As mentioned previously, titanium has a high affinity for light elements at temperatures of ~500°C and above. Consequently, rigorous inert gas shielding is used when welding titanium alloys to prevent discoloration and possible embrittlement of the weld metal. The choice of inert gas (either helium or argon) is likely to be determined by the wavelength of the incident laser radiation. However, the inert shielding gases are a potential source of hydrogen, which, according to the hydrogen solubility diagram produced by Lakomski and Kalinyuk [1963], may be absorbed by the melt pool as it cools prior to solidification. Therefore, an increased amount of hydrogen present in the shielding gases may increase the possibility of hydrogen porosity present in the solidified weld metal.

In certain instances, wire addition may be required to correct geometric defects present in the weld profile, such as undercut at the weld face and/or root. Investigations performed by Gorshkov and Tret'Yakov [1963] when arc welding titanium alloys have shown that increased hydrogen content in the filler metals tended to increase weld metal porosity. Many welding consumables are now extra-low-interstitial grade with nominal hydrogen contents. As a result, the hydrogen content of welding consumables should not be of concern provided that a suitable grade is chosen. However, as with the parent material, a hydrated layer can form on the surface of titanium welding wires which may increase the content of hydrogen in the melt pool.

2.4.4.2 Processing Porosity

Despite taking care in workpiece preparation and shielding gas purity, porosity can still form in weld metal. Furthermore, larger pores may also form in the weld metal when laser welding, which cannot be attributed to hydrogen precipitation as the cooling rate is too high [Pastor et al, 1999]. It has been reported [Matsunawa, 2001] that keyhole instability can lead to metal vapour and/or inert shielding gases being trapped in the weld metal. This occurs when the forces trying to hold the keyhole open are not in equilibrium with those trying to close it. Keyhole observation techniques using micro-focussed X-rays and a high speed video camera have shown that the dimensions of the keyhole fluctuate, both parallel and perpendicular to the laser beam [Katayama et al, 2003]. The proceeding chapter provides extensive details on the reported causes of keyhole stability and on potential methods for eliminating or reducing them.

2.5 Weld Quality Criteria for Titanium Alloys in Aerospace Applications

Several published welding standards exist relating to the laser welding of metallic materials. For instance, BS EN ISO 15609-4:2009 '*Specification and qualification of welding procedures for metallic materials, Welding procedure specification, Laser beam welding*' provides details for the content of welding procedure specification for laser welding.

In terms of acceptable levels of weld defects when laser welding titanium alloys, BS EN ISO 5817:2007 '*Welding. Fusion-welded joints in steel, nickel, titanium and their alloys (beam welding excluded). Quality levels for imperfections*' gives guidance on the quality levels of welded joints in titanium alloys, but excludes beam welding processes. BS EN ISO 13919-1:1997 and BS EN ISO 13919-2:2001 give guidance on the quality levels of welded joints in steel and aluminium alloys respectively. The stated weld imperfection limits in these two standards are detailed for three different quality levels; B, C and D. There are no standards published by the International Standards Organisation which relate to acceptable limits of imperfections in laser welded titanium alloys. However, AWS D17.1:2001, '*Specification for Fusion Welding for Aerospace Applications*', by the American Welding Society, details the requirements for welding aircraft and space hardware in titanium alloys and other metallic materials. The AWS D17.1 standard incorporates electric arc, plasma arc, oxyfuel, laser beam and electron beam welding processes. Furthermore, the stated quality criteria in AWS D17.1 are more stringent than those found in BS EN ISO 13919-1, which contains more stringent criteria than BS EN ISO 13919-2.

It is known [Hilton et al, 2007] that the quality acceptance criteria for aeroengine applications are more stringent than those prescribed for aircraft and space hardware in AWS D17.1. The criteria are company specific and have not been formally published by an international standards body. An example of such typical acceptance criteria, in terms of weld profile and weld metal porosity, has been detailed by Hilton et al [2007]. A summary of the typical quality criteria detailed in AWS D17.1 and a company specific standard is given in the subsequent Sections. Attention is given to the potential weld defects which may occur when keyhole laser welding titanium alloys, as summarised previously, specifically; embrittlement, profile defects and weld metal porosity.

Figure 2-9 details the terminology that has been adopted here to allow a comparison of the stated weld profile criteria in AWS D17.1 and the company specific standard. For comparison of weld metal porosity criteria, the term 'accumulated length' has been adopted, which can be calculated by summing the diameter's of all the pores in a nominated weld length. For this project, the nominated weld length is 76 mm and is taken around the lowest quality portion of the entire weld length.

2.5.1.1 AWS D17.1: 2001

AWS D17.1:2001, '*Specification for Fusion Welding for Aerospace Applications*' by the American Welding Society, is an American National Standard which specifies, among other things, the weld quality criteria for fusion welded aerospace hardware. The weld quality requirements are detailed for three different quality classes; Class A, Class B and Class C. Table 2-3, Table 2-4 and Table 2-5 detail acceptance limits, for all three classes, relating to discoloration, weld profile and weld metal porosity respectively. Lack of fusion or cracks in the weld metal are not permitted for any class. For undercut and concavity at the weld face or root, the defect listed is the maximum size of an individual defect allowed. Allowable limits for defects running the full length of the weld are 0.05 mm for undercut and 0.13 mm for concavity (both to Class A). Also stated in AWS D17.1, but not in Table 2-4, are criteria relating to the weld profile for certain joint geometries, such as fillet and butt joint configurations. The porosity requirements in Table 2-5 indicate the minimum spacing between individual pores. If this limit is exceeded, the diameters of the pores are summed.

Table 2-3. Acceptance limits relating to discoloration for Class A, Class B and Class C weld qualities, as specified in AWS D17.1:2001.

Class	**Level of discoloration**										
	Bright silver	Silver	Light straw	Dark straw	Bronze	Brown	Violet	Green	Blue	Gray	White
A	Accept	Accept, remove discoloration before further welding					Reject			Reject unless proven embrittlement has not occurred	
B	Accept	Accept, remove discoloration before further welding						Reject if further welding required		Reject unless proven embrittlement has not occurred	
C	Accept	Accept, remove discoloration before further welding						Reject if further welding required		Reject unless proven embrittlement has not occurred	

Table 2-4. Acceptance limits relating to weld profile for Class A, Class B and Class C weld qualities, as specified in AWS D17.1:2001.

Imperfection	**Acceptance limit**		
	Class A	Class B	Class C
Face undercut (Ca)†	0.07 T or 0.76 mm, whichever is less	0.10 T or 1.27 mm, whichever is less	0.20 T or 1.78 mm, whichever is less
Root undercut (ca)†	0.07 T or 0.76 mm, whichever is less	0.10 T or 1.27 mm, whichever is less	0.20 T or 1.78 mm, whichever is less
Face concavity (Cr)††	0.07 T or 0.76 mm, whichever is less	0.07 T or 0.76 mm, whichever is less	0.07 T or 0.76 mm, whichever is less
Root concavity (cr)††	0.07 T or 0.76 mm, whichever is less	0.07 T or 0.76 mm, whichever is less	0.07 T or 0.76 mm, whichever is less
Excess weld metal (R)	0.33 T or 0.76 mm, whichever is greater	No stated requirement	No stated requirement
Excess penetration (r)	0.33 T or 0.76 mm, whichever is greater	No stated requirement	No stated requirement
Face weld width (L)	No stated requirement	No stated requirement	No stated requirement
Root weld width (l)	No stated requirement	No stated requirement	No stated requirement
Minimum weld width (I_0)	No stated requirement	No stated requirement	No stated requirement

†individual defect, maximum for a defect running the entire weld length is 0.05mm (Class A)
†† individual defect, maximum for a defect running the entire weld length is 0.13mm (Class A)

Table 2-5. Acceptance limits relating to subsurface weld metal porosity for Class A, Class B and Class C weld qualities, as specified in AWS D17.1:2001.

Imperfection	**Acceptance limit**		
	Class A	Class B	Class C
Maximum dimension or diameter of an isolated pore	0.33 T or 1.5 mm, whichever is less	0.50 T or 2.3 mm, whichever is less	No stated requirement
Cumulative length of porosity per 76 mm weld length	1.33 T or 6.0 mm, whichever is less	2.0 T or 9.0 mm, whichever is less	No stated requirement
Minimum spacing between two pores	4 x size of larger adjacent pore	2 x size of larger adjacent pore	No stated requirement

2.5.1.2 Company Specific Standards

An example of a typical company specific standard, which has been adapted from Hilton et al [2007], is detailed in Table 2-6 and Table 2-7. In comparison with Class A of AWS D17.1, the acceptance limits relating to defects in the weld profile are similar. However, additional criteria relating to the width of the weld at the face, root and its minimum dimension, are also stated in the company specific criteria. This is most likely a consequence of the standard being derived from experience with electron beam welding [Hilton et al, 2007]. No criteria regarding the discoloration of the weld metal was reported, although it is expected that only bright silver welds (i.e. no discoloration) would be acceptable [Hilton, 2007].

In terms of weld metal porosity, the company specific criteria is several times more stringent than AWS D17.1. This is true for the maximum pore dimension, the maximum accumulated length, and the minimum spacing between adjacent pores. Although no criteria have been listed regarding cracks or lack of fusion in the welded joint, neither are believed permitted in the company specific standards [Hilton, 2007].

Table 2-6. Acceptance limits relating to weld profile for a typical company specific aeroengine. Adapted from Hilton et al [2007].

Defect type	Acceptance limit
Face undercut (Ca), mm	≤0.05 T
Root undercut (ca), mm	≤0.05 T
Face concavity (Cr), mm	≤0.1 T, Max. 0.5
Root concavity (cr), mm	≤0.1T, Max. 0.5
Excess weld metal (R), mm	≤0.2+0.15 T
Excess penetration (r), mm	≤0.2+0.15 T
Face weld width (L), mm	≤2.2+0.7 T
Root weld width (l), mm	0.3 T, Max. 2.0 ≤ I ≤ 2.2 + 0.7 T
Minimum weld width (I_0), mm	0.3 T, Max. 2.0 ≤ I ≤ 2+0.1 T

Table 2-7. Acceptance limits relating to weld metal porosity for a typical company specific aeroengine. Adapted from Hilton et al [2007].

Defect type	Acceptance limit
Maximum dimension or diameter of an isolated pore	0.3 T, Max 1.5
Cumulative length of pores per 76mm weld length	0.2 + 0.5 T
Minimum spacing between two pores	10 times the dimension of the largest imperfection

2.6 Advances in Solid-State Laser Technology

In recent years significant development has taken place in solid-state laser sources. This is a result of the poor beam quality available from diode or lamp pumped Nd:YAG rod lasers, when compared with CO_2 laser sources. It was initially thought that the pumping of the Nd:YAG rods would be homogeneous and the rods would have no temperature dependent properties [Koechner, 1970]. However, in reality the pumping is parabolic and the thermal conductivity variation with temperature in the rod led to a temperature dependence on the rod radius [Xiang, 2009]. Primarily, the beam quality is limited by the poor cooling in the rods which results in thermal lensing and birefringence [Vollertsen, 2009]. This led to the development of the fibre and the thin disc laser, both making use of large aspect ratios to increase surface area and reduce thermal effects in the active medium.

High power disc laser sources ordinarily utilise a thin disc, of approximately 100-200 μm in thickness and several millimetres in diameter, of ytterbium doped yttrium-aluminium-garnet (Yb:YAG). Hosts doped with ytterbium, thulium and neodymium can also be utilised as active mediums [Hügel and Bohn, 1998]. A highly reflective coating (for the lasing wavelength and the wavelength of the diode pumps) is applied to the rear of the disc to act as a mirror in the laser cavity. An antireflective coating (for the lasing wavelength and the wavelength of the diode pumps) is applied to the front of the thin disc. The rear of the disc is soldered, with an indium-based or gold-tin solder, to a water impingement cooled heat sink [Giesen, 2005]. Despite the thinness of the disc laser source, which limits absorption of the light from the pump diodes, overall efficiency is much higher than Nd:YAG rod laser sources [Vollertsen, 2009]. This is, in part, achieved by a set of mirrors parabolically orientated around the thin disc to achieve ~90% absorption of the pump power by the disc. The high surface area cooled by the heat sink when compared with the disc's volume, results in temperature gradients which are only co-axial with to the central axis of the disc. Giesen [2005] reported that the radial temperature gradients are only very slight. As a result, the thermal lensing and birefringence effects observed in Nd:YAG rod laser sources are significantly reduced, and the beam quality from disc laser sources can be less than 8 mm.mrad for 16 kW laser sources [Trumpf, 2010a].

The first fibre laser was proposed by Snitzer [1961a], who subsequently demonstrated the lasing action of a neodymium-doped glass fibre [Snitzer, 1961b]. However, it was not until the development of the erbium-doped fibre amplifier [Mears et al, 1987] that the foundations for the high-power fibre lasers now used for materials processing were laid. A detailed review of the current state of fibre laser technology is out of the scope of this literature review. However, Canning [2005] gives a good review of this area and should be referred to as a source of further information. Briefly, modern high-power fibre laser sources, utilise an optical fibre, typically 10-50 μm in diameter and several metres long, doped with ytterbium as the active medium. Similarly to thin disc laser sources, they are pumped with semiconductor laser diodes, which provide the high pump powers required. The light emitted from the diodes is focussed into the active medium using a double-clad fibre to achieve high absorption. Consequently, only a small proportion of the pump energy supplied is converted into heat, which limits thermal degradation of beam quality [Platonov et al, 2002]. The fibres are coiled to: (i) reduce the footprint of the laser source, and (ii) maintain beam quality [Clarkson et al, 2003].

State-of-the-art solid state lasers utilising either thin disc or fibre technology are now available with output powers of multiple kilowatts; 50 kW average power Yb-fibre laser

sources [IPG Photonics, 2010] and 16 kW average power Yb:YAG disc laser sources [Trumpf, 2010a] are now available. Optical fibre core diameters used for the delivery of the laser beam are ordinarily greater than 50 μm in diameter, although core diameters of ~15 μm are used for single mode laser sources. The beam qualities of these laser sources are typically around 0.33 – 10 mm.mrad, depending on the output power. As a result, the light emitted from Yb:YAG disc and Yb-fibre laser sources can be focussed into smaller focal spot sizes, and hence higher power densities, than Nd:YAG rod lasers, whilst maintaining an acceptable stand-off distance and depth-of-focus (as detailed in Sub-section 2.2.1).

In comparison with Nd:YAG rod laser sources, the welding performance (in terms of depth of penetration and melting efficiency) possible with these multi-kilowatt, high beam-quality, Yb:YAG disc and Yb-fibre laser sources has been studied by numerous researchers (for example; Verhaeghe and Hilton, 2005; Weberpals et al, 2005; Verhaeghe and Dance, 2008). Verhaeghe and Hilton [2005] compared the welding performance of laser beams with different beam qualities, whilst maintaining a constant laser power and focal spot diameter of 4.0 kW and 400 μm respectively. It was noted that the welding performance, when performing melt runs on a 5000 series aluminium alloy and C-Mn steel, could be increased by utilising a higher beam quality laser beam. However, at laser powers exceeding 4 kW both Verhaeghe and Hilton [2005] and Weberpals et al [2005] reported that there exists an optimum spot diameter, below which the increase in penetration depth resulting from a smaller spot diameter is negligible.

Verhaeghe and Hilton [2005] introduced the concept of beam brightness. This term is defined as the power density in the focussed spot per solid angle in the cone of the focussed beam, as detailed in Equation 2-13.

$$Brightness = \frac{4PF^2}{\pi^2 w^2 (2R)^2} \tag{2-13}$$

where P is the power density at the workpiece, F is the focal length of the focussing lens, and R is the radius of the laser beam at the focussing lens

According to the above equation, a large focussing length in combination with a small beam width and small laser beam aperture (i.e. small angle of convergence) results in a high brightness laser beam. In the research performed by Verhaeghe and Hilton [2005] laser beams within the brightness range 0.3-5.5 $MWmm^{-1}.sr^{-1}$ were evaluated at a constant power and focussed spot diameters from 0.14 to 0.61 mm. It was demonstrated that when welding either aluminium or steel there existed an optimum laser beam brightness for maximising the depth of penetration. Nevertheless, the advances made in solid-state laser technology have

led to welds which can be produced with an exceptionally high aspect ratio. Verhaeghe and Dance [2008] reported that the high quality beams from Yb-fibre and Yb:YAG laser sources are now capable of producing welds with an aspect ratio which only previously could have been produced with in-vacuum electron beam welding.

2.7 Summary

Two Sections in this chapter reviewed the laser weldability of titanium alloys and the weld quality criteria relating to laser welded titanium alloys for aerospace applications. As stated earlier, of particular concern when utilising titanium alloys for high performance aerospace applications is embrittlement of the weld bead, and the formation of cracks, porosity and geometrical defects in the weld. This is evidenced by the low tolerance to these defects in the two weld quality standards compared previously, particularly in the company specific standard. However, contamination cracks in the weld metal may be prevented if stringent workpiece preparation and inert gas shielding procedures are adopted. Furthermore, other crack formation mechanisms are not of particular concern when welding titanium alloys. Correct workpiece preparation and inert gas shielding procedures should also prevent embrittlement of the weld metal, another criterion stipulated in both AWS D17.1 and the company specific weld quality criteria. The severity of geometrical defects in the weld profile can be reduced by adjusting process parameters, whilst not compromising other joint characteristics (for example, penetration and heat input). Nevertheless, if the process parameters cannot be adjusted to produce an acceptable weld profile, filler material, an over-sized joint thickness (followed by subsequent machining), or a cosmetic pass can be utilised to eliminate remaining geometrical defects in the weld profile.

The formation of porosity in the weld metal as a result of hydrogen rejection during solidification may also be reduced by adopting stringent workpiece preparation and inert gas shielding procedures. However, porosity in the weld metal is still known to occur when keyhole laser welding, from what was referred to in Section 2.4 as processing porosity. As will be discussed in the proceeding chapter, this is a consequence of keyhole instabilities (i.e. the forces maintaining the vapour cavity are not in equilibrium with those trying to close it).

Chapter 3

Literature Review; Part II: Keyhole Behaviour, and the Formation and Prevention of Porosity

3.1 Introduction

The second part of the literature review intends to establish the mechanisms by which porosity forms in the weld metal. This can only be achieved by first discussing the forces which act on the keyhole and determine its stability. Section 3.2 details the forces for a simplified keyhole geometry, and Section 3.3 for realistic keyhole geometries. The potential origins of the porosity are then detailed, in terms of its gas content and the observed formation mechanisms of pores using an X-ray transmission high speed observation system. The attenuation of the incident laser radiation by a plasma or a plume is then detailed. Finally, methods of controlling the keyhole behaviour and reducing weld metal porosity are discussed, and the aim and objectives of this project are specified.

3.2 Keyhole Behaviour - Low Péclet Number

The Péclet number, P_e, is a ratio which compares the advection rate of a physical quantity to the diffusion rate of the quantity driven by an appropriate gradient. When utilising the Péclet number, P_e, in keyhole laser welding, the physical quantity examined is ordinarily heat and can be defined by the product of the Reynolds number, R_e, and the Prandtl number, P_r, as detailed in Equation 3-1 [Steen 1998, p.191].

$$P_e = \frac{VR_k}{2k_d} \tag{3-1}$$

where V is the welding speed, R_k is the keyhole radius, and k_d is the thermal diffusivity.

For stationary keyholes, or keyholes with a small Péclet number (i.e. moving through a substrate with a very low translational speed) the keyhole shape can be approximated to a simple cylinder or truncated cone which is rotationally symmetric around the propagation direction of the incident laser beam. This is a result of heat conduction being the dominant method of heat transfer and consequently the isotherms are considered to have rotational symmetry around the central axis of the laser radiation, as indicated in Figure 3-1 [Dowden et al, 1987].

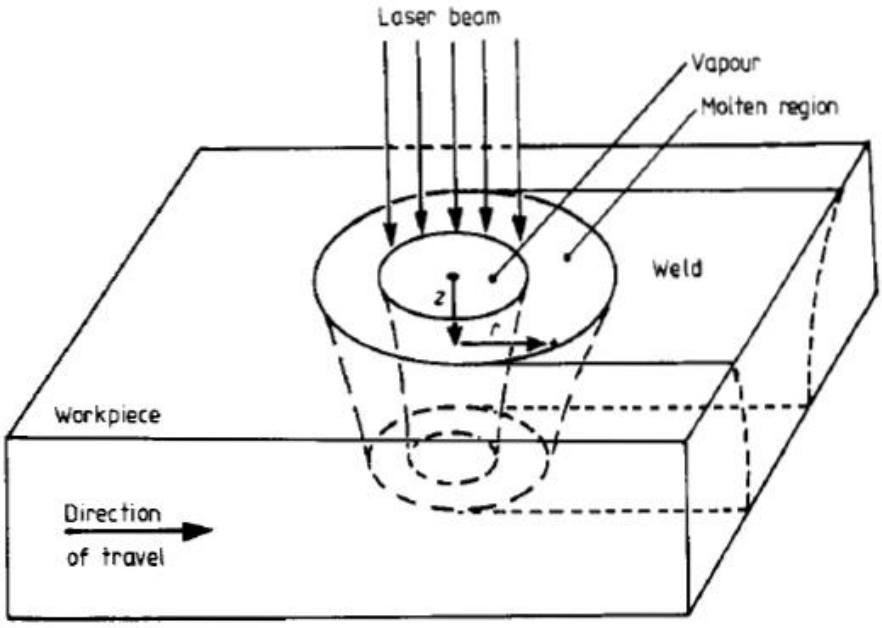

Figure 3-1. Keyhole with rotational symmetry and concentric to the central axis of the incident laser radiation [Dowden et al, 1987].

As discussed in Section 2.2, a high intensity focussed laser beam (~10^4 Wmm^{-2}) impinged on the surface of a metallic substrate will result in melting and vaporisation of the substrate,

and, subsequently, the formation of a vapour cavity. The vapour cavity will be surrounded by a sheath of molten metal. It is the forces which act on the molten sheath which will determine the stability of the vapour cavity, or keyhole. Equation 3-2 [Kroos et al, 1993; Klein et al, 1994] details the forces acting on the keyhole wall.

$$p_{abl} + p_v = p_g + p_h + p_\gamma \tag{3-2}$$

where p_{abl} is the ablation pressure, p_v is the vapour pressure, p_g is the hydrostatic pressure, p_h is the hydrodynamic pressure, and p_γ is the surface tension.

The keyhole is maintained by the ablation pressure, which is generated as molten material is vaporised from the inner surface of the keyhole, and the vapour pressure filling the keyhole. Restoring forces acting to close the keyhole are the surface tension of the molten material, the hydrostatic pressure, and the hydrodynamic pressure acting to transport molten material around the keyhole. Numerous theoretical models of the keyhole have been produced to determine the magnitude of the forces acting upon the keyhole using the geometry detailed in Figure 3-1 (for example; Dowden et al, 1987; Kroos et al, 1993; Klein et al, 1994). The ablation pressure, p_{abl}, caused by the vaporisation of molten metal on the inner surface of the keyhole wall due to absorption of the incident laser radiation, can be calculated from Equation 3-3 [Kroos et al, 1993].

$$p_{abl} = m_g n_g u_g{}^2 \tag{3-3}$$

where m_g is the mass of the particles, n_g is the density of the particles, and u_g is the velocity of the particles.

The values of density and velocity of the particles should be taken from where the Knudsen layer; a layer, several free mean path lengths (average length moved by a particle in between successive collisions which would change its direction or energy) thick, where the matter is between the liquidus and gaseous phases. The other force maintaining the keyhole is the vapour pressure, p_v, which is due to the flow of vaporised metal exiting the keyhole and can be calculated from Equation 3-4 [Klein et al, 1994]. A typical value of the ablation pressure generated when keyhole laser welding iron is $\sim 10^4$ Nm^{-2}, whereas the vapour pressure in the keyhole is $\sim$50 Nm^{-2} [Duley, 1999, p.84]

$$p_v = \left(\frac{1}{3}\right) m_g n_g u_g{}^2 \left(\frac{d}{R_k}\right)^2 \tag{3-4}$$

where d is the thickness of the workpiece.

Expressions for the forces acting to close the keyhole, specifically the surface tension, the hydrostatic pressure and the hydrodynamic pressure, have also been determined. The hydrodynamic pressure due to the flow of molten metal around the keyhole was determined by Kroos et al [1993], based on earlier work by Dowden et al [1983], to be particularly small (10 Nm^{-2}) when dealing with keyholes which have a low Péclet number. It can be calculated from Equation 3-5 [Kroos et al. 1993].

$$p_v - p_b = -\left(\frac{\rho_m}{2}\right) V^2 \left[\left(\frac{8}{R_e}\right) R_{km} \cos\Theta\right] \tag{3-5}$$

where p_b is a constant dependent upon the boundary condition between the melt-pool and the solid substrate, p_m is the density of the molten metal, R_{km} is a function of the keyhole radius and the surrounding melt pool radius, and Θ is the polar angle defined from the direction of the welding speed.

The hydrostatic pressure, at a depth z, can be determined from Equation 3-6 [Kroos et al, 1993].

$$p_g = \rho_m g z \tag{3-6}$$

where g is the gravitational acceleration constant.

Similarly to the hydrodynamic pressure, the maximum force acting to close the keyhole due to hydrostatic forces is very low compared with the ablation pressure. However, it is a function of the workpiece thickness and hence will become more important for thicker section workpieces. Conversely, the force acting to close the keyhole as a result of the surface tension is particularly large ($\sim 10^4$ Nm^{-2}) in comparison with the other restoring forces, and can be calculated from Equation 3-7 [Klein et al, 1994].

$$p_\gamma = \gamma\left[\left(\frac{1}{R_1}\right) + \left(\frac{1}{R_2}\right)\right] \tag{3-7}$$

where γ is the surface tension coefficient of the molten material and R_1 and R_2 are the Radii of curvature of the keyhole (where $R_1 = R$ and $R_2 = 0$ for a cylinder).

From comparison of the forces acting upon the keyhole, for keyholes with a low Péclet number the forces of most interest are the ablation pressure and the surface tension. If these forces are not in equilibrium the keyhole will either be expanding (i.e. $P_{abl} \gg p_\gamma$) or shrinking (i.e. $p_\gamma \gg p_{abl}$).

3.3 Keyhole Behaviour - High Péclet Number

The assumptions made in Section 3.2 only allow simplistic keyhole geometries to be considered (as shown graphically in Figure 3-1). However, these assumptions cannot be made for keyholes with higher translational speeds, such as those commonly utilised in industrial environments. Specifically, these assumptions relate to the geometry of the keyhole, the absorption mechanisms of the incident laser radiation, and the hydrodynamic forces present in the melt pool.

3.3.1 Keyhole Geometry

In Section 3.2, the keyhole was simplified to the geometry of a truncated cone. For keyholes with a low Péclet number this is an acceptable approximation, since the dominant transfer mechanism of thermal energy is conduction. Consequently the isotherms were assumed to have rotational symmetry in the direction of the laser beam propagation into the workpiece (as indicated in Figure 2-1). However, for keyholes with a high Péclet number, thermal energy will also be convected from the front keyhole wall (FKW) to the rear keyhole wall (RKW) by the transportation of vaporised metal, which would be expected to produce asymmetric isotherms. Arata et al [1985] utilised a CO_2 laser to produce a moving keyhole in soda-lime glass, allowing the behaviour of the vapour cavity to be easily observed from the side with a high speed camera. The observations have shown that the keyhole does not have rotational symmetry around the direction of laser beam propagation into the workpiece. As graphically detailed in Figure 3-2 [Arata et al, 1985], the FKW is inclined away from its translation direction and the variation in the keyhole width dimension (as viewed from the side) from the upper portion to the lower portion of the keyhole is not a simple linear relationship.

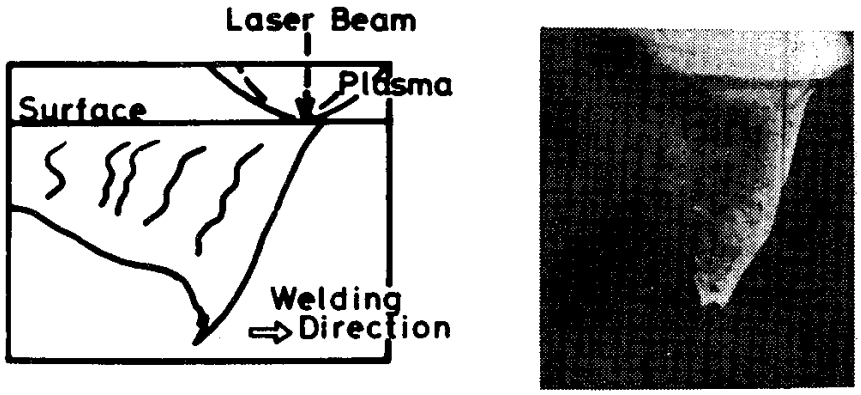

Figure 3-2. Side view of keyhole laser welding of soda-lime glass, with a 15 kW CO_2 laser [Arata et al, 1985].

It was observed that this inclination angle has a strong relationship with the translation speed, and at increasing translation speeds the inclination of the FKW will increase [Arata et al, 1985]. Experimental research [Semak et al, 1995] has shown that for translation speeds exceeding 50 mms^{-1} and laser powers above several kilowatts, the rear portion of the keyhole may not be exposed to the incident laser radiation (at least not before any reflections as a result of Fresnel absorption), which further contravenes the assumptions made at low Péclet numbers. The inclination of the FKW is likely a consequence of two possible reasons, specifically [Matsunawa and Semak, 1997]:

1. Deformation of the isotherms as a result of the incident laser radiation's movement across the workpiece.
2. The keyhole formation time exceeding the interaction time (incident beam diameter/translation speed), causing the keyhole to be in a state of permanent growth.

The keyhole formation time is the duration for a stationary keyhole to become fully penetrating (or partially penetrating at a desired depth). If this time is greater than the incident laser beam diameter divided by the translation velocity, then the keyhole will remain in a state of permanent growth [Matsunawa and Semak, 1997]. Effectively, it will have a drilling velocity perpendicular to the FKW.

As a result of the FKW inclination, no direct optical path may exist between the incident electromagnetic radiation and the lower portions of the keyhole. However, absorption may still occur in the lower portion as a result of multiple reflections, which is discussed in Sub-section 3.3.2.1. It is therefore reasonable to assume that the mechanism by which the electromagnetic radiation is absorbed may have an effect on the keyhole geometry. Furthermore, it was assumed that the forces relating to the hydrodynamic behaviour of the melt flow would be small in comparison with the ablation pressure and the surface tension forces. However, this restricts the melt flow velocities to below the beam translation velocity. For keyholes with a high Péclet number the hydrodynamic behaviour of the melt pool and the resultant forces on the keyhole need to be considered.

3.3.2 Absorption Mechanism(s)

In Section 3.2 the absorption mechanism of the incident laser radiation was not considered. It was assumed that the incident radiation was approximately absorbed through the depth of the keyhole in a uniform manner, producing an almost constant ablation pressure in the keyhole. However, when keyhole laser welding with high translation speeds, it has been

demonstrated [Arata et al, 1985] that the keyhole shape is not rotationally symmetric. Furthermore, the centre line is not straight, since the keyhole is inclined in a direction opposite the translation direction. Consequently, the uniform absorption assumed previously is invalid since the walls of the keyhole cannot all be directly irradiated by the incident laser beam.

The mechanism(s) by which the incident laser radiation is absorbed should be considered, since the subsequent heat transfer and keyhole geometry will be influenced by these physical processes. The specific absorption mechanisms occurring are dependent upon the wavelength of the incident radiation and the chemical composition of the substrate. For metallic substrates, Fresnel absorption (i.e. absorption at the keyhole walls) and/or inverse Bremsstrahlung absorption (i.e. absorption by free-free electrons in the metal vapour) will be the dominating mechanism(s).

3.3.2.1 Fresnel Absorption

Fresnel absorption refers to the partial absorption and partial reflection of light incident on an opaque surface. The energy absorbed at the keyhole walls results in ablation of the molten material. Portions of the absorbed energy are also conducted away to maintain the molten sheath and trailing melt pool, with a small amount subsequently diffusing into the solid workpiece. Equation 3-8 can be utilised to calculate the absorption coefficient for parallel polarised light incident on metals, if it is assumed that the light beam couples to the metal electron gas which will absorb a portion of the beam as a result of Joule heating [Stratton 1941, p.125].

$$A = 1 - \frac{2cos^2\emptyset - 2\varepsilon cos\,\emptyset + \varepsilon^2}{2cos^2\emptyset + 2\varepsilon cos\,\emptyset + \varepsilon^2} \tag{3-8}$$

where $\emptyset$ is the angle of incidence and ε is a value relating to the material properties and the wavelength of the incident laser radiation.

The above equation is highly dependent upon the angle of incidence, whereby the absorption at a glancing angle of incidence is an order of magnitude larger than at a normal angle of incidence for a CO_2 laser and a typical metal [Schulz et al, 1986]. The energy which is not absorbed is reflected and may consequently be [Kaplan 2009, p. 71];

(i) partly absorbed and reflected at another point in the keyhole;

(ii) reflected from out the top of the keyhole; or,

(iii) transmitted through the keyhole (applicable for full penetration welding only).

From the above, it is apparent that Fresnel absorption of the incident laser light may lead to multiple reflections inside the keyhole with small changes in the angle of incidence leading to non-uniform absorption at the front of the keyhole. The portion of energy absorbed is highly dependent upon the angle of incidence the radiation makes with the opaque surface. Consequently, a detailed knowledge of the keyhole wall geometry is required so that theoretical models can be established to determine the initial absorption and all subsequent absorptions as a result of multiple reflections. Knowing these, an understanding of keyhole geometry and behaviour can be established.

3.3.2.2 Inverse Bremsstrahlung Absorption

Inverse Bremsstrahlung absorption, or free-free absorption, is the absorption of a photon by a free electron in the proximity of an ion (i.e. the ionised gas inside the keyhole either absorbs the incident laser radiation directly, or as it is reflected through the keyhole). A portion of the energy absorbed by the vapour will then be thermally conducted to the keyhole walls providing energy for melting and vaporisation of the metallic workpiece, with the remaining portion being re-radiated in the vapour [Dowden 2009, p. 97].

Inverse Bremsstrahlung absorption can only occur if the vapour inside the keyhole is ionised, thereby having a mechanism for the presence of free electrons. Numerous spectroscopic studies have been performed to determine the species present in the keyhole vapour and its temperature (for example; Tu et al, 2003). The majority of these have been performed for CO_2 laser welding of ferrous metals, for reasons which will be discussed later.

If the following assumptions are made:

1. The metallic vapour observed is optically thin (i.e. no self absorption occurs within the plasma, allowing the analysis to be simplified).
2. Local thermodynamic equilibrium (LTE) is assumed (i.e. all particles have a Maxwellian velocity distribution, and that collisional processes dominate the rate equations such that Boltzmann Statistics apply).

The electron temperature in the metallic vapour can be determined by comparing the relative intensities of two or more emission lines from the same state by utilising the 'Boltzmann plot' method.

The spectral intensity, I_{nm}, of individual optical emission lines associated with a transition from the upper state, n, to the lower state, m, can be calculated by (Griem, 1997),

$$\boldsymbol{I_{nm} = N_n A_{nm} h v_{nm}} \tag{3-9}$$

where N_n is the population density in the n state, A_{nm} is the atomic transition probability between the states n and m, and hv_{nm} is the energy of the emitted photon.

The population of the excited state, N_n, can be found from the Boltzmann distribution,

$$N_n = N\left(\frac{g_n}{Z(T_e)}\right) exp^{(-eE_n|k_bT_e)} \tag{3-10}$$

where $Z(T_e)$ is the partition function, N the total density of the state, k_b the Boltzmann constant, g_n the degeneracy of state n, and E_n the energy level of state n.

Combining the two previous equations yields,

$$ln\left(\frac{I_{nm}\,\lambda_{nm}}{A_{nm}\,g_n}\right) = ln\left(\frac{Nhc}{Z(T_e)}\right) - \left(\frac{eE_n}{k_bT_e}\right) \tag{3-11}$$

where λ_{nm} is the wavelength of the studied spectral line, h is Planck's constant, and c is the speed of light (~3x10^8 ms^{-1}).

The Boltzmann plot technique can then be utilised, plot $ln\left(\frac{I_{nm}\,\lambda_{nm}}{A_{nm}\,g_n}\right)$ against E_n, for at least two emission lines. The gradient of the resultant line is equal to $^{-1}/_{k_bT_e}$ and thus the electron temperature can be determined. The difference between the upper state energy levels of the chosen spectral emission lines (i.e. E_n and E_l for wavelengths λ_{lk} and λ_{nm}) must be greater than the sum of the Boltzmann constant and the calculated electron temperature. This ensures that lines belonging to the same multiplet are not chosen. The Saha equation can be utilised to determine the relationship between the electron, ion and neutral number densities in the gas. If the gas is assumed to be quasi-neutral (i.e. $N_e = N_i$) and the perfect gas law is utilised (i.e. $P_0 = N_0 k_b T$) then the ionisation fraction, α, of the gas can be calculated using the equation below [Choudhuri, 1998].

$$\alpha^2 = \left(\frac{2g_i}{g_0}\right)\left[\left\{(2\pi m_e)^{3/2}\right\}P_0h^3\right](k_bT_e)^{5/2}exp^{\left(^{-eE_i}/_{k_bT_e}\right)} \tag{3-12}$$

The electron temperature can then be utilised to calculate the ionisation fraction of the metallic vapour and, with knowledge of the electron density, the inverse Bremsstrahlung absorption coefficient of the ionised vapour can be determined. The inverse Bremsstrahlung

absorption, α_{ib}, coefficient is the sum of the electron-neutral atom, α_{ea}, and the electron-ion, α_{ei}, absorption coefficients [Mitchener and Kruger 1973, p. 241].

$$\alpha_{ib} \approx \alpha_{ea} + \alpha_{ei} = \frac{{v_p}^2 v_{cf}}{c v^2} \tag{3-13}$$

where v_p is the plasma frequency, v_{cf} is the collision frequency between the different species, c is the speed of light, and v is the frequency of the incident light.

Sokolowski et al [1998] estimated that the vapour temperature in the keyhole when CO_2 keyhole laser welding steel would be in the range 9500 to 12000K, whereas the electron densities were in the range $1x10^{17}$ to $3.1x10^{18}$ cm^{-3}. For this range of temperatures the electron-neutral atom absorption coefficient is negligible compared to the electron-ion absorption coefficient and can therefore be neglected [Greses, 2003]. Consequently, the inverse Bremsstrahlung absorption coefficient can be calculated from Equation 3-10 if LTE is assumed.

$$\alpha_{ei} = \frac{4}{3}\left(\frac{2\pi}{3k_b T_e}\right)^{\frac{1}{2}}\left(\frac{n_e n_i Z^2 e^6}{h c {m_e}^{\frac{3}{2}} v^3}\right)(1 - exp^{(\frac{-hv}{k_b T_e})}) \tag{3-14}$$

3.3.2.3 Absorption of 1 and 10 µm Wavelength Laser Beams

Industrial laser sources utilised for thick section welding applications will almost certainly have a wavelength of either ~1 µm (such as Nd:YAG rod, Yb-fibre, Yb:YAG disc and diode laser sources) or ~10 µm (CO_2 laser sources). As discussed above, both the Fresnel and inverse Bremsstrahlung absorption coefficients are dependent upon the wavelength, and consequently 1 and 10 µm wavelength electromagnetic radiation will be absorbed differently.

For laser sources emitting light with a wavelength of ~1 µm the radiation is almost entirely absorbed by the Fresnel absorption mechanism. Some ionisation of the metallic vapour may occur, although the rise in temperature is not sufficient for large electron densities to be present [Dowden 2009, p. 97]. Hence, any inverse Bremsstrahlung absorption can be considered negligible. However, particularly high power densities are now available from modern solid-state lasers, single mode lasers delivered through a ~15 µm core diameter fibre optic cable are now available at powers exceeding 1 kW [IPG Photonics, 2010], and it remains unclear whether or not these laser sources are capable of producing a highly ionised plasma in the keyhole and what absorption effects this will have on the incident electromagnetic radiation.

For CO_2 laser sources the absorption of the incident electromagnetic radiation by the inverse Bremsstrahlung effect is greater, as evidenced in research by Tu et al [2003], and cannot be ignored. Tu et al [2003] determined the electron temperature and density at different heights in the keyhole when welding C-Mn steel with a CO_2 laser source. Higher temperatures and increased electron densities were found to be present at the top of the keyhole compared to the bottom, which led to an increased absorption of the laser beam in the top portion of the keyhole and, consequently, a nail shaped weld profile was observed indicating the non-uniform absorption. A typical inverse Bremsstrahlung absorption coefficient for 20 kW CO_2 keyhole laser welding of C-Mn steel at 45 mms^{-1} was calculated to be 6 - 7.5% at the top (0-3 mm) of the keyhole and 1.5 – 2% at the bottom (3-9 mm) of the keyhole [Tu et al, 2003].

Numerous models (for example; Kaplan, 1994; Solana and Negro, 1997; Fabbro and Chouf, 2000; Ki et al, 2002) have been developed to simulate the absorption of electromagnetic radiation by a keyhole and determine its influence on the keyhole geometry. Kaplan [1994] calculated the keyhole geometry by determining the energy balance at the keyhole, whilst considering both Fresnel and inverse Bremsstrahlung absorption of the laser beam. The calculated geometry of the keyhole, as shown in Figure 3-3 [Kaplan, 1994], resembles the geometry observed by Arata et al [1985] more closely than previous models.

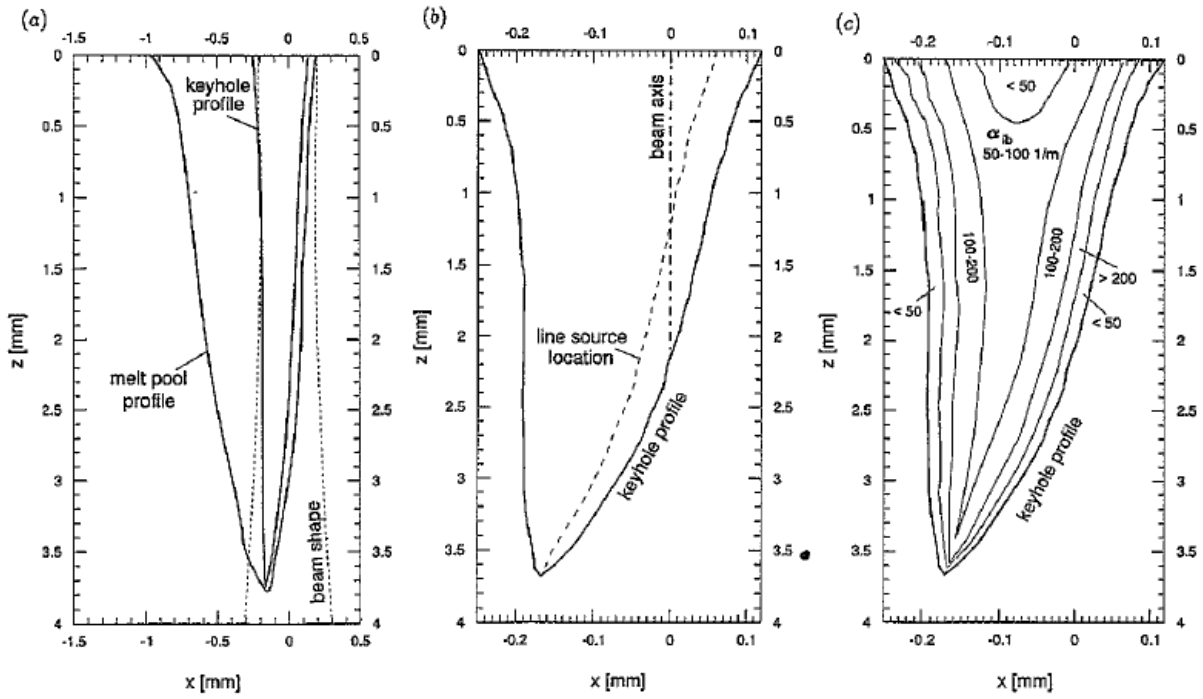

Figure 3-3. Geometry of beam, keyhole and melt pool for 4 kW CO_2 laser welding of steel at 50 mms^{-1} (a), magnified keyhole profile (b), and inverse Bremsstrahlung absorption coefficients in the keyhole [Kaplan, 1994].

Solana and Negro [1997] developed an axisymmetrical model of a keyhole which incorporated the potential for multiple reflections inside the keyhole, using a ray-tracing technique and assuming an initial conical shaped keyhole. The results allow the effects of utilising different beam profiles and different absorption mechanisms to be compared. A Gaussian beam profile was found to result in a deeper (~6%) and narrower keyhole than a uniform top-hat profile for a constant laser power. Perhaps more significantly, the inverse Bremsstrahlung absorption coefficient was adjusted from 0 – 300 m^{-1} (where 100 m^{-1} and 300 m^{-1} correspond to temperatures of approximately 9000 and 19000K respectively) and its effect on penetration modelled. The introduction of an inverse Bremsstrahlung absorption coefficient led to a decrease in penetration and increase in upper keyhole width, since a higher proportion of the energy was accumulated in the upper region of the keyhole. Increasing the coefficient further increased the width, agreeing with the later work performed by Tu et al [2003], of the upper keyhole and decreased the penetration depth.

A similar ray tracing method to that used by Solana and Negro [1997] was adopted by Fabbro and Chouf [2000] to study the keyhole geometry as a function of translation speed, incident intensity and sample material. The initial FKW inclination angle was calculated as a function of the beam translation velocity and a drilling velocity perpendicular to the inclination angle, based on previous work by Poueyo-Verwaerde et al [1994] and Fabbro et al [1997]. The ray tracing method was then utilised to determine the effect of multiple reflections on the keyhole geometry. It was determined that the FKW can be particularly stable, but it is perturbed by reflections from the RKW, whereas the RKW will be inherently unstable unless the incident laser intensity is adequate [Fabbro and Chouf, 2000]. The importance of correctly assuming the initial geometry of the keyhole was highlighted in theoretical research by Ki et al [2002], who determined that the multiple reflections are highly geometry dependent and that an incorrect preassumed keyhole geometry would lead to inadequate results.

Jin et al [2002] experimentally observed the keyhole produced when CO_2 laser welding of GG17 glass (a glass with a SiO_2 content of 80% and a softening point of 820°C), with a mathematical keyhole profile subsequently calculated by polynomial fitting. This calculated geometry allowed a model to be constructed which determined the laser intensities absorbed in different regions of the keyhole. Since GG17 glass is primarily constituted of SiO_2, which has very high ionisation energy, inverse Bremsstrahlung absorption was deemed negligible and only Fresnel absorption was considered [Jin et al, 2002]. It was established that the majority of energy was absorbed at the FKW by direct incidence. The RKW was found to have

no direct absorption of the incident laser beam and was maintained by the multiple reflections and convection of thermal energy by transported metal vapour.

Equation 3-8 indicated that the Fresnel absorption of light incident on an opaque surface could be calculated if the optical properties of the material, the angle of incidence and the wavelength of the incident laser radiation are known. However, Equation 3-8 is only valid for parallel polarised light and different equations must be utilised for other polarisations. Cho and Na [2007] indicated that the keyhole will consequently take on different geometries depending upon the light's polarisation. For laser sources which emit laser light with a random polarisation (such as multi-mode Yb-fibre lasers), calculation of the absorption coefficients for specific angles of incidence is further complicated, although Cho and Na [2007] suggested the keyhole would be similar in shape to one produced with a circularly polarised laser beam.

3.3.3 Melt pool Behaviour and Hydrodynamic Forces

In Section 3.2 it was assumed that the forces relating to the hydrodynamic behaviour of the melt flow around the keyhole would be small in comparison with the ablation pressure and the surface tension forces. For keyholes with a low Péclet number this assumption is reasonable since; (i) the laser energy is absorbed uniformly in the keyhole; and, (ii) the dominant heat transfer mechanism is conduction and the isotherms will be axisymmetric. Consequently, the flow of molten material around the keyhole has a low velocity and the trailing melt pool is similar, or identical, in size to the leading melt front. However, for keyholes with a high Péclet number the isotherms become elongated, as indicated in Figure 3-4 [Wang et al, 2006], and a trailing melt pool forms behind the keyhole.

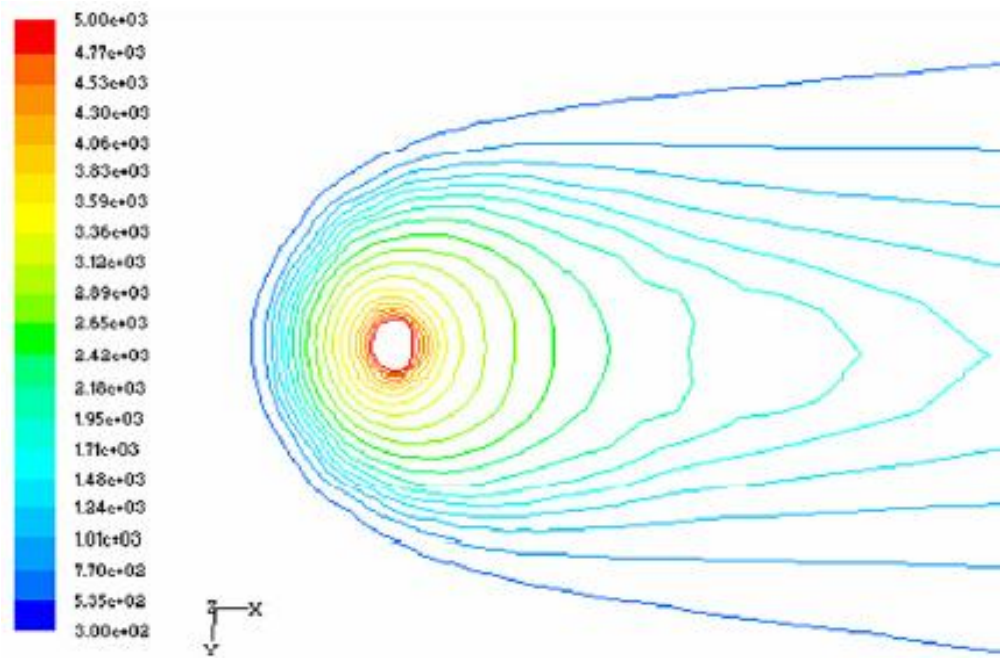

Figure 3-4. Numerical model, using the control volume method, of the induced isotherms at the top surface when welding Ti-6Al-4V with a Gaussian heat source [Wang et al, 2006].

The geometry of the melt pool, which is defined by the solid-liquid and liquid-vapour phase-change boundaries in the workpiece, is a result of the properties of the incident laser radiation, the conduction and convection of the absorbed thermal energy, and the motion of the workpiece relative to the incident laser beam. Observations of the melt pool behaviour (for example; Fabbro et al, 2006) have indicated that the fluid flow in the melt pool is particularly complex and it is driven by numerous mechanisms.

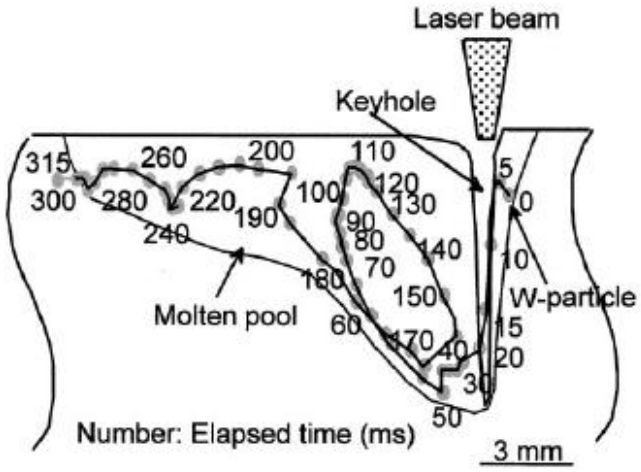

Figure 3-5. Fluid flow in melt pool, observed by the trajectory of a tungsten particle, when keyhole laser welding a 5000 series aluminium alloy with a CO_2 laser [Matsunawa et al, 1998].

Matsunawa et al [1998] observed the fluid flows during continuous-wave CO_2 keyhole laser welding of A5083 aluminium alloy, by sandwiching a tungsten particle between two sheets which were subsequently welded together. A high speed X-ray transmission observation method allowed the behaviour of the particle to be observed. The observed trajectory of the tungsten particles, shown in Figure 3-5 [Matsunawa et al, 1998], has revealed that eddy currents are established in the melt pool. Speeds of up to 350 mms^{-1} were observed in the eddy currents, which was considerably faster than the welding speed. Similar fluid flows were modelled in the melt pool by Geiger et al [2009], using a three dimensional, transient finite volume model of the keyhole laser welding process.

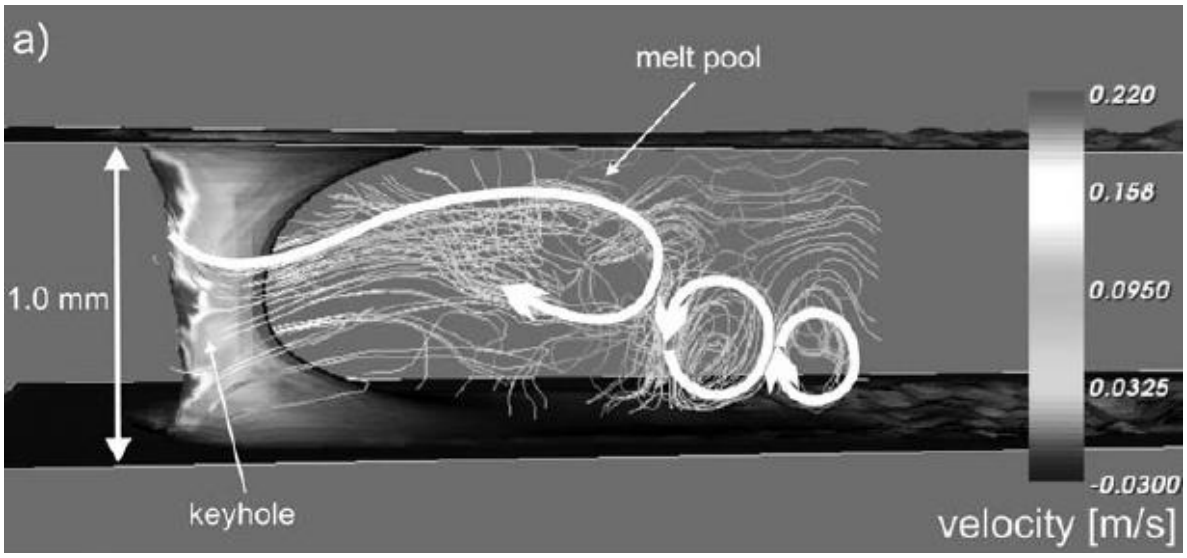

Figure 3-6. Modelled eddy currents in melt pool when welding 1 mm thickness steel with a 3.8 kW laser source, with a focussed spot diameter of 200 μm, and a welding speed of 100 mms^{-1} [Geiger et al, 2009].

As summarised by Fabbro et al [2004] and Kaplan [2009, p. 85] the specific mechanisms influencing the fluid flow are:

- Molten material driven around the keyhole by the ablation pressure at the front of the keyhole.
- Frictional fluid flow induced by the metal vapour ejected from the keyhole.
- Flow of molten material in the melt pool due to Marangoni convection (thermocapilliary flow).

It can be reasonably assumed that combination of a few of these forces will have a significant effect on the hydrodynamic behaviour of the melt pool, causing effects such as the eddy currents discussed above. In turn, these hydrodynamic behaviours may lead to; (i) the formation of geometrical defects in the weld seam; and/or (ii) a force on the keyhole which

introduces keyhole instabilities, and potentially keyhole collapse, leading to the inclusion of bubbles in the melt pool – which may not have sufficient time/buoyancy to escape and will become entrapped as porosity. Therefore, a comprehensive understanding of the melt pool hydrodynamics is necessary to produce defect free welds [Fabbro et al, 2004].

3.3.3.1 Keyhole Ablation Pressure Effects

It was discussed in Sub-section 3.3.2 that the majority of the incident laser radiation is absorbed at the FKW and the molten material is subsequently ablated which induces an ablative pressure, also referred to as a recoil pressure, on the molten material. Thermal conduction determines the rate at which this molten material is thrust towards the front of the keyhole. However, only a small proportion of the processed material is transported across the keyhole in the vapour phase, and the majority remaining is moved sideways around the keyhole in the liquid phase [Klemens, 1976]. This displacement of molten material is driven by the ablation pressure at the front of the keyhole.

Depending upon the thermal conductivity and the welding speed, the thickness of molten material on either side of the keyhole (transverse to the welding direction) may be small compared with the diameter of the keyhole. As a result, the velocity of the melt flow around the keyhole must be sufficiently high to ensure the conservation of mass law is not contravened [Semak et al, 1995]. For lower welding speeds the thickness of molten material on either side of the keyhole (transverse to the welding direction) increases and the velocity of the molten material decreases. A similar situation is found when welding materials with very high thermal conductivity and/or with a large temperature differential between their melting and boiling points [Kaplan 2009, p. 86].

Geiger et al [2009] modelled the keyhole and melt pool behaviour produced when welding 1 mm thickness steel with a 3.8 kW laser source, with a beam width of 200 μm, and a welding speed of 100 mms^{-1}. As is detailed in Figure 3-7 [Geiger et al, 2009], the velocity of the melt flowing around the keyhole (~200 mms^{-1}) was approximately twice that of the welding speed – even at this low welding speed. For higher welding speeds the velocity of the melt flow around the keyhole has been determined to be much greater [Lampa et al, 1998]. Kaplan [2009, p. 88] reported that accelerated molten metal flow towards the solidification front may result in undercut at the side of the weld and a peak in the centre.

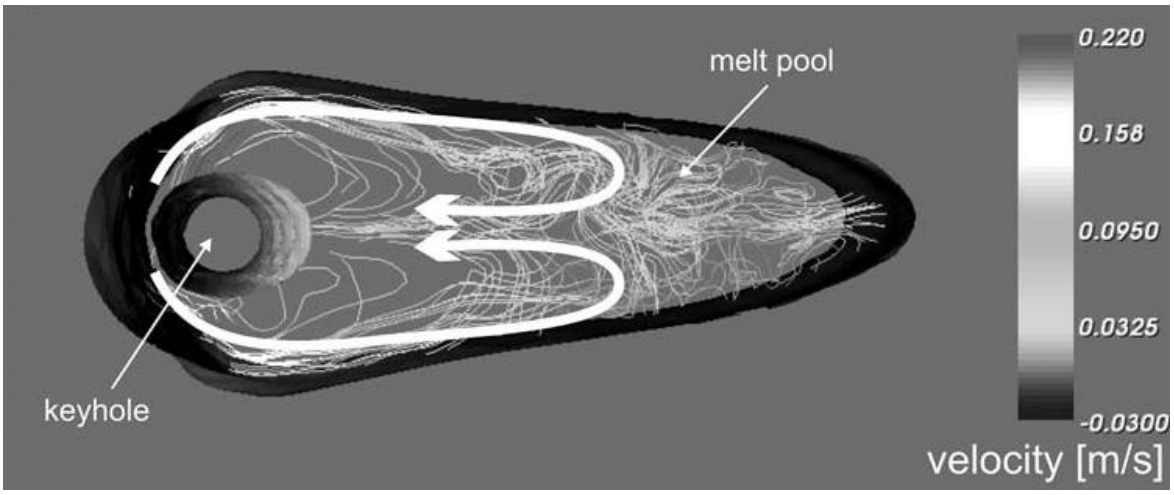

Figure 3-7. Surface melt pool velocities produced when welding 1 mm thickness steel with a 3.8 kW laser source, with a focussed spot diameter of 200 μm, and a welding speed of 100 mms^{-1} [Geiger et al, 2009].

3.3.3.2 Metallic Vapour Ejection Effects

In addition to driving the flow of molten material around the keyhole, the ablation of the front of the keyhole by the incident laser beam generates vapour inside the keyhole. Studies by Fabbro et al [2004; 2006] have reported that the ejection of the vapour from the keyhole can have a significant effect on the fluid dynamics in the melt pool.

Observation of the melt pool behaviour when Nd:YAG laser welding of C-Mn steel with a dual or treble focussed laser beam (i.e. two or three focussed spots) allowed the effects of the vapour friction effects to be observed at a welding speeds of ~ 10-80 mms^{-1} [Fabbro et al, 2004]. Swellings around the top of the keyhole were inferred to be a direct consequence of the vapour friction effects, which induced an upward melt flow. According to Semak and Matsunawa [1997] the friction of the gas flowing out of the keyhole may cause an upward force on the keyhole walls. The calculated induced upward melt flow velocity, which was contained in a boundary layer a few hundred microns thick, was similar to that from the induced from the sideways melt flow around the keyhole, and consequently cannot be ignored [Fabbro et al, 2004]. At these low welding speeds it was further reported by Fabbro et al [2006] that a bump was generated at the RKW (as indicated in Figure 3-8) which led to oscillations in the melt pool.

At increased welding velocities (100-150 mms^{-1}) the inclination of the FKW increases away from the beam translation direction and the absorbed energy at the front of the keyhole is expected to increase (as a result of the mechanisms discussed in Sub-sections 3.3.1 and 3.3.2). This leads to a significant increase in the amount of ablated material which impinges

on the keyhole wall, which has the effect of widening the top portion of the keyhole [Fabbro et al, 2006]. In further studies performed by Fabbro et al [2007] using identical equipment, it was noticed that in this range of speeds a periodic oscillation was induced in the melt pool by the vapour which led to spatter ejection from the rear of the keyhole. This vapour ejection induced effects on the keyhole and melt pool geometries at slow (15mms^{-1}) and moderate (85mms^{-1}) welding speeds are shown schematically in Figure 3-8 [Fabbro et al, 2006].

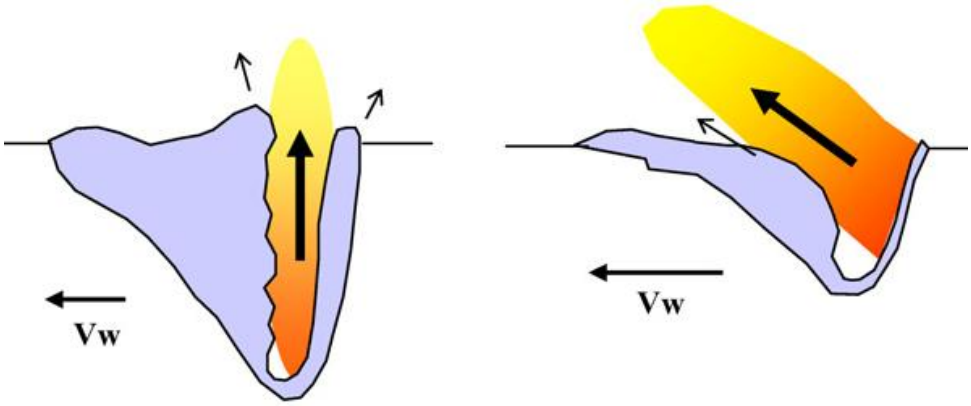

Figure 3-8. Schematic of the effect of the vapour ejection on the keyhole and melt pool geometries at welding speeds of (left) 15 mms^{-1} and (right) 100 mms^{-1} [Fabbro et al, 2006].

At moderate welding speeds the pressure exerted by the metallic vapour on the rear of the keyhole is sufficient to cause geometric defects in the weld profile, such as undercut [Kaplan 2009, p. 90]. Furthermore, If the welding speed is sufficiently high, it has been observed [Fabbro et al, 2007] that the pressure exerted on the rear of the keyhole is sufficient to cause humping of the weld bead [Fabbro et al, 2007].

3.3.3.3 Marangoni Convection Effects

Marangoni convection, which is also referred to as thermocapilliary flow, in the melt pool is generated by the presence of surface tension gradients. These surface tension gradients arise as a result of the surface tensions dependence on temperature and the large temperature differentials present in the melt pool; the melt temperature is near the solidification point at the liquid-solid phase boundaries, whereas the melt temperature is near the vaporisation temperature at the liquid-gas phase boundaries. For most metals the surface tension decreases as a function of temperature. As a result, surface tension gradients will exist from; (i) the melt surrounding the keyhole towards the solid-liquid interface; and, (ii) from the centre of the melt pool outwards to either the face or root of the weld [Fan et al, 2001]. The

molten metal flow will then be driven towards the areas of high surface tension at the solidification boundaries and at the face and root of the weld.

The presence of excessive concentrations of surface active elements, such as phosphorous and oxygen, can lead to lower surface tensions at the solidification boundaries and reverse the flow of molten material towards the centre of the weld. However, for titanium alloys which are rigorously cleaned before welding to remove surface contaminants and hydroxide layers, and shielded with inert gases during welding to prevent absorption of light elements, this is unlikely to be the case.

3.4 Origins of Weld Metal Porosity

3.4.1 Pore Gas Analysis

No research has been reported on the gas content of pores produced when keyhole laser welding titanium alloys. A small amount of research has been published on the specific gas content of the weld metal porosity formed when keyhole laser welding aluminum and magnesium alloys. A study [Kutsuna and Kurokawa, 2004] of the gas contents of pores from CO_2 keyhole laser welding of AZ361 and AZ61 magnesium alloys indicated that hydrogen was the major contributor, with a small fraction of argon (the shielding gas). A similar result was also reported by Kutsuna and Yan [1998] for pores produced in 5000 series aluminium alloys with a CO_2 laser. Hydrogen was the major constituent (77-87%) and the remaining gas was the shielding gas [Kutsuna and Yan, 1998].

The above research is perhaps confusing given the statements in the previous chapter regarding the formation of porosity due to hydrogen rejection during melt pool solidification. However, it would be expected that the formation of porosity in aluminium-magnesium alloys is significantly different from that in titanium alloys as a result of the large difference in melting and vaporisation temperatures between the aluminium and magnesium. Furthermore, the solubility of hydrogen in aluminium is significantly more conducive to the formation of hydrogen porosity than in titanium alloys [Kutsuna and Yan, 1998]. It is known from previous experience at TWI that with identical work preparation and inert gas shielding procedures, the porosity content in the weld metal can vary significantly depending upon the process parameters [Hilton, 2006]. Du et al [2003] came to a similar conclusion whilst investigating CO_2 keyhole laser welding of TC-1 titanium alloy.

Nevertheless, it can be inferred from the results presented by Kutsuna and Yan [1998] and Kutsuna and Kurokawa [2004] that it is possible for shielding gas to be entrapped in the weld

metal. Given the velocity of the metal vapour exiting the keyhole, at first consideration it is surprising that shielding gas may enter this particularly high pressure area. However, if the keyhole were to collapse, either as a combined result of the mechanisms discussed in Section 3.3 or as a result of the laser beam attenuation [which is discussed in Section 3.5) preventing/reducing ablation in the keyhole, then shielding gas may be drawn in.

3.4.2 Transient Behaviour of the Keyhole Laser Welding Process

It is apparent from the preceding Sections that the forces acting on the keyhole and the melt pool are particularly complex. Furthermore, the discussions in Sub-sections 3.3.1, 3.3.2 and 3.3.3 have only been considered for incident electromagnetic radiation with a constant power output. The introduction of a modulated power or a pulsed laser output would significantly alter the interaction between the keyhole and the melt pool, as would introducing other process parameters detailed in Table 2-1.

The mechanisms which induce the forces on the keyhole and melt pool are sufficiently intertwined that their interactions are very complex and it is hard to envisage a quasi steady-state process. Observations of the transient behaviour of the keyhole laser welding process using X-ray transmission methods have been performed by Matsunawa et al [1998], during CO_2 laser welding of A5083 in helium shielding. Figure 3-9 [Matsunawa et al, 1998] details one of the observations over a period of 90 ms. Despite the constant welding parameters the process exhibits particularly unsteady behaviour with fluctuations in penetration depth and the formation of porosity in the weld metal.

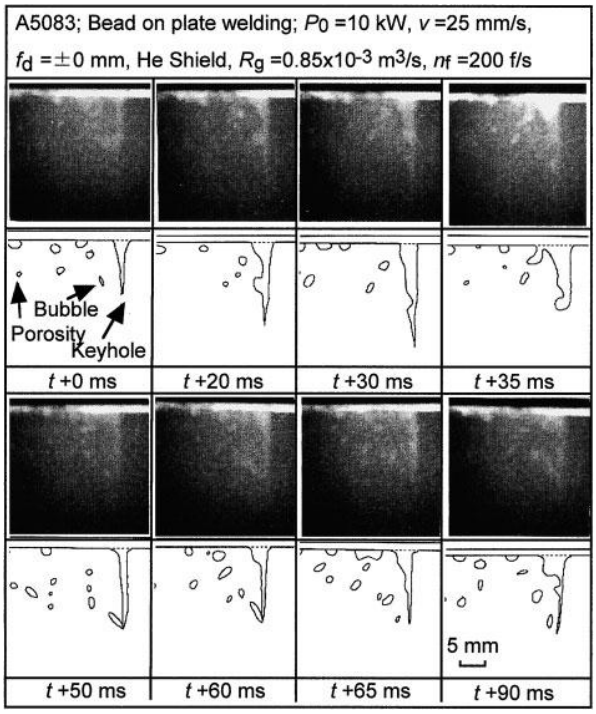

Figure 3-9. On-line X-ray measurements of porosity formation resulting from an unstable keyhole produced with a CO_2 laser in A5083 [Matsunawa et al, 1998]

The formation of porosity in Figure 3-9 [Matsunawa et al, 1998] is primarily observed in the lower half of the keyhole as a result of a non-steady keyhole geometry. In particular the depth of the keyhole and the geometry of the RKW are particularly dynamic. A change in the front keyhole wall inclination angle can be seen and a corresponding depression can be noted in the rear keyhole wall. These results have shown that the evaporation of the front keyhole wall occurs locally and not uniformly, as the rear keyhole wall depression is caused by the dynamic pressure exerted by the evaporated vapour jet [Matsunawa, 2001]. As the region of the front keyhole wall moves progressively down towards the keyhole tip because of the evaporation, the depression on the rear keyhole wall follows, until a bubble is formed at the keyhole tip, as can be seen in Figure 3-10 [Matsunawa et al, 2003] below.

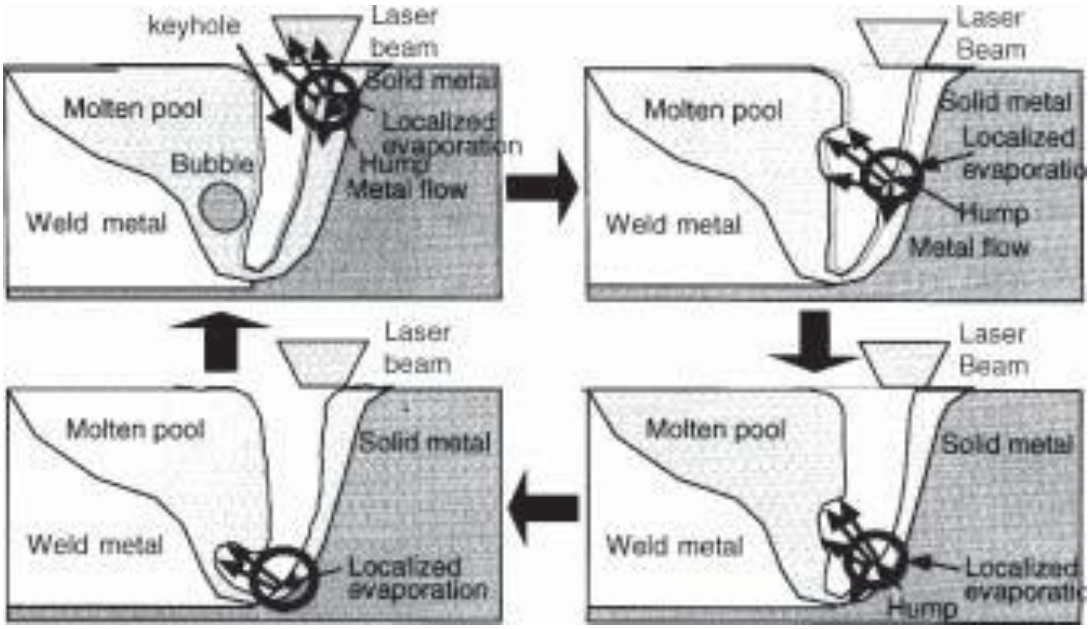

Figure 3-10. Porosity formation from the localised evaporation at the front keyhole wall [Matsunawa et al, 2003].

However, the behaviour observed in Figure 3-9 and graphically detailed in Figure 3-10 has been for partial penetration welds. For fully penetrating welds it would be expected that the hump would be ejected from the rear of the keyhole and not result in a bubble entering the molten pool. Du et al [2003] reported that a large reduction in porosity occurred when moving from a partially to a fully penetrating welding condition.

Theoretical models, based on relatively simplistic keyhole geometry, analysing the effects of a non-equilibrium state between the forces in the keyhole indicates that fluctuations in absorbed beam power may introduce fluctuations which may be amplified by the keyhole [Kroos et al, 1993]. Development of this theoretical research by Klein et al [1994] found that a simplified cylindrical keyhole can perform radial, axial and azimuthal oscillations. At absorbed laser powers which are significantly above a certain threshold value the amplitude of these oscillations is particularly small. However, if the absorbed laser power is near, or at, the threshold value then the keyhole is more prone to oscillations which are intimated to cause welding defects [Klein et al, 1994]. Further research [Klein et al, 1996] on keyhole oscillations induced by a fluctuation in the incident laser power has shown that fluctuations ≥ 1% are able to generate oscillations in the keyhole with sufficient amplitude to cause keyhole collapse if they occur at the resonant frequencies of the keyhole. This collapse would most likely result in the shielding gas entering the keyhole and becoming trapped as porosity.

The forces acting on the keyhole and the melt pool during laser welding are primarily determined by the properties of the incident laser radiation (i.e. wavelength, power density

etc), the material properties (i.e. thickness, chemical composition etc), the welding speed and the surrounding environment (i.e. the gas utilised to shield the welding process). It would be expected that the material properties, the welding speed and the shielding of the welding process would not be subject to change. However, the properties of the incident laser radiation, in terms of total power and power density, can be perturbed by the metallic vapour exiting the keyhole which provides a mechanism for the fluctuation in laser power and, as a result, the keyhole instabilities.

3.5 Plasma and Plume Attenuation Effects

3.5.1 Introduction

It has been discussed previously that the formation of a keyhole is dependent on the vaporisation of the workpiece, and the subsequent metal vapour pressure acts to maintain the keyhole. If the incident electromagnetic radiation is from a CO_2 laser source (~10 μm wavelength), the metal vapour may be partially ionised and will absorb a portion of the incident laser beam. The interaction of the metallic vapour, whether it be ionised or not, with the keyhole walls and the trailing melt pool can significantly influence the process dynamics, as a result of vapour friction effects (discussed in Sub-section 3.3.3.2). In addition to the forces exerted on the keyhole walls, the metal vapour exiting the keyhole will also interact with the incident laser radiation. Potentially, the laser beam can be absorbed, defocussed or reflected by the metal vapour, depending upon the attenuation mechanisms.

It is important at this stage to establish the terminology used to describe the thermally excited metal vapour exiting the keyhole, since ambiguity is observed when comparing the relevant literature. In this report, the term 'plasma' refers to the ionised metal vapour emitted from the keyhole during laser welding with a 10 μm wavelength laser source, since the wavelength of this electromagnetic radiation is conducive to plasma formation. Ordinarily, plasma cannot be present when welding with 1 μm wavelength laser radiation. Some ionisation of the metallic vapour may occur although the rise in temperature is not sufficient for large electron densities to be present [Dowden 2009, p. 97]. As a result, in this report the term 'plume' refers to the thermally excited metal vapour emitted when laser welding with a 1 μm wavelength laser source.

The exact attenuation mechanism(s) are primarily dependent upon the wavelength of the incident laser radiation. Numerous spectroscopic studies (for example; Poueyo-Verwaerde et al, 1993; Szymański and Kurzyna, 1994; Lacroix et al, 1997; Greses, 2003) have been

performed to determine the specific content of metal vapours produced by ~1 μm and ~10 μm wavelength lasers during keyhole laser welding of metallic materials. Determining critical parameters such as the electron temperature and density has allowed the attenuation mechanisms for the different wavelength laser sources to be determined. For instance, it has been reported [Greses 2003] for Nd:YAG laser welding of C-Mn steel that the dominant beam attenuation mechanism is through absorption of the beam by a population of metallic spheres ~20-40 nm in diameter. However, when CO_2 laser welding C-Mn steel, the dominant beam attenuation mechanism is through defocussing of the incident laser radiation by the gradient refractive index (produced by a gradient electron density) of the ionised metallic vapour [Greses 2003].

Xie [1999] observed the behaviour of the ionised metal vapour exiting the keyhole with a high speed camera at an imaging frequency of 9000 Hz, when welding steel with a CO_2 laser source. Significant fluctuations were observed in the size and position of the plasma and it was identified that this behaviour was related to the keyhole instability. A similar link between the keyhole and plasma behaviours was also identified by Seto et al [2000] when simultaneously observing their behaviours during CO_2 laser welding of either a 5000 series aluminium alloy or 304 stainless steel. As has been reported by several researchers (e.g. Matsunawa and Ohnawa, 1991), understanding the interaction between the incident laser light and the plasma or plume above the laser-workpiece interaction point is critical to achieving a stable keyhole.

3.5.2 Plasma Attenuation Mechanisms

Plasma formation was briefly discussed in Sub-section 2.2.5, where it was stated that the ratio of the electron and ion density to the density of the vapour atoms can be established calculated using the Saha equation. Knowing this ratio the proportion of inverse Bremsstrahlung absorption coefficient, as discussed in Sub-section 3.3.2.2, can be calculated using Equation 3-10. Beer's law, Equation 3-11, can then be utilised to determine the intensity of the incident radiation travelling through the plasma as a function of the plasma height (z), assuming that the inverse Bremsstrahlung coefficient is constant throughout the plasma.

$$I(z) = I_0 e^{-\alpha_{ei} z} \tag{3-15}$$

Szymański et al [1997] studied the plasma that was emitted when CO_2 laser welding Ti-1.5Al-1.3Mn, and reported that temperatures up to ~11500K were calculated for the plasma. This corresponds to a transmittance of at least 94% when argon shielding gas was utilised.

According to the results presented by Klein et al [1996], this absorption is sufficient to cause keyhole instabilities, provided there is some transient variation in the plasma's intensity. Several other studies have been performed (e.g. Poueyo-Verwaerde et al, 1993), although predominantly on ferrous metals, that have reported similar findings. It should be noted that a portion of the energy absorbed in the plasma may be radiated back to the keyhole, thereby returning a portion of the energy lost by the inverse Bremsstrahlung absorption.

It is assumed in Equation 3-11 that the inverse Bremsstrahlung absorption coefficient is constant through the depth of the plasma. The spectroscopic results reported by Poueyo-Verwaerde et al [1993] show that the electron density and temperature in the plume decreases as a function of height above the surface of the workpiece. As a result, the absorption of the incident laser radiation is strongest immediately above the keyhole which will influence the total absorption of the laser beam. These temperature and electron density gradients present in the plasma will result in the plasma behaving like a lens as a result of the gradient refractive index. This gradient refractive index can act to defocus and deflect the laser beam, which will further influence the power density and its position on the surface of the workpiece affecting the absorption of the radiation and the keyhole. Research by Poueyo-Verwaerde et al [1992] and numerous others indicated that these effects were present by modelling the incident laser radiations propagation through the plasma.

Further modelling of the laser beam propagation through the plasma by Beck et al [1995] allowed the effects on the intensity distribution and the focal plane position to be calculated. The propagation of a CO_2 laser beam through a non-uniform plasma was found to be both absorbed and refracted. Comparison of the two effects by Beck et al [1995] indicated that the dominant mechanism for perturbing the incident laser radiation was the defocussing of the beam and not the absorption. A highly fluctuating temperature in the plasma was calculated which would result in a constantly changing focal plane position and, consequently, power density at the surface of the workpiece. Szymański et al [1997] did not calculate what defocussing may occur due to a gradient in the electron density.

The absorption of the incident laser radiation by the inverse Bremsstrahlung effect in the plasma, its deflection by a gradient refractive index in the plasma, and the potential for a portion of the incident laser radiation to be reflected by the plasma, can be significantly influenced by the choice of shielding gas utilised. Beck et al [1995] modelled the attenuation effects of a CO_2 laser beam in a number of different gas environments. The attenuation could be reduced by utilising helium shielding gas as a result of its high thermal conductivity and ionisation potential, compared with those of argon and nitrogen (as detailed in Table 3-1).

Table 3-1. Thermal conductivity, at room temperature, and ionisation potential of common shielding gases used when laser welding [Lide, 1997].

Gas	Thermal Conductivity	1st Ionisation Potential
Ar	0.0001772	15.759
He	0.00152	24.587
N	0.0002598	14.534

Glowacki [1995] compared the relationship between plasma temperature and the electron density as a function of different shielding gases (argon, helium and nitrogen were considered). The refractive index and inverse Bremsstrahlung absorption coefficient could then be calculated for single shielding gases or two-component mixtures. An argon-helium mixture with a minimum of 50% helium (by volume) was found to be the most satisfactory solution since less defocussing of the incident laser light was calculated. Mixtures containing less than 50% helium resulted in a large defocussing of the incident laser beam, as indicated in Figure 3-11 [Glowacki, 1995].

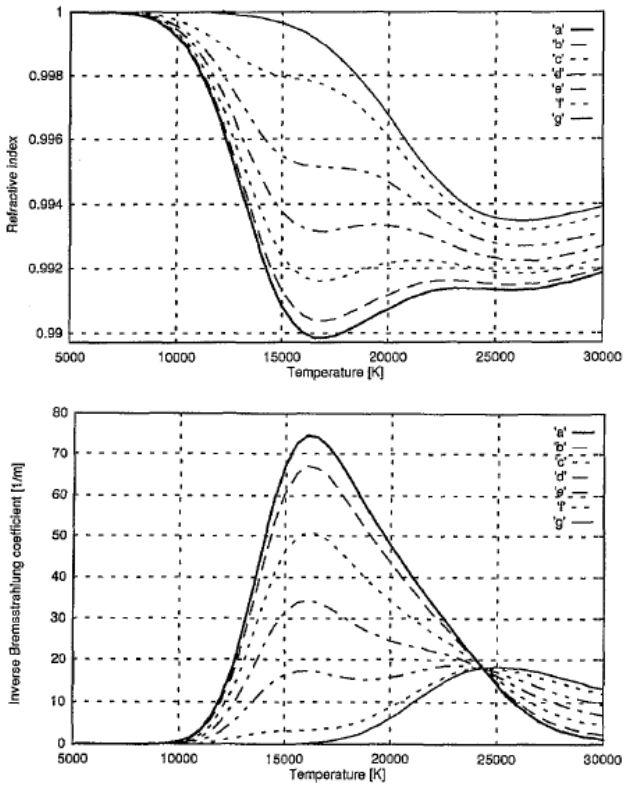

(a)

(b)

Figure 3-11. The refractive index of the plasma (a) and the inverse Bremsstrahlung absorption coefficient (b) as a function of temperature (K) for various helium-argon volume ratios: 'a' 100% - 0%, 'b' 90% - 10%, 'c' 70% - 30%, 'd' 50% - 50%, 'e' 30% - 70%, 'f' 10% - 90%, and 'g' 0% - 100% [Glowacki, 1995].

3.5.3 Plume Attenuation Mechanisms

The temperature of the plume emitted during welding with 1 μm wavelength laser sources has also been investigated using optical spectroscopy by several researchers (for example; Lacroix et al, 1997; Greses, 2003). In general, the temperatures of the metal vapour exiting the keyhole are significantly less than those calculated during CO_2 laser welding. For instance, Lacroix et al [1997] calculated a maximum electron density and plume temperature of $6.5x10^{16}$ and 7100K respectively, when pulsed Nd:YAG laser welding steel. A much lower average temperature was calculated by Greses [2003] of between 1800 and 2600K when continuous-wave Nd:YAG laser welding C-Mn steel, and these are more representative of the calculated temperature in other reported literature for continuous-wave laser sources.

It has been reported [Lacroix et al, 1997; Greses, 2003], at least for C-Mn steel, that absorption (by inverse Bremsstrahlung) and defocussing (by the gradient electron density) effects of the laser beam are very weak, if applicable at all, in the case of Nd:YAG laser welding. Scattering and absorption of the laser beam by ultrafine particles is the dominant effect in Nd:YAG laser attenuation when welding C-Mn steel. Scattering of light is a result of the electromagnetic wave interacting with a particle whose refractive index is different from the surrounding medium. The Mie solution to the Maxwell equations can be applied to determine the extinction (combination of scattering and absorption) of the laser light through the vapour plume. According to Mie theory the extinction coefficient can be calculated using Equations 3-12, 3-13 and 3-14 [van de Hulst 1957, p. 290].

$$Q_{EXT} = Q_{ABS} + Q_{SCA} \tag{3-16}$$

$$Q_{ABS} = \frac{-8\pi r_p}{\lambda} Im\left\{\frac{m^2-1}{m^2+2} + \frac{4}{15}\left(\frac{\pi r_p}{\lambda}\right)^3 \left(\frac{m^2-1}{m^2+2}\right)^2 \frac{m^4+27m^2+38}{2m^2+3}\right\} \tag{3-17}$$

$$Q_{SCA} = \frac{8}{3}\left(\frac{2\pi r_p}{\lambda}\right)^4 \left|\frac{m^2-1}{m^2+2}\right|^2 \left[1+\frac{6}{5}\left(\frac{2\pi r_p}{\lambda}\right)^2 \frac{m^2-1}{m^2+2}+\ldots\right] \tag{3-18}$$

Where Q_{EXT}, Q_{ABS}, and Q_{SCA} are the extinction, absorption and scattering efficiencies, m is the complex index of refraction for the sphere, r_p is the radius of the particles and λ is the wavelength of the incident light.

In order to apply the above equations, the particles are considered to be identical in size and composition, and that they are isotropic and optically linear. These equations can be simplified if the second part of the scattering efficiency term is less than 0.2 [van de Hulst 1957, p. 312]. For a titanium sphere (i.e. complex index of refraction of 3.8 + 4.0i) this equates

to the radius of the sphere being less than 70 nm. Observed particle sizes [Greses, 2003; Lacroix et al, 1997], at least for steels are typically smaller than this size. The equations can then be simplified.

$$Q_{ABS} = \frac{-8\pi r_p}{\lambda} Im\left\{\frac{m^2-1}{m^2+2}\right\} \tag{3-19}$$

$$Q_{SCA} = \frac{8}{3}\left(\frac{2\pi r_p}{\lambda}\right)^4 \left|\frac{m^2-1}{m^2+2}\right|^2 \tag{3-20}$$

The attenuation of the Nd:YAG laser beam can then be determined using Beer's Law

$$I(z) = Ie^{-(Q_{ABS}+Q_{SCA})\pi r_p{}^2 N_p z} \tag{3-21}$$

Where $I(z)$ is the proportion of incident laser radiation transmitted through the plume along the propagation direction z, I is the incident laser intensity, and N_p is the density of the particles in the plume.

This attenuation may be somewhat pessimistic as it does not take into account the direction of the scattered radiation (i.e. some of the scattered radiation may be parallel with the incident beam). Nevertheless, calculations of the beam attenuation by Greses [2003] have shown that up to ~30% of the beam intensity may be attenuated for particles with a diameter 10-30 nm when Nd:YAG laser welding C-Mn steel.

3.5.4 Laser Beam Brightness Effects

The commercial availability of 1 μm wavelength solid-state lasers with particularly high powers and excellent beam qualities (see Section 2.6) allows power densities of ~ $MWmm^{-2}$ levels to be produced on the surface of the workpiece. These power densities are significantly greater than with traditional Nd:YAG rod laser sources, which were capable of being focussed into power densities of $kWmm^{-2}$ levels whilst still maintaining an acceptable working distance.

Hilton and Verhaeghe [2009] compared the welding performance of focussed laser beams with power densities ranging from 15 – 500 $kWmm^{-2}$ and brightness levels (see Section 2.6) from 0.3 – 20 $MWmm^{-1}.sr^{-1}$, when welding C-Mn steel. The optimum performance in terms of melt run penetration in steel was found for the focussed laser beam with the highest brightness and not the smallest spot size. However, this could only be achieved if; (i) a side jet of argon was directed at the laser-workpiece interaction point opposite to the direction of travel, and (ii) additional cross jets of argon (directed perpendicular to the direction of

travel) were used to disturb the air flow in the region between the beam focussing lens and the workpiece. It was noted that this was a solution that was not appropriate for all the focussed beams examined. In particular, when welding with a Yb:YAG disc laser focussed into a 0.1 mm diameter spot with a 200 mm focussing lens, the performance curves were nominally identical. Nevertheless, the results reported by Hilton and Verhaeghe [2009] indicate that both the side and cross jets were required to maximise performance of the brightest laser (20 $MWmm^{-1}.sr^{-1}$). It was postulated that the effects seen could involve changes to the refractive index of the gas column between the focussing lens and the workpiece.

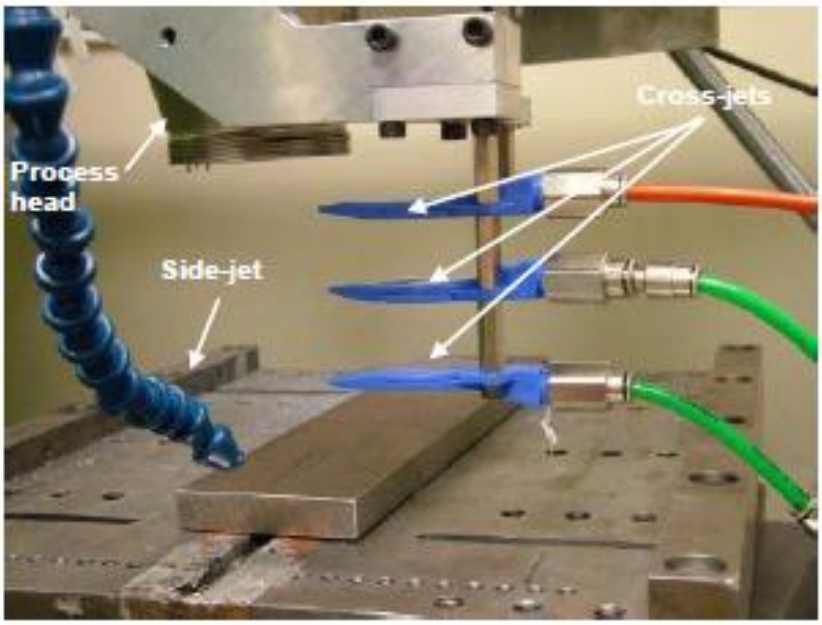

Figure 3-12. Arrangement of side jets and cross jets utilised by Hilton and Verhaeghe [2009]. Courtesy of TWI Ltd.

In terms of the characteristics of the plume present when welding with high-brightness Yb-fibre laser sources, Kawahito et al [2007] performed spectroscopic analysis of the metal vapour emitted from the keyhole during welding of 304 stainless steel with a 10 kW Yb-fibre laser. High speed observation of the plume behaviour above the keyhole when welding at a speed of 50 mms^{-1} with a power density of ~0.9 $MWmm^{-2}$ indicated that the plume reached a minimum height of 12 mm above the keyhole. During the same experiment, the vapour plume temperature was calculated to be approximately 6000K using the Boltzmann plot method. This corresponded to an ionisation fraction of 0.02 according to the Saha equation, which classifies the plume as a weakly ionised metal vapour. High speed observation of the plume behaviour above the keyhole during the same experiment indicated that the plume reached a minimum height of 12 mm above the keyhole. Therefore any attenuation which is

prevented by eliminating the plume immediately above the keyhole is most likely related to preventing absorption and scattering of the incident laser beam by ultrafine particles, as specified for Nd:YAG laser welding by Lacroix et al [1997].

The requirement for the cross jets when welding with a high brightness laser source can be explained by examining the work reported by Oiwa et al [2009], who investigated the optical properties of a gas column between the workpiece and the focussing lens when welding zinc-coated steel sheets with a 10 kW Yb-fibre laser. A Michelson interferometer was utilised to observe the refractive index distributions in the gas column between the workpiece and the focussing lens. It was observed that low refractive index distributions were present in the column up to a maximum height of 400 mm (stand-off distance was 1250 mm). When present, these regions of varying refractive index were sufficient to cause a loss of penetration in the workpiece such that the welding process moved from a fully penetrating to partially penetrating. These refractive index gradients could be eliminated by utilising a fan, positioned perpendicular to the laser beam, to create a movement of air between the focussing lens and the workpiece. Consequently, a fully penetrating welding condition occurred despite the presence of a plume, circa 20 mm in height, still present directly above the keyhole.

A similar investigation performed by Hilton and Blackburn [2010] investigated the optical properties of the plume produced when welding C-Mn steel with a 4 kW Yb-fibre laser (beam parameter product of 1.6 mm.mrad) with two different focussing lenses (300 and 500 mm). Schlieren imaging was utilised to confirm the presence of regions with different refractive index present between the workpiece and the focussing lens, and optical spectroscopy was utilised to characterise the properties of the plume immediately above the keyhole (up to a height of 22.5 mm). The results from the laser Schlieren provided evidence that the column of gas in the path of the laser beam has a different refractive index to the surroundings. However, a gradient refractive index was not detected when cross-jets were utilised, agreeing with the results presented by Oiwa et al [2009]. The calculated values of the plume temperature were ~6900K, using the Boltzmann plot method (see Page 71). This corresponds to an ionisation fraction of 0.074 for the metallic component of this vapour and ~0.0001 for the argon portion.

An interesting result noted by Hilton and Blackburn [2010] is that at the two different stand-off distances examined, the cross jets and side jet had no effect on the welding performance when the 300mm focussing lens was utilised. This is significant since the effective brightness of both focussed beams is nominally identical, as per Equation 2-13, indicating that the beam

attenuation mechanisms observed are more prevalent when using focussing lenses with a longer focal length. Referring to the results presented by Hilton and Verhaeghe [2009], the jets were found ineffective when used with lower brightness laser beams. For all the lower brightness beams examined, the longest stand-off distance utilised was 280 mm.

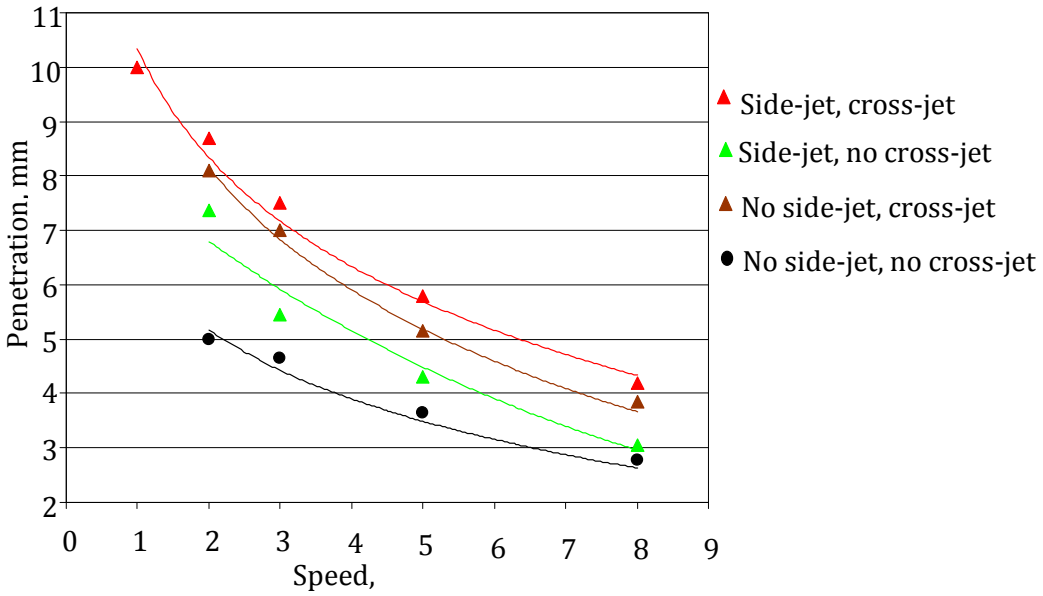

Figure 3-13. Penetration depth observed by Hilton and Blackburn [2010] when welding C-Mn steel with a 4 kW Yb-fibre laser, with a 500 mm focussing lens and 0.2 mm diameter beam width. Courtesy of TWI Ltd.

In summary, for high-brightness laser beams, it appears that two mechanisms contribute to the beam attenuation; (i) the presence of a plume immediately above the laser-material interaction point, and (ii) the establishment of regions of low refractive index in the region between the top of the plume and the focussing lens. The first of these mechanisms is present in all situations, whereas the second appears to be much more of a concern when processing with a stand-off distance exceeding 500 mm. Although this is a relatively newly observed phenomenon, which requires further investigation, it is evident that there is sufficient attenuation to cause a lack of penetration so certainly there would be enough attenuation to cause keyhole instability and possible porosity formation.

3.6 Potential Porosity Prevention Methods

Despite the reported mechanisms for introducing keyhole instability resulting in weld metal porosity, several techniques have been developed to suppress keyhole instabilities which

cannot be controlled through optimisation of the basic process parameter set (i.e. welding speed, focussed beam diameter, power density etc). Specifically, these methods are:

1. Manipulation of the shielding atmosphere in which the welding is performed (e.g. Arata et al, 1985).
2. The utilisation of a jet of inert gas directed towards the keyhole (e.g. Kamimuki et al, 2002).
3. Dual focus laser welding (e.g. Xie, 2002).

The above methods all intend to prevent the initiation of keyhole instabilities either by interacting with the plasma or plume above the keyhole or by modifying the geometry of the keyhole such that it is more resistant to variations in the forces maintaining and restoring it. Furthermore, modulating the output of the laser beam has also been reported as a method of producing keyhole laser welds with very low levels of porosity. These four potential methods for producing high quality laser welds in titanium alloys when utilising 1μm wavelength laser sources are reviewed below. Additionally, the potential for stirring the melt pool with magnetic fields for porosity prevention is also discussed.

It is worth noting that the vast majority of the published data on porosity prevention when keyhole laser welding refers to ferrous metals and aluminium alloys. A small amount of research has been published which concerns titanium alloys, however the results are generally not quantified and are therefore particularly difficult to compare. Even if the results have been quantified, the method utilised to assess the porosity of the content varies significantly. Conventional radiography and sectioning are the two methods most commonly utilised, with the former providing the most reliable results. However, the size of imperfections visible on radiographs is subject to variation in the radiography process (as a result of film sensitivity, radiation source etc), and the subsequent analysis will only amplify this (i.e. human error).

3.6.1 Shielding Atmosphere

It was previously discussed (Section 3.5) that a portion of the incident laser radiation may be attenuated by a plasma or a vapour plume, therefore providing one possible mechanism for keyhole instability and the formation of weld defects. Keyhole laser welding performed under vacuum has shown [Arata et al, 1985] that plasma formation can be easily suppressed. Katayama et al [2001] also studied the effect of processing in a vacuum when CO_2 and Nd:YAG keyhole laser welding aluminium alloys and austenitic stainless steel. Welds were produced with no porosity at lower pressures, whereas those made under identical conditions but at

atmospheric pressure contained porosity. Observation of the keyhole and melt pool behaviour indicated that both the keyhole and melt pool exhibited different behaviours when welding at lower pressures which were beneficial for preventing porosity formation; this is a result of the plasma or plume formation above the keyhole being dispersed before having time to attenuate the incident laser beam. Unfortunately, welding at lower pressures limits the inherent flexibility of laser welding and would require the utilisation of a moving vacuum chamber.

It has been reported [Caiazzo et al, 2004] that shielding of the melt pool with helium when CO_2 laser welding Ti-6Al-4V results in a higher weld quality than when using argon as a shielding gas. When keyhole laser welding with a CO_2 laser beam, helium gas (>99.995% purity) is ordinarily used to shield the welding process since its ionisation potential and thermal conductivity are higher than other shielding gases, such as argon, which will inhibit the formation of plasma outside the keyhole. The use of helium shielding gas can therefore reduce the variation in the vaporisation pressure and increase keyhole stability/internal weld quality. However, this would not be applicable when welding with 1μm wavelength laser sources since the inverse Bremsstrahlung absorption is negligible.

Katayama et al [1998] assessed the influence of using nitrogen as a shielding gas when CO_2 laser welding 5000 and 6000 series aluminium alloys. Under the correct combination of welding speed and focussed power density the output power of the laser could effectively be modulated, as a result of the cyclic formation of an attenuating plasma above the keyhole. Significantly, Katayama et al [1998] observed a reduction in porosity when utilising nitrogen shielding gas instead of helium under certain welding conditions, which was attributed to the keyhole being controllably collapsed before instabilities occurred. Nevertheless, a similar behaviour would not be expected when welding with 1 μm wavelength solid-state laser sources for the reason discussed above. Furthermore, titanium cannot be welded in a nitrogen atmosphere due to its affinity for light elements at temperatures exceeding 500°C.

3.6.2 Directed Gas Jet

Despite the reduction of porosity that can be achieved when utilising helium as a shielding gas during CO_2 keyhole laser welding (for example; Caiazzo et al, 2004), keyhole fluctuations may still occur, resulting in weld defects [Seto, 1999]. Miyamoto et al [1985] reported that a jet of inert gas, directed towards the laser-material interaction point, could be utilised to further prevent the plasma formation above the keyhole when CO_2 laser welding and produce weld beads with few defects. This approach has also been reported [Denney and Metzbower,

1989; Li et al, 1997] to be successful for reducing porosity when keyhole laser welding titanium alloys with a CO_2 laser.

The mechanisms for beam attenuation when welding with 1μm wavelength lasers are not related to ionisation and therefore shielding gases with particularly high ionisation potentials are not required. Nevertheless, a directed jet of gas has also been reported to reduce keyhole fluctuations and improve weld quality when welding with 1μm laser beams [Kamimuki et al, 2002; Fabbro et al, 2006]. Typically, the jet of gas is directed towards the keyhole using a delivery tube which is in-line with and parallel to the welding direction.

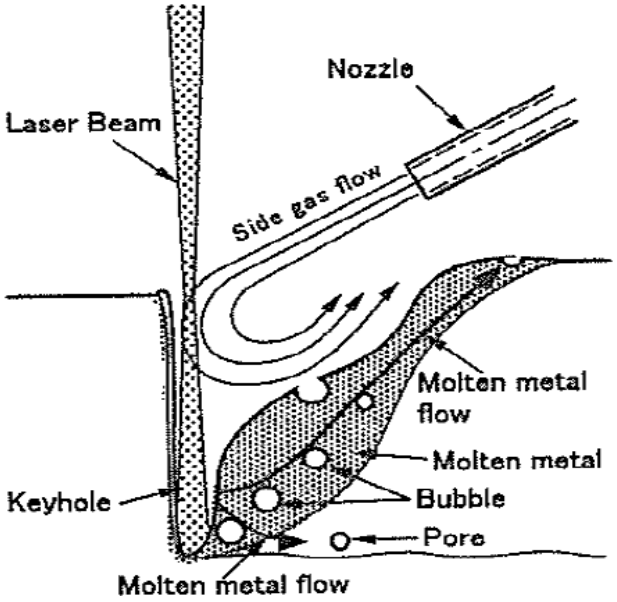

Figure 3-14. Schematic illustration of the position of the directed gas jet [Kamimuki et al, 2002].

Kamimuki et al [2002] studied the effects of utilising a jet of argon directed towards the keyhole when Nd:YAG laser welding 10 mm thickness 304 stainless steel plates. Figure 3-14 [Kamimuki et al, 2002] details the general position of the directed gas jet with respect to the keyhole laser welding process. Porosity and weld spatter could be significantly reduced by utilising the directed gas jet. This effect was attributed to the interaction with the gas jet and the melt pool which induced a flow of molten material conducive to the escape of porosity from the melt pool. This proposal was supported by high speed video observations which detailed an elongated opening at the top of the keyhole. Results were presented by Kamimuki et al [2002] assessing the influence of the positional parameters associated with the directed gas jet, and it was found there was an optimum position of the directed gas jet for reducing weld metal porosity, as indicated in Figure 3-15 [Kamimuki et al, 2002]. Monitoring of the optical signals emitted from the plume during welding process using a photodiode indicated

that the plume exhibited a much more constant behaviour when the directed gas jet was applied. It is worth noting that these results were reported for partial penetration welds only.

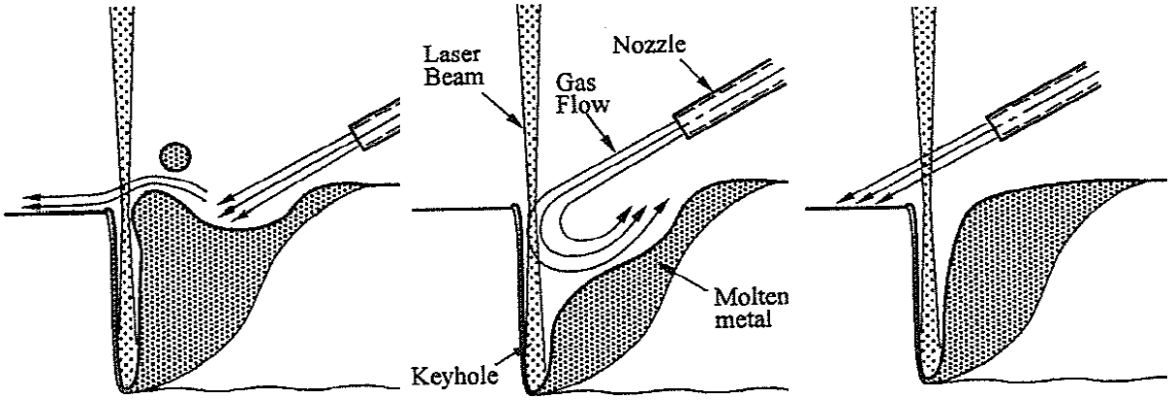

Figure 3-15. Schematic illustration of the influence of the interaction between the directed gas jet and the welding process for different nozzle positions from; (a) central gas jet axis behind the keyhole, (b) central gas jet axis centred on the keyhole, (c) central gas jet axis in front of the keyhole [Kamimuki et al, 2002].

The influence of the directed gas jet on the keyhole and melt pool during continuous-wave Nd:YAG laser welding was modelled by Amara and Fabbro [2008]. Although the gas jet was pointing opposite the direction of travel, the results presented by Amara and Fabbro [2008] indicate that the gas jet produces a slightly wider keyhole opening but also creates a much more laminar flow in the melt pool which would encourage the escape of bubbles trapped in the melt pool.

Recent publications [Hilton et al, 2007; Mueller et al, 2008] have shown that welds in titanium alloys with a high internal quality and good weld profile can be produced using 1 μm wavelength laser beams if a directed gas jet is utilised. Hilton et al [2007] used a 7 kW Yb-fibre laser to produce butt welds in Ti-6Al-4V, in thicknesses up to 9.3 mm, with internal porosity contents lower than specified in internal aeroengine weld criteria and significantly lower than AWS D17.1 Class A. Mueller et al [2008] utilised a 5 kW Yb-fibre laser to weld two titanium alloys, up to 6.5 mm in thickness, to within the weld quality criteria specified by AWS D17.1 Class A. In both cases [Hilton et al, 2007; Mueller et al, 2008] an inert assist gas still had to be utilised to stabilise the welding process and produce high quality welds. However, in both cases, no details were given regarding the parameters of the directed gas jet.

3.6.3 Dual Focus Keyhole Laser Welding

Dual focus forming optics allow manipulation of the foci separation, the foci orientation (i.e. in-line with the joint direction, transverse to it, and any angle in between), and the relative intensity distribution between the two focussed spots. Consequently, there is the potential for a wide variety of possible power density combinations, which allow the keyhole and melt pool shape to be manipulated. Researchers have reported (for example; Xie, 2002; Haboudou et al 2003; Hayashi et al, 2003) that keyhole laser welding with a dual focus laser beam can reduce weld metal porosity compared with a single spot arrangement for metallic materials other than titanium alloys.

Gref et al [2003] used a 4 kW Nd:YAG laser to keyhole weld a 6000 series aluminium alloy and found that the distance between the two focal spots has an effect on the keyhole geometry and thus the stability of the keyhole and porosity formation in the weld metal. If the two focal spots were not far enough apart the process was unstable and much porosity was produced. By increasing the distance between the two focal spots (0.6 mm was found to be ideal), pores with diameters above 0.3 mm could be reduced, although the depth of penetration was also reduced. An equal split of the laser power between the two focal spots was found to be the most advantageous power ratio with respect to porosity formation.

Haboudou et al [2003] also used a 4 kW Nd:YAG laser to weld aluminium allots with a dual focus configuration (aligned both parallel to the welding direction and perpendicular to the welding direction). It was noted that the use of the dual beam method could suppress porosity to a level of 2% volume fraction in AA5083 and 1% for A356. Analysis of the melt pool via a high speed camera by Haboudou et al [2003] confirmed that, the use of the dual spot welding technique stabilises the melt pool. Xie [2002] used a 6 kW dual beam CO_2 laser split into two equal laser beams using a simple wedge mirror. It was reported that, porosity was substantially decreased using the dual-beam laser welding technique. Xie [2002] gave no quantitative data regarding porosity formation.

In terms of utilising a dual focus keyhole laser welding technique for the prevention of porosity when joining titanium alloys, Coste et al [1999] investigated its effect on 4mm thickness Ti-6Al-4V for Nd:YAG laser welding (two 600μm diameter focal spots). No quantitative data was given regarding the amount of porosity in the weld, although it was commented that the dual focus technique can give an improved weld quality compared to a single focussed spot.

Hayashi et al [2002] also researched the effect of an in-line dual focus configuration for CO_2 laser welding of austenitic stainless steel SUS 304. Observation of the keyhole by an in situ X-ray transmission method showed that the keyholes coalesced to form one large keyhole. It was suggested that this prevents the generation of bubbles and hence the formation of porosity; as a result of the larger keyhole being more resistant to process instabilities. High speed observation of the plasma behaviour above the keyhole during CO_2 keyhole laser welding [Xie, 2002] suggested that there was less variation for the dual focus method compared to the single spot set-up.

3.6.4 Modulated Keyhole Laser Welding

Modulating the output power of a laser beam has previously been reported as a successful method of reducing weld metal porosity when welding ferrous materials and aluminium alloys (for example; Eberle and Richter, 1994; Matsunawa et al, 2003). Matsunawa et al [2003] used a modulated Nd:YAG laser to weld a 5000 series aluminium alloy. Powers ranging from 2.5 to 5.0 kW were utilised with a laser duty cycle of between 50 and 100%. It was shown that, at the same welding speed a modulated output (rectangular pulse) was capable of reducing weld metal porosity compared with a continuous wave CO_2 laser.

Kuo and Jeng [2005] reported that modulating the output power of an Nd:YAG laser reduced the resultant porosity levels when welding 3 mm thickness SUS 304L and Inconel 690 compared with a continuous wave output power. The same effect has also been reported when CO_2 laser welding aluminium alloy A5083 [Katayama et al, 2003]. A comparison of modulation amplitudes by Kawaguchi et al [2006] indicated that larger modulation amplitudes were more effective in reducing the occurrence of porosity when CO_2 laser welding SM490C steel. A similar trend relating modulation amplitude to porosity content was also established when welding SUS 304L and Inconel 690 with a 1 μm laser beam [Kuo and Jeng, 2005].

Eberle and Richter [1994] carried out modulated-power Nd:YAG laser welding of Al-alloys, reporting that welds made with a 50 Hz square wave modulation were improved, but did not quantify their results or advance an improvement mechanism. Matsunawa and Katayama [2002] performed power modulated CO_2 laser welding of AA5182 Al-alloy at 100 Hz. They observed a significant decrease in porosity when using a beam duty of ≤80% per cycle. They attributed the reduction in porosity as being due to pores entrapped in the melt pool generated by one laser pulse having a second chance to escape, when a part of the weld was re-melted by the subsequent pulse.

3.6.5 Magnetic Fields

The application of magnetic fields during conventional arc welding has been studied by several researchers (for example; Willgoss, 1981), with the intention of inducing an electromagnetic force to modify the melt flow and influence the quality of the weld. The effects observed during arc welding are most likely a result of the magnetic field's interaction with the arc current. However, the magneto-hydrodynamic forces should also be considered. Magneto-hydrodynamic forces are present in an electrically conducting fluid when it passes through a magnetic field. Ordinarily, the fluid is either a liquid (for example, the melt pool during arc welding metallic materials) or a plasma. An electric field is induced in the conductor as it moves through the magnetic field, according to Lenz's law, which causes a Lorentz force to act on the fluid, affecting its motion.

Recently, the effects of applying magnetic fields during Keyhole laser welding has been examined (for example; Kern et al, 2000; Vollertsen and Thomy, 2006). Kern et al [2000] first studied the effects on weld quality of applying magnetic fields during CO_2 laser welding of C-Mn steel StE 600 and AA6110. When applying transverse electromagnetic fields during welding of StE 600 they observed that the maximum welding speed before humping occurs could be significantly extended. The electromagnetic fields also provided beneficial effects on the process stability and the top bead appearance in both StE 600 and AA6110 [Kern et al, 2000].

Considering the potential mechanisms causing the observed effect on the weld quality, the magneto-hydrodynamic forces induced in the melt pool should not be neglected. However, the results presented by Kern et al [2000] indicate that the polarity of the magnetic field was found to be critical in positively affecting the welding process, which indicates that a net electric current must always flow in the same direction. Consequently, it would be expected that the forces were not solely magneto-hydrodynamic forces. Further experiments [Kern et al, 2000] revealed that an electric current, of the order of ~10 A, was present in the welding process without the aid of the magnetic field, a result of a thermoelectric voltage between the solidified metal and the melt pool. It is this current combined with the applied transverse magnetic field, which is thought influenced the melt flow in the experiments performed by Kern et al [2000] and improved process stability.

Vollertsen and Thomy [2006] also performed studies on the influence on magnetic stirring during CO_2 laser welding of aluminium alloys. Welding over a Al- Cu foil – Al sandwich allowed the effect of magnetic stirring to be assessed by performing EDX analysis on the resultant weld section and comparing the dilution of copper through the weld. It was

reported that the applied alternating magnetic field has a considerable effect on the dilution area and the homogeneity within this area [Vollertsen and Thomy, 2006].

Whilst no experiments have been performed assessing the influence of magnetic stirring of the melt pool on the formation of porosity in the weld metal, the results presented above indicate that magnetic fields can be utilised to influence the melt flow. Most likely, inducing a laminar flow in the melt pool using the methods reported by Kern et al [2000] would be more favourable than stirring of the melt pool [Vollertsen and Thomy, 2006] in preventing the formation of porosity.

3.7 Summary, Project Aim and Project Objectives

It is apparent from Section 2.4 that in order to achieve a weld quality that is suitable for aerospace applications then criteria relating to the visual appearance of the face and root of the weld, the geometry of the weld profile, and the occurrence of cracks and weld metal porosity must be met. Of these potential defects, the formation of porosity is of primary concern, since the remaining defects can be avoided through the adoption of rigorous workpiece preparation and inert gas shielding, and the utilisation of filler material.

Hydrogen porosity in the weld will also be influenced by the workpiece preparation and inert gas shielding procedures. Nevertheless, the formation of porosity in the weld may still occur, as a result of keyhole instability. Critically, the stability of the keyhole is determined by the forces acting to maintain it and those acting to close it. For keyholes with a high Péclet number the forces generated from the absorption of the incident laser radiation and those present in the melt pool are heavily interdependent, and it is particularly difficult to achieve a quasi steady-state condition.

The absorption of the incident laser radiation may be perturbed by the formation of a plasma or a plume exiting the keyhole. In the case of welding with a beam of adequate brightness and stand-off distance, the incident radiation may also be defocussed by a column of gas, situated between the workpiece and the focussing lens, which has regions of gradient refractive index. These perturbations may negatively influence the stability of the keyhole. Analysis of the gas contents, by mass spectroscopy, of pores formed when keyhole laser welding has indicated that it is constituted primarily of the shielding gas. The pressure inside the keyhole is such that the entrance of shielding gas into the vapour cavity is only possible if the ablation of the keyhole walls is perturbed, which will lead to the collapse of the keyhole, leading to keyhole collapse and the entrapment of shielding gas in the melt pool which becomes porosity on solidification.

Numerous potential methods for preventing the formation of weld metal porosity have been discussed, including; the shielding atmosphere, a directed gas jet, magnetic fields, dual focus laser welding and modulated laser welding. Despite the fact that the majority of the reported literature concerning ferrous metals and aluminium alloys, results can be inferred from these. A small number of papers have also been published regarding the prevention of porosity when keyhole laser welding titanium alloys. Quantitative comparison of these has not been possible since most results are stated qualitatively and not compared to a stated international standard. Nevertheless, porosity prevention methods have been developed for ferrous-metals and aluminium alloys and there is a significant knowledge gap relating to whether or not these can be transferred to titanium alloys. It has also been noted that there is little published data concerning the weld quality possible with the new generation of high brightness laser sources.

As stated previously, the aim of this research project was to *establish an understanding of the formation of weld metal porosity when keyhole laser welding titanium alloys with 1 μm wavelength laser sources and develop techniques which could prevent its formation*. This aim is driven by the commercial reasons discussed in Chapter 11.

Three potential methods for preventing the formation of porosity when welding titanium alloys with 1 μm wavelength laser beams have been identified from this chapter; specifically: an accurately positioned jet of inert gas directed at the laser-material interaction point; a modulated laser power; and, a dual focus laser beam. The primary advantage of these methods over others discussed in Section 3.6 is that they maintain the inherent flexibility of fibre delivered laser beams. Operating in a reduced pressure environment would give little advantage over electron beam welding techniques, whereas inducing an electromagnetic force in the melt pool could potentially limit the component geometries which could be processed. The first three objectives of this project were therefore:

a. *To determine whether an accurately positioned jet of inert gas directed at the laser-material interaction point can be used for reducing weld metal porosity when welding titanium alloys relevant to the aerospace industry with an Nd:YAG laser. Furthermore, determine the influence of key process parameters on the resultant weld quality and the welding process.*
b. *To determine whether a modulated laser power can be used for reducing weld metal porosity when welding titanium alloys relevant to the aerospace industry with an Nd:YAG laser. Furthermore, determine the influence of key process parameters on the resultant weld quality and the welding process.*

c. *To determine whether a dual focus laser beam can be used for reducing weld metal porosity when welding titanium alloys relevant to the aerospace industry with an Nd:YAG laser. Furthermore, determine the influence of key process parameters on the resultant weld quality and the welding process.*

Meeting these objectives would enable critical knowledge of the effects of these methods on the resulting weld quality to be gained. Relating the weld qualities to changes in welding process would develop a fundamental understanding of the porosity formation and prevention mechanisms.

It was previously stated that a new generation of solid-state 1 μm wavelength laser sources, with excellent beam qualities, are emerging. The potential weld qualities available with these laser sources have not yet been established. Consequently, the fourth objective of this project was to:

d. *Establish the weld qualities possible when keyhole laser welding titanium alloys relevant to the aerospace industry with excellent beam quality 1 μm wavelength laser sources.*

In order to benchmark laser welding as a technique for producing near-net-shape titanium alloy components for the aerospace industry, the process, including the potential advancements resulting from this project, should be compared against competing processes. Therefore, the final objective of this was to:

e. *Compare the potential benefits for adopting keyhole laser welding as a production process for titanium aerospace components with the competing manufacturing processes.*

Part II

Technical Aspects

Chapter 4: Research Methodology

Chapter 5: Nd:YAG Laser Welding with a Directed Gas Jet

Chapter 6: Modulated Nd:YAG Laser Welding

Chapter 7: Dual Focus Nd:YAG Laser Welding

Chapter 8: Welding with Excellent Beam Quality 1 μm Wavelength Laser Sources

Chapter 9: Porosity Formation

Chapter 4

Research Methodology

4.1 Introduction

In the previous chapter, the formation and subsequent behaviour of the keyhole were discussed in detail. The potential mechanisms which may act to close the keyhole, and thereby lead to the formation of porosity were highlighted. Potential porosity prevention techniques were identified by reviewing the literature concerning porosity formation during keyhole laser welding. Knowledge gaps relating to the use of these techniques when welding titanium alloys were identified. The objectives of this project, which are detailed in Section 3.7, were borne from the identified knowledge gaps. Following on from the project's objectives, it is the purpose of this chapter to:

1. Outline the approach taken to achieve the objectives of this project.
2. Provide sufficient details concerning equipment, experimental procedures and data analysis techniques so that the experiments may be repeated by another researcher.
3. Justify why certain techniques were used and others were not.
4. Detail the scope of research performed - to act as a precursor to the proceeding results chapters.

Initially, the research approach is discussed. Details are then provided of the titanium sheets sourced for this investigation and an overview of the laser sources utilised to process these sheets is given. The calculated properties, including depth of focus and the focussing cone half angle etc, of all the focussed beams used during experimentation are given. The procedures relating to focal plane positioning, test piece clamping, shielding gas configuration and material preparation are then specified. Details of the analytical techniques employed, such as high speed video observations and optical emission spectroscopy, are given along with

information regarding the processing of the data with MATLAB® programs. Techniques used to evaluate the weld quality, in terms of discoloration, porosity content, and profile are stated, as well as those relating to characterisation of individual pores. Finally, the scope of research performed is clarified.

4.2 Research Approach

For achieving the project's objectives, stated in Section 3.7, different research approaches existed. Three possible research approaches are ordinarily considered for materials processing research.

1. The research could be focussed around the development of a model, numerical or analytical, which describes the process in sufficient detail that the process mechanisms and key process parameters can be understood.
2. The research could be driven by experimental research. Using statistical techniques to identify key process parameters, and analytical techniques to develop a fundamental understanding of the process mechanisms and the effects of key process parameters.
3. A considered combination of the above two techniques.

The research approach taken in this project is one driven by experimental research. Experiments have been performed in a systematic manner to identify the effects of process parameters on the resultant formation of porosity in the weld metal. Where necessary, statistical techniques have been used to design and/or analyse experiments. The analysis of results has focussed around a quantitative assessment of weld metal porosity, although weld quality has also been assessed in terms of discoloration and geometric profile. After identification of the key process parameters, their effects on the process behaviour have been studied using analytical techniques. High speed video has enabled the dynamic behaviour of the keyhole, weldpool and vapour plume to be studied. The data was quantitatively analysed using specifically designed MATLAB programs. The physical and chemical properties of the vapour plume have also been studied using optical emission spectroscopy and scanning electron microscopy.

The development of a model, capable of predicting the formation of porosity in the weld metal would also have allowed the objectives of this project to be met. The most feasible approach would have been numerical modelling of the laser welding process using an appropriate multiphysics software package, such as COMSOL, that enables the interactions between the four states of matter (solid, liquid, gas and plasma) to be determined. However,

the efforts required to develop such a model are not easily understood, and it is likely such efforts would be far outside the duration of this project (see for example the development of the laser cutting software, CALcut, by Dirk Petring). Furthermore, the validation of such a model would require development of the quantitative experimental techniques, such as those utilised in this project. For these reasons, a model driven research approach was not adopted for this project.

A research approach driven by experimental research but supported with an analytical model was also considered for this project. However, an analytical model would be very unlikely to have the capability to predict the formation of porosity in the weld metal, due to the simplifications that must be made.

Presented in the remainder of this chapter are the materials, equipment, experimental procedures and analytical techniques used throughout the experimental research performed in this project. As a result of the project's objectives, defined in Section 3.7, the scope of experimental research performed in this project is best described as four separate work packages. The first three of these work packages relate to the research performed with Nd:YAG laser sources (i.e. using a directed jet of inert gas, a modulated laser power output, and a dual focus laser beam). The final work package is the assessment of using excellent beam quality 1 μm wavelength laser beams for welding titanium alloys.

4.3 Materials

4.3.1 Titanium Sheets

A variety of different titanium alloy grades are utilised in the aerospace industry, with the specific choice depending upon the component's service requirements. It would be practically and economically unfeasible to perform experiments on numerous grades and thicknesses of titanium alloys within this project. Ti-6Al-4V is an α/β alloy which accounts for 60% of the total production of titanium alloys and is used in aeroengine components at temperatures below 315°C and throughout most airframe sections. Consequently, sheets of Ti-6Al-4V in thicknesses of 2.0, 3.25 and 7.0 mm were sourced in order to broaden the industrial relevance of this research. The majority of sheets were 3.25 mm thick. Sheets of 3.25 mm thickness Ti-2.5Cu, which is a near-α alloy and is utilised in airframe structures, were also obtained to provide an indication of the transferability of developed welding procedures between different grades of titanium alloys. The chemical compositions of the Ti-6Al-4V

sheets are detailed in Table 4-1. The chemical composition of the Ti-2.5Cu (also referred to as TA-21, MSRR8603 or IMI 230) is detailed in Table 4-2.

Table 4-1. Chemical compositions of the Ti-6Al-4V sheets.

	Element, wt% (except where stated ppm)								
Thickness	C	Al	Cu	Fe	H(ppm)	N	O	V	Ti
2.0mm	0.008	6.34	<0.01	0.19	56	0.009	0.18	3.98	Bal.
3.25mm	0.011	6.33	<0.01	0.20	61	0.007	0.16	3.83	Bal.
7.0mm	0.012	6.33	<0.01	0.20	51	0.009	0.16	3.91	Bal.

Table 4-2. Chemical composition of the Ti-2.5Cu sheets.

	Element, wt% (except where stated ppm)								
Thickness	C	Al	Cu	Fe	H(ppm)	N	O	V	Ti
3.25mm	0.006	<0.01	2.34	0.07	17	0.006	0.16	<0.01	Bal.

Test pieces, of at least 100 mm in the welding direction (width), were guillotined from the sheets. Typically, the test pieces were 200-300 mm in length allowing numerous autogeneous melt runs to be performed on the same test piece. Test pieces of 7.0 mm thickness Ti-6Al-4V plate were cut to size with a band saw. Machining of the 7.0 mm test pieces allowed 4.0, 5.0 and 6.0 mm thickness test pieces to also be utilised in certain experiments.

4.3.2 Material Preparation

The titanium plates were received in a chemically pickled condition after rolling. However, the elapsed time between pickling and welding was not controlled. No further chemical pickling was applied to any of the test pieces. Immediately prior to performing each melt run, the surfaces of individual test pieces were acetone degreased, cleaned with an abrasive paper and then degreased again with acetone. An identical procedure was performed when producing butt welds, except that the abutting edges of the test pieces were dry machined prior to welding. Butt welds were performed within 8 hours after machining.

4.3.3 Filler Material

Certain experiments were performed using wire as a filler material in order to correct geometrical defects in the weld profile. Ti-6Al-4V wire, manufactured by Daido Steel Co. Ltd., of 0.8 mm diameter was chosen. This wire was applied with a proprietary coating by Daido Steel Co. Ltd. which has been previously shown to aid the liquid-metal transfer when inert gas

arc welding [Pike, 2009]. Consequently, this filler material was preferred to an uncoated wire. Although not metallurgically matched to the Ti-2.5Cu titanium alloy, a small number of trials were performed with this combination.

4.4 Laser Processing Equipment

Five different solid-state laser sources were utilised for the laser processing of the titanium test pieces, all emitting electromagnetic radiation of approximately 1 μm wavelength, specifically:

- GSI-Lumonics JK1002 Nd:YAG laser
- Trumpf HL 4006 Nd:YAG laser
- IPG YLS-1000 SM Yb-fibre laser
- IPG YLR-4000 Yb-fibre laser
- IPG YLS-5000 Yb-fibre laser

The choice of laser sources was influenced by the thickness of titanium sheets sourced and the availability of high power solid-state lasers for experimental trials. The Sub-sections 4.4.1 and 4.4.2 provide details of the Nd:YAG and Yb-fibre laser sources, and the properties of the focussed beams utilised in this research. It was deemed that the above selection of laser sources, combined with the available focussing optics, offered the potential for a wide variation in focussed beam properties suitable for processing the range of titanium sheets acquired.

All the laser sources incorporated beam delivery through a flexible optical fibre to a process head containing the collimating and focussing optics. In all experiments, except those performed with the YLR-4000 Yb-fibre laser, the process head was mounted to a Kawasaki 6-axis robot. The 6-axis robot was used to manipulate the incident angle of the focussed beam and accurately position the beam waist relative to the top surface of the workpiece. An Aerotech x-y manipulation table provided motion of the workpiece relative to the stationary processing head. In experimental work using the YLR-4000 Yb-fibre laser, the focussing head was manipulated with a Cartesian ‘z’ axis traversed over a stationary welding jig.

4.4.1 Nd:YAG Laser Sources

Table 4-3 details the characteristics of the JK1002 and HL4006 Nd:YAG laser sources utilised, and their focussed beam properties. A Trumpf processing head with a collimating optic of 200 mm focal length was utilised for trials with both Nd:YAG laser sources. Focussing optics

of focal length 100 and 150 mm, and 150 and 200 mm were chosen for experimental work performed with the JK1002 and HL4006 Nd:YAG laser sources respectively. Additionally, a HIGHYAG process head with 200 mm focal length collimating optic, and 150 mm focal length focussing optic was used in combination with the HL4006 Nd:YAG laser source. The HIGHYAG process head incorporated a beam splitting module which allowed two focussed beams, of 450 μm beam waists, to be produced from one collimated beam.

Table 4-3. Characteristics of the GSI-Lumonics JK1002 and Trumpf HL 4006 Nd:YAG laser sources , and their focussed beam properties.

Parameters	**Laser Source**			
	JK1002		HL4006	
Maximum output power, W	2000		4000	
Maximum Average power, W	1000		4000	
Modulation waveforms	sine, square		square	
Modulation frequency, Hz	≤1000		≤500	
Delivery fibre diameter, μm	600		600	
Beam parameter product, mm.mrad	25.0		23.0	
Collimating optic focal length, mm	200		200	
Focussing optic focal length, mm	100	200	150	200
Raw beam diameter, mm	33.3	33.3	30.6	30.6
Nominal beam waist, μm	300	600	450	600
Focussing cone half angle, degrees	9.46	4.76	5.84	4.38
Rayleigh length, mm	0.90	3.60	2.20	3.91
Depth of Focus (5%), mm	0.57	2.29	1.40	2.49

4.4.2 Yb-fibre Laser Sources

Table 4-4 details the characteristics of the YLS-1000 SM, YLR-4000 and YLS-5000 Yb-fibre laser sources, and their focussed beam properties. An Optoskand process head with a collimating optic of 160 mm focal length was utilised for the experimental trials with the YLS-1000SM and YLS-5000 Yb-fibre lasers. Three different focal length focussing optics (160, 250 and 500 mm) allowed a number of different focussed beams to be employed. Research with the YLR-4000 Yb-fibre laser was performed at the Fraunhofer IWS, Dresden, Germany, with a process head assembled by Fraunhofer IWS.

Table 4-4. Characteristics of the IPG YLS-1000 SM, IPG YLR-4000 and IPG YLS-5000 Yb-fibre laser sources, and their focussed beam properties.

Parameters	**Laser Source**							
	YLS-1000 SM			YLR-4000		YLS-5000		
Maximum output power, W	1000			4000		5000		
Delivery fibre diameter, μm	17			50		150		
Beam parameter product,	0.39			1.6		6.0		
Collimating optic focal length,	160			120		160		
Focussing optic focal length,	160	250	500	300	500	160	250	500
Raw beam diameter, mm	14.68	14.68	14.68	15.35	15.35	25.59	25.59	25.59
Nominal beam waist, μm	17	27	53	125	208	150	234	469
Focussing cone half angle,	2.63	1.68	0.84	1.47	0.88	4.57	2.93	1.47
Rayleigh length, mm	0.19	0.45	1.81	2.44	6.78	0.94	2.29	9.16
Depth of Focus (5%), mm	0.12	0.29	1.15	1.56	4.32	0.60	1.46	5.83

4.5 Procedures

4.5.1 Beam Waist Position and Power Measurements

The position of the beam waist with respect to the top surface of the test piece was measured by performing a series of low-power constant-energy laser beam releases on anodised aluminium sheet with the height of the process head increased/decreased between successive releases. The distance adjusted between successive releases was dependent upon the calculated Rayleigh length of the focussed beam. Measurement of the spot sizes (measured based on the removal of the black anodised layer) was performed with an optical microscope, allowing the beam waist position to be determined. A piece of processed anodised aluminium plate that had been used for determining the position of one of the beam waists used in this research is shown in Figure 4-1.

Figure 4-1. Anodised aluminium plate which had been subjected to constant energy beam releases, with the beam waist positioned at different distances from the top surface of the plate.

Power measurements were performed before and after a series of experiments utilising the same laser source and optical set-up. The requested power was correlated with the measured power using a water-cooled power meter, manufactured by Ophir Optronics Ltd. An average of three readings was taken provided the values were in close agreement. Unless stated otherwise, the power reported in all subsequent experiments is the power measured at the workpiece (i.e. after all optical elements in the beam delivery system).

4.5.2 Test Piece Clamping

The same steel clamping jig, incorporating a copper efflux channel, was utilised for all experiments. Top-down clamps were utilised in all melt runs and butt welds, allowing the clamping pressure applied to the test piece to be adjusted in order to ensure it remained horizontal along its entire length. Additionally, transverse clamps were employed for butt welds to ensure the gap between the abutting edges remained tight and constant. Figure 4-2 details the typical experimental set-up.

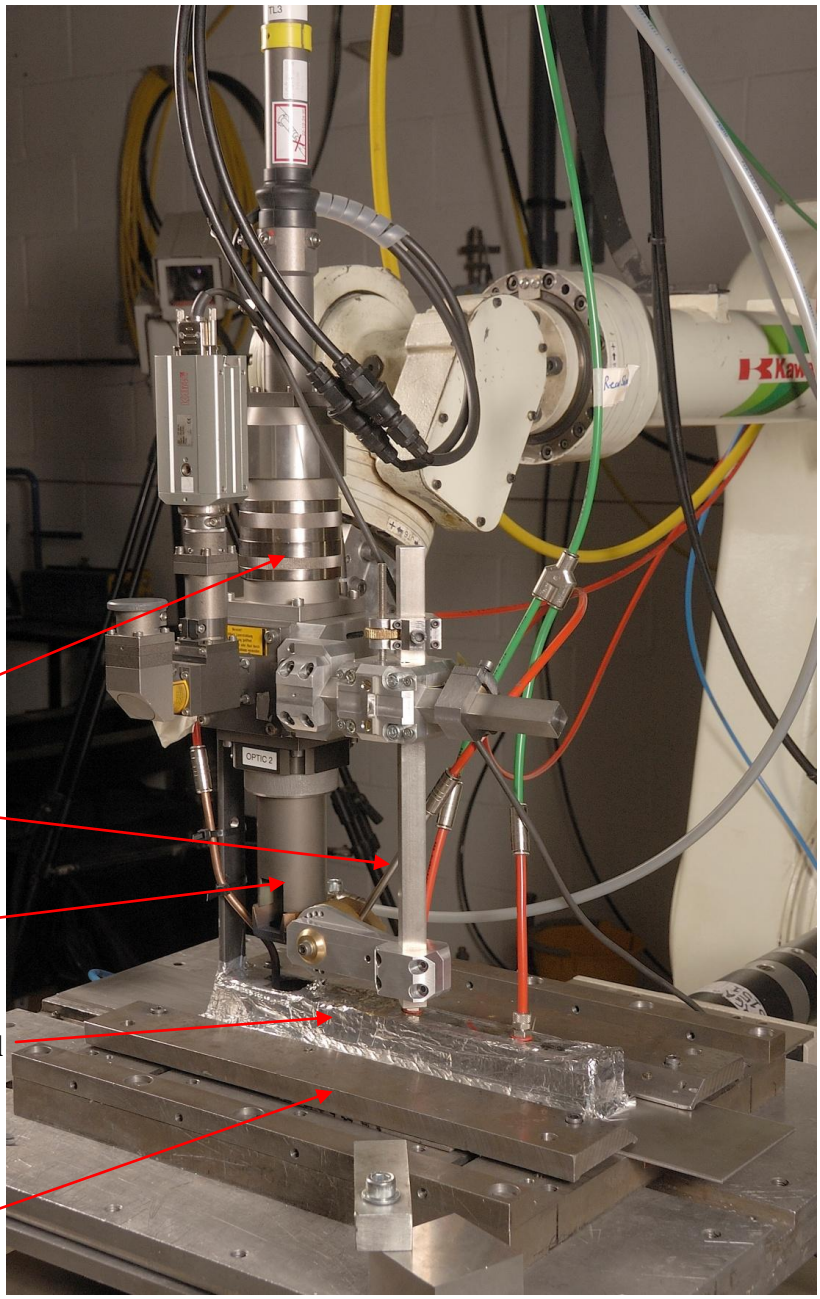

Figure 4-2. Typical experimental set-up, showing: the clamping jig; the shielding shoe; the process head; the air-knife; and, the bracket used for positioning of the directed gas jet.

4.5.3 Shielding Gas

As stated previously, titanium has a high affinity for light elements (such as H, N and O) at temperatures exceeding 500°C, and consequently the melt pool and cooling weld metal must be shielded with an inert gas to prevent discoloration and embrittlement of the weld bead. The weld face and root were shielded with argon gas, of 99.998% purity (BS EN ISO 14175), delivered through a trailing shield and a 10 mm^2 section copper efflux channel respectively. The shielding gas was delivered through three 4.0 mm diameter orifices at different locations

along the top of the trailing shield; 15 mm in front of the laser impingement point, and 83 and 171 mm behind the laser impingement point. A flexible 'skirting' material attached to the trailing shield ensured a smooth interface with the workpiece and reduced the potential of air entering the shield. For the experiments performed with the JK1002, HL4006, YLS-1000SM and YLS-5000 laser sources, the trailing shield was supplied with 30 ℓmin^{-1} of argon gas (measured using Platon flow meters), directed to the three entry locations simultaneously, and 5 ℓmin^{-1} argon was supplied to the efflux channel. The shielding gas was not controlled in the same way when welding with the YLR-4000 Yb-fibre laser and, consequently, the flow rates were adjusted until bright silver weld face and root beads were achieved. The focussing optic was protected with a cover slide and a high pressure transverse air knife positioned between the lower surface of the focussing lens and the workpiece in all the experiments performed.

4.5.4 Directed Gas Jet Positioning

A directed jet of inert gas, aligned towards the laser beam/material interaction point, was utilised in one phase of experiments (detailed in Section 4.9). A dedicated bracket was manufactured to allow the positional parameters associated with the gas jet to be set to the accuracy required. A CMOS camera/monitor system, arranged co-axially with the laser beam allowed the impingement point of the gas jet with the workpiece to be positioned with an accuracy of <0.25 mm. A Platon flow meter allowed the flow rate of gas to be set with an accuracy of ±0.5 ℓmin^{-1}. The generic set-up of the bracket is shown in Figure 4-2. Figure 4-3 shows the co-axial camera system used to position the directed gas jet.

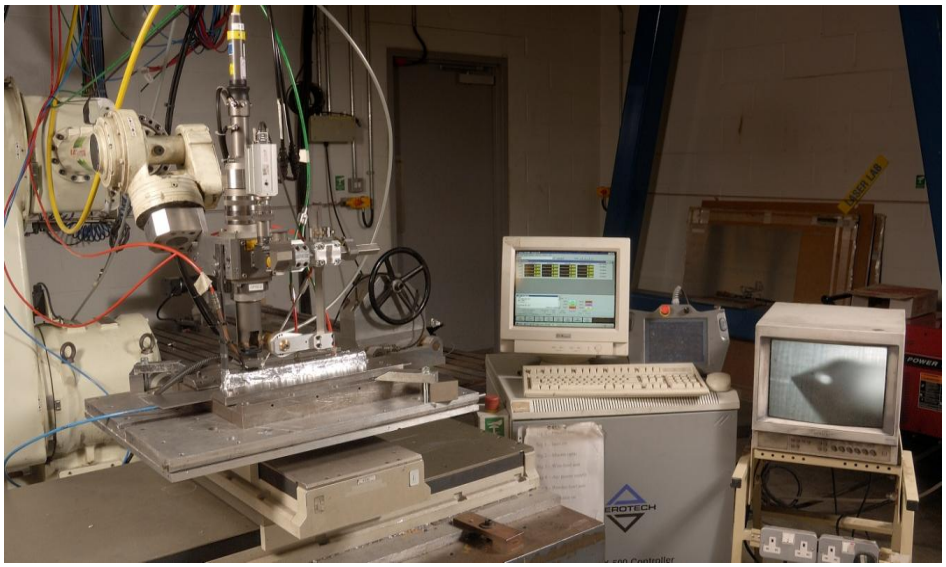

Figure 4-3. Experimental set-up showing the positions of the robot, Aerotech table and controller, and the co-axial camera system used to position the directed gas jet.

4.5.5 Modulated Waveform Programming

The JK1002 Nd:YAG laser is a super-modulated laser source and is specifically designed to deliver a modulated power output. The required output was achieved by selecting the frequency, peak power and one of two waveforms available (sine or square wave). Utilisation of a pulse-shape editor allowed a modulated power output to be emitted from the HL4006 Nd:YAG laser. A minimum segment time of 1 ms was viable with the HL4006 Nd:YAG laser which allowed a maximum modulation frequency of 500 Hz. Example modulated waveforms are shown in Figure 4-4.

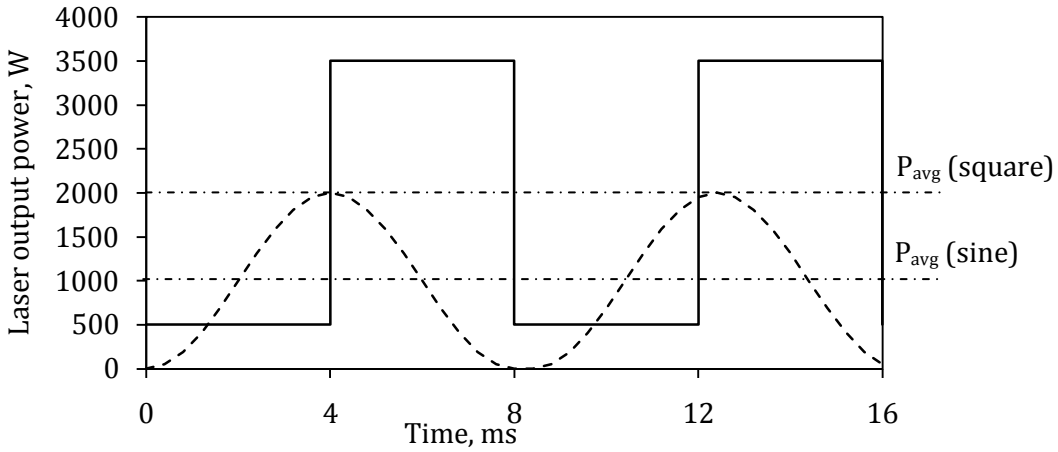

Figure 4-4. Square and sine waveforms with average powers (P_{avg}) of 2.0 and 1kW respectively

4.5.6 Dual Focus Configurations

The HIGHYAG processing head utilised in this research incorporated a transmissive glass prism, which may intercept and refract a proportion of the collimated laser beam. Consequently, two foci can be produced on the surface of the workpiece. The orientation of the two foci with respect to the welding direction can be adjusted through turning the dual focus module through 0-90°, the separation between the two foci (0-1.45 mm), and the relative energy distribution between can be altered through adjustment of two micrometers.

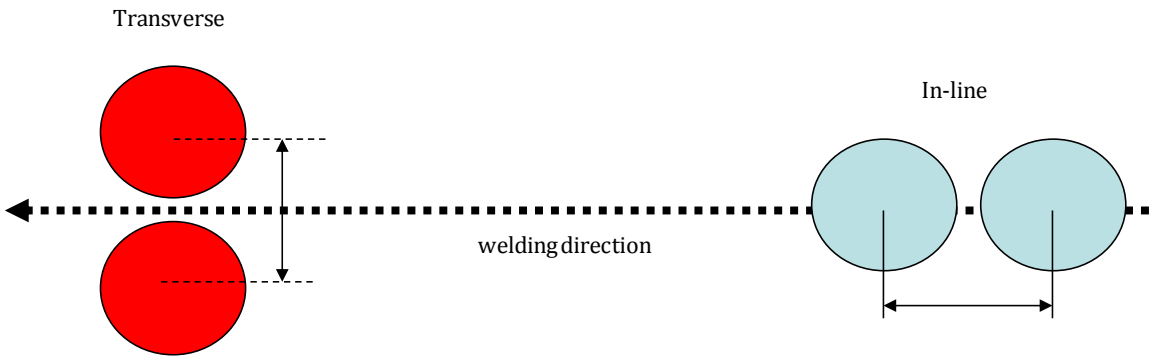

Figure 4-5. Transverse and in-line foci geometry used in the dual focus research.

4.5.7 Wire Feed

For welding trials which utilised wire feed, either a Lincoln Electric Powerfeed or Planetics 501 Saturn wire feeding unit was used. A camera/monitor system, arranged co-axially with the laser beam, allowed the wire tip to be accurately positioned (±0.25 mm) with respect to the laser impingement point. An identical bracket to that utilised for positioning of the directed gas jet allowed the positional parameters of the wire feeding unit to be accurately set.

4.6 High Speed Video Observations

In order to understand the effects of key process parameters on the keyhole laser welding process, high speed video observation (at up to 10 kHz imaging frequency) of the keyhole, melt pool and/or plume behaviour as performed during selected melt run trials. Observation of the process using a micro-focussed X-ray transmission system, such as that utilised by the Joining and Welding Research Institute (JWRI) in Osaka, Japan, could provide important information regarding the dynamic behaviour of the keyhole and melt pool through the thickness of the workpiece which cannot be obtained by high speed video observations. However, the design, manufacture and operation of such a system were not feasible within the timescales of this project. If necessary, the data generated from high speed video observations could then be related back to published findings of the JWRI to gain an understanding of the through thickness behaviour of the keyhole and melt pool.

The typical high speed video equipment configuration is shown in Figure 4-6. In general, a high speed camera observed the vapour plume behaviour (camera with a horizontal inclination of ~5°) and a secondary high speed camera observed the keyhole/melt pool behaviour (camera with a horizontal inclination of 45°). Co-axial observation of the welding process was difficult to achieve at an acceptable frame rate and image quality. Alignment of

the camera through an optics branch on the processing heads was possible although the images were always defocussed and/or obscured as a result of the vapour plume emitted from the keyhole laser welding process. For this reason, only high speed observation with the cameras orientated in lateral positions was performed. Fused-silica glass windows were fitted to either side of the shielding shoe to ensure sufficient shielding of the process when performing high speed observations.

Conventional high speed imaging can be utilised to observe the vapour plume behaviour process emissions with temporal filtering (i.e. shortened exposure times) ensuring that the images were not over exposed. However, conventional high speed imaging techniques cannot be used to image the keyhole/melt pool behaviour because of the high intensity broadband process emissions. Temporal filtering combined with spatial/wavelength filtering (i.e. a narrow bandpass interference filter) were used to effectively eliminate the process emissions. Low power laser sources, such as those detailed in Sub-section 4.6.2, synchronised with the high speed camera provided monochromatic illumination of the keyhole laser welding process.

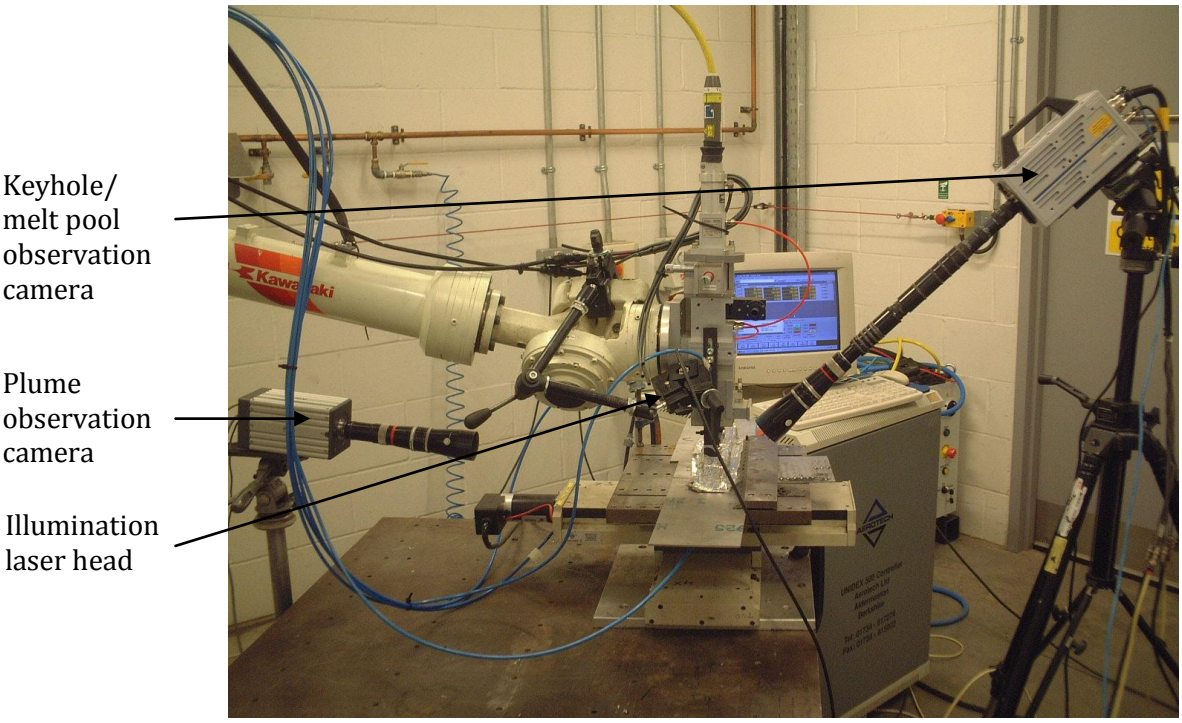

Figure 4-6. Typical configuration of the high speed video equipment.

4.6.1 High Speed Cameras

Achieving an acceptable image quality, such that the pictures could be both post-processed with the techniques detailed in Sub-section 4.6.3 and observed by eye, required a balance

between the imaging frequency and the image resolution. For the high speed cameras available during this project, this equilibrium occurred at an imaging frequency of approximately 10 kHz, which correlated well with the operational limits of the illumination laser sources. Observation of the vapour plume behaviour was performed in all cases with a MotionPro X4 camera (colour), which provided a resolution of 256 by 512 pixels at an imaging frequency of 10 kHz. A 150 mm focal length lens with 50 mm of extension tubes resulted in a field of view of approximately 3 mm by 5 mm. For the majority of keyhole/melt pool observations, a Photron SA-3 camera (monochrome) was utilised, which provided a resolution of 512 by 512 pixels at an imaging frequency of 10 kHz. A 150 mm focal length lens with ~400 mm of extension tubes gave a field of view of 2 mm by 2 mm. On a small number of occasions, observation of the keyhole/melt pool behaviour was performed with a Photron Fastcam MC-1 (monochrome) camera which offered a resolution of 512 by 512 pixels at an imaging frequency of 2 kHz. As before, a 150 mm focal length lens, but with no extension tubes, was used with this camera resulting in a field of view of 13 mm by 13 mm.

4.6.2 Illumination Laser Sources

To provide illumination of the keyhole/melt pool, three different pulsed laser sources were utilised at various points in this project; a LS20-50 copper vapour laser, a Cavilux® Smart diode laser, and a Cavilux® HF diode laser. For each laser source, the keyhole/melt pool observation camera was synchronised with the laser source by employing the camera as the master and the laser as the slave. A delayed signal sent from the master camera to the plume observation camera ensured the plume observation was not obscured by the illumination laser.

The LS20-50 copper vapour laser, manufactured by Oxford Lasers Ltd., emitted laser light at a dominant frequency of 511 nm (secondary wavelength of 578nm), with an average power of 20 W and pulse durations of ~25 ns. The laser light was delivered to a simple collimating head through a 10 m length optical fibre, allowing the light to be easily focussed and positioned.

Both the Cavliux Smart and HF diode lasers, manufactured by Cavitar Ltd., emitted laser light at a wavelength of 810 nm and are therefore only compatible with monochrome high speed cameras (the spectral response of colour high speed cameras is much lower in the infra-red wavelength range than monochrome high speed cameras). The Cavilux HF diode laser provided a maximum output power of 500 W with a maximum duty cycle of 2%, whereas the Cavilux Smart gave an output power of 200 W and a maximum duty cycle of 1%. As with the

copper vapour laser, the laser light was delivered to a simple collimating head through an optical fibre, allowing the laser beam to be easily focussed and positioned.

Table 4-5. Characteristics of the LS20-50 copper vapour laser (CVL), and the CAVITAR HF and CAVILUX Smart diode lasers.

Characteristic	**Laser type**		
	LS20-50 CVL	CAVITAR HF	CAVILUX Smart
Emission wavelength (nm)	511 and 578	810	810
Average power (W)	20	500	200
Pulse duration (ns)	~25	100-10,000	100-10,000
Maximum frequency (kHz)	50	100	2
Fibre delivered	Yes	Yes	Yes

4.6.3 Post Processing

The observation of the vapour plume and keyhole/melt pool behaviour at a sampling rate of up to 10 kHz, generated a significant quantity of data. Observation of the videos provides qualitative information regarding the effect of parameters on key process mechanisms, such as spatter generation. However, the direct comparison of numerous image sequences by this method would be particularly time-consuming and would not provide a quantitative result. Previous research has reported that fluctuations in the vapour plume are directly related to keyhole instability which can cause weld metal porosity. In order to attain quantitative data, allowing numerous different welding conditions to be directly compared, two MATLAB programs were written to extract and subsequently analyse pixel intensity data from the images.

Images of the vapour plume behaviour were acquired with the MotionPro X4 colour high camera, and consequently each pixel had an associated red, green and blue (RGB) value. A MATLAB program was written to extract the RGB values of individual pixels and convert them into a single value of intensity for each pixel. The resulting set of data, for each welding condition, contains α functions (i.e. number of pixels analysed per frame) with β discrete values (i.e. number of frames analysed). As detailed in Figure 4-7, at heights of 1.0, 2.0, 3.0, 4.0 and 5.0 mm above the laser interaction point, an average intensity value was calculated from three pixels situated in the anticipated path of the incident laser radiation (one at each extreme of the beam, and one in the centre). This allows variations in the vapour plume intensity over the analysed height to be determined.

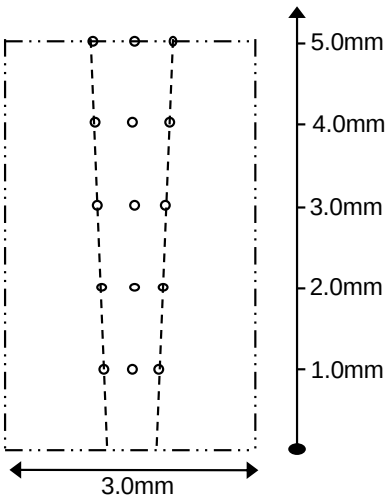

Figure 4-7. Pixel extraction points for vapour plume behaviour. Note: position of points in x-axis is dependent upon the size of the focussed spot and the incident laser beams cone angle.

Statistical analysis of this data provides only static information, such as the mean and standard deviation. For dynamic information, Fourier analysis can be utilised to ascertain the presence of periodic behaviours in the vapour plume behaviour. The discrete Fourier transform of the average values calculated at each height were computed using a fast Fourier transform. 2^{12} (4096) frames were processed for each welding condition, corresponding to a welding time of 0.41 s and resulting in a resolution frequency of ~2.4 Hz. These values could then be correlated with the corresponding weld quality.

If trends were not identified using this method, the mean pixel intensity (MPI) for each frame was calculated, using a MATLAB program, for a region of interest which approximated the position of the vapour plume. The resulting data set contains, for each welding condition, β discrete values (i.e. number of frames analysed) with each value being the MPI for a particular frame. Subsequently, the data could be analysed using statistical techniques or using a fast Fourier transform to calculate the discrete Fourier transform of the data and transform it into the frequency domain. These values could then be correlated with the corresponding weld quality and vapour plume analysis results.

The methods utilised to analyse the keyhole behaviour from the generated keyhole/melt pool observations are analogous to those utilised for the vapour plume behaviour analysis described above.

4.6.4 Optical Spectroscopy

For measurement of metallic vapour spectra emitted during keyhole laser welding of titanium alloys with different process parameters, an Ocean Optics HR4000 spectrometer

was utilised. The spectrometer was calibrated such that it recorded in the range 410-950 nm with a resolution of 0.25 nm. A fibre optic cable, with a core diameter of 400 µm, was utilised to deliver the optical signal to the spectrometer. The Numerical Aperture (NA) of the optical fibre was 0.22±0.02 which corresponds to an acceptance angle of 12.7° (half-angle of the acceptance cone). The optical fibre was positioned such that a plume of 22.5 mm height (from the surface of the workpiece) could be sampled as detailed in Figure 4-8. A bandpass filter was utilised to protect the spectrometer from reflected Yb-fibre laser light (N.B. constant transmission through 410 to 950 nm range).

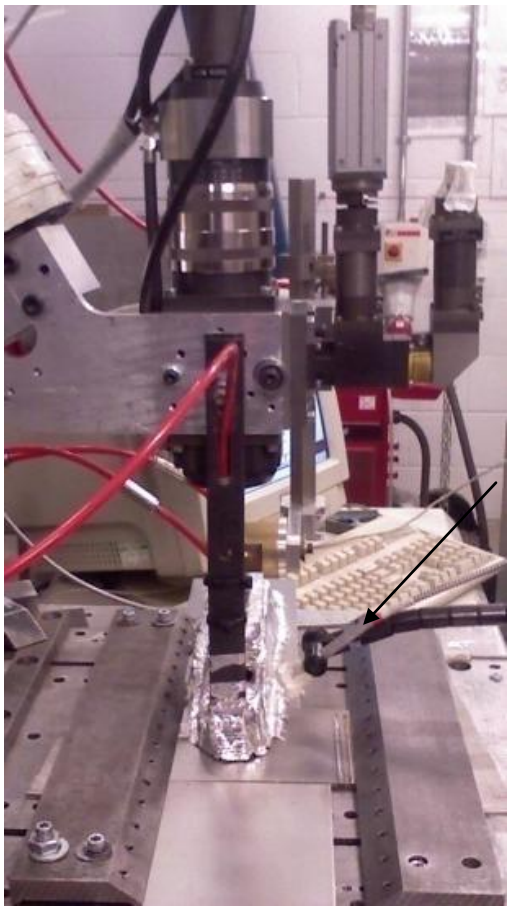

Figure 4-8. Typical configuration/position of the spectrometer's optical fibre end.

The spectrometer was controlled using the OOIBase32 software package, whereby numerous sampling parameters could be controlled. In order to minimise experimental noise, each data set stored to hard disk is an average of three spectra. The dark spectrum (i.e. ambient light) was recorded and subtracted from the recorded spectra, and all spectra were corrected for electrical darkness. Spectra were recorded through a fused-silica glass window, which has the transmission spectrum detailed in Figure 4-9. A small correction factor was applied to each spectrum in order to account for the slight variation in transmission at different wavelengths.

A spectrum was recorded to the hard disk approximately every 70 ms. The recorded spectra were analysed using a MATLAB program to determine the intensity of individual peaks.

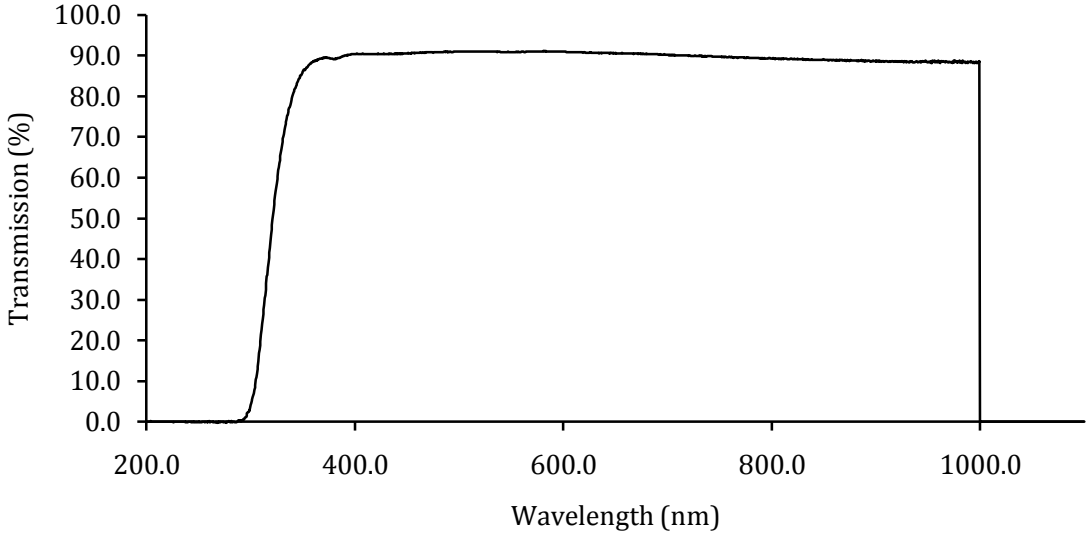

Figure 4-9. Transmission spectrum of the fused-silica glass window.

4.6.5 Particle Sampling

The condensed vapour plume particles, which were typically present on the weld face and/or root in varying quantities (dependent upon the process parameters) were collected from the surface of selected welded samples using a carbon impregnated double sided adhesive tape (to prevent the accumulation of an electrostatic charge), with the tape subsequently adhered to a metal stub. Typical particle sizes were determined using field emission gun (FEG) scanning electron microscopy (SEM). The elements contained in the vapour plume were determined using SEM with energy dispersive X-ray (EDX) analysis.

4.7 Weld Quality Evaluation

4.7.1 Discoloration

All melt runs and butt welds were inspected visually on both the weld face and root for discoloration and are subsequently described according to the discoloration scale outlined in AWS D17.1:2001 and the guide shown in Figure 4-10 [Smith et al, 1999].

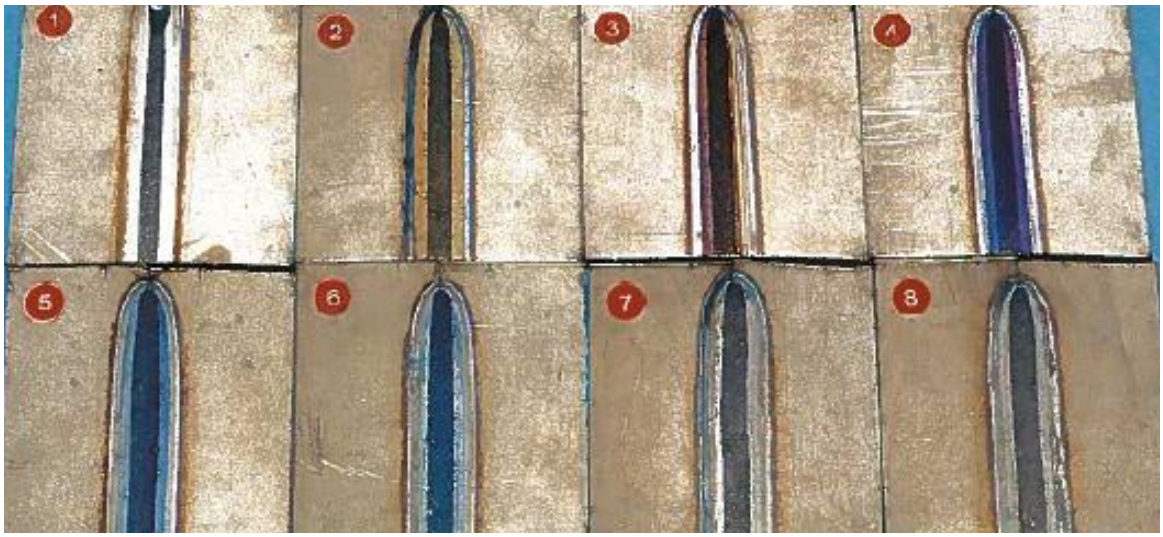

Figure 4-10. TIG welds in commercially pure titanium sheet made with successively greater air contamination of the shielding gas [Smith et al, 1999].

4.7.2 Weld Metal Porosity

Radiographic examination of all melt runs and butt welds was performed according to the standards outlined in BS EN 1435:1997, always using the same equipment and X-ray films of the highest resolution available. A minimum indication size of approximately 0.05 mm was visible on the radiographs, although any indications down at this detection limit had their sizes rounded up to 0.1 mm. Henceforth, all references to 0.1 mm diameter pores therefore include pores in the diameter range from the detection limit up to and including 0.1 mm. Pore counts were always carried out by the same individual on radiographs, over a 76 mm analysis length, as prescribed in AWS D17.1. The pore count is expressed as an accumulated length, defined by AWS D17.1 as the summation of all the pore diameters counted in the 76 mm analysis length. As surface breaking porosity was not detected in any of the melt runs or butt welds examined, all pore counts refer to subsurface, or internal, porosity.

It is acknowledged that a radiographic examination of bead-on-plate melt runs and butt welds is not ideal as the pores are assumed to be spherical. Transverse weld sections have indicated that all the pores observed in the weld metal were spherical. However, in certain instances several pores were found ‘stacked’ on top of each other, with the smaller diameter pores in the stack not visible by conventional two dimensional radiography. For this reason, a small number of samples were analysed using a computed tomography instrument. A Metris X-tek 320 kV Custom Bay fitted with a 225 kV X-ray source and tungsten target, operating at 115 kV and 95 μA was utilised. The resultant three dimensional radiographs had a resolution of 13.2 μm.

4.7.3 Profile

For selected melt runs and butt welds, profile sections were taken transverse to the welding direction. Samples were cut out at positions which were representative of the entire weld length, mounted, ground, polished and etched using an aqueous solution of 10% HF, 25% HNO_3 and 15% HCl. Macrographs of the section allowed accurate measurements of any weld defects at the weld face and/or root to be determined, as well information relating to the weld width at the face, root and centre of the weld. The three dimensional radiographs produced with the computed tomography instrument outlined above were utilised to confirm the consistency of the defects in the weld profile.

4.8 Pore Characterisation

Characterisation of the gas contents of specific pores would provide invaluable data in determining the source and, subsequently, the mechanisms of pore formation. It was detailed in Chapter 2 that the most likely sources of porosity when keyhole laser welding titanium alloys are from the rejection of hydrogen upon weld solidification and/or the entrapment of shielding gases. An ONH-2000 oxygen/nitrogen/hydrogen determinator, manufactured by ELTRA GMBH, was utilised to determine (by hot extraction) the difference in hydrogen content between a small number of welded samples containing porosity and their relevant parent materials. A small number of sectioned weld samples were also viewed using SEM to observe the internal structure of the pores. EDX analysis of the chemical composition of the pores internal walls was also performed to determine if any elements were present in a higher concentration than the parent material.

4.9 Scope of Work

From the previous Section it can be seen that a broad range of solid-state laser sources have been utilised during this research. Different process heads and process head configurations have also enabled focussed laser beams with different characteristics to be utilised.

Furthermore, keyhole laser welding techniques such as welding with a directed gas jet, modulating the output of the laser power, and using a dual focus technique have been examined when welding with the Nd:YAG laser sources. For clarity, and as a pre-cursor to the following results chapters, it is therefore worth outlining the scope of work that has been performed. The experimental research can be efficiently segregated into four distinct phases, as previously indicated.

- Nd:YAG laser welding with a directed gas jet
- Modulated Nd:YAG laser welding
- Dual focus Nd:YAG laser welding
- Welding with excellent beam quality 1 μm wavelength laser sources

Table 4-6 provides details of the laser sources, optical configurations and titanium test pieces utilised for each of the phases of work. Also detailed in Table 4-7 are the weld quality evaluation and process characterisation techniques employed during the individual phases of work.

Table 4-6. Detailed scope of work performed, segregated into four distinct phases.

	Laser source, optical configurations and techniques utilised					
	JK1002 (600µm dia. optical fibre)	HL 4006 (600µm dia. optical fibre)	YLS-1000 SM (17µm dia. optical fibre)	YLR-4000 (50µm dia. optical fibre)	YLS-5000 (150µm dia. optical fibre)	Titanium grades and thicknesses
Nd:YAG laser welding with a directed gas jet	-	Trumpf process head with 200mm F_c† and 200mm F_f‡. Inert gas jet utilised.	-	-	-	3.25mm Ti-6Al-4V, 3.25mm Ti-2.5Cu.
Modulated Nd:YAG laser welding	GSI process head with 200mm F_c and 100 and 200mm F_f. Sine and square waveforms.	Trumpf process head with 200mm F_c and 200m F_f. Square waveforms.	-	-	-	2.0 and 3.25mm Ti-6Al-4V, 3.25mm Ti-2.5Cu.
Dual focus Nd:YAG laser welding	-	HIGHYAG process head with 200mm F_c and 150mm F_f. Dual focussing module.	-	-	-	3.25mm Ti-6Al-4V, 3.25mm Ti-2.5Cu.
Welding with excellent beam quality 1 µm wavelength laser sources	-	-	Optoskand process head with 160mm F_c and 160, 250 and 500mm F_f.	Custom process head with 120mm F_c and 300 and 500mm F_f.	Optoskand process head with 160mm F_c and 160, 250 and 500mm F_f.	2.0, 3.25, 4.0, 5.0, 6.0 and 7.0mm Ti-6Al-4V

† Fc is the focal length of the collimating lens, ‡ Ff is the focal length of the focussing lens.

Table 4-7. Process characterisation and weld quality evaluation techniques utilised for the four distinct phases of work.

	Process characterisation techniques				**Weld quality evaluation techniques**			
	Keyhole/melt pool observation	Vapour plume observation	Optical spectroscopy	Particle sampling	Discoloration	Porosity		Sectioning
						2D X-ray	CT	
Nd:YAG laser welding with a directed gas jet	YES	-	YES	YES	YES	YES	YES	YES
Modulated Nd:YAG laser welding	YES	YES	-	-	YES	YES	YES	YES
Dual focus Nd:YAG laser welding	YES	YES	-	-	YES	YES	YES	YES
Welding with excellent beam quality 1 µm wavelength laser sources	-	-	-	-	YES	YES	-	YES

Chapter 5

Nd:YAG Laser Welding with a Directed Gas Jet

5.1 Introduction

This journal paper was submitted to the *Journal of Laser Applications* on the 21st December 2009 and accepted for publication on the 23rd May 2010. The paper was published on the 23rd July 2010 in the May 2010 edition, volume 22(2), of the *Journal of Laser Applications*. The research for the paper was performed with Dr Chris Allen, Dr Paul Hilton and Professor Lin Li.

In terms of the co-author's involvement, Dr Chris Allen assisted with specifying the range of variables that were considered for the initial welding trials. All the experimental works, including the statistical design and analysis of the experiments was performed by the author of this thesis. Dr Paul Hilton provided guidance and suggested utilisation of high speed video observation techniques to observe the effects of the directed gas jet on the melt pool. Optical spectroscopic analysis of the vapour plume behaviour was performed by the primary author of the thesis. Professor Lin Li gave guidance on the interpretation of the high speed video and spectroscopy results.

Nd:YAG laser welding of titanium alloys using a directed gas jet

Jonathan Blackburn[a)]
Laser Processing Research Centre, The University of Manchester, Manchester M60 1QD, United Kingdom

Chris Allen and Paul Hilton
TWI Ltd., Granta Park, Abington, Cambridge CB21 6AL, United Kingdom

Lin Li
Laser Processing Research Centre, The University of Manchester, Manchester M60 1QD, United Kingdom

(Received 21 December 2009; accepted for publication 23 May 2010; published 23 July 2010)

The increasing utilization of titanium alloys in the aerospace industry, a direct result of socioeconomic pressures, has created the need for a production process which can produce high quality near-net-shape titanium alloy components. Keyhole laser welding is a joining technology which could be utilized for this requirement. In general, when laser welding titanium alloys, a jet of inert gas, directed at the region of the laser beam/material interaction point is utilized to achieve the weld quality required. A statistical study has been performed in order to determine the optimum position and flow rate of this directed gas jet, with respect to reducing the weld metal porosity and optimizing the weld profile, for autogeneous Nd:YAG laser welding of 3.25 mm thickness Ti-2.5Cu and Ti-6Al-4V. As a result, butt welds have been reproducibly made with a quality that exceeds the most stringent aerospace weld quality criteria. High speed imaging and spectroscopic analysis of the welding process have revealed that, when correctly set-up, the directed inert gas jet disperses the formation of excited metal vapor above the keyhole and also significantly changes the hydrodynamic behavior of the weld pool. © *2010 Laser Institute of America.*

Key words: laser, weld, titanium, Nd:YAG, porosity, aerospace

I. INTRODUCTION

The increasing utilization of titanium alloys in the aerospace industry, a direct result of socioeconomic pressures, has created the need for a production process which can produce high quality near-net-shape titanium alloy components. Keyhole laser welding is a joining technology which could be utilized, after appropriate classification of the resultant weld qualities, for this requirement. As a result of their high specific strength, corrosion resistance, fatigue resistance, and their ability to operate at elevated temperatures, titanium alloys are already exploited throughout the aerospace industry. The specific alloy employed depends upon the exact service requirements of the component, but α, α/β, and β alloys are all exploited.[1] Current demand for titanium products in the aerospace industry is primarily being driven by the commercial sector, which is utilizing an increasing amount of titanium alloys to achieve weight savings.[2] The adoption of large volumes of carbon fiber reinforced polymers (CFRPs) into the fuselages of modern airframes is adding further to the use of titanium alloys because of their galvanic compatibility with graphite.

High quality components can be produced by forging and subsequent machining. However, this process is labor intensive and finished components can have uneconomical buy-to-fly ratios. The production of near-net shape components with a high integrity joining process could significantly reduce material wastage and increase production rates. Keyhole laser welding is a high energy density joining technology that produces deep penetration welds with a relatively low heat input when compared to inert gas arc welding. Furthermore, it can be performed at atmospheric pressure and the fiber optic delivery of near infrared laser beams, provides increased flexibility when compared to CO_2 laser systems and other joining technologies. However, the formation of porosity in the weld metal is of particular concern when laser welding titanium alloys with a 1 μm wavelength laser source. For high-performance, fatigue-sensitive components whose weld profiles are dressed, pores can break the surface of the dressed weld and reduce its fatigue resistance.[3] A direct result of this is the stringent weld quality criteria that are applied to welded components in the aerospace industry.[4]

During fusion welding, the formation of porosity in the weld metal can occur as a result of soluble gases dissolved in the weldpool, such as hydrogen, being rejected upon solidification of the molten material. The presence of hydrogen in the joint zone can be significantly reduced by shielding the process with low moisture content shielding gas and a suitable preweld purge time. The hydrogen content in modern titanium alloys is typically <150 ppm and is not of concern. However, since TiO_2 is hygroscopic it will adsorb moisture from the atmosphere and a hydrated layer will form on the surface of the parent material. Removal of this layer prior to welding has been reported to reduce weld metal porosity in laser welded titanium alloys.[5]

[a)]Electronic mail: jon.blackburn@affiliate.twi.co.uk

TABLE I. Chemical compositions of the titanium alloys investigated.

Material	Element, wt% (except where stated ppm)								
	C	Al	Cu	Fe	H (ppm)	N	O	V	Ti
3.25 mm Ti-2.5Cu	0.006	<0.01	2.34	0.07	17	0.006	0.16	<0.01	Bal
3.25 mm Ti-6Al-4V	0.011	6.33	<0.01	0.20	61	0.007	0.16	3.83	Bal

It has been reported that keyhole instability can lead to metal vapor and/or inert shielding gases being trapped in the weld metal.[6] This occurs when the forces trying to hold the keyhole open (i.e., vaporization pressure and radiation pressure) are not in equilibrium with those trying to close it (i.e., surface tension, hydrostatic pressure, and hydrodynamic pressure).[7] The vaporization pressure can be affected by a vapor plume exiting the keyhole that attenuates the incident laser radiation. The specific attenuation mechanism(s) depends upon the wavelength and power density of the laser beam, as well as the chemical properties of the workpiece.[8] As the dynamic behavior of the vapor plume is not constant the power density delivered to the workpiece can fluctuate.[9] Consequently, changes in vaporization pressure can lead to an unstable keyhole, periodic collapses of the keyhole, and the generation of porosity in the weld metal.

When welding C-Mn steel with a CO_2 laser it has been demonstrated that the primary mechanisms responsible for beam attenuation are absorption and defocusing of the laser radiation through a partially ionized plasma with a gradient refractive index.[8] For CO_2 laser welding of titanium alloys, it has been reported that shielding of the weld pool with helium gives a higher weld quality than when using argon shielding gas.[10] This is a result of the lower ionization potential of argon, which promotes inverse Bremsstrahlung absorption of the incident 10.6 μm laser radiation at lower irradiances than when helium shielding is used. The use of helium shielding gas can therefore reduce the variation in the vaporization pressure and increase keyhole stability/internal weld quality. Conversely, for Nd:YAG laser welding, of C-Mn steels at least, beam attenuation takes place by absorption and scattering of the laser light by a population of Fe nanoparticles ($\sim$50 nm in diameter).[8,11]

Previous studies have shown that an inert gas jet, directed toward the laser beam material interaction point, can reduce the occurrence of weld metal porosity when CO_2 or Nd:YAG laser welding of 304 stainless steel.[12–14] Furthermore, recent publications have reported that butt welds in titanium alloys with a low level of weld metal porosity can be produced using a near-infrared laser beam.[4,15] In order to achieve a low level of weld metal porosity, both Hilton *et al.*[4] and Mueller *et al.*[15] reported the use of an inert assist gas. No information regarding the parameters associated with this assist gas jet were disclosed by the authors. It is not known whether these parameters have been optimized and what the set-up tolerances are if a consistently low level of weld metal porosity is to be achieved.

In this paper, the directed gas jet parameters for Nd:YAG laser welding of 3.25-mm-thick titanium alloys have been optimized, with respect to minimizing weld metal porosity and achieving a favorable weld profile, using a parametric approach. Furthermore, the interaction between the directed gas jet and the welding process has been observed with a high speed camera, and the vapor plume has been characterized.

II. EXPERIMENTAL PROCEDURES

A. Laser welding procedures

Experimental trials were performed on 3.25-mm-thick Ti-2.5Cu and Ti-6Al-4V (Table I). The materials had been chemically pickled after rolling, although the time between pickling and welding was not controlled. Immediately prior to performing bead-on-plate (BOP) tests, the surfaces of test pieces were cleaned with an abrasive paper and acetone degreased. An identical procedure was followed when performing butt welding trials, except that the abutting edges of the test pieces were dry machined prior to abrading and degreasing.

A Trumpf HL4006D Nd:YAG laser source was utilized for all welding trials. Relevant information for the laser source and its focused beam is shown in Table II. The process head was attached to a Kawasaki JS30 robot, which allowed accurate control of the focal plane position. The average laser powers at the workpiece were measured using a water cooled Ophir power meter. A measured power of 4.1 kW (at workpiece) was used in all trials. The focusing optic was protected with a high pressure air-knife and a cover

TABLE II. Trumpf HL4006D Nd:YAG laser source information and focused beam properties.

Delivery fiber diameter, μm	600
Nominal beam parameter product, mm.mrad	23.2
Collimating lens focal length, mm	200
Focusing beam focal length, mm	200
Nominal beam diameter at waist position, μm	600
Calculated beam focusing angle, °	4.42
Nominal power density (at beam waist for 1 kW), kW/mm^2	3.54
Calculated Rayleigh length, mm	±3.88
Calculated depth of focus (5%), mm	±2.47

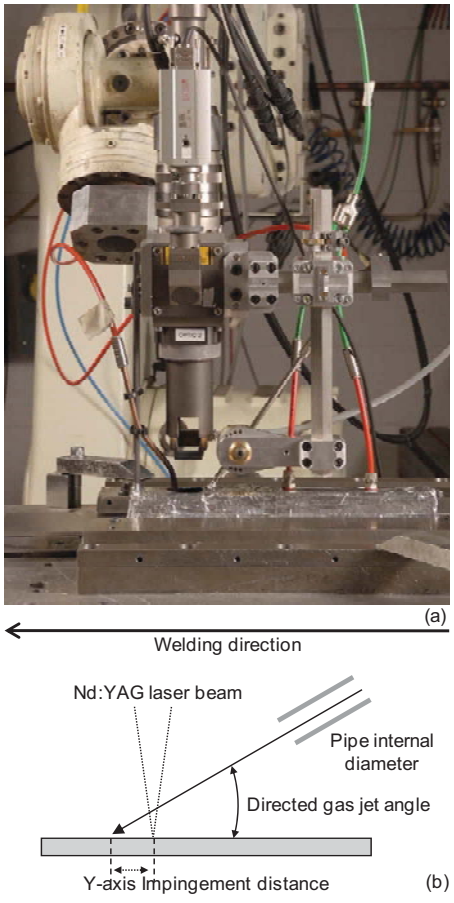

FIG. 1. (a) Experimental setup and (b) schematic of the directed gas jet configuration.

slide positioned between the lower surface of the focusing lens and the workpiece. All BOP tests and butt welds were performed in the 1 G position.

Since titanium reacts with oxygen and nitrogen at relatively low temperatures (~500 °C), a stainless steel trailing shoe was used to prevent oxidation and embrittlement of the weld metal. The trailing shield and a 10 mm^2 cross-section copper efflux channel were both supplied with a regulated supply of pureshield argon (gas type I1 to BS EN 14175).[16] A directed jet of pureshield argon was used in the majority of experiments. The positional parameters of the argon jet could be manipulated by the use of a dedicated bracket, and the flow rate of gas was measured using a Platon flow meter. Figure 1 details the experimental setup.

B. Parametric study

A three stage parametric study, consisting of preliminary screening trials and two separate design of experiments (DOE), was carried out in order to determine the significant processing variables and their optimum values with respect to minimizing weld metal porosity (the response variable investigated). Initially, the effects of seven processing variables on the weld metal porosity were evaluated. The variables investigated are given in Table III. Evaluation of the weld metal porosity and profile results from these experiments allowed the range of variables examined in the first DOE to be defined. A two-level factorial experiment was created, using DESIGN-EXPERT software, for four process variables (i.e., 2^4) associated with the directed gas jet. The results from this DOE were subsequently used to define the range of variables investigated in the second DOE—a general factorial experiment used to determine the optimum position of the directed gas jet and its operating windows if a consistently low-level of weld metal porosity is to be achieved.

C. Weld quality assessment

All BOP tests and butt welds were assessed visually for oxidation. Radiographic examination was performed, according to BS EN 1435:1997,[17] to determine the weld metal porosity content, which allowed indications ≥0.05 mm in diameter to be detected. Selected samples were also sectioned, transverse to the welding direction, at representative positions, to assess their weld profile. Weld profile and weld metal porosity results were compared to typical aeroengine quality criteria, as reported previously by the authors.[4] Table IV details the weld quality criteria.

D. Process characterization

High speed video observations and optical spectroscopy were performed during selected welding experiments. A Photron Fastcam MC1 high speed video camera was utilized to observe the behavior of the keyhole and the weld pool

TABLE III. Process variables investigated.

Variables	Fixed value or range investigated		
	Initial trials	First DOE	Second DOE
Welding speed (mm/s)	10 to 100	67	67
Laser focal plane position (mm)	+3 to −3	0	0
Directed gas type	Argon, helium	Argon	Argon
Directed gas jet pipe internal diameter (mm)	1.4, 2.0, 4.0	4.0	4.0
Measured gas flow rate (l/min)	5 to 26	16, 20	16, 18, 19
Directed gas jet angle off plate surface (deg)	30 to 55	35, 55	35, 45, 55
Y-axis impingement point of gas jet axis (mm)	0 to 3.0	1.5, 2.5	1.5, 1.75, 2.0, 2.25
X-axis impingement point of gas jet axis (mm)	0	−0.5, 0.5	0

TABLE IV. Typical aeroengine weld quality criteria for 3.25-mm-thick titanium alloys. Derived from Hilton *et al.* (Ref. 4).

Weld profile		Subsurface porosity	
Undercut (Ca) (mm)	0.16	Maximum dimension for a single pore, mm	1
Excess weld metal (R) (mm)	0.69	Accumulated length in 76 mm of weld, mm	1.7
Excess penetration (r) (mm)	0.69		
Incompletely filled groove (Cr) (mm)	0.33		
Root concavity (cr) (mm)	0.33		
Shrinkage groove (ca) (mm)	0.33		
Face weld width (L) (mm)	<4.2		
Minimum weld width (I_0) (mm)	$1.1<I_0<2.1$		
Root weld width (I) (mm)	$1.1<I<4.2$		

during selected welding experiments. Temporal and spatial filtering effectively eliminated the inherently bright process emissions and a CAVILUX® Smart fiber-delivered diode laser (808 nm) provided illumination. An Ocean Optics HR4000 spectrometer was utilized to record the spectrum of the vapor plume. The spectrometer was calibrated such that it recorded in the range 400–1000 nm with a spatial resolution of 0.3 nm and a sampling frequency of ~30 Hz. The spectrometer was controlled using the OOIBASE32 software package and the recorded data analyzed using MATLAB. Furthermore, typical condensed vapor plume particle sizes were determined using field emission gun (FEG) scanning electron microscopy (SEM). The elements contained in the vapor plume were determined using conventional SEM with energy dispersive x-ray (EDX) analysis.

III. RESULTS AND DISCUSSIONS

A. Parametric study

1. Initial BOP tests

Autogeneous BOP tests were produced at welding speeds between 10 and 100 mm/s, and at different focal plane positions without using a directed gas jet. The weld face and root of all the BOP tests were bright silver in color, indicating that they had been adequately shielded. A welding speed of 67 mm/s was the fastest welding speed that gave a consistent fully penetrating weld, with a root wide enough for practical application.

Numerous BOP tests were performed at a welding speed of 67 mm/s with different combinations of parameters shown in Table III. Not all permutations of the parameters were performed. With certain parameter combinations, the weld quality criteria stipulated in Table IV could be achieved. In general, lower weld metal porosity results were achieved with the laser beam focal plane positioned on the surface of the workpiece, when using argon rather than helium, and with a 4.0 mm internal diameter pipe. Henceforth, these parameters were fixed to the above values. A large variation in the weld metal porosity, both in terms of the number and size of pores, was observed with relatively small adjustments in the remaining parameters.

2. First design of experiments

In order to determine the significance of single factors as well as two and three level factor interactions, on the weld metal porosity, a two-level factorial experiment for four variables (shown in Table III) was designed using the DESIGN-EXPERT software. The variables examined were the measured gas flow rate (variable A), the jet angle off the plate surface (variable B), the impingement point of the jet axis ahead of laser impingement point (variable C), and the impingement point of the jet axis with respect to either side of the joint line (variable D). The values of the variables examined in this DOE were chosen based on the results of the earlier trials. Experimental noise was reduced by choosing parameter values that were expected to produce fully penetrating BOP tests, performing three replications of each parameter set, and randomization of the run order.

Radiographic evaluation of the weld metal porosity revealed a range of contents depending on the gas jet condition used, with 25 of the 48 BOP tests meeting the internal weld quality criteria stipulated in Table IV. Using the DESIGN-EXPERT software, statistically significant factors were selected, including those supporting hierarchical terms. An analysis of variance (ANOVA) model including these terms was fitted to the natural logarithm of the response variable. A single BOP test did not fit this model and was excluded from further analysis. The t values of the factors, and their interactions, are shown in Table V. The t values suggest that variable C is several times more significant in its effect on internal porosity content than the next most significant factors, B and A. However, it should be noted that these values are only relevant to the high-low range of values used in the study, as chosen from initial screening trials, whereby some parameters may have been closer to their optimum settings than others.

All but one of the BOP tests made with a flow rate of $16\ell/\text{min}$ were silver colored in appearance, indicating adequate shielding. Conversely, most of the BOP tests produced with a flow rate of $20\ell/\text{min}$ were oxidized, ranging from light straw to blue colored. This is a result of turbulence in the shielding shoe and air being drawn in, allowing the weld metal to oxidize. Fine spatter was

TABLE V. ANOVA table of weld metal porosity model from the first DOE.

Source	Σ squares	Df	Mean square	F value	Prob >F	Significance
Model	27.21	11	2.47	63.43	<0.0001	Significant
A-flow rate	0.79	1	0.79	20.21	<0.0001	Significant
B-angle	1.38	1	1.38	35.49	<0.0001	Significant
C-Y offset	23.04	1	23.04	590.80	<0.0001	Significant
D-X offset	0.094	1	0.094	2.41	0.1299	Not significant
AB	0.031	1	0.031	0.79	0.3793	Not significant
AC	0.29	1	0.29	7.44	0.0099	Significant
BC	0.064	1	0.064	1.64	0.2088	Not significant
BD	0.40	1	0.40	10.15	0.0030	Significant
CD	0.018	1	0.018	0.45	0.5049	Not significant
ABC	0.46	1	0.46	11.91	0.0015	Significant
BCD	0.36	1	0.36	9.15	0.0046	Significant
Lack of fit	0.14	4	0.034	1.14	0.3553	Not significant
Pure error	0.92	31	0.030			
Cor total	30.41	46				

invariably present on the underside of all the BOP tests but could be much reduced on the top side if certain gas jet conditions were used.

3. Second design of experiments

A general factorial parametric study was designed in order to determine the optimum position of the gas jet and the flow rate through it, with respect to minimizing weld metal porosity content. The values used for these three factors were chosen based on the results of the first DOE and are given in Table III. The directed gas jet was pointed directly at the joint line, to conserve symmetry. All other parameters were fixed at the same values as used in the first DOE. A total of 36 individual BOP tests were made. The order in which these were made was again randomized. The first DOE had indicated that results were sufficiently reproducible to forgo repeats, particularly when a given combination of parameters led to a low internal porosity content weld. All BOP tests produced were fully penetrating and bright silver in color.

Statistical analysis of the porosity formation data was performed using the DESIGN-EXPERT software package. An appropriate power transformation (in this case a natural log transformation) was determined using a Box-Cox plot. Factors to be included in the polynomial model were selected using a backward selection with an Alpha out value of 0.100. Further diagnostic graphical plots (e.g., normal plot of studentized residuals, externally studentized results, and the studentized residuals versus predicted values) were utilized to check for any time-related variables unaccounted for and any data points having an excessive influence and/or leverage on the model. None of the data points were found to be problematic. An ANOVA analysis was performed and a calculated Model F-Value of 16.56 implied that the model was significant. This analysis confirms that the statistically significant terms in this model are; the jet angle off the plate surface (B), the impingement point of the jet axis ahead of the laser impingement point (C), and the measured gas flow rate (A). Additionally the factor BC was found to be significant suggesting that the height above the keyhole at which the gas jet passes is important. The terms AB, AC, and any high order terms were determined to be statistically insignificant. A cube plot of the three factor interactions is shown in Fig. 2. The final equation in terms of the natural log of the accumulated length of porosity and for the actual factors is shown below;

$$\mathrm{Ln(Porosity)} = +3.68 - (0.126A) - (0.081B) - (2.064C) + (0.071BC). \quad (1)$$

It should be remembered that this equation is only valid within the range of parameters investigated in the second DOE. Comparison of the relative significances of factors determined from the first and second DOEs revealed some differences. In the first DOE, factor C was the most significant. In the second DOE, factor C was only the second most significant. However, in the second DOE a smaller range for factor C had been chosen deliberately, this being perceived as a parameter requiring tight control for achievement of low internal porosity content. Therefore,

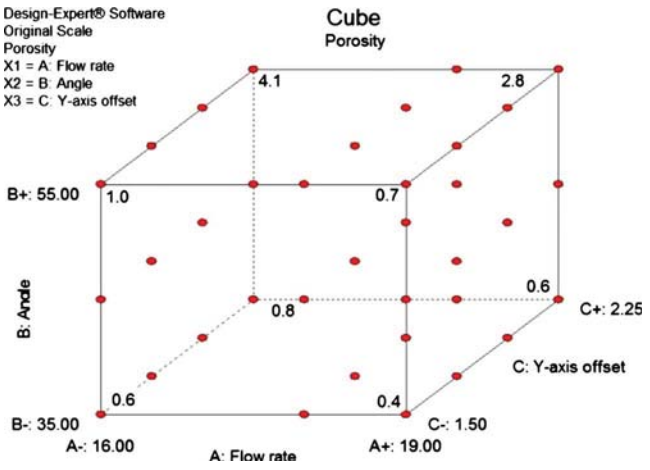

FIG. 2. Cube plot of the three factor interactions from the second DOE.

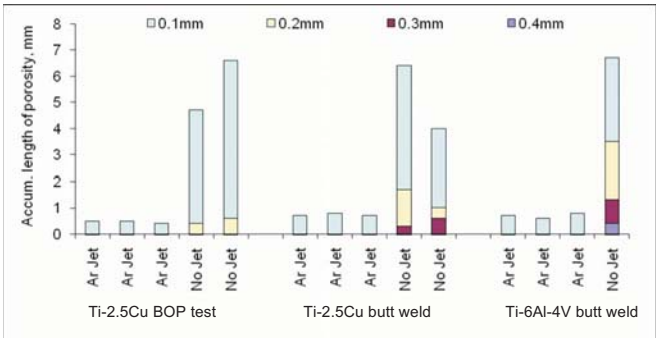

FIG. 3. Weld metal porosity in Ti-2.5Cu BOP tests and butt welds and Ti-6Al-4V butt welds—for optimized directed gas jet conditions and no directed gas jet.

using such a small range, the second DOE determined C to be of less absolute significance than it actually was. A similar situation also held true for factor A, in that both DOEs determined this to be a less significant factor. Nevertheless, the range of factor A was tightly controlled deliberately in both DOEs, as the earlier screening trials had indicated this was necessary.

B. Optimized weld quality

Butt welds in 3.25 mm thickness Ti-2.5Cu and Ti-6Al-4V were made with the optimized directed gas jet conditions determined from the second DOE. For comparison, butt welds were also made under the same conditions without using a directed gas jet. All welds were fully penetrating and bright silver in color. Any spatter on the weld face was avoided when using the directed gas jet. The porosity content of the weld metal is shown in Fig. 3. The maximum pore diameter of 0.4 mm was reduced to 0.1 mm by using the optimized directed gas jet. The accumulated length of porosity was reproducibly reduced in all cases to within internal aeroengine standards. These results suggest that these gas jet conditions can be used successfully when butt welding both Ti-2.5Cu and Ti-6Al-4V, producing welds that easily meet all the subsurface porosity criteria stipulated in stringent aeroengine standards. Figure 4 details the cross sections of butt welds made with and without a directed gas jet in both Ti-2.5Cu and Ti-6Al-4V. The welds made with a directed gas jet are free of top bead undercut, but both have a small amount of root undercut, to a maximum defect depth of 0.06 mm. Conversely, in the welds made without a directed gas jet, an unacceptable level of both top bead and root undercut is observed. Those BOP tests or butt welds produced with an optimized directed gas jet met all of the weld quality criteria stipulated in Table IV.

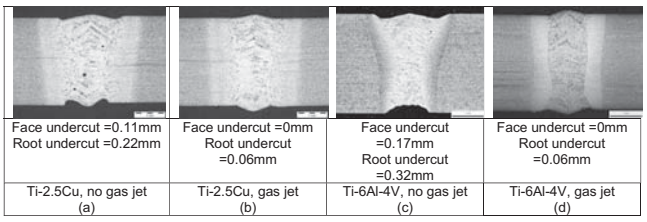

FIG. 4. Weld profiles of Ti-6Al-4V and Ti-2.5Cu butt welds produced—for optimized directed gas jet conditions and no directed gas jet.

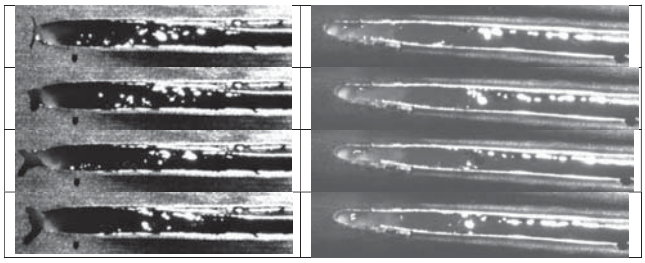

FIG. 5. High speed images of Nd:YAG laser welding of Ti-2.5Cu without (left) and with (right) an optimized a directed gas jet, 0.5 ms intervals.

C. High speed video observation

Selected images from high speed observations of BOP melt runs made in Ti-2.5Cu without and with an optimized directed gas jet are shown in Fig. 5. Without the gas jet the keyhole frequently collapses and much spatter is ejected from the front of the keyhole. This is most likely the result of the keyhole momentarily being covered over by molten metal (keyhole collapse), vapor pressure in the keyhole then leading to the ejection of this overlying molten material. This also explains the presence of top surface weld spatter, undercut and underfill observed in welds made without the argon gas jet. Conversely, when welding with a gas jet, the keyhole is markedly more constant in size and quiescent, and the keyhole does not collapse. Consequently, no top bead weld spatter is observed, either in the high-speed video or in the resulting welds. In addition to considerations of spatter and weld profile, a more stable keyhole process will reduce the tendency of the process itself to generate pores, from collapses of the keyhole.

Differences in the length and width of the weldpool when using a directed jet of gas can be seen by comparing the images in Fig. 5. When using the gas jet the weld pool is narrower (~0.9 mm) immediately behind where the laser beam impinges on the material surface and is also longer (~10 mm with the gas jet and ~8 mm without). After some lag, related to the low thermal conductivity of titanium, the pool then widens out to a width similar to that

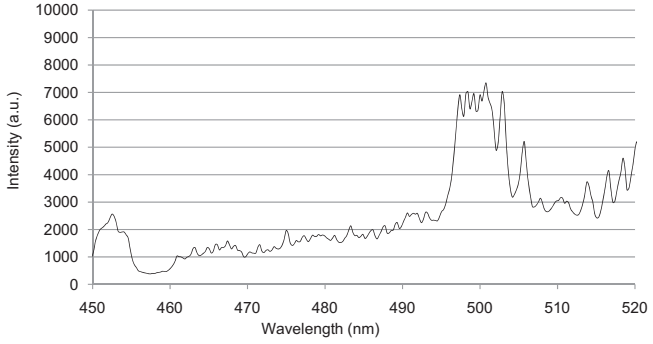

FIG. 6. Emission spectra of the vapor plume when Nd:YAG laser welding Ti-2.5Cu within the range 450–520 nm.

TABLE VI. TiI emission lines used to calculate electron temperature (Ref. 18).

Transition wavelength λ_{mn} (nm)	Transition probability A_{mn} (10^8 s^{-1})	Statistical weight g_m	Upper energy level E_m (eV)
453.324	8.83×10^{-1}	11	3.5826549
468.192	2.35×10^{-2}	11	2.6953807
498.173	6.60×10^{-1}	13	3.336502
517.375	3.80×10^{-2}	5	2.395745
521.039	3.57×10^{-2}	9	2.4268626

of the pool formed without using an Ar gas jet (~1.9 mm with the gas jet and ~2.2 mm without). Weld pool lengthening would prolong solidification time, in turn allowing more time for any gas bubbles trapped in the weldpool to escape prior to freezing of the weldpool.

D. Vapor plume analysis

An example of the emission spectrum taken when Nd:YAG laser welding of Ti-2.5Cu is shown in Fig. 6. Only TiI or ArI emission lines were detected in the data. The atomic lines shown in Table VI were used to calculate the TiI electron temperature, T_e, using the equation below and the Boltzmann plot method;[18,19]

$$\ln(I_{mn}\lambda_{mn}/g_mA_{mn}) = \ln(Nhc/Z) - E_m/kT_e, \quad (2)$$

where I_{mn} is the spectral line intensity, λ_{mn} is the wavelength of the transition, g_m is the statistical weight at level m, A_{mn} is the transition probability, N is the atomic number density, h is Planck's constant, c is the velocity of light, E_m is the energy at level m, and k is the Boltzmann constant. An average vapor plume temperature of ~3100 K was calculated from the gradient of the Boltzmann plot. According to the Saha equation, and assuming a quasi-neutral vapor plume at atmospheric pressure, the ionization fraction of a titanium vapor plume at this temperature is <1% and the vapor plume can be categorized as a negligibly ionized vapor. Therefore any attenuation of the laser beam by inverse Bremsstrahlung absorption and/or defocusing by a gradient of electron density can be considered negligible.

Particle diameters collected from the condensated Ti-2.5Cu vapor plume ranged from 30–60 nm, with the majority being in the 40–50 nm range. The EDX analysis indicates that both alloying elements from the parent material (titanium and copper) were present in the vapor plume. A degree of oxidation of one or both of these elements may have also have taken place. Carbon was also detected, which most likely originated from inadvertent sampling of the adhesive film beneath the particles.

The Mie solution to Maxwell's equations has been applied to determine the extinction coefficient (combination of scattering and absorption) of the laser radiation through the vapor plume. The simplified solutions can be applied in this case as the diameter of the spheres is less than 140 nm.[20] For calculation purposes it is assumed that the particles are all identical in size (either 40 or 50 nm) and composition and that they are isotropic and optically linear. Additionally, the particles have been assumed to be pure titanium. The complex index of refraction for titanium at 1 μm is $3.8+4.0i$ (Ref. 21);

$$Q_{\mathrm{ABS}} = (-8\pi r/\lambda)\mathrm{Im}\{m^2 - 1/m^2 + 1\}, \quad (3)$$

$$Q_{\mathrm{SCA}} = (8/3)(2\pi r/\lambda)^4|m^2 - 1/m^2 + 2|^2, \quad (4)$$

where Q_{ABS} and Q_{SCA} are the absorption and scattering terms, r is the radius of the particles, and m is the complex refractive index. The calculated absorption and scattering efficiencies for vapor plumes containing either 40 or 50 nm particles are shown in Table VII.

It can be seen that the absorption efficiency is the dominant beam attenuation mechanism at these particle sizes and compositions. The effect of preventing this attenuation by using the directed gas jet has been revealed through high speed video observation. However, it should be noted that these are only the efficiency values and in order to calculate the actual attenuation values the particle density needs to be calculated. These could be empirically determined through observation of the vapor plume and measurement of the vaporization mass loss.

IV. CONCLUSIONS

A three stage study was performed in order to minimize weld metal porosity content, using a directed gas jet, in Nd:YAG welding of 3.25-mm-thick Ti-2.5Cu and Ti-6Al-4V

TABLE VII. Calculated Q_{ABS} and Q_{SCA} efficiencies.

Particle diameter (nm)	Q_{ABS}	Q_{SCA}	Q_{EXT}
40	0.0486	5.2×10^{-4}	0.049
50	0.061	1.3×10^{-3}	0.062

titanium alloys. Initial trials determined a suitable welding speed for full penetration and outlined the influence of a number of gas jet parameters on weld porosity content. Subsequently, two DOEs were performed to optimize the directed gas jet parameters with respect to minimizing internal porosity content, as well as weld face and root undercut. The working tolerances of parameters have been determined which allow a weld quality to within internal aerospace standards to be reproducibly achieved.

Additionally, the vapor plume above the keyhole when Nd:YAG laser welding Ti-2.5Cu has been characterized using optical spectroscopy and vapor plume sampling. The plume temperature was calculated to be ~3100 K. The main mechanisms of Nd:YAG laser beam attenuation by the vapor plume have been found to be primarily absorption but also scattering of the incident laser light by a population of 30–60 nm titanium particles. High speed observation of the welding process with and without an optimized directed gas jet has revealed that it disperses the formation of the vapor plume above the keyhole. This prevents fluctuations in the keyhole's vaporization pressure and hence increases keyhole stability thus reducing weld metal porosity.

ACKNOWLEDGMENTS

This work was funded by the Industrial Members of TWI, as part of the Core Research Programme. Part of the work was also funded by EPSRC Grant No. C537750. Materials for the work were kindly provided by Aeromet International PLC and The Boeing Company. The high speed camera was loaned from the EPSRC Engineering Instrument Pool.

[1]R. R. Boyer, "An overview on the use of titanium in the aerospace industry," Mater. Sci. Eng., A **213**, 103–114 (1996).
[2]http://www.boeing.com/commercial/aeromagazine/articles/qtr_4_06/AERO_Q406.pdf, date accessed, November 25, 2009.
[3]D. V. Lindh and G. M. Peshak, "The influence of weld defects on performance," Weld. J. (London) **48**, 45s–56s (1969).
[4]P. Hilton, J. Blackburn, and P. Chong, "Welding of Ti-6Al-4V with fiber delivered laser beams," *Proceedings of ICALEO 2007*, Orlando, Florida, 29 October–1 November 2007 (Laser Institute of America, Orlando, 2007), pp. 887–895.
[5]C. Li, H. Lunji, and G. Shuili, "A study on the porosity of CO_2 laser welding of titanium alloy," China Welding **15**, 1–5 (2006).
[6]A. Matsunawa, M. Mizutani, S. Katayama, and N. Seto, "Porosity formation and its prevention in laser welding," Welding International **17**, 431–437 (2003).
[7]W. W. Duley, "Heat transfer and modelling in laser welding," *Laser Welding* (Wiley & Sons, New York, 1999), p. 83.
[8]J. Greses, "Plasma/Plume effects in CO_2 and Nd:YAG laser welding," Ph.D. thesis, University of Cambridge, 2003.
[9]W. M. Steen, "Laser welding," *Laser Material Processing*, 2nd ed. (Springer-Verlag, London, 1998), p. 155.
[10]F. Caiazzo, F. Curcio, G. Daurelio, and F. C. M. Minutolo, "Ti6Al4V sheets lap and butt joints carried out by CO_2 laser: mechanical and morphological characterization," J. Mater. Process. Technol. **149**, 546–552 (2004).
[11]D. Lacroix, G. Jeandel, and C. Boudot, "Solution of the radiative transfer equation in an absorbing and scattering Nd:YAG laser-induced plume," J. Appl. Phys. **84**, 2443–2449 (1998).
[12]H. Mauro, I. Miyamoto, and Y. Arata, "The roles of assist gas in CO_2 laser welding," Q. J. Jpn. Weld. Soc. **3**, 276–283 (1985).
[13]D. Douay, F. Daniere, R. Fabbro, and L. Sabatier, "Plasma blowing in deep penetration CO_2 laser welding," *Proceedings of ICALEO 1996*, Detroit, Michigan, 14–17 October 1996 (Laser Institute of Laser, Orlando, 1996), pp. 54–63.
[14]K. Kamimuki, T. Inoue, K. Yasuda, M. Muro, T. Nakabayashi, and A. Matsunawa, "Prevention of welding defect by side gas flow and its monitoring method in continuous wave Nd:YAG laser welding," J. Laser Appl. **14**, 136–145 (2002).
[15]S. Mueller, E. Stiles, and R. Dienemann, "Study of porosity formation during laser welding of Ti6Al4V," *Proceedings of ICALEO 2008*, Temecula, California, 20–23 October 2008 (Laser Institute of America, Orlando, 2008), pp. 133–138.
[16]BS EN ISO 14175:2008, "Welding consumables. Gases and gas mixtures for fusion welding and allied processes" (2008).
[17]BS EN 1435:1997, "Nondestructive examination of welds. Radiographic examination of welded joints" (1997).
[18]http://physics.nist.gov/PhysRefData/ASD/index.html, date accessed March 2009.
[19]H. R. Griem, "Spectroscopic temperature measurements," *Principles of Plasma Spectroscopy* (Cambridge University Press, Cambridge, England, 1997), p. 281.
[20]H. C. van de Hulst, "Non-absorbing spheres," *Light Scattering by Small Particles* (Dover, Mineola, 1981), p. 144.
[21]*American Institute of Physics Handbook*, edited by B. D. E. Gray (MacGraw-Hill, New York, 1972).

Chapter 6

Modulated Nd:YAG Laser Welding

6.1 Introduction

This journal paper was submitted to *Science and Technology of Welding and Joining* on the 14th April 2010 and accepted for publication on the 8th May 2010. The paper was published in July 2010 edition, volume 15(5) of the *Science and Technology of Welding and Joining*. The research for the paper was performed with Dr Chris Allen, Dr Paul Hilton, Professor Lin Li, Mr Mohammed Hoque and Dr Ali Khan.

In terms of the co-author involvement Dr Chris Allen, Dr Paul Hilton and Professor Lin Li assisted with defining the scope of the laser parameters that were to be considered for this experiment, based on a literature review performed by the author of this thesis and the performance capabilities of the available laser sources. The experimental work, including the high speed video observations of the keyhole and the melt pool, were performed by the author of this thesis. Relating the porosity to the behaviour of the keyhole, melt pool and the vapour plume, using the high speed video observations, was the idea of the author of this thesis. Mr Mohammed Hoque aided with the MATLAB programming, and Dr Ali Khan with the Fast Fourier Analysis.

Modulated Nd : YAG laser welding of Ti–6Al–4V

J. E. Blackburn*[1], C. M. Allen[2], P. A. Hilton[2], L. Li[1], M. I. Hoque[1] and A. H. Khan[2]

Modulating the output of Nd : YAG laser sources has been evaluated as a technique for producing high quality welds in titanium alloys. Welds with high internal quality were produced when a square wave form was used with a modulation frequency ⩾125 Hz and a duty cycle of 50%. Undercut present in the weld profile can be reduced if the correct combination of modulation amplitude and laser beam focal plane position are used. High speed observation and subsequent Fourier analysis of the vapour plume and keyhole behaviour have shown that they both exhibit the same periodic tendencies. With the correct parameters, an oscillating wave can be set up in the weld pool, which appears to manipulate the vapour plume behaviour and hence reduce porosity formation.

Keywords: Laser, Weld, Nd : YAG, Modulated, Titanium, Porosity

Introduction

There is an increasing utilisation of titanium alloys for high performance aerospace applications, which has created the need for a joining process capable of fabricating high quality, near net shape titanium alloy components. Replacing current manufacturing techniques, which are machining and labour intensive, would reduce component cost and increase productivity. Keyhole laser welding is a fusion welding process, which produces high aspect ratio welds (deep penetration and a relatively narrow weld bead) with a relatively low heat input compared with arc welding processes. Furthermore, laser welding can be performed out of vacuum, and the fibre optic delivery of near infrared solid state laser beams provides increased flexibility, compared with other joining technologies. Consequently, keyhole laser welding can be considered as a primary candidate for the production of titanium alloy components for aerospace applications.

The service requirements of high performance aerospace components include high fatigue resistance, and therefore, stringent quality standards exist.[1] These standards include criteria relating to weld profile and internal quality, such as porosity and cracks. It has been reported that weld metal porosity can easily form when keyhole laser welding.[2] This is of primary concern for components whose weld profiles are dressed (machined to remove geometric defects present in the weld profile), as pores may then break the surface, act as stress concentrators and reduce the fatigue resistance of the weld.[3]

Weld metal porosity can be caused by soluble gases dissolved in the weld pool, such as hydrogen, which are rejected during weld pool solidification.[4] Removal of the TiO_2 layer, which is hygroscopic and will adsorb moisture from the atmosphere, from the parent material before welding, has been reported to reduce weld metal porosity when CO_2 laser welding.[5] Keyhole instability has also been reported as a cause of weld metal porosity, as it can lead to metal vapour and/or inert shielding gases being trapped in the weld metal.[2] Vaporisation irregularities at the front keyhole wall[2] and attenuation of the incident laser radiation by a vapour plume[6] are two reported causes of keyhole instability.

Modulation of the output power is a reported method of reducing weld metal porosity when laser welding metallic materials other than titanium alloys.[7–9] Kuo and Jeng[7] reported that modulating the output power of an Nd : YAG laser reduced the resultant porosity levels when welding 3·0 mm thick SUS 304L and Inconel 690, compared with a continuous wave output power. The same effect has also been reported when CO_2 laser welding A5083.[8] A comparison of modulation amplitudes by Kawaguchi *et al.*[9] indicated that larger modulation amplitudes were more effective in reducing the occurrence of porosity when CO_2 laser welding SM490C.

Modulating the output of 1 μm wavelength laser sources has been evaluated here as a technique for producing high quality welds in Ti–6Al–4V up to 3·25 mm in thickness. High speed observation of the keyhole and vapour plume has been performed to understand the effects of the modulated waveform on the dynamic behaviour of the welding process.

Methodology

Materials

Trials were performed on 2·0 and 3·25 mm thick Ti–6Al–4V. Immediately before performing bead on plate

[1]School of MACE, The University of Manchester, Manchester M60 1QD, UK
[2]TWI Ltd, Cambridge CB21 6AL, UK

*Corresponding author, email: Jonathan.Blackburn@postgrad.manchester.ac.uk

Published by Maney on behalf of the Institute
Received 14 April 2010; accepted 8 May 2010
DOI 10.1179/136217110X12731414739718

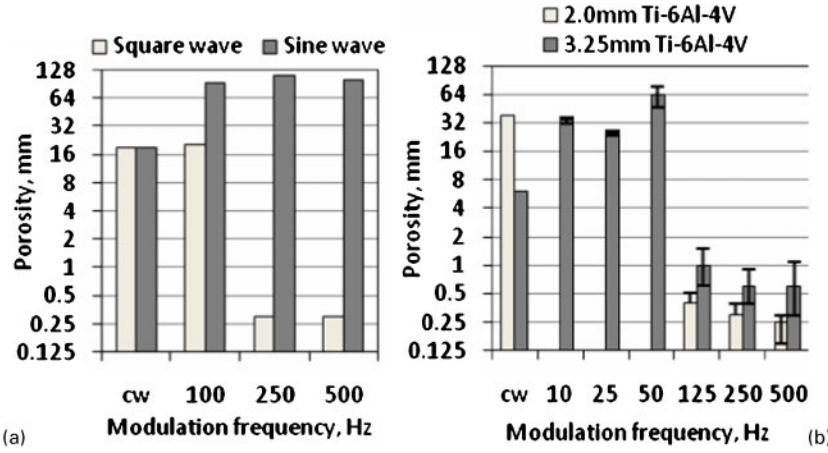

1 Porosity content of BOP tests made in *a* 2·0 mm thick Ti–6Al–4V with JK1002 laser (P_{avg}=1·0 kW, P_{amp}=2·0 kW and P_{peak}=2·0 kW) and *b* 2·0 and 3·25 mm thick Ti–6Al–4V with square waveform from HL4006D laser (P_{avg}=2·0 kW, P_{amp}=4·0 kW and P_{peak}=4·0 kW)

(BOP) tests, the surfaces of testpieces were cleaned with an abrasive paper and acetone degreased. An identical procedure was followed when performing butt welding trials, except that the abutting edges of the testpieces were dry machined before abrading and degreasing. Welding was performed within 8 h of machining.

Equipment and experimental procedure

Two Nd : YAG laser sources were used in this investigation: a GSI Lumonics JK1002 Nd : YAG laser (GSI Lumonics, GSI Group, Rugby, UK) and a TRUMPF HL4006D Nd : YAG laser (TRUMPF Laser, Schramberg, Germany). Average laser powers at the workpiece were measured using a watercooled Ophir power meter. The incident laser radiation was always delivered at an angle normal to the top surface of the workpiece. A trailing gas shield (above the weld) and a 10 mm^2 cross-section copper efflux channel (below the weld) were supplied with 30 and 5 L min^{-1} of argon gas (99·998% purity) respectively to prevent oxidation of the weld metal. Table 1 details the variables investigated. Processing with the JK1002 laser was performed on 2·0 mm thick Ti–6Al–4V only, whereas processing with the HL4006D laser was performed on 2·0 and 3·25 mm thick Ti–6Al–4V. A laser duty cycle of 50% was utilised in all experiments. To assess a large number of variables, the majority of the trials were linear BOP tests. Selected welding conditions were transferred to linear butt joints. This approach has been utilised successfully in previous research.[1]

High speed observations (10 kHz frequency) of the keyhole and vapour plume were performed during selected BOP tests in 3·25 mm thick Ti–6Al–4V. The keyhole behaviour was observed using a Photron SA-3 monochrome camera. Illumination of the keyhole was provided by a copper vapour laser. A MotionPro X4 colour camera was used to observe the behaviour of the vapour plume exiting the keyhole.

The face and root of all BOP tests and butt welds were visually assessed for discoloration. Samples were radiographed, in accordance with BS EN 1435:1997, to determine weld metal porosity content. Indications ⩾0·05 mm in diameter could be detected in the radiographs. Pore counts were performed over a 76 mm weld length, and the diameters of the pores in this length were summed to determine the accumulated length of porosity (presented in units of mm in the subsequent graphs). Selected samples were sectioned transverse to the welding direction at representative positions.

Results

Waveform and frequency

Figure 1*a* details the weld metal porosity contents of BOP tests produced with different waveforms and frequencies, in 2·0 mm thick Ti–6Al–4V using the focused beam of the JK1002 laser. It can be seen that a square waveform at frequencies ⩾250 Hz reduced the weld metal porosity considerably when compared with BOP tests produced with a continuous wave output. In contrast, the sinusoidal waveform increased the formation of porosity in the weld metal compared with continuous wave BOP tests. Weld metal porosity data

Table 1 Variables investigated in this project

Variable	Laser source	
	GSI JK1002	TRUMPF HL4006D
Average power P_{avg}, kW	1·0	2·0
Peak power P_{peak}, kW	2·0	4, 3·5, 3·0, 2·5
Minimum power P_{min}, kW	0	0, 0·5, 1·0, 1·5
Modulation amplitude $P_{amp}=P_{peak}-P_{min}$, kW	2·0	1·0, 2·0, 3·0, 4·0
Modulation waveform	Sinusoidal, square	square
Frequency P_{freq}, Hz	100, 250, 500	10, 25, 50, 125, 250, 500
Focal plane position, mm	0	−3, 0, +3
Beam waists, μm	300, 600	600

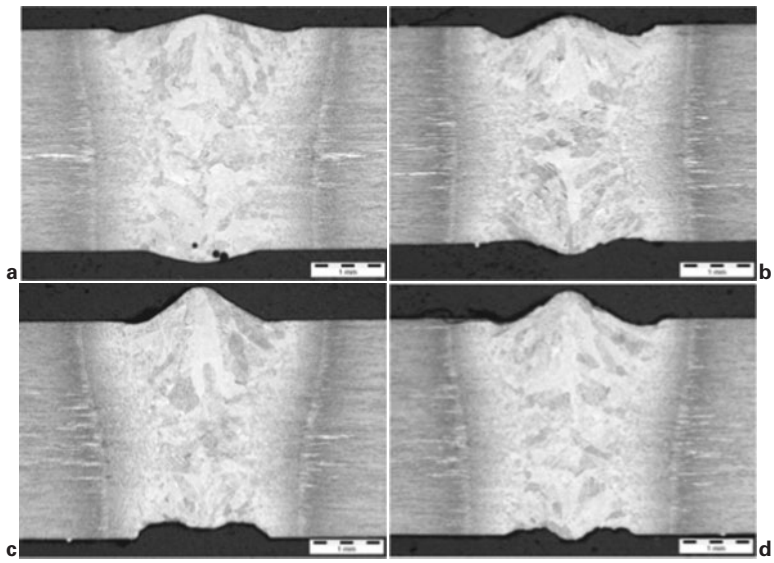

a continuous wave (face undercut=0·10 mm; root undercut=none); *b* 125 Hz (face undercut=0·20 mm; root undercut=0·09 mm); *c* 250 Hz (face undercut=0·08 mm;; root undercut=0·26 mm); *d* 500 Hz (face undercut=0·11 mm;; root undercut=0·12 mm)

2 Weld profiles of BOP tests made in 3·25 mm thick Ti–6Al–4V with HL4006D laser (P_{avg}=2·0 kW and P_{amp}=4·0 kW) at different frequencies

of BOP tests produced in 2·0 and 3·25 mm thick Ti–6Al–4V using the HL4006D laser is shown in Fig. 1*b*. Fully penetrating and stable welding speeds of 33 and 20 mm s^{-1} were determined, through continuous wave experiments, for the 2·0 and 3·25 mm thick Ti–6Al–4V respectively. A square waveform with a modulation frequency $\geqslant$125 Hz was a successful method of reducing porosity in titanium alloys up to 3·25 mm thickness. The majority of the pores observed in the radiographs of those BOP tests produced with a square waveform and a modulation frequency $\geqslant$125 Hz were $\leqslant$0·1 mm in diameter and evenly distributed throughout the weld length. Transverse cross-sections of BOP tests produced in 3·25 mm thick Ti–6Al–4V at square wave modulation frequencies of 125, 250 and 500 Hz are shown in Fig. 2. Varying amounts of continuous undercut were present at the weld face and/or root on the BOP tests produced with a modulated output.

Butt welds were produced in 2·0 and 3·25 mm thick Ti–6Al–4V, with parameters developed from BOP tests. The results in Fig. 3 suggest that the conditions developed through BOP tests are transferable to the butt joint configuration. Porosity is significantly reduced when compared with continuous wave butt welds produced with the same energy input. However, as was observed in the BOP tests, the welds produced with a modulated waveform are unacceptably undercut at the weld face and/or root.

Modulation amplitude and focal plane position

All further experiments were performed on 3·25 mm thick Ti–6Al–4V using the HL4006D laser. Modulation amplitudes in the range of 1·0–4·0 kW were considered, for a constant average power and welding speed of 2·0 kW and 20 mm s^{-1} respectively. Figure 4*a* shows the effect of using different modulation amplitudes on the weld metal porosity content. In general, BOP tests

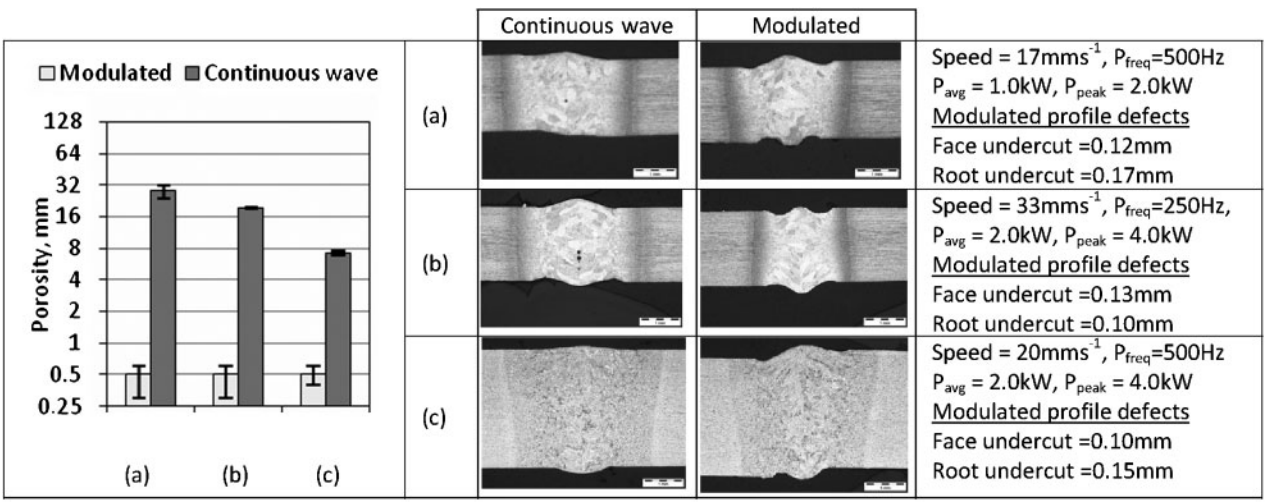

3 Weld metal porosity and weld profile results for butt welds produced in *a* 2·0 mm Ti–6Al–4V with JK1002 laser, *b* 2·0 mm Ti–6Al–4V with HL4006D laser and *c* 3·25 mm Ti–6Al–4V with HL4006D laser

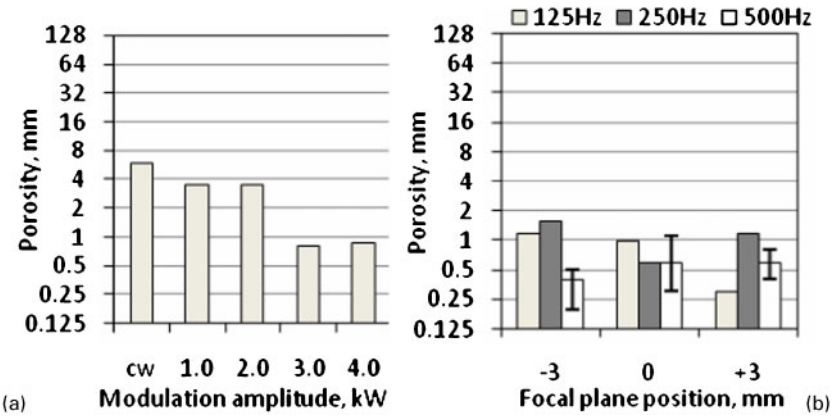

4 Weld metal porosity of BOP tests produced with P_{avg}=2·0 kW and *a* P_{freq}=500 Hz, focal plane position of 0 mm and P_{amp}=1·0–4·0 kW, *b* P_{amp}=4·0 kW, P_{freq}=125–500 Hz and focal plane positions of −3·0, 0 and +3·0 mm

produced with a modulation amplitude of either 3·0 or 4·0 kW had particularly low levels of weld metal porosity (<1·0 mm accumulated length). Modulating the output of the Nd:YAG laser with amplitudes of either 1·0 or 2·0 kW reduced the weld metal porosity content compared with BOP tests produced with a continuous wave output but not as significantly as the higher modulation amplitudes. Corresponding weld profiles are shown in Fig. 5. At higher modulation amplitudes, the amount of continuous undercut at the weld face and root increased.

The effect of defocusing the laser beam on internal weld metal porosity is shown in Fig. 4*b* for square waveform modulation frequencies in the range of 125–500 Hz with a 2·0 kW average power. A ±3·0 mm focal plane shift was examined, which corresponds to a beam width of ~750 μm at the workpiece surface. In contrast with the other parameters investigated, a ±3·0 mm shift in the focal plane position had a relatively small effect on the weld metal porosity content and the weld profile. However, it can be seen from Fig. 6 that when combining a ±3·0 mm shift in the focal plane position with a modulation amplitude of 3·0 kW, at a modulation frequency of 125 Hz, the undercut at the weld root can be eliminated while still achieving low levels of weld metal porosity. Approximately 0·1 mm of continuous undercut at the weld face is still present.

Vapour plume behaviour

A significantly large amount of data was generated from the high speed observations of the vapour plume, which complicated a straightforward comparison of the vapour plume behaviours during different welding conditions. A MATLAB program was used to extract the red, green and blue values of individual pixels and

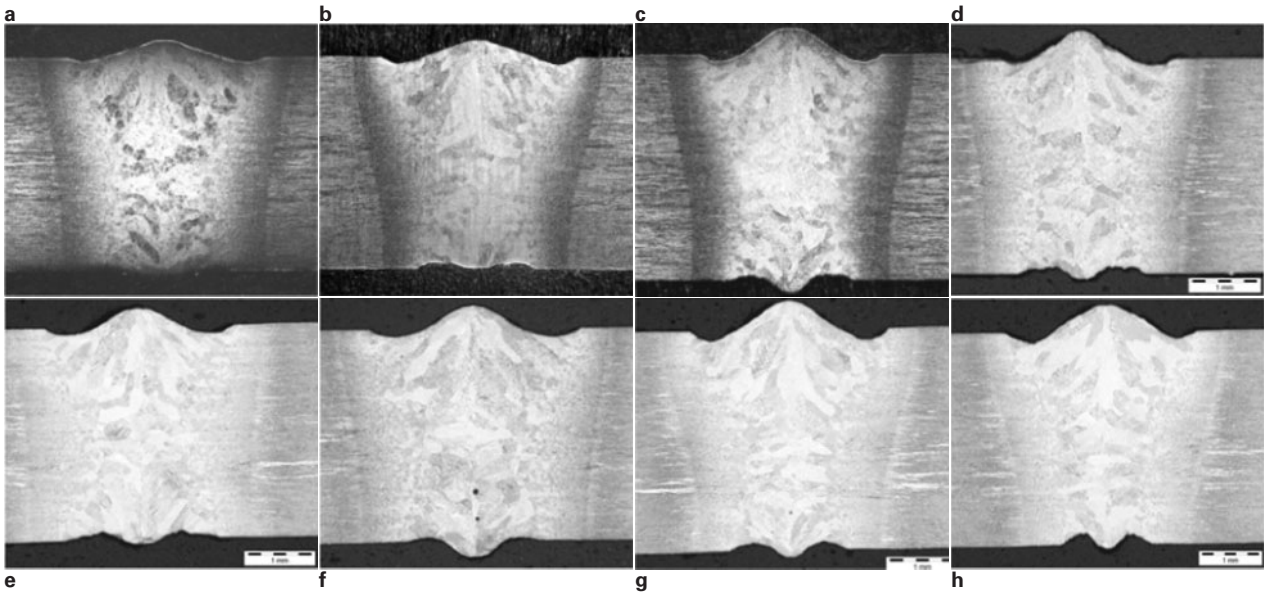

5 Profiles of BOP tests produced in 3·25 mm thick Ti–6Al–4V with P_{freq}=500 Hz, P_{avg}=2·0 kW and P_{amp} of *a* 1·0 kW (face undercut=0·06 mm; root undercut=none), *b* 2·0 kW (face undercut=0·13 mm; root undercut=0·09 mm), *c* 3·0 kW (face undercut=0·11 mm; root undercut=0·12 mm) and *d* 4·0 kW (face undercut=0·11 mm; root undercut=0·14 mm). BOP tests produced with P_{freq}=125 Hz, P_{amp}=4·0 kW and focal plane positions of *e* −3·0 mm (face undercut=0·14 mm; root undercut=0·16 mm) and *f* +3·0 mm (face undercut=0·13 mm; root undercut=0·09 mm). BOP tests produced with P_{freq}=500 Hz, P_{amp}=4·0 kW and focal plane positions of *g* −3·0 mm (face undercut=0·18 mm; root undercut=0·15 mm) and *h* +3·0 mm (face undercut=0·18 mm; root undercut=0·18 mm)

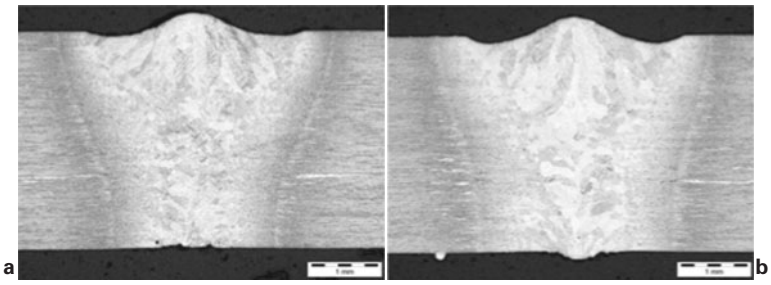

6 Weld profiles of BOP tests produced in 3·25 mm thick Ti–6Al–4V with P_{amp} of 3·0 kW, P_{freq} of 125 Hz and focal plane positions of *a* +3·0 mm (face undercut=0·08 mm; root undercut=none; porosity=1·3 mm) and *b* −3·0 mm (face undercut=0·13 mm; root undercut=none; porosity=0·8 mm)

convert them into a single value of intensity for each pixel in every frame. Statistical analysis of these data provides only static information, such as the standard deviation. Previous studies have reported that dynamic fluctuations in the vapour plume are directly related to keyhole instability, which can cause weld metal porosity.[10,11] Therefore, Fourier analysis of these data sets was performed to ascertain the presence of periodic fluctuations in the vapour plume behaviours and determine if this correlates with weld metal porosity. At heights of 1·0–5·0 mm above the laser interaction point, an average intensity value was calculated from three pixels situated in the anticipated path of the laser radiation. The discrete Fourier transform of the average values was calculated using a fast Fourier transform. A total of 2^{12} (4096) frames were processed for each welding condition, resulting in a resolution frequency of ~2·4 Hz. Comparing the frequency spectra from different heights for a given welding condition revealed that nominally identical frequency spectrums were produced at all the heights. Therefore, only the Fourier analyses performed at a height of 2·0 mm are detailed here.

Figure 7 details the frequency spectra calculated from five different modulated welding conditions, their weld metal porosity contents being shown in Fig. 1*b* or 4*a*. The frequency spectrum calculated from a 2·0 kW continuous wave welding condition (Fig. 7*a*) contains no dominant frequencies, indicating a noisy signal with no periodic behaviour. In contrast, when welding with a 250 Hz modulation frequency and 4·0 kW amplitude, numerous peaks are observed in the frequency spectrum (Fig. 7*b*). A fundamental frequency of 241·7 Hz (near the modulation frequency) was calculated, and the second, third and fifth harmonics also have amplitudes similar to this fundamental frequency. Up to the 11th harmonic frequency are visible in the frequency spectrum but with decreasing amplitudes. Figure 7*c* details the frequency spectrum produced when the output power is modulated at 50 Hz and 4 kW amplitude. A fundamental frequency of 48·8 Hz is present, again approximately matching the laser beam modulation frequency. Also present in the frequency spectrum are relatively small peaks at frequencies of 97·7 and 144·0 Hz, indicating little periodic behaviour present in the vapour plume that does not match the modulation frequency.

Figure 7*d* and *e* shows the calculated frequency spectrums of two modulated welding conditions (500 Hz modulation frequency), differing only by the modulation amplitudes of 1·0 and 3·0 kW respectively. The frequency spectrum calculated for a modulation amplitude of 1·0 kW is very similar to that produced with a continuous wave output. However, numerous peaks are found in the spectrum if the modulation amplitude is increased to 3·0 kW: a fundamental frequency (478·5 Hz) and second to sixth harmonics. The spectrum displays similar trends to that produced with a 250 Hz modulated output power and a modulation amplitude of 4·0 kW. Both of these welding conditions gave very low weld metal porosity contents.

Several of the periodic behaviours indicated from the Fourier analysis can be observed in the high speed videos. Figure 8 details the typical behaviour of the vapour plume when welding with a modulation frequency of 250 Hz and 4 kW amplitude. A 2 ms duration (the laser on time) is shown. Initially, a relatively intense

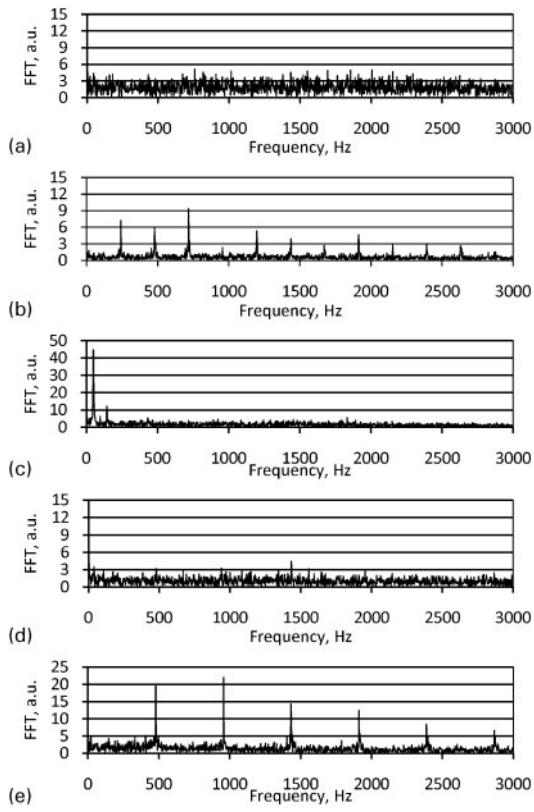

7 Frequency spectra of vapour plume behaviour for *a* 2·0 kW continuous wave, *b* P_{freq}=250 Hz, P_{amp}=4·0 kW and P_{avg}=2·0 kW, *c* P_{freq}=50 Hz, P_{amp}=4·0 kW and P_{avg}=2·0 kW, *d* P_{freq}=500 Hz, P_{amp}=1·0 kW and P_{avg}=2·0 kW and *e* P_{freq}=500 Hz, P_{amp}=3·0 kW and P_{avg}=2·0 kW. Note different *y*-axis scales

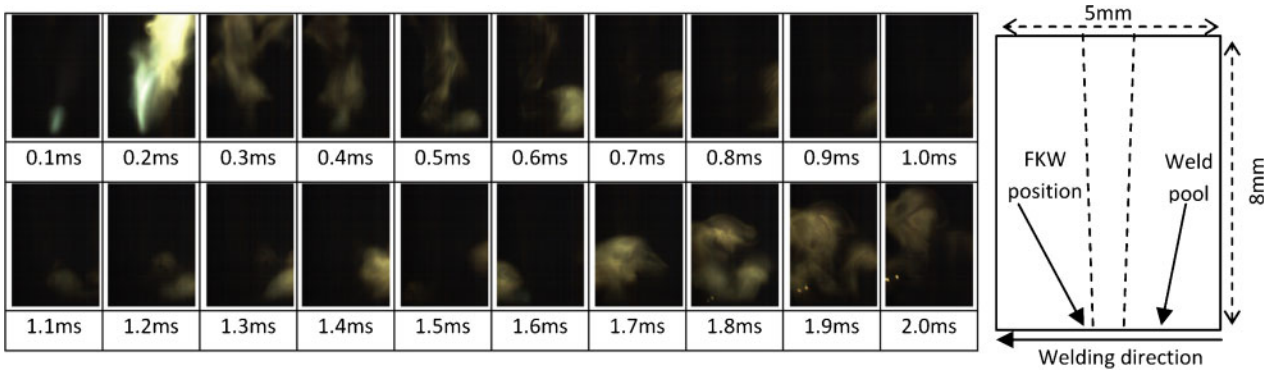

8 Behaviour of vapour plume during 2·0 ms laser on time as observed when welding with P_{freq}=250 Hz, P_{avg}=2·0 kW and P_{amp}=4·0 kW: positions of front keyhole wall (FKW) and weld pool are indicated in diagram on right hand side

vapour plume is emitted in a direction normal to the laser beam, for ~0·2 ms. This vapour plume then disperses over ~0·2 ms, before a relatively weak vapour plume is emitted towards the weld pool for ~1·0 ms. A sudden change in direction of the vapour plume is then observed, as the vapour plume is briefly emitted for ~0·3 ms towards the leading edge of the process, before dispersing. No vapour plume is then observed until the laser power is turned back on and this cyclic process is repeated, frames 2·0–4·0 ms (not shown). Similar vapour plume behaviour is observed when welding with a modulation frequency of 500 Hz and amplitude of 3·0 or 4·0 kW. In contrast, the behaviour of the vapour plume during the laser on time of a 10 ms pulse (i.e. 50 Hz modulation frequency) appears random and is similar to that of one produced with a continuous wave output power or with modulation amplitude of $\leqslant$1·0 kW.

Keyhole and weld pool behaviour

Fourier analysis of pixels in the keyhole region was performed with methods analogous to those described previously. The resulting frequency spectrum produced for a 2·0 kW continuous wave welding condition consisted of noise, as found when analysing the vapour plume behaviour. This suggests that there was no periodic behaviour present in the keyhole observations. However, what is apparent from high speed observations is that the process is particularly unstable, and the keyhole frequently collapses. A particularly unstable keyhole was also observed when welding with those parameters used for Fig. 7*c* and *d* (i.e. resulting in high levels of weld metal porosity).

The keyhole frequency spectra of those welding conditions, which resulted in low levels of weld metal porosity, had harmonic trends very similar to those shown in Fig. 7*b* and *e*. However, only the first four harmonic frequencies had significant amplitudes. When welding with modulation frequencies $\geqslant$125 Hz and amplitudes $\geqslant$3·0 kW, no uncontrolled keyhole collapses were observed. Keyhole collapses were observed, but this was due to the fact that minimum power in the waveform had insufficient energy to maintain the keyhole open. A minimum of 1·0 kW was required to maintain a keyhole at the welding speed used. It was noted from the high speed video that, under these same combinations of process parameters, a periodic oscillation was introduced into the weld pool. Weld pool oscillations were observed in the high speed videos of those welds produced with a modulation frequency $\geqslant$125 Hz and modulation amplitude $\geqslant$3·0 kW.

Discussion

The weld quality results shown above indicate that full penetration welds with low levels of weld metal porosity can be produced in Ti–6Al–4V up to 3·25 mm in thickness with the modulated output of an Nd : YAG laser. These levels of weld metal porosity meet the stringent porosity criteria stipulated in typical aero-engine weld quality standards.[1] A key to achieving an excellent internal weld quality is the appropriate choice of waveform, modulation frequency and modulation amplitude.

In the experimental results shown in Fig. 2*a*, the weld metal porosity contents of BOP tests made using a square waveform were substantially less than those produced with a sinusoidal waveform. Eberle and Richter[12] established a similar result when welding 1·0–3·0 mm thick aluminium alloys with a 2·0 kW Nd : YAG laser. They reported that welds made using square waveforms contained less weld metal porosity than those made with triangular or sinusoidal waveforms with a 50 Hz modulation frequency. Further studies are required to understand the importance of waveform since there are a large number of permutations.

At modulation frequencies $\geqslant$125 Hz, BOP melt runs and butt welds can be produced with excellent internal qualities (<1·0 mm accumulated length) when using a square waveform. However, when utilising lower modulation frequencies, such as 50 Hz, relatively large amounts of porosity (>20 mm accumulated length) are found in the weld metal. The laser duty cycle was fixed at 50%, and hence, a decrease in modulation frequency resulted in a proportionate increase in the pulse width. As seen from Fig. 7, pulse widths $\leqslant$4 ms (i.e. modulation frequencies $\geqslant$125 Hz) combined with modulation amplitudes $\geqslant$3·0 kW resulted in a periodic vapour plume behaviour, which was observed to have relatively little activity in the path of the incident laser radiation (Fig. 8). A relatively stable keyhole is also observed if these welding conditions were adopted, with the same periodic tendencies as those observed in the vapour plume being detected in the keyhole behaviour by Fourier analysis (see section 'Keyhole and weld pool behaviour'). However, at pulse widths >4 ms or at

modulation amplitudes <3·0 kW, the vapour plume behaviour did not appear to be periodic in nature, and significant plume activity in the path of the incident laser radiation was observed. The random keyhole instabilities that occur in these cases are indicated by the calculated frequency spectrums of the vapour plume and keyhole behaviour, which consisted primarily of noise. In terms of the importance of pulse width, Shimoksu *et al.*[13] reported a similar plume behaviour when Nd : YAG laser welding of SUS 304L and stated that, after laser pulses with a beam on time in excess of 5 ms, the plume began to re-emerge from the top of the keyhole, the keyhole began to destabilise and gas bubbles were introduced into the weld pool.

The principal difference, as observed from the high speed video observations of the keyhole between the two groups of conditions discussed above, is the presence of a keyhole that opens and closes on a regular basis, such that an oscillating wave is created in the weld pool. From the high speed video evidence, it appears that this wave acts to manipulate the ejection angle of the vapour plume. This is supported by the correlating periodic behaviours calculated from the Fourier analysis of the vapour plume and keyhole observations. The shifting ejection angle will reduce the attenuation of the incident laser radiation by the vapour plume and ensure that a constant power is delivered to the workpiece (during the laser on time). It is thought that the wave motion will also aid the escape of the gas bubbles in the weld pool. Kuo and Jeng[7] suggested that the laser pulse agitated the molten metal and caused bubbles to float to the surface of the weld pool, decreasing the porosity.

When a modulation amplitude of <3·0 kW is utilised, the minimum power is sufficient to maintain a keyhole of some depth, and as a result, an oscillating wave is not established in the weld pool. At increased pulse durations, the repetition rate of the keyhole opening/closing is not sufficient enough to establish a standing wave. Furthermore, instabilities similar to those observed when welding with a continuous wave output power are observed. Kuo and Jeng[7] utilised a 2·5 kW Nd : YAG laser to weld SUS 304L and Inconel 690 at an average power of 1700 W, a duty cycle of 50% and a frequency of 100 Hz. High modulation amplitude values resulted in low levels of weld metal porosity compared with lower modulation amplitudes or continuous wave results.

The production of butt welds with very low levels of weld metal porosity is likely to be insignificant if stress concentrating defects, such as undercut, are present in the weld profile. In the work reported here, it has been shown that undercut at the weld root can be eliminated through the adoption of smaller modulation amplitudes and a defocused beam. However, continuous undercut is still present at the weld face, which is of concern for fatigue sensitive components. Two possible approaches for eliminating the undercut at the weld face exist: wire feed addition and an oversized weld section, with subsequent machining.

Conclusions

The work reported here has evaluated modulating the output of 1 μm laser source as a technique for producing high quality welds in Ti–6Al–4V up to 3·25 mm in thickness. The key conclusions are the following.

1. With the appropriate choice of modulation parameters, butt welds can be produced in Ti–6Al–4V, up to 3·25 mm in thickness, which have very low levels of weld metal porosity.
2. Undercut present at the weld root can be reduced through the adoption of a defocused laser beam and a decreased modulation amplitude.
3. High speed observation and subsequent Fourier analysis has shown the presence of common periodic behaviours in the vapour plume and keyhole when low porosity welding conditions are utilised.
4. An oscillating wave was created in the weld pool when low porosity welding conditions were used, which is thought to act in manipulating the ejection angle of the vapour plume and aiding the escape of the gas bubbles in the weld pool.

Acknowledgements

This work was funded by the Industrial Members of TWI, as part of the Core Research Programme. Part of the work was funded by the Engineering and Physical Sciences Research Council (EPSRC) under grant no. C537750. Materials were provided by Aeromet International PLC (London, UK) and The Boeing Company (Seattle, WA, USA). The Photron SA-3 camera and the LS20-50 copper vapour laser were loaned from the EPSRC Engineering Instrument Pool (Didcot, UK).

References

1. P. Hilton, J. Blackburn and P. Chong: 'Welding of Ti–6Al–4V with fibre delivered laser beams', Proc. Laser Material Processing Conf. (ICALEO), Orlando, FL, USA, November 2007, LIA, 887–895.
2. A. Matsunawa: 'Problems and solutions in deep penetration laser welding', *Sci. Technol. Weld. Join.*, 2001, **6**, 351–354.
3. D. V. Lindh and G. M. Peshak: 'The influence of weld defects on performance', *Weld. J.*, 1969, **48**, 45–56.
4. V. I. Lakomski and N. N. Kalinyuk: 'The solubility of hydrogen in liquid titanium', *Automat. Weld.*, 1963, **16**, 28–32.
5. L. Chen, L. Hu and S. Gong: 'A study on the porosity of CO_2 laser welding of titanium alloy', *China Weld.*, 2006, **15**, (1), 1–5.
6. T. Klein, M. Vicanek, J. Froos, I. Decker and G. Simon: 'Oscillations of the keyhole in penetration laser beam welding', *J. Phys. D*, 1994, **27D**, 2023–2030.
7. T. Y. Kuo and S. L. Jeng: 'Porosity reduction in Nd–YAG laser welding of stainless steel and inconel alloy by using a pulsed wave', *J. Phys. D*, 2005, **38D**, 722–728.
8. A. Matsunawa, M. Mizutani, S. Katayama and N. Seto: 'Porosity formation mechanism and its prevention in laser welding', *Weld. Int.*, 2003, **17**, 431–437.
9. I. Kawaguchi, S. Tsukamoto, G. Arakane and H. Honda: 'Characteristics of high power CO_2 laser welding and porosity suppression mechanism with nitrogen shielding – study of high power laser welding phenomena', *Weld. Int.*, 2006, **20**, 100–105.
10. A. Matsunawa, J. D. Kim, N. Seto, M. Mizutani and S. Katayama: 'Dynamics of keyhole and molten pool in laser welding', *J. Laser Appl.*, 1998, **10**, 247–254.
11. J. Xie: 'Dual beam laser welding', *Weld. J.*, 2002, **81**, 223–230.
12. H. G. Eberle and K. Richter: 'Welding of aluminium alloys with modulated lasers', Proc. Laser Materials Processing Conf. on 'Industrial and microelectronics applications', Vienna, Austria, April 1994, SPIE, 185–191.
13. Y. Shimoksu, S. Fukumoto, M. Nayama, T. Ishide, S. Tsubota, A. Matsunawa and S. Katayama: 'Application of pulse-modulated high-power YAG laser welding to welding of heavy plates', *Weld. Int.*, 2003, **17**, 534–540.

Chapter 7

Dual Focus Nd:YAG Laser Welding

7.1 Introduction

This paper has been accepted for publication in *Lasers in Engineering*. The paper is an extended version of a peer reviewed conference paper, which was published in the proceedings of the 36th International MATADOR Conference in July 2010. After presentation of the research on the 14th July, the paper was selected to be considered for publication in *Lasers in Engineering*. This research is presented in the format it was submitted to *Lasers in Engineering*, but retains the pagination sequence of this thesis. The research was performed with Dr Chris Allen, Dr Paul Hilton and Professor Lin Li.

In terms of the co-author involvement Dr Chris Allen and Dr Paul Hilton assisted with defining the scope of the laser parameters that were to be considered for this experiment, based on a literature review performed by the author of this thesis and the performance capabilities of the available laser sources and dual focus forming process head. All the experimental trials, including the high speed video observations, weld quality evaluation and statistical analysis was performed by the author of this thesis. Dr Paul Hilton and Professor Lin Li provided guidance on the statistical analysis.

Dual Focus Nd:YAG Laser Welding of Titanium Alloys: Effect on Porosity Formation

J.E. BLACKBURN[1]*, C.M. ALLEN[1], P.A. HILTON[1] AND L. LI[2]
[1]*TWI Ltd, Cambridge, Cambridgeshire, CB21 6AL, UK*
[2]*School of Mechanical, Aerospace and Civil Engineering, The University of Manchester, Manchester, Greater Manchester, M60 1QD, UK*
*Corresponding author: Phone: +44 1223 899000; Fax: +44 1223 892588; E-mail: jon.blackburn@twi.co.uk

ABSTRACT

The dual focus technique has been considered as a method for reducing porosity formation when Nd:YAG laser welding titanium alloys. Response surface methodology has been used to examine the effects four process variables - foci orientation, foci separation, welding speed and power ratio – have on the formation of porosity. The statistical results and high speed imaging have shown that both transverse and in-line foci orientations, with controlled foci separations and welding speeds, can be used to establish a stable elongated keyhole, promoting low porosity welds.

1 INTRODUCTION

Keyhole laser welding is a non-contact joining technology characterised by the high power densities ($>10^4 Wmm^{-2}$) applied to the surface of the substrate, which produces a high aspect ratio (depth:width) keyhole, in most metallic materials. Fusion welds produced by this technology have minimal thermal distortion compared with arc welding processes. Moreover, keyhole laser welding has advantages compared with electron beam and friction welding processes, including; the ability to operate out of vacuum, and the flexibility provided by fibre delivered 1µm wavelength laser sources allowing easy robotic manipulation. However, observations of the keyhole laser welding process, first by Arata et al [1] and later by Matsunawa et al [2], have shown that dynamic instabilities in the keyhole geometry may occur even with a constant set of process parameters. These instabilities may lead to the formation of weld defects, such as undercut and porosity [2], and are as a result of an imbalance between the forces acting to open the keyhole and those acting to close it.

Forces acting to close the keyhole are the surface tension and metallostatic forces of the surrounding molten material, and the hydrodynamic forces generated during the transfer of molten material from the front of the keyhole to the trailing melt pool [3]. In addition, the forces generated in the trailing melt pool as a result of Marangoni convection and vapour friction effects may lead to further forces acting to close the keyhole [4]. The keyhole is held open by the recoil pressure, generated as the laser beam is absorbed and ablates a portion of the molten material sheath, and the vapour pressure in the keyhole [5]. The physical mechanisms causing these forces are so intertwined that it is hard to envisage a quasi steady-state keyhole even with constant process parameters. Theoretical research [6] has shown that keyhole instabilities can be induced by a $\geq 1\%$ fluctuation in the incident

laser power, which have sufficient amplitude to cause keyhole collapse if they occur at the resonant frequencies of the keyhole.

For high-performance components, particularly those subjected to fatigue loads, stringent weld quality criteria exist [7] which define maximum allowable defect levels. The occurrence of porosity in the weld metal is of primary concern (particularly if the weld is dressed) as a result of its negative effects on the fatigue life [8]. Reducing the severity and/or occurrence of porosity would enable the keyhole laser welding process to be utilised in the construction of high-performance components. For titanium alloy aerospace components there are considerable cost savings to be made, in terms of reduced material consumption and increased productivity, by replacing conventional machining techniques with a near-net-shape welding process [9].

Several different techniques have been considered for manipulating the keyhole behaviour and consequently preventing weld metal porosity when keyhole laser welding, including; a gas jet directed towards the keyhole [10], modulation of the laser output [11], and dual focus laser welding [12]. Dual focus forming optics can be utilised with a single laser beam input to produce two focused spots on the surface of the workpiece. The optics allow manipulation of the foci separation, the foci orientation and the relative power ratio between the two focused spots. It was reported [12] that weld metal porosity could be reduced when welding aluminium alloys with a Nd:YAG laser if a dual focus configuration was utilised, compared with a single spot configuration. Similar results have also been reported [13] when welding type 304 stainless steel with a CO_2 laser.

In this study, the dual focus technique has been considered as a method for reducing porosity formation when Nd:YAG laser welding of titanium alloys. The effects of foci orientation, foci separation, welding speed and the power ratio between the two foci on the resulting penetration, profile and, primarily, the porosity content have been assessed. High speed (10kHz) imaging has been performed to determine the effects of these parameters on the keyhole and vapour plume behaviour.

2 METHODOLOGY

2.1 Materials and material preparation

Experimental trials were performed on 3.25mm thickness Ti-2.5Cu plates, of a length up to 150mm in the welding direction. The plates had been chemically pickled after rolling, although the time between pickling and welding was not controlled. Plate surfaces were cleaned with an abrasive paper and acetone degreased prior to processing.

2.2 Equipment and experimental procedure

Figure 1 details the typical equipment configuration. Welding was performed with a Trumpf HL4006D Nd:YAG laser, of 23mm.mrad beam parameter product. A 600µm core diameter optical fibre transmitted the laser light to a HIGHYAG dual focus process head.

The calculated diameters of the beam waist were 450µm. The beam waists were kept coincident with the top surface of the workpiece; since operating out of focus when using a dual focus forming module does not give a simple beam profile. A laser power of 4.1kW at the workpiece, measured with a water-cooled Ophir power meter, was used for all experiments. The downhand (1G) position was adopted throughout all tests. A stainless steel trailing shield and a square-section copper efflux channel were supplied with a regulated supply of argon (99.998% purity) in all experiments.

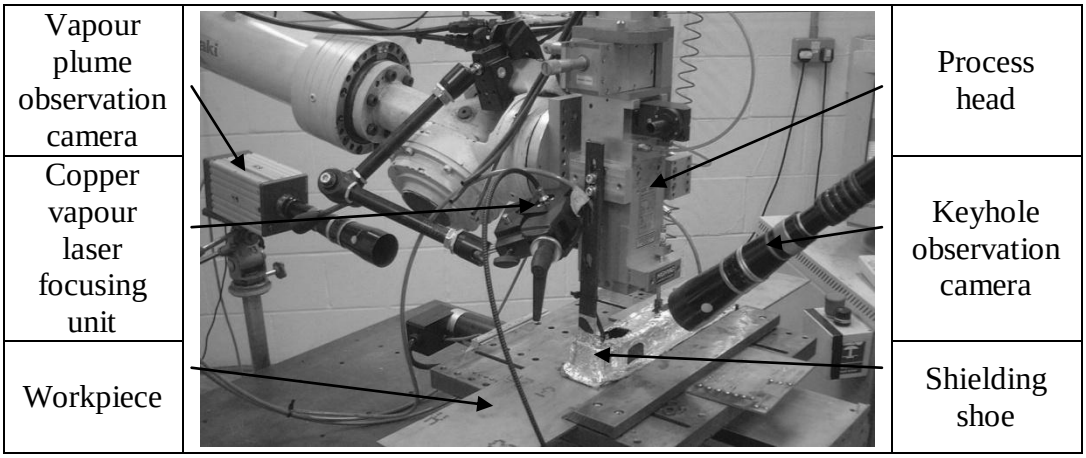

FIGURE 1 Typical equipment configuration.

2.3 Process variables

The dual focus forming module allowed manipulation of the foci orientation (with respect to the welding direction), the foci separation, and the power ratio between the two focused spots. The ranges of the four process parameters investigated are detailed in Table 1 [14]. The relative intensity between the foci was only varied in the in-line configuration. In order to assess a large number of parameter combinations, autogeneous melt run trials on plate were performed. This method also prevents other, potentially uncontrolled, variables (i.e. joint-gap and edge cleanliness) from interfering with the interpretation of results. It is known from previous research by the authors [15, 16] that welding conditions developed through melt runs can successfully be transferred to close fitting butt joints.

TABLE 1 Process variables investigated [14].

Parameter	Range
Foci orientation	transverse or in-line to welding
A: Welding speed (mm/s)	33.33 – 116.67
B: Foci separation (mm)	0[†] , 0.15, 0.30, 0.45, 0.54, 0.90,
C: Power ratio[‡]	50:50, 60:40, 78:22

[†]i.e. a single 450µm diameter spot, [‡]Only varied in the in-line spot configuration

2.4 Weld quality evaluation

All melt runs were assessed visually for discoloration, and radiographed to determine their weld metal porosity content. Radiography was performed in accordance with BS EN 1435:1997, allowing indications ≥0.05mm in size to be detected. The weld metal porosity was determined by summing the diameters of all the pores in a 76mm weld length, giving

an accumulated length of porosity (presented in units of mm in the subsequent figures) for each melt run; as specified in AWS D17.1:2001 '*Specification for Fusion Welding for Aerospace Applications*' by the American Welding Society. Selected melt runs were also sectioned, transverse to the welding direction, at representative positions, to assess their weld profile.

2.5 High speed imaging

High speed imaging (10kHz) of the keyhole and vapour plume behaviours were performed during selected melt runs. Temporal and spatial filtering techniques were used to reduce the inherently bright broadband process emissions for the keyhole observations. Illumination of the keyhole was then provided by an Oxford Lasers LS20-50 copper vapour laser (CVL). Quartz glass windows in the shielding shoe ensured the weld pool remained shielded.

Observation of the images provides qualitative information regarding the effect of parameters on key process mechanisms. In order to attain quantitative data, allowing numerous different welding conditions to be compared directly, a MATLAB® program was used to extract and subsequently analyse pixel intensity data from the images. The mean pixel intensity (MPI) for each frame was calculated for a region of interest which approximated either the position of the keyhole or the path of the laser beam. The resulting MPI data sets were then analysed to determine their behaviour and correlated with the corresponding weld quality and statistical results.

3 RESULTS

3.1 Welding performance

Figure 2 [14] details the maximum welding speeds which resulted in consistent full penetration for the range of parameters investigated. Four separate data sets are shown, corresponding to the transverse orientation and the in-line orientations with power ratios of 50:50, 60:40 and 78:22. In terms of welding performance, operation in the in-line orientation has advantages compared with the transverse orientation. For the in-line orientation and at foci separations exceeding 0.45mm, the penetration is determined by the power ratio – a larger difference between the two relative intensities tending to increase the penetration depth for a given welding speed.

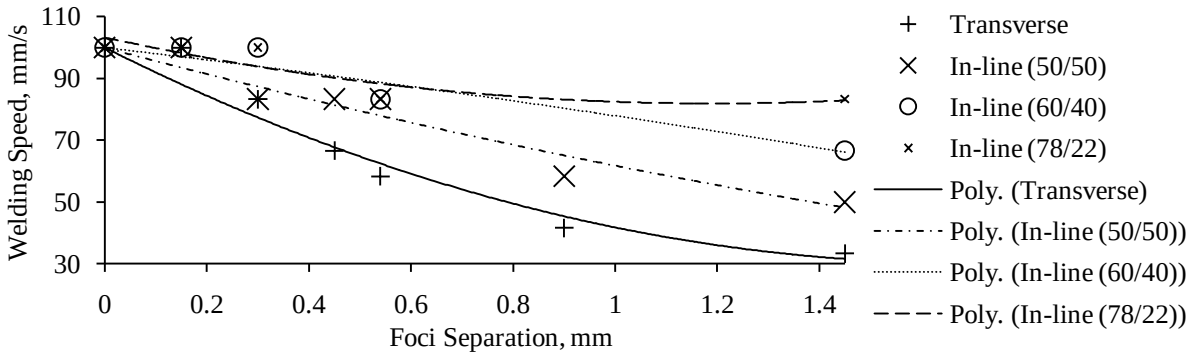

FIGURE 2 Limits of full penetration for transverse and in-line spot orientations [14].

3.2 Statistical analysis

Design of Experiment techniques were not used for experimental design, although the scope of parameter permutations executed is similar to two fractional high-order factorial experiments. The accumulated length of porosity data obtained from the analysis of the radiographs provides a historical quantitative response which can be statistically analysed. Furthermore, a large number of parameter combinations were repeated, allowing prediction variances to be minimised. The statistical software package, Design-Expert 8.0.1 was used to historically analyse the weld metal porosity data using response surface methodology (RSM); which determines a suitable approximation for the true functional relationship between a quantitative response and a set of input variables (process variables). Constraints, established from Figure 2 [14], were positioned on the design space to ensure that only parameter combinations which resulted in consistent full penetration were permitted. Analysis of the transverse foci and in-line foci orientations was performed separately to simplify the analysis.

For both analyses, a response transformation was necessary in order to reduce the residuals; a square root and a $\log_{10}$ transformation were applied to the transverse (62 melt runs) and in-line (92 melt runs) data sets respectively. A cubic model provided the most complete description of the response for both data sets. To minimise the prediction variances, those melt runs produced in the transverse foci orientation with a foci separation >0.54mm (10 melt runs) were removed from the analysis. A single melt run was also excluded from the analysis of the in-line orientation data. Linear regression analysis, and a backward elimination technique was utilised to remove non-significant terms from the cubic model. The p-values, or statistical significance, of individual terms were determined using analysis of variance (ANOVA). Those terms with p-values >0.10 were deemed statistically insignificant and removed from the model unless they were required to support hierarchical terms. Table 2 and 3 detail the terms, and their p-values, included in the transverse and in-line models.

TABLE 2 ANOVA for transverse foci orientation model.

Source	Sum of Squares	df	Mean square	F value	Prob > F	Effect
Model	34.20	7	4.89	24.07	< 0.0001	significant
A	3.68	1	3.68	18.12	0.0001	significant
B	2.20	1	2.20	10.83	0.0019	significant
AB	3.15	1	3.15	15.51	0.0003	significant
A^2	4.40	1	4.40	21.69	< 0.0001	significant
B^2	5.42	1	5.42	26.72	< 0.0001	significant
A^2B	1.63	1	1.63	8.05	0.0068	significant
AB^2	2.09	1	2.09	10.28	0.0025	significant
Residual	9.13	45	0.20			
Lack of Fit	2.88	16	0.18	0.83	0.6416	not significant
Pure Error	6.26	29	0.22			
Cor Total	43.33	52				

TABLE 3 ANOVA for in-line foci orientation model.

Source	Sum of Squares	df	Mean square	F	Prob > F	Effect
Model	9.73	11	0.88	17.66	< 0.0001	significant
A	0.28	1	0.28	5.59	0.0205	significant
B	0.41	1	0.41	8.26	0.0052	significant
C	0.05	1	0.05	0.96	0.3295	not significant
AB	0.00	1	0.00	0.02	0.8923	not significant
AC	0.50	1	0.50	10.07	0.0021	significant
BC	0.35	1	0.35	6.98	0.0099	significant
A^2	0.01	1	0.01	0.11	0.74	not significant
B^2	0.19	1	0.19	3.77	0.0557	not significant
ABC	0.20	1	0.20	3.90	0.0516	not significant
A^2B	0.79	1	0.79	15.71	0.0002	significant
B^2C	0.41	1	0.41	8.26	0.0052	significant
Residual	4.01	80	0.050			
Lack of Fit	1.33	45	0.030	0.39	0.9985	not significant
Pure Error	2.67	35	0.076			
Cor Total	13.74	91				

Diagnostic graphical checks were performed on the residuals of both models to ensure that the factors were fixed and not random, thereby meeting the ANOVA assumptions. Studentised forms of the residuals were used in all the checks. No abnormalities were found in the normal plot of residuals. The plots of residuals against the predicted values and the run order (Figure 3a and 3b) indicated that no assumptions were contravened. The random scatter of results about the centre line in the residuals versus run order plots signify that there are no time-related variables that have not been accounted for in the analysis. Additional graphical tests (not shown in this paper) were carried out to provide a measure of the influence, potential or actual, that individual melt runs may have. No melt runs were found to have a high degree of influence or leverage over either model. The final β coefficient values for both models, in terms of actual factors, are detailed in Table 4 [14].

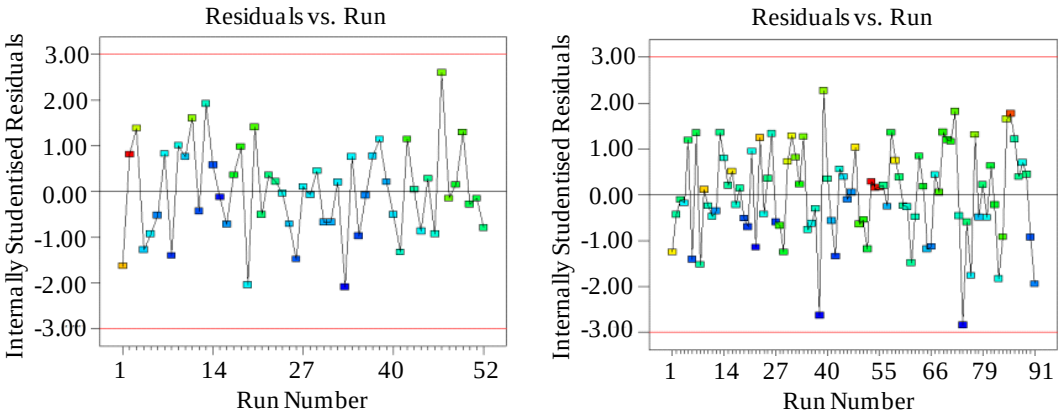

(a) (b)

FIGURE 3 Plots of the externally studentised residuals for the transverse (a) and the in-line (b) data.

TABLE 4 β coefficient values, in terms of actual factors, for the transverse and in-line models [14].

Coefficient	Transverse	In-line
ϐ0	9.76E+0	7.58E+0
ϐA	-1.74E-1	-1.78E-1
ϐB	4.11E+1	-8.84E+0
ϐC	n/a	not significant
ϐAB	-1.29E+0	not significant
ϐAC	n/a	8.31E-5
ϐBC	n/a	-1.91E-2
ϐABC	n/a	5.15E-4
$ϐA^2$	9.15E-4	not significant
$ϐB^2$	4.76E+1	not significant
$ϐA^2B$	8.07E-3	-1.62E-3
$ϐAB^2$	1.03E+0	not significant
$ϐB^2C$	n/a	-2.22E-2

3.3 Transverse foci orientation

3.3.1 Porosity formation

There were significant differences in the amount of porosity observed in the melt runs produced in the transverse foci orientation. Foci separations of 0.54mm and above had an accumulated length of porosity >40mm, and were not included in the statistical analysis since they exerted too much influence on the model. The remaining 52 melt runs had accumulated lengths of porosity in the range 0.7 to 27.6mm. Pore diameters were in the range 0.1 - 0.4mm, with predominantly smaller diameter pores (0.1 – 0.2mm) present at speeds >70mm/s.

Figure 4 details the perturbation curves (Figure 4a) and response surface (Figure 4b) for the transverse foci orientation model detailed in Table 4 [14]. The perturbation curves indicate that at welding speeds between 33 and 60mm/s the porosity content in the weld metal is primarily determined by the welding speed and negligibly influenced by the foci separation. According to the response surface in Figure 4b, those melt runs produced with

a welding speed <60mm/s will have an accumulated length of porosity >4.0mm. Conversely, at welding speeds above 60mm/s the foci separation and welding speed have similar influences on the porosity content of the melt run (Figure 4a).

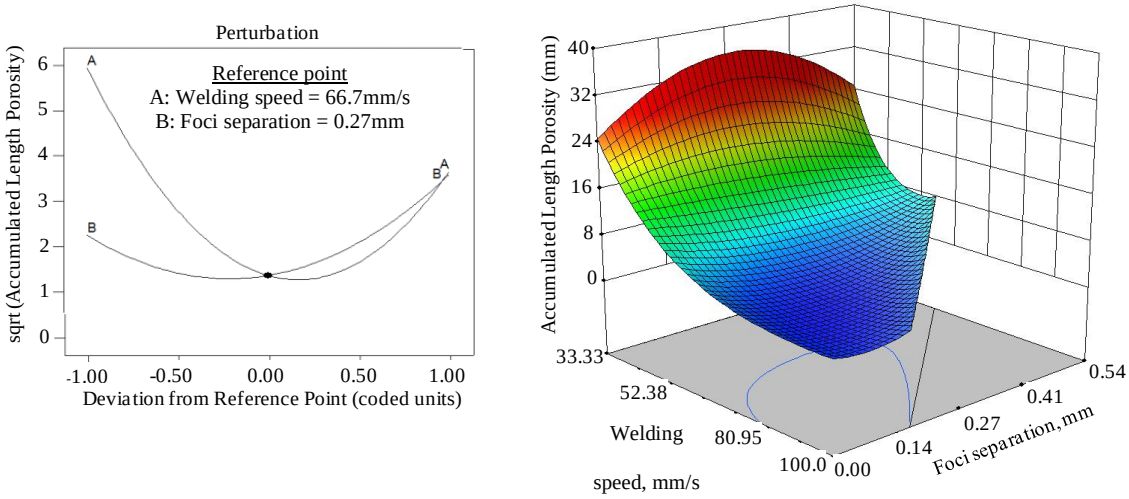

(a) (b)

FIGURE 4 Perturbation curves (a) and a contour graph (b) detailing the effects of the welding speed and the foci separation on the formation of porosity in the weld metal.

Parameter combinations in the response surface indicate that melt runs can be readily produced which contain relatively low levels of weld metal porosity. For instance, melt runs with <1.7mm accumulated length porosity can be produced if a welding speed of 70-100mm/s is adopted with an appropriate foci separation. Within this range of welding speeds, an increase in the heat input (i.e. decrease in welding speed) necessitated an increase in the foci separation in order to minimise the resultant porosity content. Very small accumulated lengths of porosity (≤1.0 mm) are predicted by the model to occur at a welding speed of ~80mm/s and a foci separation of ~0.15mm. Two separate melt runs produced with parameters very close to these parameters had accumulated lengths of porosity of 0.8 and 1.4mm. In comparison, two melt runs produced with a 0mm spot separation had accumulated lengths of porosity of 2.0 and 4.2mm.

3.3.2 Profile

Transverse cross-sections of melt runs produced at a welding speed of 66.7mm/s (the fastest welding speed giving full penetration at foci separations of up to 0.54mm) with increasing spot separations are detailed in Figure 5. Face and root undercut are present on the melt run produced with a single spot to a maximum depth of 0.14mm (both on face and root). At spot separations ≥0.30mm the weld profile improves, as the undercut at the weld root is eliminated.

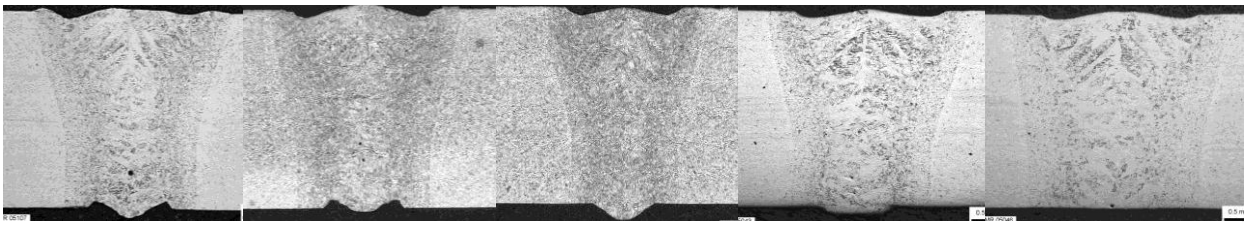

(a) (b) (c) (d) (e)

FIGURE 5 Transverse cross-sections of melt runs produced in 3.25mm thickness Ti-2.5Cu with a transverse foci orientation, a welding speed of 66.7m/s, and foci separations of 0 (a), 0.15 (b), 0.30 (c), 0.45 (d) and 0.54mm (e).

3.4 In-line foci orientation

3.4.1 Porosity formation

Similar to the porosity formation observed in the transverse foci orientation, a wide range of porosity contents (between 0.8 and 37.6mm accumulated length) and pore diameters (between 0.1 and 0.5mm) were observed using an in-line foci orientation. Pore diameters of up to 0.5mm were produced, although the majority of pores were ≤0.2mm diameter. All 91 melt runs produced were included in the model. Perturbation curves and response surfaces, calculated from the β coefficients, for the three different focus power ratios examined, are detailed in Figure 6. In the response surface graphs, the design space has been limited in order to ensure only fully penetrating welds are considered.

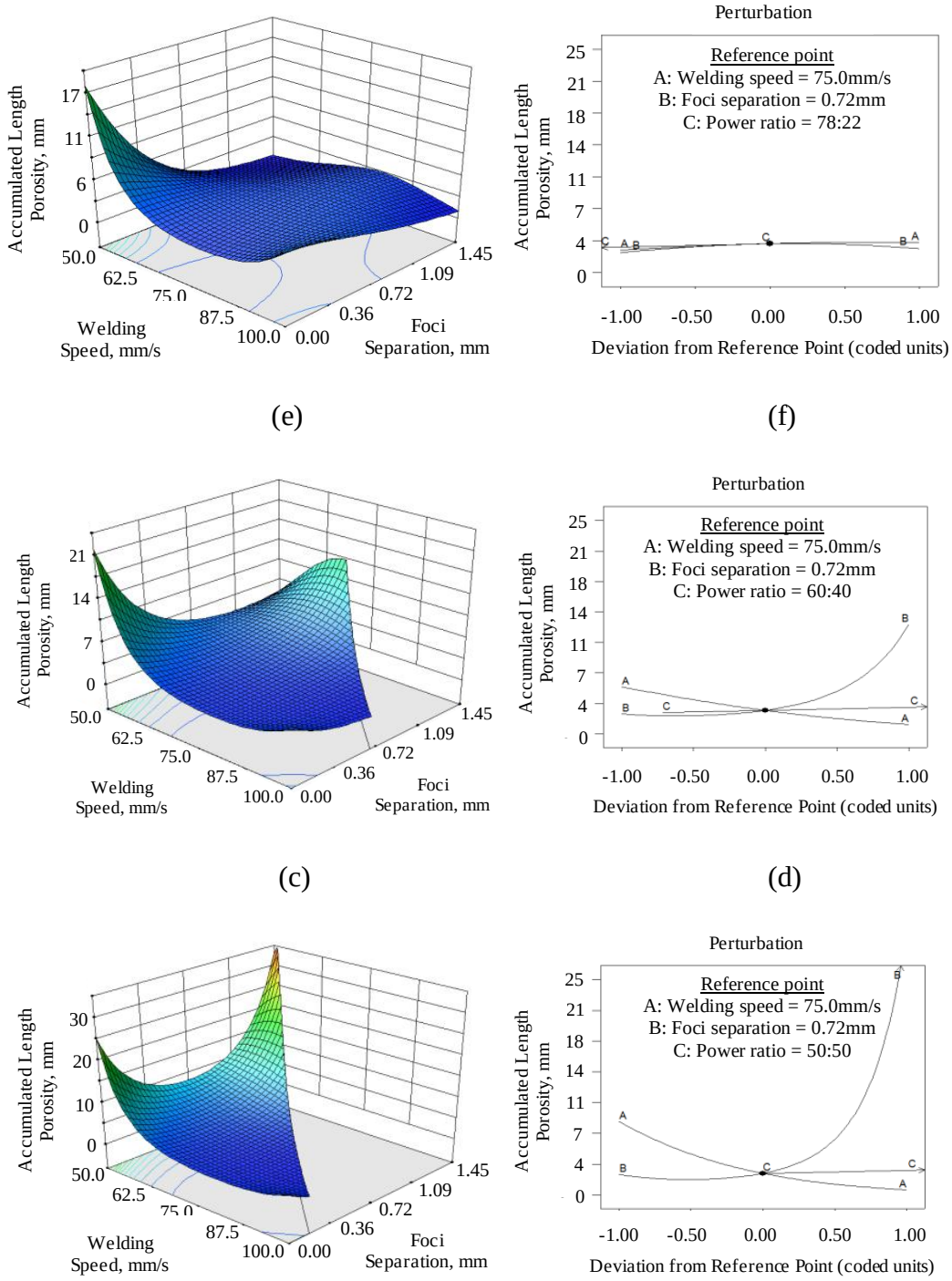

FIGURE 6 Perturbation curves and response surfaces showing the effect of welding speed and foci separation on porosity formation, for power ratios of 50:50 (a, b), 60:40 (c, d), and 78:22 (e, f).

Figures 6a and 6b are the response and perturbation curves produced with a power ratio of 50:50. As observed in the transverse foci orientation model, the porosity content increases significantly at welding speeds below ~67mm/s. However, with a foci separation of ~0.70mm this increase is limited. At increased welding speeds, the level of subsurface

porosity formed in the weld metal is significantly less for all foci separations giving full penetration. Positioning the foci with a separation of ~0.15mm leads to a reduction in porosity compared with a single spot condition. The modeled response and perturbation curves when operating with an in-line configuration with a power ratio of 60:40 are detailed in Figures 6c and 6d. The range of conditions giving full penetration is increased compared with that shown in Figure 6a; as a result of the higher leading power density. As with a 50:50 power ratio, the porosity formation can be limited at slower welding speeds by adopting an appropriate foci separation. The modelled response surface indicates the best results possible with a 60:40 power ratio are at higher welding speeds and with a slight foci separation. Figures 6e and 6f are the response and perturbation curves produced with a power ratio of 78:22. Apart from the significant increase in porosity formation when operating with a foci separation of 0mm and low welding speeds, the response surface is particularly flat. From Figure 6e it can be seen that using a foci separation of 1.45mm is conducive to producing a comparatively low porosity melt run at all welding speeds. A similar behaviour, although not as beneficial, is also noticed in Figure 6c (60:40 power ratio).

The response surfaces produced for the three different focus power ratios indicate that an increased power density in the leading focus will reduce considerably the occurrence of porosity at lower welding speeds when welding with foci separations of 0.45mm and above. Nevertheless, the lowest levels of weld metal porosity when using an in-line foci orientation are modeled to occur when using a 50:50 power ratio with a welding speed >75.0mm/s and a foci separation of between 0.15 and 0.30mm. The model predicts that a single melt run produced with a foci separation of 0.30mm and a welding speed of 83.3mm/s will have an accumulated length of porosity of 1.4mm. Three melt runs produced with an identical combination of parameters, which were included in the analysis, contained 0.8, 1.0 and 1.1mm accumulated length of porosity; indicating very little experimental noise.

3.4.2 Profile

Transverse cross-sections, representative of the entire weld length, of melt runs produced at welding speeds of 66.7 and 83.3mm/s, and with different foci separations, are detailed in Figure 7. Figures 7a – 7e detail the melt runs produced at a welding speed of 66.7mm/s. All the melt runs produced at this welding speed have varying amounts of undercut at the weld face. Undercut at the weld root can be significantly reduced by using a foci separation ≥0.30mm. The melt runs produced at a welding speed of 83.3mm/s had a more inconsistent weld bead appearance compared with those produced at 66.7mm/s. The profiles detailed in Figures 7f-7j indicate varying amounts of face and root undercut, and no benefit to the weld profile by operating with increased spot separations.

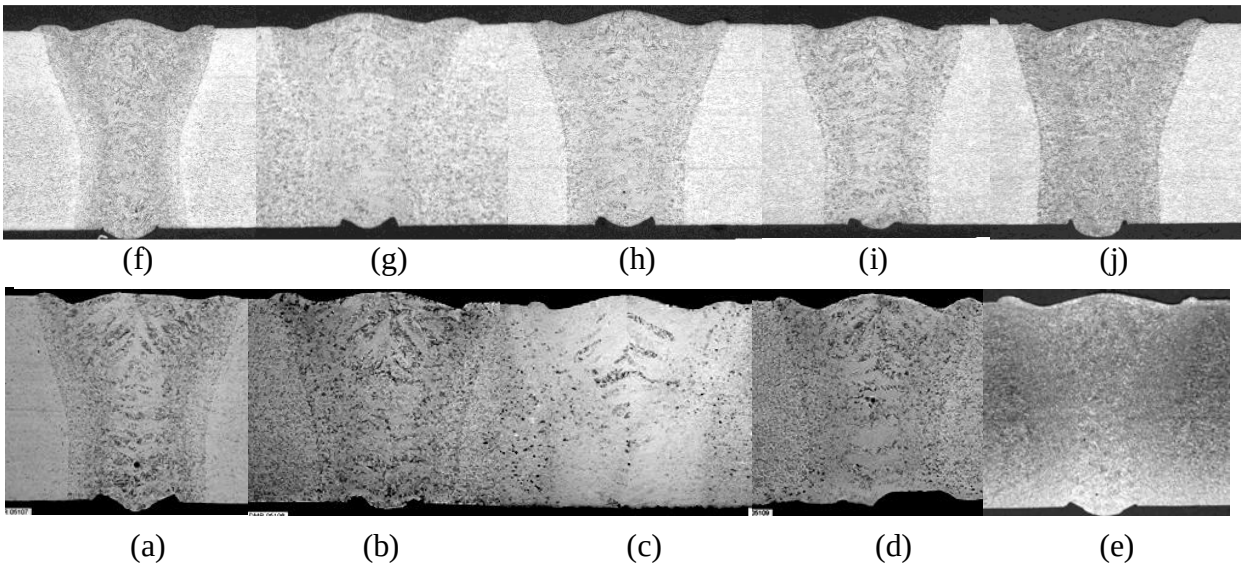

FIGURE 7 Transverse cross-sections of melt runs produced in 3.25mm thickness Ti-2.5Cu with an in-line foci orientation, a 50:50 power ratio, a welding speed of either 66.7 (a - e) or 83.3mm/s (f – j), and foci separations of 0 (a, f), 0.15 (b, g), 0.30 (c, h), 0.45 (d, i) and 0.54mm (e, j).

3.5 Wire feed

Wire feed was considered as a means of reducing undercut. The wire was fed into the front of the weld pool. An angle of 45° and a position 1mm ahead of the laser impingement point were adopted from previous experience, and wire feed rates of 2- 5m/min were examined for two parameter combinations: (i) in-line foci orientation, 0.30mm foci separation, 83.3mm/s welding speed and a 50:50 power ratio; and, (ii) transverse foci orientation, 0.30mm foci separation and a 66.7mm/s welding speed.

The introduction of wire necessitated a reduction in welding speed in order to maintain full penetration for both foci orientations; although this effect was more pronounced with the in-line foci orientation. Wire feed rates of 66.7-83.3mm/s eliminated undercut entirely but necessitated a decrease in welding speed, which significantly increased porosity content. The most favourable result was produced with the transverse foci orientation, particularly with a wire feed rate of 50mm/s and a welding speed of 58mm/s; giving a 1.8mm accumulated length of porosity and a melt run free of undercut.

3.6 High speed imaging

3.6.1 Keyhole behaviour

The images produced were analysed with a MATLAB program to determine their MPI in the keyhole area. It was envisaged that quantitative trends in keyhole closure could have been detected by this method. A similar method has been used previously by the authors during modulated Nd:YAG laser welding of titanium alloys [15]. The contrast in the images was insufficient for the MATLAB program, and the pictures have been analysed qualitatively. In the in-line foci orientation, high speed videos were taken with a 50:50 power ratio between the spots. Three different welding regimes were noted:

1. Single keyhole: this regime occurred when the foci separation was ≤0.30mm, irrespective of welding speed. As detailed in Figure 8a.

2. Dual keyhole: this regime occurred with foci separations ≥0.90mm, irrespective of welding speed. As detailed in Figure 8b.
3. Transitional: in this regime periodic transitions between the single and dual keyhole regimes occurred, as detailed in Figure 8c-8f. This regime occurred at foci separations of 0.45-0.54mm.

The same welding regimes were present in images of the keyhole(s) behaviour with a transverse foci orientation. In both foci orientations, foci separations ≥0.90mm led to particularly complex melt flow interactions between the two keyholes and frequent keyhole collapses resulted. Similarly, in the transitional regime, frequent keyhole collapses were observed. With the single spot regime, much fewer keyhole collapses occurred, particularly at high welding speeds.

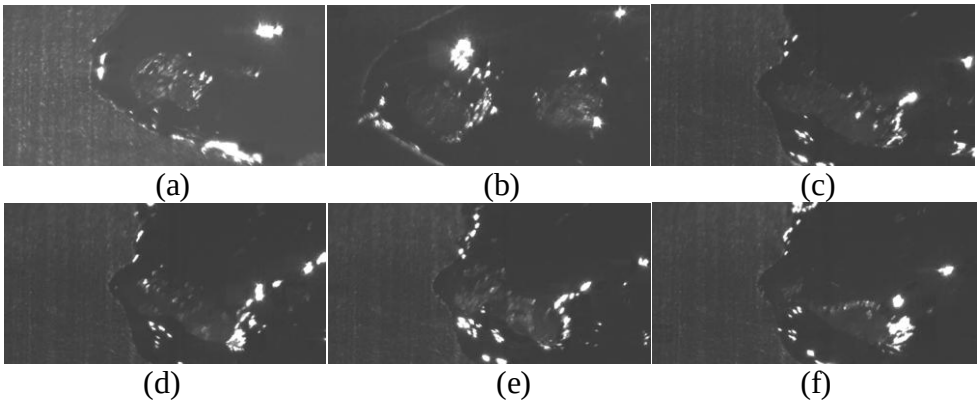

FIGURE 8 Images of the in-line foci orientation, a 50:50 power ratio, and: (a) a 0.15mm foci separation and a 83mm/s welding speed; (b) a 1.45mm foci separation and a 50mm/s welding speed; and (c)-(f) a 0.54mm foci separation and a welding speed of 66.7mm/s, intervals of 100µs.

3.6.2 Vapour plume behaviour

The images of the vapour plume produced with the in-line foci orientation indicated that at foci separations of 0.15 and 0.30mm the vapour plume had a more constant behaviour and did not fluctuate as frequently compared with a single focused beam, as detailed in Figure 9 [14]. The MPI technique was used to analyse the vapour plume behaviour of melt runs produced with the foci orientated in-line with the welding direction, a power ratio of 50:50, foci separations of 0-1.45mm and welding speeds of 41.7-83.3mm/s. The MPI of the vapour plume in the path of the laser beam, up to 3mm above the keyhole, was individually calculated for 5000 images (0.5s of real time) per welding condition. The resulting data set for each welding condition therefore contained 5000 data points each having a value between 0 and 255 (average of RGB intensities). The standard deviation of the individual data sets was then calculated to determine the variation of pixel intensities from the average; and thereby infer the variation in vapour plume behaviour in the path of the laser beam.

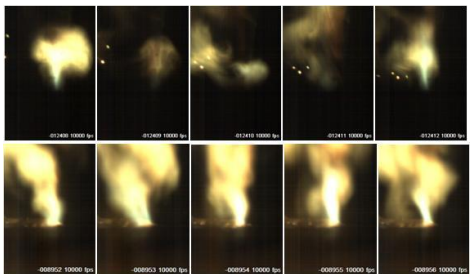

FIGURE 9 Images of the vapour plume when welding with a single focus (top) and an optimised dual focus (below), at 100µs intervals [14].

Table 5 details the results for six different welding conditions, and their observed accumulated lengths of porosity. There is a correlation between the standard deviation of the MPI and the resultant internal quality of the weld. Melt runs produced with the transverse foci orientation were not analysed as imaging of the vapour plume could not be performed in-line with the welding direction.

TABLE 5 Standard deviation of the vapour plume mean pixel intensity (MPI) for melt runs produced with an in-line foci orientation and a power ratio of 50:50.

Foci Separation (mm)	Welding Speed (mm/s)	Standard Deviation of MPI	Porosity - Accumulated Length (mm)
0	83.3	33.5	2.0, 4.2
0.15	83.3	23.7	0.8, 1.4
0.30	83.3	26.9	2.3
0.45	83.3	33.1	5.6
0.90	41.7	44.7	43.9, 50.5, 46.7
1.45	41.7	50.1	59.3, 50.5

4 DISCUSSION

The welding performance data shows that if the foci separation is increased, the welding speed must be reduced in order to maintain full penetration. This is a result of the interaction between the two focused laser beams decreasing, leading to a significantly reduced power density at the workpiece. This decrease in welding performance at increasing foci separations is more noticeable in the transverse configuration; as an additional volume of material must be processed with each increment in foci separation.

The statistical analysis of porosity formation in melt runs, produced in 3.25mm thickness Ti-2.5Cu using the dual focus Nd:YAG laser welding technique, has enabled the influence of foci separation, welding speed and power ratio to be determined. The statistical models produced for both foci orientations indicate that a foci separation of 0.15-0.30mm can reduce porosity formation at higher welding speeds (~80mm/s). Qualitative analysis of the keyhole behaviour, in both foci orientations, has shown a single keyhole is still present with these spot separations and welding speeds, which appeared more stable than the dual keyhole or transitional regimes. The quantitative vapour plume behaviour analysis has shown less variation occurs in vapour plumes produced from the single keyhole regime than the transitional and dual keyhole regimes. High variations in the vapour plume behaviour are indicative of an unstable keyhole, since:

1. The ejection angle of the vapour plume is directly related to the absorption angle of the incident laser radiation at the front keyhole wall.
2. No vapour plume is ejected from the keyhole immediately after keyhole collapse.

Previous observations of the plasma behaviour when welding a 5000 series aluminium alloy with a CO_2 laser beam also suggested that, there was less variation in its behaviour if a dual focus technique was utilised [17]. A dual focused CO_2 laser has also been reported to reduce weld metal porosity when welding type 304 stainless steel with the focused spots arranged in-line with the welding direction [13]. The keyhole behaviour was observed using an in-situ X-ray transmission method, which revealed that the two keyholes coalesced to form one larger keyhole. It was argued that this prevents the generation of bubbles and hence weld metal porosity [13]. The results presented here agree with this argument; certainly closely separated foci resulted in keyholes which coalesced at the top surface in the single keyhole regime.

The levels of weld metal porosity reported in this research easily meet the criteria demanded by AWS D17.1 Class A (limit of 4.3mm accumulated length for 3.25mm thickness plate) and are very near to the criteria required for aeroengine applications (0.9mm accumulated length [7]). However, the levels of undercut are unacceptable and have necessitated the use of wire feed addition into the melt pool. The welding process was particularly sensitive to the wire feed rate, since the welding speed needed to be dropped considerably in order to maintain full penetration. In the in-line configuration the wire tended to choke the keyhole, destabilising the process and significantly increasing porosity content. In the transverse configuration the wider keyhole accommodated wire feed more easily, and at the correct wire feed rate the undercut on the weld face could be removed. This approach resulted in a level of porosity which would be suitable for applications requiring AWS D17.1 Class A criteria, but not suitable for aeroengine applications. In this situation, a different approach to eliminating undercut at the weld face and root, whilst minimising porosity formation with the optimum choice of dual focus parameters, would be to use an oversized joint thickness followed by subsequent machining of the weld bead.

5 CONCLUSIONS

This work has investigated the feasibility of reducing the formation of porosity in the weld metal when Nd:YAG laser welding titanium by using a dual focus technique. The results have been analysed by RSM and the models indicate that the weld metal porosity can be reduced to within levels stipulated by stringent aerospace criteria, if a relatively small foci separation and a suitable welding speed are utilised. Observation and subsequent analysis of the welding process using two high speed cameras has shown that small foci separations (0.15-0.30mm) increase keyhole stability; and hence reduce the occurrence of keyhole collapse and the formation of weld metal porosity.

6 ACKNOWLEDGEMENTS

This work was funded by the Industrial Members of TWI, and also by EPSRC grant no. C537750. Materials were kindly provided by Aeromet International PLC and The Boeing Company. A high speed camera and the CVL were loaned from the EPSRC Engineering Instrument Pool.

7 REFERENCES

[1] Arata, Y., Abe, N. and Oda, T. Beam hole behaviour during laser beam welding. *The International Congress on Application of Lasers and Electro-Optics (ICALEO 1983): Materials Processing Symposium*. Los Angeles, CA., USA, pp.59-66.

[2] Matsunawa, A., Kim, J.D., Seto, N., Mizutani, M. and Katayama, S. Dynamics of keyhole and molten pool in laser welding. *Journal of Laser Applications*, **10**(6) (1998), 247-254.

[3] Kroos, J., Gratzke, U. and Simon, G. Towards a Self-Consistent Model of the Keyhole in Penetration Laser Beam Welding. *Journal of Physics D: Applied Physics* **26**(3) (1993) 474-480.

[4] Kaplan A. Keyhole welding: the solid and liquid phases. in Dowden J.M. (Ed.) *The theory of laser materials processing: heat and mass transfer in modern technology*. Bristol: Canopus 2009, pp.71-93.

[5] Klein, T., Vicanek, M., Kroos, J., Decker, I. and Simon, G. Oscillations of the keyhole in penetration laser beam weld. *Journal of Physics D: Applied Physics* **27**(10) (1994), 2023-2030.

[6] Klein, T., Vicanek, M. and Simon, G. Forced oscillations of the keyhole in penetration laser beam welding. *Journal of Physics D: Applied Physics* **29**(2) (1996), 322-332.

[7] Hilton, P., Blackburn, J. and Chong, P. Welding of Ti-6Al-4V with fibre delivered laser beams. *The 26th International Congress on Application of Lasers and Electro-Optics (ICALEO 2007): Laser Materials Processing Section*. 29 October – 1 November 2007, Orlando, FL., USA. pp.887-895.

[8] Lindh, D.V. and Peshak, G.M. The influence of weld defects on performance. *Welding Journal*, **48** (1969), 45s-56s.

[9] Threadgill, P., Wynne, B., Russell, M. and Davies, P. Prefabricated materials preforms in titanium alloys using stationary shoulder friction stir welding. *TMS 2008 Collected proceedings of the 137th Annual Meeting and Exhibition*, 9-13 March 2008, New Orleans, LA., USA, pp.333-338.

[10] Kamimuki, K., Inoue, T., Yasuda, K. Muro, M., Nakabayashi, T. and Matsunawa, A. Prevention of welding defect by side gas flow and its monitoring method in continuous wave Nd:YAG laser welding. *Journal of Laser Applications*, **14**(3) (2002), 136-145.

[11] Kuo, T.Y. and Jeng, S.L. Porosity reduction in Nd-YAG laser welding of stainless steel and inconel alloy by using a pulsed wave. *Journal of Physics D: Applied Physics*, **38**(5) (2005) 722-728.

[12] Haboudou, A., Peyre, P., Vannes, A.B. and Peix, G. Reduction of porosity content generated during Nd:YAG laser welding of A356 and AA5083 aluminium alloys. *Materials Science and Engineering*, **363**(1-2) (2003), 40-52.

[13] Hayashi, T., Matsubayashi, K., Katayama, S., Abe, S., Matsunawa, A. and Ohmori, A. Reduction mechanism of porosity in tandem twin-spot laser welding of stainless steel. *Welding International*, **17**(1) (2003), 12-19.

[14] Blackburn, J.E., Allen, C.M., Hilton, P.A. and Li, L. Dual focus Nd:YAG laser welding of titanium alloys. *The 36th International MATADOR 2010 conference*. 14-16 July (2010), Manchester, United Kingdom. pp.279-282.

[15] Blackburn, J.E., Allen, C.M., Hilton, P.A., Li, L., Hoque, M.I. and Khan, A.H. Modulated Nd:YAG laser welding of Ti-6Al-4V. *Science and Technology of Welding and Joining* **15**(5) (2010), 433-439.
[16] Blackburn, J.E., Allen, C.M., Hilton, P.A. and Li, L. Nd:YAG laser welding of titanium alloys using a directed gas jet. *Journal of Laser Applications* **22**(2) (2010), 71-78.
[17] Xie, J. Dual Beam Laser Welding. *Welding Journal* **10** (2002), 283s-290s.

Chapter 8

Welding with Excellent Beam Quality 1µm Wavelength Laser Sources

8.1 Introduction

This paper has been prepared for publication in a suitable peer reviewed Journal. The paper combines the results of research reported at the 4th Pacific International Conference on Applications of Lasers and Optics (PICALO) in Wuhan, China [Blackburn et al, 2010] and more recent results. The unpublished research is currently under embargo by TWI, and consequently the paper will be submitted for publication on the expiration of this embargo. This paper is presented in a format suitable for submission to a relevant peer reviewed Journal. The research was performed with Dr Paul Hilton, Dr Chris Allen, Dr Ali Khan and Professor Lin Li.

In terms of the co-author involvement Dr Paul Hilton, Dr Chris Allen and Dr Ali Khan assisted with defining the scope of the laser parameters that were to be considered for this experiment, based on a literature review performed by the author of this thesis and the availability of excellent beam quality laser sources. Professor Lin Li provided input on the presentation of results.

Welding Ti-6Al-4V with Excellent Beam Quality 1µm Wavelength Laser Sources

J.E. Blackburn[1], P.A. Hilton[1], C.M. Allen[1], A.H. Khan[1], L. Li[2]

[1]TWI Ltd, Cambridge, Cambridgeshire, CB21 6AL, UK
[2]School of Mechanical, Aerospace and Civil Engineering, The University of Manchester, Manchester, Greater Manchester, M60 1QD, UK

Abstract

Excellent beam quality 1µm wavelength laser sources have been considered here for producing high quality welds in titanium alloys. Three different Yb-fibre laser sources, with beam parameter products in the range 0.33-6.0mm.mrad, focused with different optical combinations, have been used to process 2.0-7.0mm thickness Ti-6Al-4V. The results indicate that butt welds which meet the AWS D17.1:2001 Class A criteria can be produced with very different focused beams in the beam parameter product range 1.6-6.0mm.mrad. No special techniques, such as a directed jet of inert gas, were required to produce these high quality welds, as is the case with poorer beam quality Nd:YAG rod laser sources.

Keywords

Laser welding, titanium alloys, Yb-fibre, Yb:YAG disc, porosity

1. Introduction

Keyhole laser welding is already an established technique for the joining of metallic components in a number of industry sectors; for instance, in the automotive sector to join body panels [1,2]. The technique is characterised by its ability to produce high aspect ratio welds in a wide range of metallic materials at atmospheric pressure. In comparison with electric arc based welding processes, the heat inputs for a similar depth of penetration are significantly lower when keyhole laser welding. Furthermore, the delivery of 1µm wavelength laser beams through fibre optic cables, allows straightforward integration with robotic manipulators and consequently, the capability to process components of high geometric complexity.

Modern solid-state fibre delivered laser sources, such as Yb-fibre and Yb:YAG disc lasers, are commercially available with rated output powers exceeding 10kW and near diffraction limited beam quality [3,4]. High power fibre and disc laser technologies were developed as a result of the poor beam quality available from Nd:YAG rod laser sources, when compared with CO_2 laser sources; CO_2 laser sources offer good beam quality at high powers but their output cannot be delivered through an optical fibre. Studies of welding performance as a function of beam quality [5,6] have enabled the potential benefits, in terms of welding performance, of replacing Nd:YAG rod lasers with Yb-fibre or Yb:YAG disc lasers, to be highlighted. Verhaeghe and Dance [7] reported that the high quality beams emitted from Yb-fibre and Yb:YAG disc laser sources are now capable of

producing welds with an aspect ratio which only previously could have been produced by in-vacuum electron beam welding. However, for high-performance welded components detailed knowledge of the resulting weld quality is required.

A potential application for keyhole laser welding is in the production of near-net-shape titanium alloy components for aerospace applications. Defect free components can be manufactured by machining billets or forgings, although these techniques can have buy-to-fly ratios (the mass of material prior to machining compared with the mass of the finished component) exceeding 10:1 [8]. The production of neat-net-shape components by keyhole laser welding, or another welding process, would significantly reduce component cost and increase productivity. Nevertheless, it must be determined if welds of the required quality can be reproducibly produced by keyhole laser welding prior to it being considered as a manufacturing technique for this application. Potential weld defects when fusion welding titanium alloys are [9]: (i) embrittlement of the weld bead; (ii) solidification and/or contamination cracks in the weld metal; (iii) geometrical weld profile defects; and, (iv) subsurface porosity.

Embrittlement of the weld bead and the formation of cracks in the weld metal can be avoided by adopting stringent inert gas shielding and joint preparation techniques. As reported by Hilton et al [10], stringent weld quality criteria exist for primary airframe structures and aeroengine components, as a result of their service environments. The most difficult to meet of these criteria, for keyhole laser welding, relate to the formation of geometrical defects in the weld profile and subsurface porosity in the weld metal. Geometrical defects in the weld profile (eg undercut or concavity at the weld face/root) can be attributed to the complex interaction of forces in the melt pool [11]. The severity of geometrical defects can be influenced through an appropriate choice of process parameters, whilst not trying to compromise other joint characteristics (eg penetration and heat input). Nevertheless, if the process parameters cannot be adequately adjusted, filler material, an over-sized joint thickness (followed by subsequent machining), or a cosmetic pass, may potentially eliminate remaining geometrical defects.

The formation of porosity as a result of fine scale hydrogen rejection during weld pool solidification [12] is not of particular concern if stringent joint preparation techniques are implemented; particularly given the low hydrogen content of titanium alloys and high purity shielding gases. Nevertheless, subsurface porosity may form during keyhole laser welding as a result of dynamic instabilities in the keyhole [13]. It has been reported that for solid-state laser sources with a beam parameter product of 18.0-24.0mm.mrad, subsurface porosity requirements cannot be achieved unless techniques such as a directed gas jet [10], power modulation [14] or a dual focus configuration [15] are used.

The research presented in this paper has examined the potential to weld titanium alloys, up to 7mm in thickness, with excellent beam quality 1μm wavelength laser sources, for aerospace applications. Three different Yb-fibre lasers, with beam parameter products in the range 0.33-6.0mm.mrad, have been used in this investigation. Weld qualities have been

assessed in terms of their subsurface porosity content and weld profile, and compared against a relevant aerospace welding standard.

2. Research Methodology

2.1 Laser Sources

Three different solid-state laser sources all emitting electromagnetic radiation of ~1µm wavelength were used in this investigation; specifically, a YLS-1000-SM Yb-fibre laser, a YLR-4000 Yb-fibre laser, and a YLS-5000 Yb-fibre laser. All three laser sources incorporated beam delivery through a flexible optical fibre to a process head containing the collimating and focusing optics. The collimating and focusing optic combinations used in this investigation, along with the calculated properties of the resulting focused laser beams, are specified in Table 1.

Table 1 Details of the laser sources and calculated properties of the focused beams used in this investigation.

Property	**YLS-1000-SM**		**YLR-4000**		**YLS-5000**		
Maximum rated output power, W	1000		4000		5000		
Beam parameter product, mm.mrad	0.33		1.6		6.0		
Delivery fibre diameter, µm	17		50		150		
Collimating optic focal length, mm	120		120		160		
Raw beam diameter, mm	10.6		15.3		25.6		
Focusing optic focal length, mm	250	500	300	500	160	250	500
Nominal beam waist (w_0) diameter, µm	30	60	125	210	150	230	470
Power density per kW, kW/mm^2	1300	330	82	29	57	23	5.8
Focusing cone half angle (θ), deg	1.2	0.6	1.46	0.88	4.6	2.9	1.5
Rayleigh length, mm	1.5	3.0	4.9	13.6	1.9	4.6	18.3
5% Depth of focus (Z_f), mm	0.9	1.9	3.1	8.6	1.2	2.9	11.7

2.2 Materials

Ti-6Al-4V is a readily fusion weldable α/β alloy [9] used in aeroengine components at temperatures below 315°C and throughout airframes [16]. Sheets of Ti-6Al-4V in thicknesses of 2.0, 3.25 and 7.0mm were sourced to broaden the industrial relevance of this research. The sheets of 2.0 and 3.25mm thickness Ti-6Al-4V were guillotine sheered to size, with a minimum dimension of 150mm in the welding direction. Test pieces of the 7.0mm thickness Ti-6Al-4V plate were cut into 300mm lengths, with subsequent dry machining of the plate giving four 75mm (length) steps of 4.0, 5.0, 6.0 and 7.0mm thickness. Immediately prior to performing each melt run, the surfaces of individual test pieces were acetone degreased, cleaned with an abrasive paper and then degreased with acetone. The same procedure was followed for butt welds, apart from the abutting edges were dry machined immediately prior to welding.

2.3 Experimental Scope and Procedures

Table 2 details the parameters, and their ranges, investigated for the three different laser sources, although not all permutations of parameters were performed. The majority of experimental trials performed were autogeneous melt runs. Based on previous results by

the same authors [14,15], the transfer of single spot conditions from a melt run configuration to a well fitting butt joint requires no alteration of parameters. Nevertheless, a small number of butt welds were also produced to determine the transferability of conditions developed through melt run trials.

Table 2 Parameters investigated in the experimental trials on 2–7mm thickness Ti-6Al-4V.

Parameters	YLS-1000-SM	YLR-4000	YLS-5000
Power, W	1000	1000-4000	4000
Nominal beam waist (w_0), μm	30, 60	125, 210	150, 230, 470
Welding speeds, mm/s	8.3-150	16.7-233.3	33.3-133.3
Focal plane position†, mm	-5 to +5	-5 to +5	-8 to +4
Material thickness, mm	2.0	3.25	4, 5, 6, 7

†A focal plane position of 0mm indicates the beam waist was positioned on the top surface of the workpiece, whereas a negative and a positive focal plane position indicate the beam waist was positioned below or above the top surface of the workpiece respectively.

Figure 1 details the typical equipment configuration, although the process head was controlled with an XYZ gantry system when processing with the YLR-4000 Yb-fibre laser. Laser powers were measured with a water-cooled Ophir power meter; the powers reported subsequently are those measured at the workpiece (i.e. after all optical elements). The focusing optic was protected with a cover slide and a high pressure air-knife, as detailed in Figure 1. Welding was performed in the downhand (1G) position; a 3° inclination angle was included to avoid back reflection when processing with the YLS-1000-SM. The same steel clamping jig, incorporating a copper efflux channel, was used for all experiments. The efflux channel and a shielding shoe, detailed in Figure 1, were supplied with 99.998% purity argon shielding gas in order to prevent discoloration and embrittlement of the weld root and face respectively.

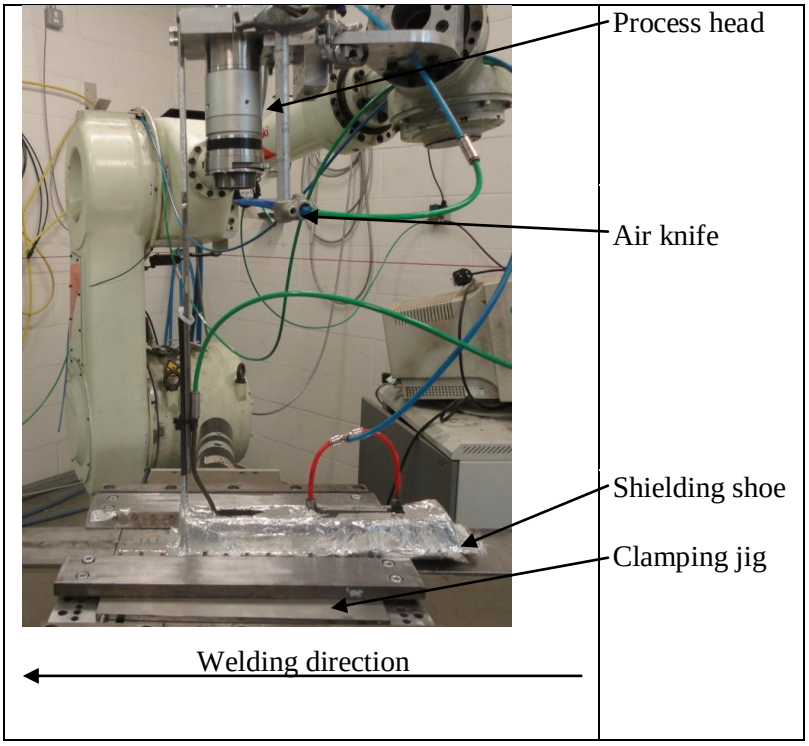

Figure 1 Typical experimental set-up detailing position of the air-knife immediately below the cover slide holder.

2.4 Weld Quality Assessment

All melt runs and butt welds were inspected visually on both the weld face and root for discoloration. They were classified according to the discoloration scale outlined in AWS D17.1:2001 *Specification for Fusion Welding for Aerospace Applications*. Radiographic examination of the melt runs and butt welds was performed according to the standards outlined in BS EN 1435:1997 *Non-destructive examination of welds*. Indication sizes >0.05mm were visible on the radiographs, although any indications of this size were rounded up to 0.1mm. Pore counts were performed by the same individual over a 76mm analysis length, as prescribed in AWS D17.1; although a 50mm analysis length was used for the 4-7mm thickness material, which was extrapolated to 76mm. Weld profile sections, transverse to the welding direction, were taken of selected melt runs and butt welds at positions representative of the entire weld length.

Table 3 Acceptance limits relating to weld profile and subsurface porosity criteria for Class A, B, C weld qualities, as specified in AWS D17.1:2001.

Imperfection	Acceptance limit		
	Class A	Class B	Class C
Face undercut (Ca)†	0.07 T or 0.76 mm, whichever is less	0.10 T or 1.27 mm, whichever is less	0.20 T or 1.78 mm, whichever is less
Root undercut (ca)†	0.07 T or 0.76 mm, whichever is less	0.10 T or 1.27 mm, whichever is less	0.20 T or 1.78 mm, whichever is less
Face concavity (Cr)††	0.07 T or 0.76 mm, whichever is less	0.07 T or 0.76 mm, whichever is less	0.07 T or 0.76 mm, whichever is less
Root concavity (cr)††	0.07 T or 0.76 mm, whichever is less	0.07 T or 0.76 mm, whichever is less	0.07 T or 0.76 mm, whichever is less
Maximum dimension or diameter of an isolated pore	0.33 T or 1.5 mm, whichever is less	0.50 T or 2.3 mm, whichever is less	No stated requirement
Cumulative length of porosity per 76 mm weld	1.33 T or 6.0 mm, whichever is less	2.0 T or 9.0 mm, whichever is less	No stated requirement
Minimum spacing between two pores	4 x size of larger adjacent pore	2 x size of larger adjacent pore	No stated requirement

†individual defect, maximum for a defect running the entire weld length is 0.05mm (Class A)
†† individual defect, maximum for a defect running the entire weld length is 0.13mm (Class A)

3. Results

3.1 YLS-1000-SM Yb-fibre Laser

The face and root of the majority of melt runs produced were bright silver in colour; indicating that they had been adequately shielded. When melt runs with a discoloured face or root were produced, the shielding shoe was adjusted and the condition repeated.

Melt runs were produced with the range of parameters detailed in Table 2. In terms of welding performance, full penetration could be achieved at welding speeds up to 150 and 66.7mm/s with the 250 and 500mm focusing lenses respectively. This was achieved with a 0mm focal plane position, and could not be increased by moving the focal plane position beneath or above the top surface of the workpiece.

Accumulated lengths of subsurface porosity in the range 1.1-21.5mm were observed in the melt runs produced, although the majority of melt runs had accumulated lengths of porosity exceeding the Class B limit. The vast majority of pores observed were ≤0.1mm in diameter. A small number of melt runs were produced with the 250mm focusing lens which had accumulated lengths of porosity meeting the Class A criteria, but these were not reproducible. For instance, five melt runs made with the 250mm focusing lens, a welding speed of 66.7mm/s and a focal plane position of 0mm had accumulated lengths of porosity in the range 2.2-4.5mm. No melt runs were produced with the 500mm focusing lens which met the Class A criteria for accumulated length of subsurface porosity when the inert gas cross-jet was used.

Figure 2 details the profiles of melt runs produced with the 250mm focusing lens, a 0mm focal plane position and with welding speeds of 66.7-133.3mm/s. The profiles are nail-shaped, indicative of an increased absorption of the incident radiation at the top of the keyhole. All the cross-sectioned melt runs made with this optical configuration had profiles which met the Class A weld profile criteria. Undercut at the weld face and/or root concavity was present on the majority of melt runs cross-section, although these were within the levels specified by Class A. Figure 3 shows the profiles of melt runs produced with the 500mm focusing lens, a 0mm focal plane position and with welding speeds of 50-83.3mm/s. All the fully penetrating melt runs sectioned were unacceptably undercut at the weld face, as indicated in Figure 3a and 3b, not meeting the Class A criteria.

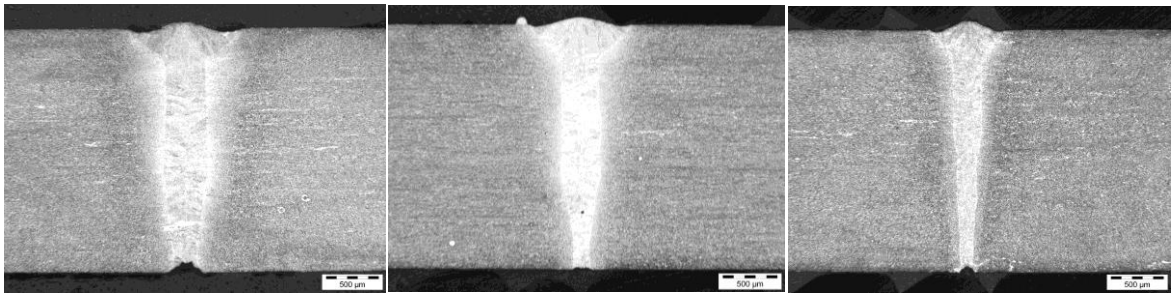

(a) (b) (c)

Figure 2 Melt runs produced with the YLS-1000-SM Yb-fibre laser in 2mm thickness Ti-6Al-4V using a 250mm focusing lens, a 0mm focal plane position, and welding speeds of (a) 66.7mm/s, (b) 83.3mm/s, and (c) 133.3mm/s.

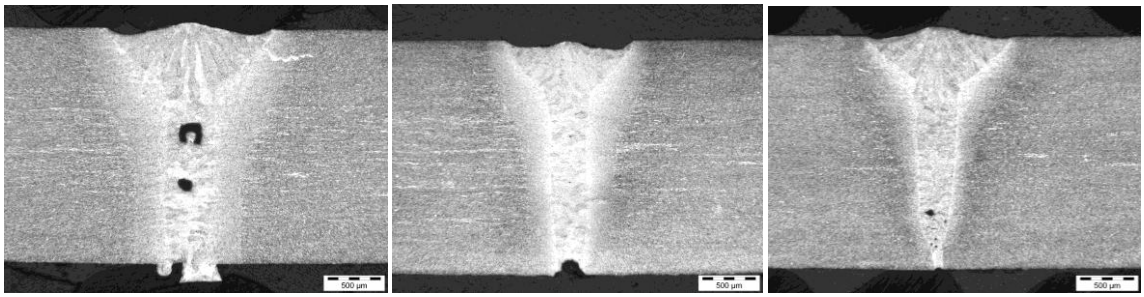

(a) (b) (c)

Figure 3 Melt runs produced with the YLS-1000-SM Yb-fibre laser in 2mm thickness Ti-6Al-4V using a 500mm focusing lens, a 0mm focal plane position, and welding speeds of (a) 50mm/s, (b) 66.7mm/s, and (c) 83.3mm/s.

3.2 YLR-4000 Yb-fibre Laser

Melt runs were produced in 3.25mm thickness Ti-6Al-4V, with two different focusing optics (300 and 500mm) and at laser powers of 2.0, 3.0 and 4.0kW. Welding speeds of 16.7-233.3mm/s were examined. For the results reported here, the beam waist position was coincident with the top surface of the workpiece when processing with the 300mm focal length lens. However, a beam waist positioned 4mm below the top surface of the workpiece was used when processing with the 500mm focal length lens; since this resulted in the most desirable visual appearance of the weld bead. All conditions reported here were fully penetrating. Spatter at the weld face was invariably observed on melt runs produced with a welding speed of 16.7-50mm/s. Above 50mm/s only occasional spatter was observed either side of the weld track. The roots of all melt runs were bright silver in colour – indicating that the flow rate of argon gas supplied through the efflux channel was adequate. However, several of the melt runs produced were oxidised on the top surface, but a chevron pattern was still observed on the top surface indicating that this oxidation most likely occurred after solidification.

Table 4 details the accumulated length of subsurface porosity for selected melt runs produced with the YLR-4000 Yb-fibre laser. The maximum pore diameter observed was 0.4mm, although the majority of pores were in the range 0.1 to 0.2mm in diameter. In general, melt runs with particularly low levels of subsurface porosity content could be produced with both focusing lenses, easily meeting all the Class A criteria relating to subsurface porosity.

Table 4 Subsurface porosity content for selected melt runs produced in 3.25mm thickness Ti-6Al-4V with the YLR-4000 Yb-fibre laser.

Beam width diameter, µm	Power (kW)	Welding Speed, mm/s	Porosity, mm
125	3.0	16.7	0.9 (Class A)
125	3.0	33.3	0.9 (Class A)
125	3.0	50.0	0.2 (Class A)
125	4.0	41.7	0.2 (Class A)
125	4.0	50.0	0.7 (Class A)
125	4.0	58.3	0.4 (Class A)
210	3.0	33.3	0.8 (Class A)
210	3.0	41.7	1.9 (Class A)
210	3.0	50.0	1.3(Class A)
210	4.0	66.7	0.7 (Class A)
210	4.0	83.3	0.9 (Class A)

The melt runs produced at 4kW had a more desirable weld profile than those produced at lower powers and only these are detailed here. Figure 4 shows images of three transverse cross-sections of melt runs produced with the Yb-fibre laser, focused with a 300mm lens, at welding speeds of 41.7-133mm/s. With regards to defects at the weld face and root, concavity, to a maximum value of 0.17mm was invariably present at the root of the profile of those melt runs produced at welding speeds of 60mm/s and above. A small amount, ~0.05mm, of non-continuous face undercut was also observed on those welds produced at relatively high welding speeds. Face undercut and root concavity was not observed in the

profile of those melt runs made at welding speeds of ~50mm/s or less. In fact, the Class A weld quality criteria relating to undercut and root concavity were consistently achieved on the melt runs produced with the YLR-4000 Yb-fibre laser.

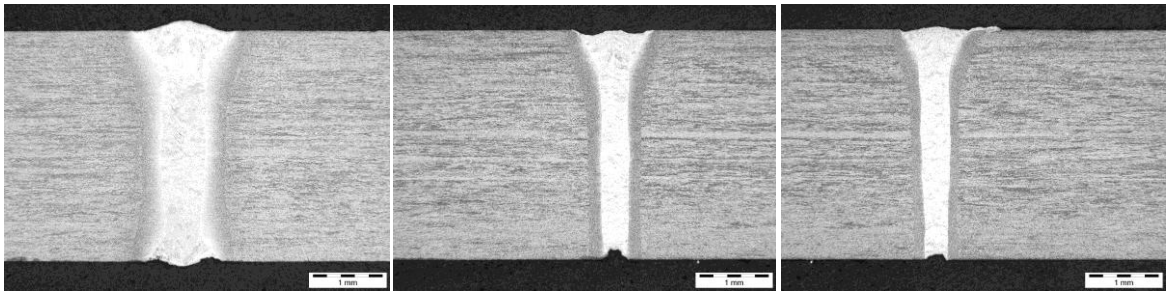

(a) (b) (c)

Figure 4 Melt runs produced with the YLR-4000 Yb-fibre laser in 3.25mm thickness Ti-6Al-4V using a 300mm focusing lens, a 0mm focal plane position and welding speeds of (a) 41.7mm/s, (b) 100mm/s, and (c) 133.3mm/s.

3.3 YLS-5000 Yb-fibre Laser

The face and root of the majority of melt runs produced with the YLS-5000 Yb-fibre laser were bright silver in colour; indicating that they had been adequately shielded. When melt runs with a discoloured face or root were produced, the shielding shoe was adjusted and the condition repeated.

Using the 160mm focusing lens resulted in consistent full penetration in 4mm thickness Ti-6Al-4V, for welding speeds of 50-100mm/s with a 0mm focal plane position. Consistent full penetration was not achieved at thicknesses >4mm at any of the welding speeds and focal plane position combinations examined. All the melt runs produced with the 160mm focusing lens and a 0mm focal plane position exhibited large amounts of spatter at the weld face. It was found that positioning the focal plane at least 2mm below the workpiece surface resulted in a condition free of heavy spatter. Furthermore, operating with a -2mm focal plane position increased the welding speed which resulted in consistent full penetration in 4mm thickness Ti-6Al-4V, to 116.7mm/s.

With the 250mm focusing lens consistent full penetration in 4mm thickness Ti-6Al-4V could be achieved at welding speeds up to 100mm/s with a focal plane position of -2 to 2mm. With the lowest welding speed examined (33mm/s), consistent full penetration could be achieved in thicknesses $\leq$ 6mm. Those melt runs which were fully penetrating were nearly free of weld spatter. The 500mm focusing lens enabled consistent full penetration in 4mm thickness Ti-6Al-4V at welding speeds $\leq$66.7mm/s with a focal plane position of 0mm. Consistent full penetration could also be achieved in 5mm thickness Ti-6Al-4V at welding speeds of 33.3mm/s. Melt runs produced with the 500mm focusing lens were typically free of heavy weld spatter.

Accumulated lengths of subsurface porosity in the range 0.2 to 24.3mm were observed in the melt runs produced with the YLS-5000 Yb-fibre laser. The majority of pores counted

were ≤0.2mm in diameter, although diameters up to 0.5mm were present. The melt runs produced with the 160mm focusing lens in thicknesses ≥5mm all had accumulated lengths of porosity exceeding the Class B limit. Nevertheless, melt runs meeting the Class A subsurface porosity criteria were produced in the 4mm thickness Ti-6Al-4V. With a focal plane position of -2.0mm, an accumulated length of subsurface porosity ≤1.5mm was produced at all welding speeds between 50 and 116.7mm/s, as detailed in Table 5.

Table 5 Subsurface porosity content of fully penetrating melt runs produced in 4mm thickness Ti-6Al-4V with the YLS-5000 Yb-fibre laser, a 160mm focusing lens, a -2mm focal plane position and at different welding speeds.

Speed, mm/s	Porosity, mm
50	0.9 (Class A)
66.7	0.6 (Class A)
83.3	0.3 (Class A)
100	1.1 (Class A)
100	1.5 (Class A)
116.7	1.2 (Class A)

Similarly to the melt runs produced with the 160mm focusing lens, the consistent full penetration melt runs produced with the 250mm focusing lens had internal qualities meeting the criteria stipulated in Class A. As detailed in Table 6, accumulated lengths of porosity in the range 0.2-4.4mm were observed in the fully penetrating melt runs. Fully penetrating melt runs produced when using the 500mm focusing lens contained accumulated lengths of subsurface porosity exceeding the Class B limit for all welding speeds examined, except 50mm/s. Fully penetrating melt runs produced with a 50mm/s welding speed were just inside the Class A limit. In contrast to the other optical configurations, partially penetrating melt runs of excellent internal quality were produced at welding speeds of 66.7 and 83.3mm/s in all the workpiece thicknesses and for a wide range of focal plane positions. The Class A subsurface porosity contents of melt runs produced with a focal plane position of -2mm, giving the least weld spatter with this focusing optic, are detailed in Table 7.

Table 6 Subsurface porosity content of fully penetrating melt runs produced in 4-7mm thickness Ti-6Al-4V with the YLS-5000 Yb-fibre laser, a 250mm focusing lens, and at different welding speeds and focal plane positions.

Focal plane position, mm	Speed, mm/s	Thickness, mm	Porosity, mm
-2	33.3	4	1.4 (Class A)
-2	33.3	5	4.4 (Class A)
-2	33.3	6	1.2 (Class A)
0	33.3	4	0.5 (Class A)
-2	50	4	2.1 (Class A)
0	50	4	0.2 (Class A)
2	66.7	4	1.1 (Class A)
2	66.7	5	0.8 (Class A)
0	83.3	4	1.5 (Class A)
-1	100	4	1.8 (Class A)
0	100	4	1.7 (Class A)
1	100	4	0.9 (Class A)
2	100	4	2.3 (Class A)

Table 7 Subsurface porosity content of partially penetrating melt runs produced in 4-7mm thickness Ti-6Al-4V with the YLS-5000 Yb-fibre laser, a 500mm focusing lens, a welding speed of 66.7mm/s and different focal plane positions.

Focus plane position, mm	Thickness, mm	Porosity, mm
-6	7	0.3 (Class A)
-6	6	0.2 (Class A)
-6	5	0.5 (Class A)
-6	4	1.3 (Class A)
-2	7	0.8 (Class A)
-2	6	1.2 (Class A)
-2	5	1.8 (Class A)

Figure 6 details the cross-sections of selected melt runs in 4mm thickness Ti-6Al-4V which also met the Class A subsurface porosity criteria. All the melt runs produced with a 0mm focal plane position did not meet the weld profile criteria stipulated in Class A, B or C of AWS D17.1. However, manipulating the focal plane position to -2.0mm below resulted in profiles which were met the Class A criteria at welding speeds of 50, 66.7, and 83.3mm/s. The cross-sections of further fully penetrating melt runs produced in 4 and 5mm thickness Ti-6Al-4V with the 230µm diameter beam waist are shown in Figure 7. In general, the severities of geometric defects occurring were greater than those produced with the smaller focused beam waist. Nevertheless, with the correct combination of welding speed and focal plane position (50mm/s and 0mm) a melt run in 4mm thickness Ti-6Al-4V was produced which met the Class A weld profile criteria (Figure 7b). This combination of process parameters also resulted in an accumulated length of subsurface porosity content of 0.2mm, easily meeting the Class A criteria.

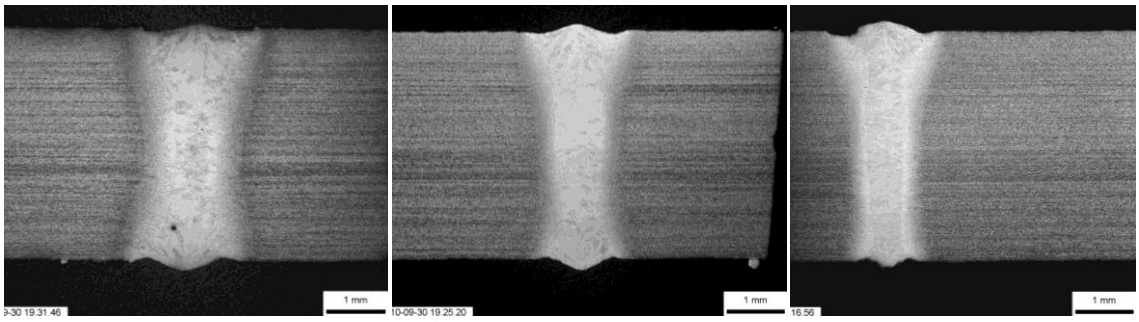

(a) (b) (c)

Figure 6 Melt runs produced in 4mm thickness Ti-6Al-4V with the YLS-5000 Yb-fibre laser using a 160mm focusing lens, a -2.0mm focal plane position and welding speed of (a) 83.3mm/s, (b) 66.7mm/s, and (c) 50mm/s.

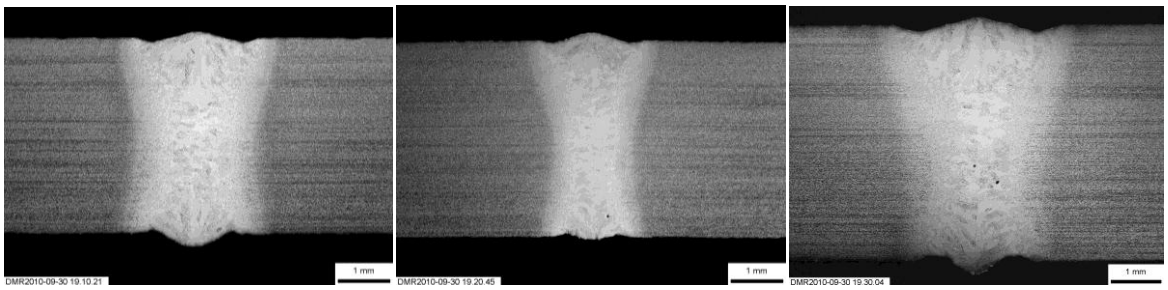

(a) (b) (c)

Figure 7 Melt runs produced in 4 (a,b) and 5mm (c) Ti-6Al-4V with the YLS-5000 Yb-fibre laser using a 250mm focusing lens and welding speed of (a) 33.3mm/s, focal plane position of -2.0mm, (b) 50mm/s, focal plane position of 0mm, and (c) 33.3mm/s, focal plane position of -2.0mm.

Figure 8 shows the cross-sections of melt runs produced in 5-7mm thickness Ti-6Al-4V with the 500mm focusing lens, a welding speed of 66.7mm/s and a focal plane position of -2.0mm. Recalling from above, the partially penetrating melt runs in 6 and 7mm thickness Ti-6Al-4V detailed in Figure 8 resulted in an internal quality which easily met the Class A subsurface porosity criteria. All these melt runs exhibited undercut at the weld face, but this was within the Class A criteria.

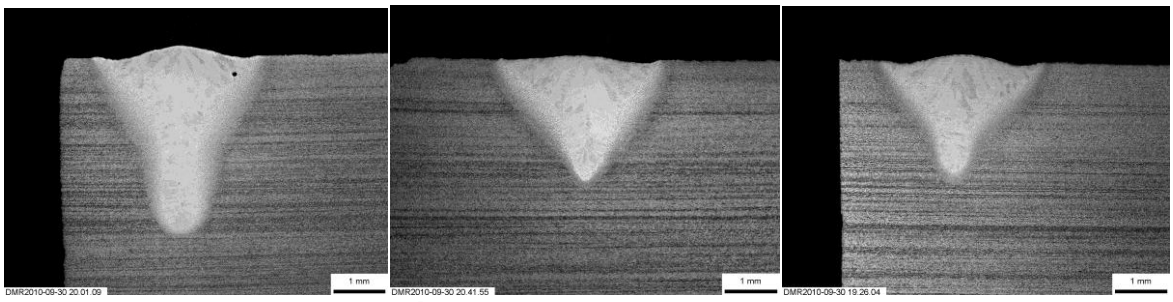

(a) (b) (c)

Figure 8 Melt runs produced in 5 (a), 6 (b), and 7mm (c) thickness Ti-6Al-4V with the YLS-5000 Yb-fibre laser, a 500mm focusing lens and welding speed of 66.7mm/s and focal plane position of -2.0mm.

3.4 Butt Welds

Based on the results of the melt run trials, butt welds were produced with the YLS-5000 Yb-fibre laser and the following conditions:

1. 160mm focusing lens, a focal plane position of -2mm, a welding speed of 66.7mm/s, and in 4mm thickness Ti-6Al-4V.
2. 500mm focusing lens, a focal plane position of -2mm, a welding speed of 66.7mm/s, and in 7, 6, 5 and 4mm thickness Ti-6Al-4V.

All the butt welds produced were free of spatter and had a bright silver face and root. The quality of these butt welds, in terms of their subsurface porosity contents, is detailed in Table 8 and Figure 10 respectively. From these results it can be seen that the welding conditions developed as melt runs can be successfully transferred to close fitting butt joints, for the beam widths at least ≥150µm in diameter.

Table 8 Subsurface porosity content of butt welds produced using 4-7mm thickness Ti-6Al-4V with the YLS-5000 Yb-fibre laser; produced with a focal plane position of -2mm and a welding speed of 66.7mm/s.

Beam width diameter, µm	Thickness, mm	Penetration	Porosity, mm
150	4	Full	1.0 (Class A)
150	4	Full	0.5 (Class A)
470	7	Partial	1.4 (Class A)
470	6	Partial	0.6 (Class A)
470	5	Partial	1.4 (Class A)
470	4	Partial	1.1 (Class A)

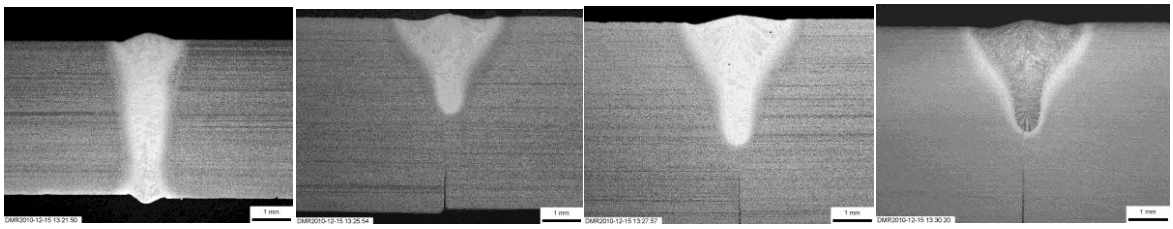

(a) (b) (c) (d)

Figure 9 Butt welds produced using 4 (a), 5 (b), 6 (c) and 7mm (d) thickness Ti-6Al-4V with the YLS-5000 Yb-fibre laser, a welding speed of 66.7mm/s, a focal plane position of -2.0mm, and a focusing lens of 160mm (a) and 500mm (b,c,d).

4. Discussion

4.1 Aerospace Weld Quality Requirements

The results indicate that excellent beam quality 1µm wavelength laser sources are capable of producing fully penetrating welds in Ti-6Al-4V which easily meet the criteria stipulated in Class A of AWS D17.1. Furthermore, partially penetrating welds may also be produced to a similar quality. These weld qualities have been achieved without the techniques required when welding with poorer beam quality 1µm wavelength laser sources. The excellent weld quality has been achieved with two different laser sources, the YLR-4000 and the YLS-5000 Yb-fibre lasers, and a total of five different focused beams. Importantly,

this gives increased flexibility to the end-user when considering what focused beam properties are required for a particular application.

However, it is known that company specific weld quality standards exist for particularly high-performance aerospace applications. An example of such a standard was reported by Hilton et al [10], who detailed the weld profile and subsurface porosity criteria which must be achieved if a particular welding process is to be adopted for the manufacture of aeroengine components. In comparison with the subsurface porosity criteria detailed in Class A of AWS D17.1, the company specific criteria are more stringent. In particular, the accumulated length of subsurface porosity is 1.7, 2.1 and 2.7mm for 3.25, 4.0 and 5.0mm thickness workpieces respectively. Nevertheless, the majority of melt runs reported in this research had accumulated lengths of porosity meeting this criterion. Furthermore, all the butt welds also met the accumulated length criterion. The company specific criterion relating to the maximum dimension of a single pore (1.0, 1.2 and 1.5mm for 3.25, 4.0 and ≥5.0mm thickness workpieces respectively) was achieved with the YLR-4000 and YLS-5000 Yb-fibre lasers.

In terms of weld profile requirements, the company specific criteria are very similar in value to those required by Class A of AWS D17.1 [10]. Consequently, those melt runs and butt welds with profiles meeting the Class A requirements, also met the company specific criteria for these defects. However, further weld profile criteria exist in the company specific standard, relating to the dimensions of the fusion-zone at the weld face, waist and root. These Criteria are detailed in Table 9 [10].

Table 9 Company specific criteria relating to the dimensions of the fusion zone in welded titanium alloys [10].

Weld profile	**Material thickness (mm)**		
	9.3	**5.0**	**3.0**
Face weld width, mm	≤9.0	≤5.0	≤4.0
Minimum weld width, upper limit, mm	3.0	2.5	2.0
Minimum weld width, lower limit, mm	2.0	1.5	1.0
Root weld width, upper limit, mm	9.0	5.0	4.0
Root weld width, lower limit, mm	2.0	1.5	1.0

The face weld width was met on all melt runs and butt welds produced. However, the lower limits of the minimum weld width and the root weld width were not routinely achieved. The weld profile detailed in Figure 7a did meet the criteria, but this was produced with a relatively large beam waist (230µm) and a slow welding speed (33.3mm/s). All other fully penetrating melt runs and butt welds sectioned did not meet this requirement. To meet these weld width requirements with such finely focused laser beams, beam oscillation, with a suitable waveform, amplitude and frequency, may provide a potential solution.

Potential weld qualities produced with the YLS-1000-SM Yb-fibre laser are not currently suitable for high-performance aerospace applications, at least with the optical

configuration examined, as indicated by their subsurface porosity contents being Class B or worse. Nevertheless, processing with these beam waists may be suitable for applications where the welded component is not under cyclic loads. One particular example is the welded assemblies of titanium pacemakers which are currently produced using pulsed laser sources necessitating lower speeds and higher heat inputs (although the components utilise sub 1mm wall thicknesses). Using beam waists of the order of ~50µm and a continuous-wave process would increase productivity and potentially reduce distortion in the welded assembly.

4.2 Beam Quality

As can be seen from Sections 3.2 to 3.3, the focused outputs of the YLR-4000 and the YLS-5000 Yb-fibre lasers are both capable of producing fully penetrating welds in Ti-6Al-4V with a relatively low subsurface porosity content. Such a result was not possible with the YLS-1000-SM Yb-fibre laser, with the optical configurations and material thickness considered, which was only capable of consistently producing melt runs to a Class B quality.

From previous published works [10,14,15,17] it is known that special techniques are required to produce welds of similar quality when using 1µm wavelength laser beams with beam parameter products in the range 18-24mm.mrad. For instance, Hilton et al [10] used a 7kW Yb-fibre laser, of beam parameter product 18mm.mrad and focused into a 600µm diameter beam waist, to butt weld Ti-6Al-4V up to 9.3mm in thickness. Butt welds of a similar quality to those produced here were reported, but a jet of inert gas finely positioned so that it impinged on the laser-material interaction point was required. Similarly, Blackburn et al [14,15] required power modulation and dual focus techniques to produce high internal quality welds in titanium alloys up to 3.25mm in thickness with a 4kW Nd:YAG rod laser (beam parameter product of 24mm.mrad).

The fundamental difference between the laser sources used in this investigation and those in previous research [10,14,15,17] is their beam quality; which is translated into different diameter beam waists, power densities, focusing cone half angles, and Rayleigh lengths depending upon the optical configuration used. The properties of the focused beam widths used in previous research are detailed in Table 10.

Table 10 Properties of the focused laser beams used in previous research to weld titanium alloys.

Property	**YLS-7000**	**HL4006D**	
Beam parameter product, mm.mrad	18.0	24.0	
Collimating optic focal length, mm	120	200	
Raw beam diameter, mm	28.8	32	
Focusing optic focal length, mm	250	150	200
Nominal beam waist (w_0), µm	625	450	600
Power density per kW, kW/mm^2	3.3	6.3	3.5
Focusing cone half angle (θ), deg	3.3	6.1	4.6
Rayleigh length, mm	10.8	4.2	7.5
5% Depth of focus (Z_f), mm	6.9	2.7	4.8

As can be identified by comparing the properties of the focused beam widths in Table 10 to those detailed in Table 1, the primary difference is the change in power density for a given beam power. Excluding the results produced with the YLS-5000 Yb-fibre laser focused with a 500mm optic (since this only produced high quality partial penetration welds), melt runs and butt welds of very high internal quality were produced in the power density range 23-82kW/mm^2. This trend is likely to be related to the keyhole being more stable at higher power densities. Keyhole stability is dependent on the balance of the forces trying to keep the vapour cavity open (vaporisation pressure and radiation pressure) and the restoring pressures (surface tension, hydrostatic pressure and hydrodynamic pressure).

The radiation pressure, ρ_l, tends to keep the keyhole open and can be described in its functional form as [18]:

$$\rho_l = (I/c)\,[A + 2R] \qquad \text{(Equation 1)}$$

Where I is the incident laser intensity, c is the speed of light, A the absorptivity and R the reflectivity.

Therefore, a significant increase in the incident laser intensity will increase the radiation pressure inside the keyhole which will increase the resistive forces trying to keep the keyhole open, reduce keyhole instability, and decrease the formation of porosity in the weld. However, further research is required to understand the dynamic behaviour of the melt pool, keyhole and vapour plumes at different power densities, since a limit has been reached (~82kW/mm^2) where power densities above this have a negative effect on the internal quality of the weld.

4.3 Joint Configuration

The bulk of trials performed in this study have been autogeneous melt runs on plate. This has primarily been performed to allow a large number of parameter combinations to be assessed without the influence of joint fit-up and edge preparation interfering with the interpretation of results. The butt welds in this study were made with beam widths of ~150µm and ~470µm diameter, and the results indicate that conditions developed through melt run trials can successfully be transferred to close fitting butt joints.

Nevertheless, operating with beam widths ~150µm diameter presents challenges in a production environment. This research has been performed in a research and development laboratory, enabling weld paths to be pre-programmed in onto a high accuracy XY table. Furthermore, high precision joint preparations have been used. Translating this into a production environment would significantly increase cost compared with using a beam widths >450µm diameter. The combined errors from robotic manipulators, joint preparation and in-process component distortion could lead to instances where the beam becomes misaligned with the joint, potentially leading to lack of fusion problems. Potential solutions to this problem include using a seam tracker to track the joint line, and/or using a process head incorporating a beam oscillator to produce an increased tolerance to joint gap variations.

5. Conclusions

This research has evaluated the suitability of using excellent beam quality 1µm wavelength solid-state laser sources for producing near-net-shape titanium alloy aerospace components. Three Yb-fibre lasers, with beam parameter products in the range 0.33-6.0mm.mrad, have been used to process Ti-6Al-4V using a continuous-wave power output. Analyses of subsurface porosity contents and weld profiles have allowed the following conclusions to be drawn:

1. Fully penetrating autogeneous butt welds can be produced in up to 5.0mm thickness Ti-6Al-4V with a suitable focused YLS-5000 Yb-fibre laser, of beam parameter product 6.0mm.mrad, with a quality meeting the Class A criteria of AWS D17.1. In addition, partially penetrating welds can be produced to a similar quality.
2. Fully penetrating melt runs in 3.25mm thickness Ti-6Al-4V can be produced with a suitably focussed YLR-4000 Yb-fibre laser, of beam parameter product 1.6mm.mrad, with a quality meeting the Class A criteria of AWS D17.1.
3. The subsurface porosity content of melt runs produced with the single mode Yb-fibre laser in 2mm thickness Ti-6Al-4V are outside the criteria stipulated in Class A of AWS D17.1, although melt runs with acceptable profiles were produced.
4. Melt runs and butt welds were also produced with an internal quality which met the most stringent company specific weld quality criteria. Profile defects at the weld face and root were within the allowable levels stipulated in these company specific weld quality criteria. However, the company specific weld quality criteria relating to minimum weld thickness and weld root thickness were not achieved at any of the welding conditions evaluated.

Acknowledgements

The work was funded by the Industrial Members of TWI Ltd, as part of its Core Research Programme. Part of the work was also funded by the EPSRC grant no. C537750. The assistance of IWS, Dresden, Germany, for the use of their IPG Yb-fibre laser and Dr Gunther Göbel in particular is acknowledged.

References

[1] Larsson, J.K. (2003) ‘Laser welding applications within the european automotive industry’, Welding Research Abroad, 49(11), 20-27.

[2] Tang, H. (2010) ‘Latest advances in joining technologies for automotive body [3] manufacturing’, International Journal of Vehicle Design, 54(1), 1-25.

[3] IPG Photonics Website (2010) http://www.ipgphotonics.com/apps_materials.htm (Accessed May 2010).

[4] Trumpf Website (2010) http://www.trumpf-laser.com/en/products/solid-state-lasers/disk-lasers/trudisk.html (Accessed May 2010).

[5] Verhaeghe, G. & Hilton, P. (2005) ‘The effect of spot size and laser beam quality on welding performance when using high-power continuous wave solid-state lasers’, in *Proc. Int. Conf of Appl. of Lasers and Electro-Opt., ICALEO, Miami, November 2005*, 264-271.

[6] Weberpals, J., Russ, A., Dausinger, F. & Hügel, H. (2005) 'Influence of the focus diameter in laser welding with thin disk laser', in *Proc. of the 3rd Int. Conf. on Lasers in Manufacturing. LIM, Munich, June 2005*, 39-42.
[7] Verhaeghe, G. & Dance, B. (2008) 'An assessment of the welding performance of high-brightness lasers and a comparison with in-vacuum electron beams', in *Proc. Int. Conf of Appl. of Lasers and Electro-Opt., ICALEO, Temecula, October 2008*, 406-414.
[8] Threadgill, P.L., Leonard, A.J., Shercliff, H.R. & Withers, P.J. (2009) 'Friction stir welding of aluminium alloys', *International Materials Reviews*, 54(2), 49-93.
[9] Donachie, M.J. (2000) 'Titanium: a technical guide', 2nd edition, ASM International, Ohio.
[10] Hilton, P., Blackburn, J. & Chong, P. (2007) 'Welding of Ti-6Al-4V with fibre delivered laser beams', in *Proc. Int. Conf of Appl. of Lasers and Electro-Opt., ICALEO, Orlando, November 2007*, 887-895.
[11] Kaplan, A. (2009) 'Keyhole welding: the solid and liquid phases', in: Dowden, J.M. (ed.) *The theory of laser materials processing: heat and mass transfer in modern technology*, Canopus, Bristol (England), 71-93.
[12] Lakomski, V.I. & Kalinyuk, N.N. (1963) 'The solubility of hydrogen in liquid titanium', *Autom. Weld.*, 16, 28-32.
[13] Matsunawa, A., Kim, J.D., Seto, N., Mizutani, M. & Katayama, S. (1998) 'Dynamics of keyhole and molten pool in laser welding', *J. Laser Appl.*, 10(6), 247-254.
[14] Blackburn, J.E., Allen, C.M., Hilton, P.A., Li, L., Hoque, M.I. & Khan, A.H. (2010) 'Modulated Nd:YAG laser welding of Ti-6Al-4V', *Sci. and Technol. of Weld. and Joining,15(5), 433-439.*
[15] Blackburn, J.E., Allen, C.M., Hilton, P.A. & Li, L. (2010) 'Dual focus Nd:YAG laser welding of titanium alloys', *Proc. of MATADOR conference, Manchester (England)*, 279-282.
[16] Boyer, R.R. (1996) 'An overview on the use of titanium in the aerospace industry', *Mater. Sci. and Eng. A (Struct. Mater.: Prop., Microstruct. and Process.)*, 213(1-2), 103-114.
[17] Blackburn, J., Allen, C., Hilton P. & Li, L. (2010) 'Nd:YAG laser welding of titanium alloys using a directed gas jet', *J. Laser Appl.*, 22(2), 71-78.
[18] Duley, W.W. (1999) 'Laser Welding', Wiley: New York.

Chapter 9

Porosity Formation

9.1 Introduction

Chapters 5-7 have presented the results and analysis of research performed using three different techniques to reduce weld metal porosity when welding titanium alloys with an Nd:YAG rod laser. In addition, Chapter 8 has presented the results of research performed using three different excellent beam quality 1 μm wavelength laser sources to weld titanium alloys from 2.0-7.0 mm thickness. Individual discussions of the results were presented in each of these four chapters. This Chapter builds on the results and discussions presented in Chapters 5-8, in order to develop an understanding of the origins of weld metal porosity when keyhole laser welding titanium alloys with 1 μm wavelength laser beams. A small number of further results, related to the analysis of pores in the weld metal, are included.

9.2 Porosity Formation Mechanisms

It was discussed in sub-Section 2.4.4 that weld metal porosity may occur during keyhole laser welding as a result of:

1. Hydrogen rejection during solidification of the melt pool.
2. Keyhole instability leading to the presence of metal vapour or shielding gases in the melt pool, which are then entrapped as pores on solidification of the melt pool.

Based on the results of the literature review, it was decided that three different keyhole laser welding techniques (a jet of inert gas directed towards the laser-material interaction point, a modulated laser power output, and a dual focus technique) should be investigated to determine their ability to reduce porosity formation when keyhole laser welding titanium alloys with Nd:YAG rod laser sources. The results presented in Chapters 5-7 have shown that

the dynamic behaviour of the keyhole, melt pool and vapour plume are directly related to the formation of porosity in the weld metal.

Both the directed gas jet and the dual focus (in either direction) techniques have shown that with the correct combination of parameters, the occurrences of keyhole collapse can be significantly reduced. High speed imaging and spectroscopic analysis of an optimised directed gas jet have shown that, when correctly set up, the jet disperses the formation of excited metal vapour above the keyhole and also significantly changes the hydrodynamic behaviour of the melt pool. Less instances of keyhole collapse were observed (although this was not quantified) and a particularly high internal quality melt run was produced. The high speed video analysis of the dual focus research indicated that, with the correct foci separation and welding speed, a slightly enlarged keyhole could be produced which resulted in fewer instances of keyhole collapse and a higher internal quality melt run. It is also thought that the increased power densities possible with the excellent beam quality 1 μm wavelength laser sources have a similar effect; increasing the radiation pressure within the keyhole, leading to reduced occurrences of keyhole collapse and a decreased content of weld metal porosity. Conversely, the modulated laser power output technique has relied upon the periodic closure of the keyhole to initiate an oscillating wave in the melt pool; which is thought to manipulate the angle of the vapour plume and aid the escape of any gas bubbles in the melt pool.

The results of the research performed with the directed gas jet and the dual focus techniques indicate that the majority of porosity seen in the weld metal is as a result of keyhole instability and/or collapse; with the result being the entrapment of shielding gas in the weld metal. Nevertheless, a small number of further experiments and analysis were performed in an effort to confirm the origins of the porosity, specifically:

- Analysis of the hydrogen content of welded and virgin parent material by vacuum hot extraction.
- Analysis of the grain structure and chemical composition of the inner surface of pores.
- Application of the Hadamard-Rybczynski equation to determine the necessary melt pool dimensions which would allow trapped gas bubbles to escape as a result of buoyancy forces.

9.3 Pore Gas Analysis

9.3.1 Vacuum Hot Extraction

Vacuum hot extraction was performed on virgin parent material and weld metals having both high and low accumulated lengths of weld metal porosity, to determine the hydrogen content of the samples. Details of the equipment used are given in Section 4.8. The samples chosen for analysis were:

1. 2.0 mm thickness Ti-6Al-4V parent metal, un-welded but cleaned as per the method detailed in sub-Section 4.3.2.
2. A butt weld (4W24) produced in 2.0 mm thickness Ti-6Al-4V with an accumulated length of subsurface porosity of ~20 mm per 76 mm weld length.
3. A butt weld (4W26) produced in 2.0 mm thickness Ti-6Al-4V with an accumulated length of subsurface porosity of ~0.5 mm per 76 mm weld length.

Table 9-1 summarises the results obtained, expressed as ppm of hydrogen evolved during sample heating and vacuum extraction. As Table 9-1 shows, a significant increase in hydrogen content in the weld metal when compared with the parent material was not detected, and, one sample of the high internal porosity content weld 4W24 had the lowest hydrogen content recorded. The potential explanations for this are:

- The weld metal porosity observed is not associated with hydrogen.
- The hot vacuum extraction technique is not sufficiently sensitive to detect changes in weld metal hydrogen associated with porosity.
- Hydrogen effusion out of the pores is occurring during cooling after welding.

Table 9-1. Hot vacuum extracted hydrogen contents for parent material and weld metals.

Description	Sample No.	Hydrogen content, ppm
2mm thickness Ti-6wt%Al-4wt%V parent metal, un-welded	1	39
	2	48
Weld metal 4W24	1	25
	2	50
Weld metal 4W26	1	45
	2	50

9.3.2 Mass Spectroscopy

Mass spectroscopy may be used to determine the chemical composition of the gas inside the pores, provided that it can be sampled. Research was undertaken in collaboration with a university to determine the gas contents of various size pores produced in keyhole laser welded titanium alloys, using a quadrupole gas analyser. The geometric positions of the porosity were determined using the three dimensional radiographs detailed in sub-Section 4.7.2. Samples were machined to ensure the pore was no more than 500 μm below the machined surface. Prior to a sample manipulator 'piercing' the pore, a high vacuum (10^{-9} Torr) needed to be made to ensure the safe (i.e. no leakage) transfer of the gas to the calibrated quadrupole. The quadrupole did not detect any gases inside the pore and further tests showed that the system was not capable of detecting the air in an 8 mm diameter purposely induced pore in an aluminium casting. This is unfortunate since such a result would have provided unquestionable results of whether the gas inside the pores was predominantly constituted of hydrogen or argon (the shielding gas).

9.4 Scanning Electron Microscopy

Cross-sections longitudinal to the welding direction were taken of the butt welds 4W24 and 4W26. Their cross-sections are detailed in Figure 9-1. Scanning electron microscopy was used to investigate the chemical content of the inner surfaces of the pores found in 4W24.

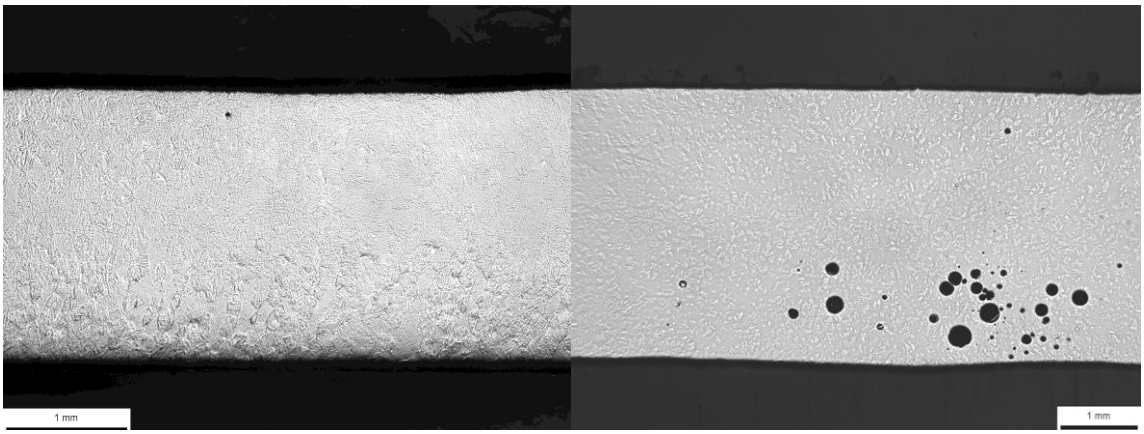

Figure 9-1. Longitudinal sections of a low porosity weld (4W26, left) and a high porosity weld (4W24, right), showing how the porosity is predominantly located in the bottom half-thickness of the weld metal of weld 4W24.

Secondary and backscattered electron images of typical pores found in the welded sampled 4W24 are detailed in Figure 9-2. In general, secondary electron images provide information on surface topography, and orientation with respect to the location of the secondary electron

detector. Similarly, backscattered electron images provide information on local chemical composition (so called 'atomic number contrast', with lighter elements having lower contrast than heavier elements), as well as surface topography and orientation. Therefore, at first, it appeared that the darker pore shown in Figure 9-2 was of a different chemical composition than the others. Nevertheless, it was not possible to obtain an energy dispersive X-ray spectrum from this pore of sufficient signal strength, despite tilting the sample surface so that it was normal to the X-ray detector. This in itself suggests that the lack of contrast from this pore is due primarily to its depth below the surface, as shown schematically in Figure 9-3.

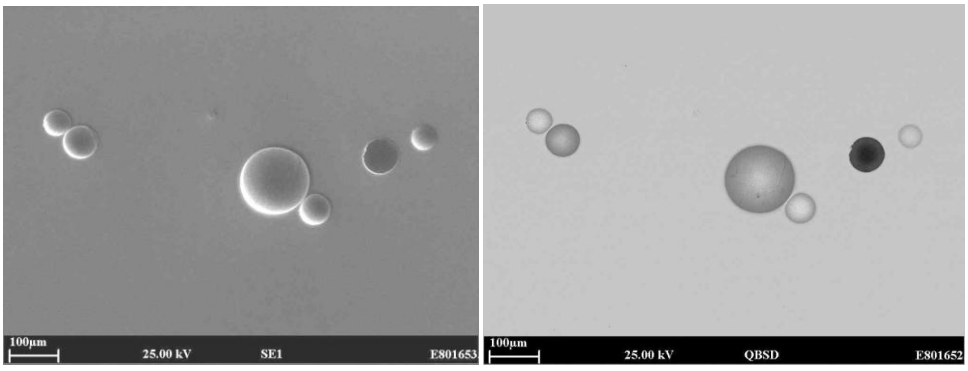

Figure 9-2. Secondary (left) and back scattered (right) electron images of pores in weld 4W24.

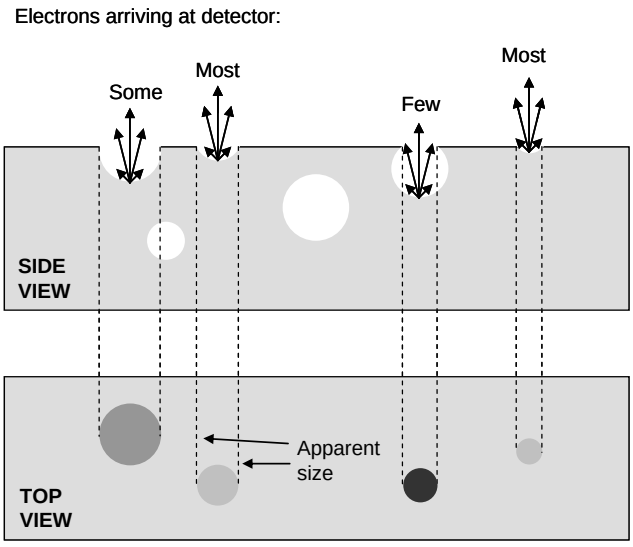

Figure 9-3. Schematic explanation of contrast observed in electron images of pores.

For shallower pores, energy dispersive X-ray spectra were obtained. These spectra only detected Ti, Al and V. Similarly, only Ti, Al and V were detected in spectra taken from the surrounding matrix. This suggests that whichever chemical species are present in the pores, they are not reacting with the matrix that encloses the pores, and are escaping on sectioning (e.g. inert or un-reactive gaseous elements), or are reacting with the matrix, but only forming a very thin reaction layer below the detection limit of SEM and EDX. Certainly, there was no

evidence of a thick reaction layer on the inner surfaces of the pores, as the solidification structure (e.g. dendrites and grain boundaries) of the Ti alloy was still clearly apparent, as shown in Figure 9-4.

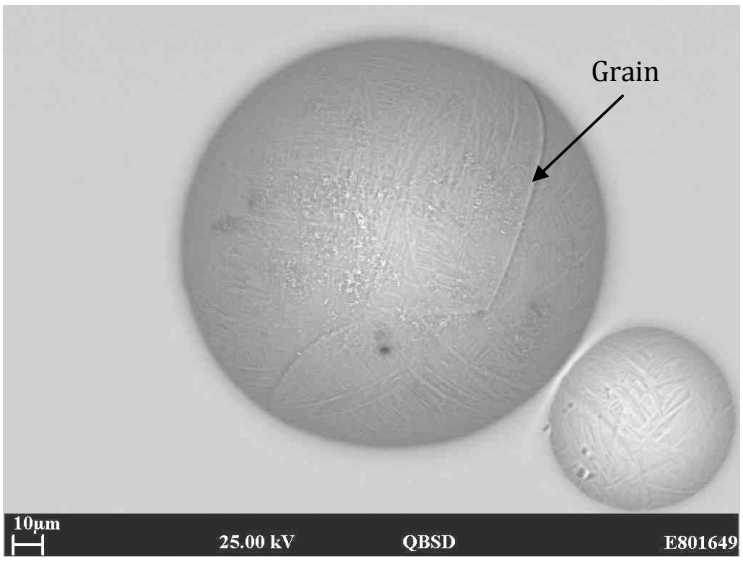

Figure 9-4. Internal structure of typical pores observed in keyhole laser welded titanium alloys.

9.5 Bubble Rise Time

As well as considering keyhole instability as a means of generating gas bubbles in the melt pool, consideration can also be given to bubble buoyancy forces, as at least some of the bubbles generated will escape from the melt pool before it solidifies. Shortly after forming, the bubbles will reach a terminal velocity, V_b, which is determined by the buoyant rise and drag forces. The Hadamard-Rybczynski equation [Clift et al, 1978], derived from the Navier-Stokes equation, can be used to calculate the rise velocity for bubbles in a fluid with a small Reynolds number (approximately <1.0):

$$V_b = \left[\frac{(2/9)gr^2(\rho_f - \rho_g)}{\mu_f}\right]\left(\frac{\mu_f + \mu_g}{2\mu_f + 3\mu_g}\right) \tag{9-1}$$

where r is the radius of the bubble, ρ_f and ρ_g the densities of the fluid and the gas respectively, and μ_f and μ_g the dynamic viscosity of the ambient fluid and the gas in the bubble respectively.

The reduced version of the Hadamard-Rybczynski equation has been used to calculate the rise velocity and hence the rise time for bubbles of various sizes in 3.25 mm Ti-6Al-4V. The density and viscosity of the gas have been ignored (permissible given their relatively low

values compared with the molten titanium) and the results are detailed in Table 9-2. It can be seen that gas bubbles with a diameter of ~0.1 mm (the majority of those observed) had a rise velocity of 22.6 mms^{-1} which equates to a rise time of 0.144s to escape from the bottom of a titanium melt pool 3.25 mm deep. As would be expected, the larger diameter bubbles rise at a faster velocity.

Table 9-2. Calculated rise speeds and times for gas bubbles in molten titanium over 3.25 mm. The viscosity and density values of molten titanium were taken at 2000 K (melting point 1943 K).

Gas bubble radius, mm	**Rise speed, mms^{-1}**	**Rise time, s**
0.05	5.64	0.576
0.1	22.6	0.144
0.2	90.2	0.0360
0.3	203	0.0160
0.4	361	0.00901
0.5	564	0.00577
0.6	812	0.00400
0.7	1110	0.00294

Images from the high speed video observations have been used to determine the melt pool lengths and hence maximum times available for the gas bubbles to escape the molten material. The shortest melt pools were in the higher speed single spot continuous power melt runs. For example a 4.0 kW Nd:YAG laser beam focussed to a 0.45 mm diameter beam width produced a trailing melt pool of length ~5.1 mm at a welding speed of 5 $mmin^{-1}$, which equates to a solidification time of 0.06 s. This would allow gas bubbles of up to ~0.2 mm in diameter to escape, which correlates well with the results achieved. However at slower welding speeds larger melt pools form and hence longer solidification times are observed. It would be expected this would facilitate the escape of gas bubbles in the melt pool, however, this is not the case. In Chapter 7 the subsurface weld metal porosity contents of melt runs produced with a 0.45 mm diameter beam width and a welding speed of ~50 mms^{-1} contained accumulated lengths of subsurface porosity of ~20 mm per 76 mm weld length. The melt pool length of such a welding condition observed from the high speed video was approximately 10mm, resulting in a solidification time of 0.2 s.

Nevertheless, this analysis ignores the complexity of molten metal flow in the melt pool. Matsunawa et al (1998) have revealed, using transmissive micro-focussed

X-ray techniques, that significant turbulence is present in the root of the melt pool, at least for partial penetration melt runs. Therefore, with certain combinations of welding parameters, the downward velocity component produced by the flow of molten metal flow in the melt pool must be comparable with or greater than the buoyancy velocity generated by the density differentials, such that gas bubbles are prevented from buoyant escape from the melt pool.

9.6 Origin of Pore Gases

The results of the above analyses combined with the results of the different keyhole laser welding techniques presented in Chapters 5-8, strongly suggest that the pores are formed as a result of keyhole instability (which is caused by the mechanisms discussed in Chapter 3) and closure which lead to the presence of shielding gases in the melt pool. These gas bubbles, as a result of the complex molten metal flows present in the melt pool are not able to escape prior to solidification and become entrapped as porosity. This statement can be made because of the following reasons:

1. All the welded samples were prepared with nominally identical cleaning procedures, in order to remove any hydrated layers present on the surface of the workpiece. Furthermore, the samples were all shielded with identical flow rates of argon delivered through the same shielding shoe and efflux channel. However, large differences in the accumulated lengths of subsurface weld metal porosity were observed in all the melt runs and butt welds produced; on occasion with nominally identical parameters. However, little difference was found in the hydrogen content of welded samples produced with a very low or very high accumulated length of subsurface porosity.
2. The grain structures present on the inner surface of typical pores indicated that an inert gas was present in the pores. The only inert gas the welding process was subjected to was argon.
3. Calculation of the time required for bubbles to escape from the bottom of a melt pool prior to solidification has shown that a large number of melt runs produced at slower welding speeds should have had a sufficiently long melt pool that the vast majority of bubbles could escape. However, the majority of melt runs produced at slower speeds (with a continuous-wave output) had a significantly higher amount of subsurface porosity than those produced at higher speeds; suggesting more gas bubbles are produced at slower speeds and once these gas bubbles are present in melt pool it is particularly difficult for them to escape. Therefore, in order to achieve a low level of subsurface porosity a particularly stable keyhole is required which does not collapse

and lead to the presence of gas bubbles in the melt pool. Such stable keyholes have been shown to be produced with the directed gas jet and dual focus techniques, leading to welds of very high internal quality.

It is acknowledged that the evidence provided for this argument is not conclusive. Nevertheless, all the evidence currently indicates that entrapment of inert shielding gas is the principal cause of weld metal porosity when keyhole laser welding adequately prepared and inert gas shielded titanium alloys with 1 μm wavelength laser beams.

Part III

Commercial Aspects

Chapter 10: The Sponsoring Company – TWI

Chapter 11: Commercial Implications

Chapter 10

The Sponsoring Company – TWI

10.1 Introduction

Part III of this thesis, which begins with this chapter, discusses the commercial implications of the project. In this chapter, the company who sponsored this research, TWI, is discussed; enabling the commercial implications of this project to be put into perspective. The chapter begins with a brief history and overview of TWI. TWI's core business and key markets are then introduced. The structure of the organisation is then described, including details on how employees fit and work together within this structure. The history of innovation at TWI, how innovation is supported and developed into revenue streams are outlined. Finally, details concerning how this project aligned itself within the sponsoring company are given.

10.2 History and Overview

Officially, the company who provided sponsorship of this research project is TWI Ltd. However, TWI Ltd is a registered Trading Company in TWI Group, and TWI (The Welding Institute) is the ultimate holding company for all the trading companies in TWI Group. TWI Ltd was incorporated in 1999 [Companies House, 2010], although its origins date back to March 1946 when the British Welding Research Association (BWRA) was incorporated. The BWRA then became The Welding Institute (TWI) in 1968 [TWI, 2010a]. The TWI group includes TWI Ltd and other companies based in the United Kingdom and across the globe.

TWI's mission is to 'deliver world class services in joining materials, engineering and allied technologies to meet the needs of a global membership and its associated community' [TWI

2010b]. To perform this mission, TWI has specific expertise in the areas of welding and joining technologies, materials processing, non-destructive testing, structural integrity, corrosion management, materials testing and failure investigations. In addition, TWI provides training and examination services for the engineering community, and offers further services including software development and information services.

The majority of services provided by TWI are at the corporate headquarters in Cambridge; although TWI has a growing presence throughout the United Kingdom and has established Technology Centres in Rotherham (incorporating laser based additive manufacture, friction stir, and surfacing research activities) and Middlesbrough (incorporating reduced pressure electron beam, arc welding, composites and coating research activities), a non-destructive testing Validation Centre in Port Talbot, and a training and examination services centre in Aberdeen. In order to maintain and develop their reputation world-wide, numerous offices have been set-up around the world in both established and developing economies (offices in China and the United States have recently been founded as a result of a growing number of Chinese and American Industrial Member companies). These offices provide a point of contact for potential customers and serve as a base to offer training and a certain amount of technical support. Agents also act as valuable points of contact in other areas of the world, including: Brazil, India, Japan, the Kingdom of Saudi Arabia, Korea, Kuwait and Taiwan.

TWI Ltd currently trades as TWI Ltd, TWI Technology Centre (North East), TWI Technology Centre (Yorkshire), TWI Technology Centre (Wales), TWI Aberdeen and The NDT Validation Centre. The majority of other companies in TWI Group offer training services, although companies such as Plant Integrity Ltd and The Test House Ltd offer services and/or products complimentary to those offered by TWI Ltd. The TWI Group of companies currently employs approximately 650 people and had a turnover in excess of £45 million in 2009 [TWI, 2010c].

In contrast to the majority of other companies operating in the private sector, TWI is limited by guarantee and does not have a share capital. It is owned by its Industrial Member companies and is a non-profit distributing organisation. TWI currently has over 3000 Industrial Member companies from 65 countries throughout the world. Industrial membership to TWI is based on an annual fee, which is determined by the Council [TWI, 2010a]. The Council, led by the President and Chairman of the Council, is constituted of up to 32 individuals who are either elected representatives of the Industrial Member companies or Professional Members of TWI. The Council is ultimately responsible for the running of TWI, although the majority of powers are delegated to the Executive Board (as indicated in Figure

10-1). The Executive Board, consisting Directors, Associate Directors and Non-executive Directors, is led by the Chief Executive.

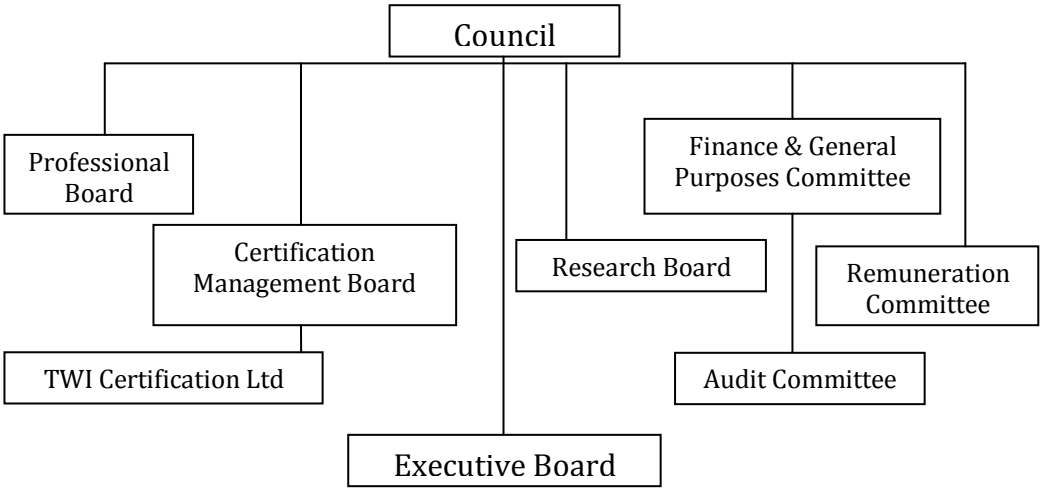

Figure 10-1. Structure of TWI from the Council to the Executive Board.

10.3 Core Business and Key Markets

TWI's revenue is generated from a number of different streams, primarily: industrial membership fees; performing consultancy, and research and development work (detailed in Figure 10-2 as SCP & GSP, and Collaborative R&D); training and exams; licensing of innovative technologies and software programs; technology transfer programmes (detailed in Figure 10-2 as Collaborative TT); and, the sale of Teletest® Focus guided wave products and services. A small amount of revenue is also generated from other companies in TWI Group; such as The Test House. The revenue split between these products throughout the last eight years is detailed in Figure 10-2 [TWI, 2010c].

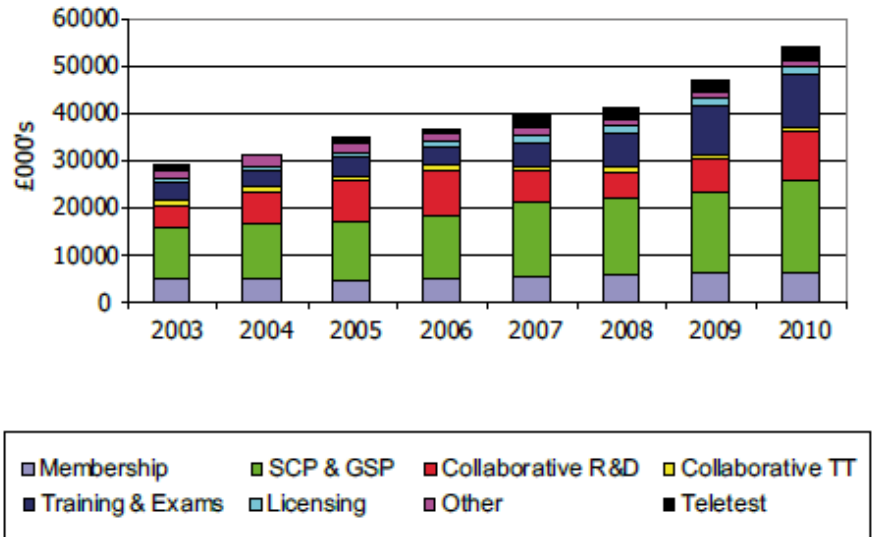

Figure 10-2. TWI's revenue by product [TWI, 2010c].

Over the past eight years an increasing proportion of TWI's income has been generated by training and examination services, and the sale of Teletest products and services. However, the majority, approximately two thirds, of TWI's revenue is currently generated from Industrial Membership fees, contract consultancy, and research and development. All the contract consultancy and research and development services are performed by TWI Ltd, and Industrial Membership of TWI is required to access these services. TWI has positioned itself as a market leader in welding and joining technologies, materials processing, non-destructive testing, structural integrity, failure investigations and training; enabling TWI to provide consultancy and research and development services to Industrial Member companies at any stage of a product's life cycle. As a consequence, TWI regularly deals with technologies which are not fully mature.

10.3.1 Technology Readiness Levels

An accepted method for assessing the maturity of a developing technology is to use Technology Readiness Levels (TRLs); a graduated scale, ordinarily incorporating nine levels, which uses specific criteria to quantitatively measure the maturity of a technology. The TRLs are a metric conceived and first used by NASA [Saden et al, 1989] to aid planning during large projects that rely on the integration of numerous technologies into a system or sub-system. Measuring the maturity of all the technologies being integrated, with a technology independent method, ensures that individual technologies are not responsible for the delay of the entire project and effort can be effectively allocated. Figure 10-3 [NASA, 2010] details a TRL scale that is currently being used by NASA to aid integrated technology planning. It

consists of nine levels, where TRL 1 represents Basic Technology Research (i.e. the goals have been identified but the path to reach them has not) and TRL 9 the System Test, Launch and Operations.

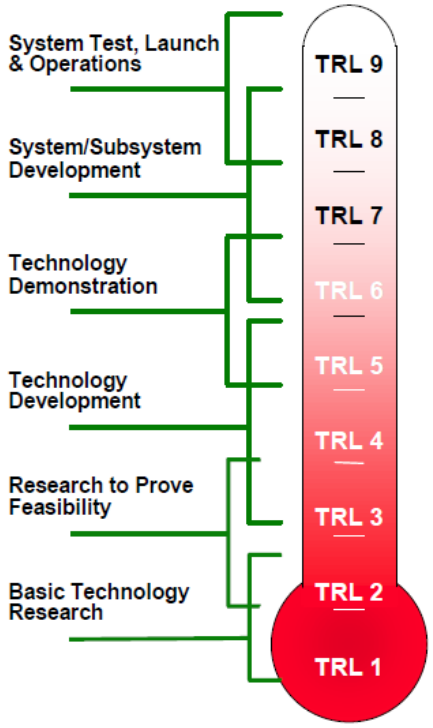

Figure 10-3. Technology Readiness Level (TRL) scale, as used by NASA [NASA, 2010].

The expertise of TWI, as a research and development organisation typically lies within TRL 2 to TRL 7. Competition at the lower end of the scale comes from universities, who ordinarily operate up to TRL 4 (although this is increasing due to the increasing number of spin-off companies from universities). Competition at the higher end of the scale comes from large enterprises which have the capabilities and resources to take a technology to market.

10.3.2 Research and Development Project Types

TWI delivers consultancy and research and development services to its Industrial Member companies through four different types of projects:

- the Core Research Programme (CRP), funded by Industrial Membership fees;
- Single Client Projects (SCPs);
- Group Sponsored Projects (GSPs); and,
- Collaborative Projects.

The CRP consists of research projects performed on behalf of Industrial Member companies. Funding for this programme is taken from the Industrial Membership fees of Industrial Member companies, and the programme is worth in excess of £3 million per year. The CRP is guided by the Research Board (see Figure 10-1); which is a committee of representatives from Industrial Member companies. Topics for research in the CRP may be suggested by TWI or Industrial Member companies, and are ordinarily discussed and chosen every three years by the Research Board; consequently the programme reflects the needs of Industrial Member companies. Funding for research projects is typically allocated for a two or three year period, and the project is managed by a Project Leader. The deliverables of the CRP projects are formal technical reports. The Research Board meets annually to discuss progress of CRP projects, guide the programme, and review technical reports. Once approved by the Research Board, to be of an acceptable standard, the reports are published as Industrial Members Reports and made available to all the Industrial Member companies of TWI.

SCPs are performed for individual Industrial Member companies. These projects are the core service provided by TWI, allowing research and development, and/or consultancy activities to be performed with the upmost confidentiality and impartiality. They are typically performed over short-medium term time frames, although longer term research projects are not uncommon. SCPs are initiated following the acceptance of a formal written proposal, where the scope duration and price of work is detailed, made by TWI to an Industrial Member company.

Where the needs of several Industrial Member companies overlap, a GSP or a joint industry project (JIP) may be a more suitable type of project. These projects are funded equally by a group of Industrial Member companies, with the results being shared by all the companies in the consortium. They are a mechanism for enabling individual companies to access the results of large projects with reduced financial risk. GSPs are typically performed over medium-long term time frames.

Collaborative projects are a funding mechanism which enables TWI to seek funding for medium-long term research and development projects. This type of project is ordinarily initiated as a response to calls for proposals. The proposal calls are issued by public sector funding bodies (such as the Technology Strategy Board in the United Kingdom, and the Framework programme by the European Commission) to invest in technologies which will benefit the wider community to which the call is issued.

TWI has operated for over 60 years and has established itself in a diverse range of industrial sectors, including: aerospace; construction, engineering and general fabrication; automotive,

electronics and sensors; equipment consumables and materials; medical; military vehicles and equipment; off-highway and mining; oil, gas and chemical; power; rail; and, shipbuilding. Industrial Member companies are typically grouped by sector, with each sector being managed by an Industrial Sector Manager; this structuring allows TWI to identify ideas for CRP, GSP and Collaborative projects which are industry sector specific.

10.4 Organisational Structure

TWI is a global organisation, with offices based in Australia, Bahrain, China, Malaysia (6 in total), Thailand, the United Arab Emirates, the United Kingdom, the United States and Vietnam. However, the majority of these offices act as training centres or points of contact for Industrial Member companies. The majority of services are offered from TWI's UK offices. Figure 10-4 details the organisational structure of TWI, from the Chief Executive down. Business Functions, such as finance and business development, are divided and typically led by a Director or an Associate Director. This division of Business Functions is in-line with most other commercial organisations.

The business functions in TWI are typically divided into Groups (led by Group Managers) and sub-divided into Sections (led by Section Managers). Sections are typically organised using a capabilities based structure, whereby employees with common expertise work together; and, for Technology-based Sections are likely to include Technical Project Leaders (highly qualified scientists and engineers who manage the projects and provide technical input), technicians and administrators. The line management structure is clear; Section Managers are responsible for the employees in their Section and report to Group Managers, and Group Managers report to the Director or Associate Director in charge of their particular Business Function.

Despite the clear divisions between business functions, typical projects performed by TWI require the expertise of employees in different Sections, Groups and Functions. After a prospect has been identified, as a result of the Business Development Function's efforts, the relevant technical Section is tasked with developing a proposal in communication with the Industrial Member company. The Section Manager will delegate this task to a Project Leader who has the relevant technical background and experience; although the proposal will require input from the Commercial Group (ensuring correct Terms and Conditions are used), and potentially other Sections if their expertise and/or resources are required. Successful proposals will then be managed by the Project Leader, who has the responsibility for co-ordinating the resources, which may spread different Groups and Business Functions,

required. Throughout the duration of the project, other Business Functions (Information Technology, Site Services etc) will also indirectly contribute to the delivery of the project. On completion of the project, the Finance and Services Business Function process payments, and the Business Development Business Function work to identify other potential projects with the client.

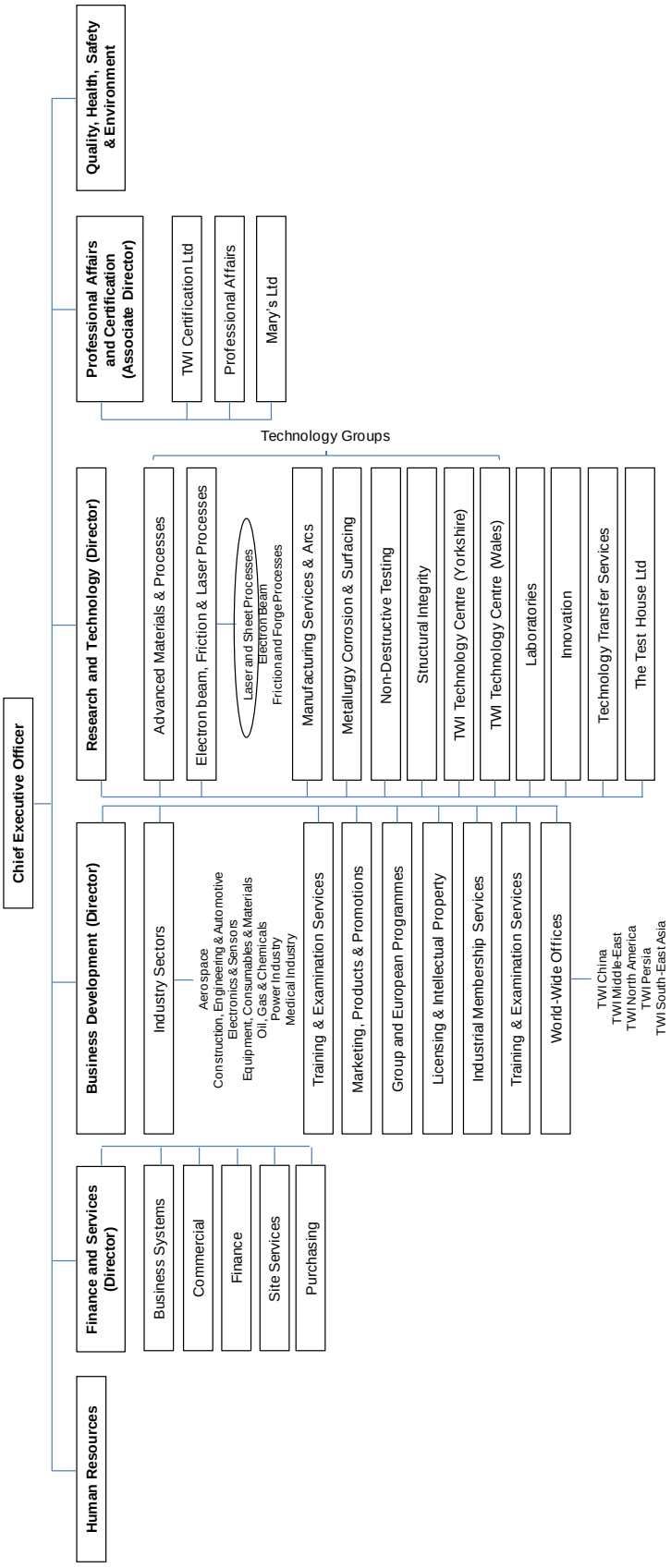

Figure 10-4. The organisational structure of TWI from the Chief Executive down to Groups and Sections.

10.5 Communication Channels

The internal Communication Channels at TWI are primarily used for three reasons:

1. To facilitate the straightforward and timely communication of information from senior management down the structure of the organisation.
2. To manage interactions with clients (i.e. proposals, visits etc).
3. To enable the successful delivery of projects to clients.

Various channels are used effectively in TWI by the senior management to ensure that important information can be communicated vertically down through the organisation. For instance, the monthly publication 'Team Brief' (accessed electronically or on noticeboards) provides regular updates for staff on financial performance, health and safety notices, and new starters, as well as information on less regular subjects such as ISO 9001 audits. Important notices can be placed on the homepage of the company's Intranet system, and, when necessary, be reproduced in hardcopy and placed onto noticeboards (positioned adjacent to refreshment machines). The company's Mission statement, Values and Vision are communicated through these methods.

Regular meetings are used at all levels in the organisation to review performance and undertake strategic planning. The monthly Executive Board meeting enables the Chief Executive and/or other Directors to provide information on the performance of the company and potential difficulties that have arisen to Group Managers. In addition, the Technology Group Managers meet on a monthly basis to discuss current and future issues facing Technology Groups. The key points of these meetings are communicated to non-management personnel through Section Meetings (led by the Section Manager), where items specific to each Section are primarily discussed. Communication upwards can be done through the relevant Section or Group Manager, or anonymously through the Staff Consultancy Committee, which meets every quarter with the Chief Executive and other senior management personnel.

To facilitate the quick communication of the company's cumulative performance throughout the year, TWI operates a balanced scorecard system. The balanced scorecard is a concise report that consists of a mixture of financial and non-financial measures of the company's performance, with each measure being compared against a target value for the year. Balanced scorecards are not intended to replace conventional financial/operational reports, but provide a summary that is easily accessed and understood by all employees. The results are presented on a monthly basis on noticeboards and in Section Meetings.

The Intranet system is TWI's primary information system. It acts as an information portal for employees in all Business Functions, having the functionality and providing the information which enables employees to perform their day-to-day tasks effectively. Financial information on specific projects can be found and time booked to that project using the timesheet system. The Human Resources and Quality, Environment, and Health & Safety manuals can be accessed. Information on Industrial Member companies can be found (such as previous and present projects and proposals, visit reports, relevant contacts). Individual Sections have their own drives allowing procedures, information etc which are specific to that Section to be stored.

As discussed in Section 10.4, projects being run at TWI, whether being CRP projects, SCPs, GSPs or collaborative projects, require a team effort by persons from different Sections, Groups and/or Business Functions within the company. Communication with others involved on specific projects is done through the usual channels; face-to-face meetings; e-mails; and phone calls.

10.6 Technology Innovation

TWI has a history of technology innovation dating back to the 1940s when the factors controlling hydrogen induced heat affected zone cracking were first identified [TWI, 2010c]. Numerous other technology innovations have followed, including: aluminium and copper ball joining; linear friction welding of metals; reduced pressure electron beam welding; friction stir welding; and, Vitolane®. Technology innovations by TWI which are specific to laser materials processing include gas assisted laser cutting, the Clearweld® process and laser Surfi-Sculpt®.

In 1967 TWI reported the use of a 300W pulsed slow flow CO_2 laser and an oxygen jet, delivered co-axially with the laser beam, to cut carbon and stainless steels up to 2.5mm in thickness at speeds of $1mmin^{-1}$ [Sullivan and Houldcroft, 1967]. In the forty-three years that have elapsed since, laser cutting has become the biggest industrial use of high-power laser sources and machine sales for this application have exceed $4 Billion for the past five years [Belforte, 2010].

The Clearweld process, which was invented by TWI and has been subsequently patented, is a method for joining plastics transmissive to infrared wavelengths with infra-red laser beams. A colourless infrared absorbing medium is applied to the interface of two plastic components, enabling a weld to be produced which does not affect the surface appearance of the components.

Surfi-Sculpt is an advanced surface texturing process invented and patented by TWI in the previous decade. The process can be used to generate complex features on the surface of materials by rapidly deflecting a focussed power beam over its surface. Material is moved from the bulk solid of the workpiece to points on its surface by a combination of vapour pressure and surface tension effects; repeating this process numerous times results in the formation of arrays of autogeneous surface features that are used to enhance the functional performance of the workpiece. Electron beams, controlled using electromagnetic coils, were first used to demonstrate this process, although more recently the process has been demonstrated using near infra-red laser beams [Hilton and Nguyen, 2008; Blackburn and Hilton, 2010].

The income generated from the licensing of innovative technologies was worth approximately £1.8 million to TWI in 2010 (see Figure 10-2); as a result of TWI holding the patents for these innovative technologies. However, patents have a finite duration for which they can be licensed. Consequently, TWI must ensure that potential future technology innovations are encouraged and financially supported in order to maintain this income stream. Figure 10-5 is a flow chart which outlines how technology innovations are progressed from the initial idea to an income stream.

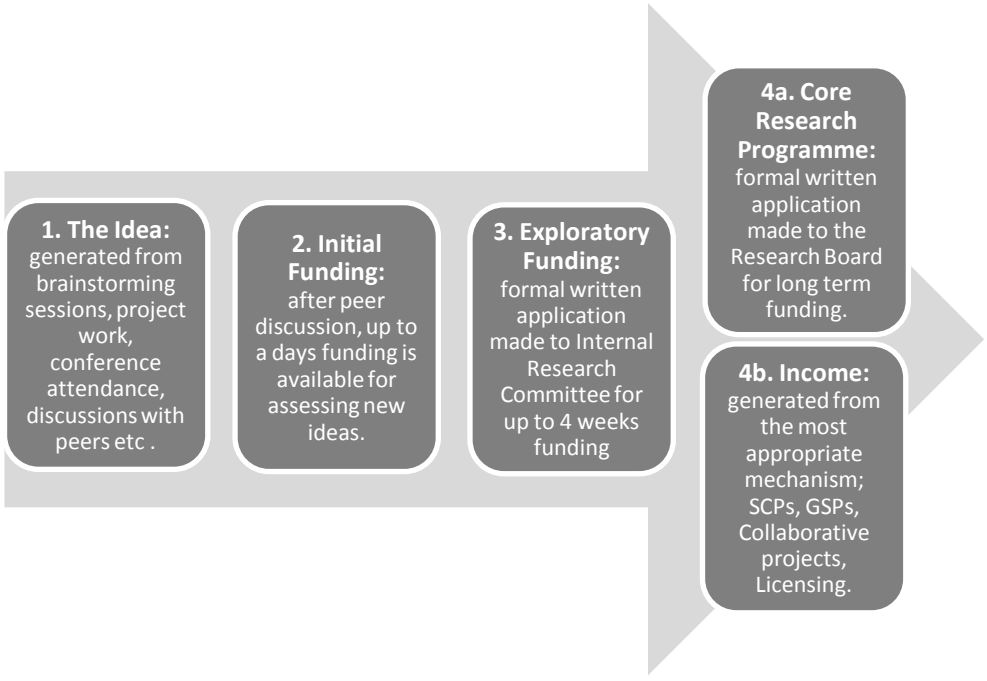

Figure 10-5. The progression of technology innovations at TWI.

Stage 1 - the idea. Innovative ideas may occur as a result of a variety of direct and indirect activities; such as brainstorming sessions, conference attendance, project work, peer discussions, a site visit. To encourage the generation of ideas, TWI have initiated systems such as The Hub (a website accessible by employees which (i) encourages the informal discussion of technology using visual and audio stimuli, and (ii) allows book groups to be established to encourage communication between staff in different Sections) and Food for Thought sessions (informal presentations and discussions of recent technology innovations at lunchtimes, open to all staff members).

Stage 2 – initial funding. A small amount, typically up to a day of financial support, of initial funding can be sought for a technology innovation by informally discussing the idea with the fund manager. Funding can be used for performing initial experiments to test the validity of an idea, performing a background literature or patent search, or acquiring an overview of the commercial demand/applications. If successful, the initial funding is likely to result in the technology being at TRL 1-2.

Stage 3 – exploratory funding. If the idea is proved viable, then a formal application can be made to the Internal Research Committee for up to 4 weeks funding. This may be to perform experimental trials or a more extensive survey of an industry sector's requirements and/or demand for a certain technology. The output at this stage is a concise technical report, which is discussed by the Internal Research Committee and ordinarily presented at a Food for Thought lunchtime networking session. This typically raises the innovation to TRL 2-3.

Stage 4 – further development or an income stream. Following a successful exploratory project, the technology innovation can either be further developed through the CRP (typically over a period of 2-3 years), and/or be exploited by generating income through SCPs, GSPs and/or Collaborative projects. The TRL attained will be dependent upon the level of funding brought in.

10.7 This Project

This project has taken place in the Lasers and Sheet Processes Section of the Electron Beam, Friction and Laser (EFL) processes Technology Group; the position of the Section in the organisational structure of TWI is indicated in Figure 10-4. The EFL Technology Group consists of six Sections based in Cambridge, Rotherham or Middlesbrough. The Lasers and Sheet Processes Section undertakes research and development work for Industrial Member companies in the field of high power laser processing. Research and development projects performed by the Lasers and Sheet Processes Section are ordinarily in the fields of welding,

hybrid laser-arc welding, cutting and surfacing. A different Section in the EFL Technology Group is tasked with performing Research and Development with laser-based additive manufacturing technologies (Laser Direct Metal Deposition, Selective Laser Melting). In addition, the Advanced Manufacturing Processes Technology Group has capabilities for lower power laser processing (i.e. welding of polymers and micro-joining).

This project has been part funded by the EPSRC (Engineering and Physical Sciences Research Council) under Grant no. C537750. The remaining funding has come from four years of TWI's CRP funding. In addition, a small amount of exploratory funding (see Section 10.6) was also obtained to develop the high speed imaging techniques necessary for this project. In both cases the funding has been assigned a project number which has been booked to by the Research Engineer, enabling TWI to determine how much effort the project has required. The project number also allows other employees to perform work related to the project; for instance, radiography of the workpieces and the machining of jigs and fixtures.

Three technical reports summarising the research performed have been prepared for and accepted by the Research Board, and are now available to all Industrial Member companies. As will be discussed in Chapter 11, the commercial drivers behind this project are from the aerospace sector. Consequently, the results have also been presented at two Aerospace Panels (meetings held every six months at TWI for Industrial Member companies in the aerospace sector).

Chapter 11

Commercial Implications

11.1 Introduction

In the previous chapter, details of the sponsoring company, TWI, and how this project fitted into their organisation were given. This chapter presents the commercial implications of the research performed, beginning with the commercial drivers of the project. Other near-net-shape welding technologies are then introduced and discussed with reference to keyhole laser welding. Following these, details of the progress made in this project, in terms of TRLs, are discussed. An overview of the necessary steps to advance this technology to higher TRLs and, ultimately, a production environment, are discussed. Finally, the potential future outcomes of the project for TWI are discussed.

11.2 Commercial Drivers

11.2.1 Increasing use of Titanium in the Aerospace Industry

Among the commonly used metallic materials in the aerospace industry are titanium and its alloys, since their mechanical properties are particularly suitable for the service requirements of both airframe and aeroengine applications. Titanium alloys are employed in applications which require corrosion resistance, weight or space savings, fatigue resistance, or when the capability to operate within a large temperature differential is required. Table 11-1 [Lütjering and Williams 2007, p.15] details the properties of titanium compared with selected other non-ferrous metallic aerospace components.

Table 11-1. Titanium properties compared with other non-ferrous metallic aerospace materials [Lütjering and Williams 2007, p.15].

Property	Ti	Al	Ni
Density (gcm^{-3})	4.5	2.7	8.9
Melting temperature, at 1 atm (K)	1943	933	1728
Thermal conductivity, at 300 K ($Wm^{-1}K^{-1}$)	20	234.5	90
Specific heat capacity ($J\ kg^{-1}K^{-1}$)	523	900	440
Linear coefficient of thermal expansion, at 300 K ($10^{-6}K^{-1}$)	8.4	23.1	13.4
Yield Stress Level (MPa)	1000	500	1000
Modulus of elasticity (GPa), at 300 K	115	72	200

Alpha (α), alpha/beta (α/β), and beta (β) titanium alloys are all used, with the specific alloy chosen dependent upon the component's operating requirements, for example [Boyer, 1996]:

- Ti-6Al-2Sn-4Zr-2Mo-0.1Si (Ti-6-2-4-2S), an α alloy, is utilised for blades, discs and rotors in aeroengines;
- Ti-6Al-4V, an α/β alloy, is used in both static and dynamic aeroengine components at temperatures below 315°C, and is also employed throughout most airframe sections; and,
- Ti-15V-3Cr-3Al-3Sn (β) is used for environmental control system ducting in the Boeing 777 as well as support brackets in certain airframe structures.

It is expected that the demand for titanium alloys in the aerospace industry will rise by ~100% throughout the next five years [Hall, 2009]. This demand is being stimulated by the commercial aerospace industry whose aircrafts are incorporating an increasing proportion of high specific strength materials as a result of environmental and fiscal pressures concerning fuel efficiency in this sector. This statement is evidenced by a statistic [Hale, 2006] regarding the 787 'Dreamliner', which will incorporate ~15% titanium alloys (by weight), whereas its predecessor, the 777, incorporated ~8% titanium alloys (by weight). The use of titanium alloys in the military aerospace sector is a secondary driving force behind the total demand for titanium alloy components in the aerospace sector, where increased functionality and performance can be achieved by using lightweight structural materials [Hill, 2007].

11.2.2 Near-Net-Shape Welding

The production of many of these titanium alloy components by traditional manufacturing methods, i.e. casting or forging and/or machining, is ordinarily the preferred current method. High quality titanium alloy components can be produced with these manufacturing techniques, although the finished components may have buy-to-fly ratios (the mass of material prior to machining compared with the mass of the finished component) which are economically unattractive, in comparison with aluminium alloys and structural steels. It has been reported that for structural aerospace components the ratio may exceed 10:1 [Threadgill et al, 2008]. Welding processes offer the potential to manufacture near-net-shape components, which may require post weld machining, that will have significantly lower buy-to-fly ratios and hence reduce material wastage and overall component cost. Furthermore, a competitive industrial advantage may be gained by a net increase in productivity. Welding technologies such as electron beam and inert gas arc are already utilised to manufacture certain titanium alloy aerospace components [Hilton et al, 2007]. The potential exists for laser based welding processes to be considered for replacing these welding technologies and/or being utilised in the manufacture of new components, because of the increase in productivity possible.

11.2.3 Keyhole Laser Welding

Keyhole laser welding is a non-contact joining process characterised by its high focussed energy density, which is capable of producing high aspect ratio (width : depth) welds in many metallic materials. In comparison with competing welding technologies, discussed in Section 11.3, keyhole laser welding can be performed at atmospheric pressure and with a relatively low heat input. The current generation of solid-state laser sources (Nd:YAG, Yb-fibre, and Yb:YAG disc lasers) emit laser light with a wavelength of ~1 μm, which can be delivered through optical fibres up to 50 m in length (depending upon the required beam quality). Consequently, the process may be easily automated using robotic manipulators, providing extensive flexibility in terms of part size and shape when compared with 10 μm wavelength laser, electron beam and friction welding systems.

The potential for utilising laser welding to manufacture structural components for the aerospace industry has been considered since the mid 1960s [Earvolino and Kennedy, 1966]. Recent advances in high-power, solid-state laser sources (e.g. Nd:YAG rod, Yb-fibre, and Yb:YAG disc lasers) have increased the flexibility of the process, allowing laser beams, of very high beam quality and particularly high power densities, to be fibre delivered to the

workpiece. Consequently, for the manufacture of metallic aerospace components laser welding has received significantly more interest in recent years [e.g. Folkes & Pashby, 2003; Iammi et al, 2008].

Despite the potential advantages for utilising keyhole laser welding as a manufacturing technique for near-net-shape welding of titanium alloy components, if the welding process is to be adopted the produced welds must be of an acceptable quality. Specifications such as EN ISO 13919-2:2001*, Welding – Electron and laser beam welded joints – Guidance on quality levels for imperfections*, detail general requirements for welds produced with a power beam. Criteria relating to the weld metal porosity, weld profile and weld discoloration are included in the specification. However, EN ISO 13919 is neither industry sector nor material specific, and the acceptance criteria are not as stringent as those detailed in AWS D17.1:2001, *Specification for Fusion Welding for Aerospace Applications*. AWS D17.1 details the quality levels for welded aerospace structures for several metallic materials, including titanium alloys, produced using electric arc, laser beam, electron beam or oxyfuel welding processes. The criteria stated in AWS D17.1 may be suitable for certain non-primary airframe applications, although for aeroengine and primary airframe applications the acceptance criteria are known to be company specific and are significantly more stringent than those detailed in AWS D17.1 and EN ISO 13919 [Hilton et al, 2007].

This thesis has presented the research performed in a joint project undertaken by The University of Manchester and TWI Ltd (the operating arm of TWI). The aim of this research project was to *establish an understanding of the formation of weld metal porosity when keyhole laser welding titanium alloys with 1 μm wavelength laser sources and develop techniques which could prevent its formation*.

11.3 Competing Technologies

In addition to keyhole laser welding, there are several other joining technologies capable of producing near-net-shape titanium alloy components for the aerospace industry; specifically, electron beam welding, friction stir welding, tungsten inert gas arc welding, and diffusion bonding. If keyhole laser welding is to be chosen above these other manufacturing techniques, to replace traditional casting and forging methods, it must offer the end-user a competitive advantage. This competitive advantage may come in the form of:

1. an overall decrease in total production costs; or,
2. an increased manufacturing capability (e.g. the possibility of manufacturing components of increased geometrical complexity, enabling greater design freedom).

Ultimately, the choice of manufacturing technique will depend upon the specific component. Detailed in the remainder of this Section is a comparison of keyhole laser welding, in terms of advantages and disadvantages, with the competing manufacturing technologies mentioned above.

11.3.1 Tungsten Inert Gas Arc Welding

Arc based welding processes use a power supply to produce an electric arc between the electrode and the workpiece; welds between abutting components are produced by traversing this arc along the joint. Several different arc welding techniques exist, depending upon the use of a consumable or non-consumable electrode, and whether an alternating or direct current is chosen.

The most common arc welding process for welding titanium based alloys is tungsten inert gas (TIG) welding [Donachie, 2000] also known as gas tungsten arc welding (GTAW). The TIG welding process uses a non-consumable tungsten electrode, and similarly to keyhole laser welding the process may be either autogeneous, if the joint-gap variation is sufficiently low, or make use of filler material (which is added separately to the weldpool) as a solution for poor joint preparations. Several variations to the TIG welding process exist; specifically activated TIG(ATIG), keyhole mode TIG (K-TIG) [Jarvis, 2001], and keyhole mode plasma arc (PAW).

A high purity inert shielding gas is used when TIG welding titanium based alloys. This shielding gas is ordinarily supplied through a trailing shield, analogous to that shown in Figure 4-2, to ensure the process and the cooling weld metal is adequately shielded from light elements. Argon and/or helium can be used as a shielding gas, whereby the addition of helium increases the arc temperature promoting increased welding speeds or weld penetration. However, the use of high purity helium, a gas which is not necessary when welding titanium based alloys with 1 μm wavelength laser beams, will increase the cost of the process.

For high production environments, TIG welding may be mechanised using, for instance, a 6-axis robot; enabling relatively complex components to be welded together. However, due to the size of the torch and the limited arc length, joints which are difficult to access (e.g. in a narrow recess) are not easily weldable using TIG welding equipment. Such joints are more readily accessible using a narrowly focussed laser beam of low divergence.

The principal advantage offered by TIG welding of titanium alloys over keyhole laser welding is the cost of capital equipment; a welding power source is approximately one order of magnitude less than a laser source. Automation equipment for both processes will be of a similar cost. However, in comparison with laser beam welding, TIG welding has a relatively high heat input. Figure 11-1 [Short, 2009] details the specific heat input for TIG and ATIG welding of titanium. For the most common thickness used in this project (i.e. 3.25 mm) a specific heat input of approximately 600 Jmm^{-1} was required, whereas with keyhole laser beam welding a specific heat input of 30-60 Jmm^{-1} was necessary.

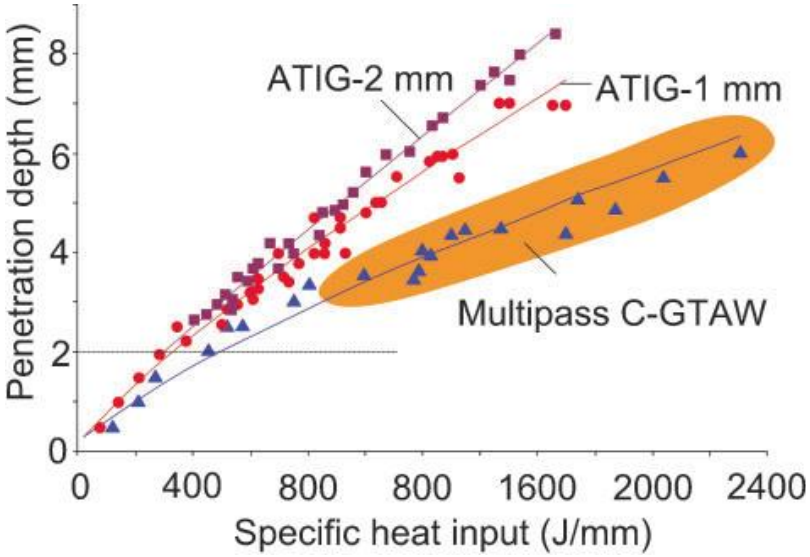

Figure 11-1. A comparison of penetration depth versus specific heat input for multipass C-GTAW and ATIG welding of titanium [Short, 2009].

11.3.2 Electron Beam Welding

Electron beam welding is also a fusion welding process. The process uses a highly focussed beam of high-velocity electrons to vaporise the workpiece and produce a keyhole, similarly to keyhole laser welding, which enables an efficient transfer of energy between the beam and the workpiece. Welds are produced by traversing the keyhole along the joint, and the process mechanisms are similar to those described in Sub-section 2.3.2; except that the kinetic energy of electrons is instantly converted into heat upon impact, rather than the Fresnel or inverse Bremsstrahlung absorption of photons. Focussed beam widths are <0.5 mm and consequently joint gap preparation as precise as that in autogeneous keyhole welding are required.

Potential single pass penetration depths for electron beam welding are significantly higher than possible with keyhole laser welding and TIG welding. High power machines (>100 kW

rated output power) are capable of producing single pass welds of at least 300 mm in low alloy steel [Sanderson, 2006]. Such high penetration depths have not yet been produced using keyhole laser welding, although penetration depths >14 mm are not often required by the aerospace industry. At lower powers and at workpiece thicknesses <10 mm, high beam quality 1 μm wavelength laser sources and electron beam welding machines are capable of similar welding performances [Verhaeghe and Dance, 2008].

High-vacuum electron beam machines require pressures of the order 10^{-5} – 10^{-2} mbar to operate effectively, resulting in the need for vacuum chambers and high-performance vacuum pumps. The high vacuum requirement limits the size of the component which can be welded, and allowances must also be made for the manipulation equipment since the component is moved underneath a stationary beam. This is a key advantage for the laser-based welding process, since it can operate out of vacuum and is capable of processing complex part geometries using a 6-axis robotic manipulator. The vacuum chamber and high-performance vacuum pumps add significantly to the investment required in capital equipment, if the electron beam welding method were chosen; although they do allow for complex inert gas shielding shoes to be avoided. Investment costs are likely to exceed those required for a laser welding facility of similar welding performance. Furthermore, productivity would be lower for electron beam welding since time also needs to be allocated for pump down of the vacuum chamber.

Advancements made in the design of the electron beam gun have allowed electron beam welding to be performed at pressures approaching 1 mbar [Sanderson, 2006]. Operating at these pressures enables local seals and/or vacuum arrangements to be used instead of a high-vacuum chamber; having knock-on effects in terms of decreased capital equipment costs and pump down times. Nevertheless, it is hard to envisage such an arrangement having the same degree of flexibility as laser welding head mounted on an articulated robot arm operating at atmospheric pressure.

11.3.3 Friction Stir Welding

Friction stir welding is a solid-state joining technique conceived by Wayne Thomas of TWI in 1991 [Dawes, 1995]. The welding technique uses a cylindrical tool, with an integral shoulder, that is driven through the joint line of two abutting components. The tool is rotated as it is driven, generating heat as a result of the friction with the workpiece. The resulting heat enables the consumable tool to be driven through the workpiece, at temperatures below the

workpiece's melting point, and the weld is made as plasticised material is transferred from the leading to the trailing edge of the tool.

The technique has found considerable uptake in the production of aluminium assemblies [Threadgill et al, 2009]. However, a study on the application of traditional friction stir welding techniques (i.e. a rotating shoulder) to join high temperature materials, such as titanium based alloys, found the following problems [Russell and Freeman, 2007]:

- high performance, high temperature and therefore expensive tool materials were required;
- the tools have an undesirable short life due to high wear;
- a narrow processing window; and,
- a process which is particularly sensitive to temperature variations.

The stationary shoulder friction stir welding (SSFSW) technique was developed to overcome these problems, and friction stir welding of 6mm thickness Ti-6Al-4V panels has now been performed [Russell and Freeman, 2007]. Temperatures exceeding 500°C occur during SSFSW of titanium alloys [Edwards and Ramulu, 2010] requiring the use of inert shielding gases during welding.

Excellent weld qualities, potentially defect free [Zhang et al, 2010], are produced during friction stir welding. Traditionally, thick section components may be welded using large gantry friction stir welding machines that are similar in cost to an electron beam welding machine. However, for thin section components, a high-performance articulated arm is capable of applying the forces required to initiate friction stir welding. Nevertheless, tool wear is still high, and tool geometry (which will limit access to certain joints) is dependent upon the mechanical performance of the tool's material properties (as a result of induced bending stresses etc).

11.3.4 Diffusion Bonding

Diffusion bonding is a solid-state joining process, sometimes referred to as diffusion welding, which uses elevated temperatures and pressures, applied over long durations, to join components. It is often used in combination with superplastic forming to produce complex assemblies. Weld qualities produced by diffusion bonding are superior to all other welding techniques, since the micro-structures are identical to the parent material (temperatures below the phase transition temperatures are used). Diffusion bonding is performed in an

inert gas, a reducing atmosphere or a vacuum and is therefore ideally suited to processing of titanium based alloys. The primary disadvantages of diffusion bonding are:

- Cost – large custom designed and built chambers are required to house large components.
- Time – a typical diffusion bonding process for Ti-6Al-4V components is generally performed at pressures of up to 13.8 MPa, temperatures of 900-950°C and for durations of 60 to 360 minutes [Donachie, 2000].

11.4 Technology Readiness Level of Current Work

The use of TRLs to determine the maturity of individual technologies was discussed in Section 10.3. Although four different techniques (Chapters 5-8) have been researched in this project, the fundamental technology has been *keyhole laser welding*. Keyhole laser welding is already an established technology in a number of industry sectors; such as the automotive sector [Tang, 2010]. Therefore, in this project it is more appropriate to use the TRLs as a metric to evaluate the progress made in using *keyhole laser welding as a process to produce near-net-shape titanium alloy components for the aerospace industry*. Table 11-2 [MoD, 2010] details the definitions and descriptions of TRLs 1-7; since these are the TRLs that TWI will most likely be involved with.

Prior to performing this project, the technology for this application was at TRL 2-3. TRL 1, which is defined as “Basic principles observed and reported” [MoD, 2010], may have been reached as early as 1966 [Earvolino and Kennedy, 1966] when the potential for using laser welding to manufacture structural components for the aerospace industry was first identified. It should be noted that this would not have been for keyhole laser welding, since the power densities available would only have been sufficient for conduction limited laser welding of structural components.

Table 11-2. Technology Readiness Level (TRL) definitions and descriptions up to TRL 7, the level reached in this project [MoD, 2010].

TRL	Definition	Description
1	Basic principles observed and reported.	Lowest level of technology readiness. Blue skies scientific research begins to be translated into applied research and development (R&D). Examples might include paper studies of a technology's basic properties.
2	Technology concept and/or application formulated.	Invention begins. Once basic principles are observed, practical applications can be invented. Applications are speculative, and there may be no proof or detailed analysis to support the assumptions. Examples are limited to analytic.
3	Analytical and experimental critical function and/or characteristic proof-of-concept.	Active R&D is initiated. This includes analytical studies and laboratory studies to physically validate the analytical predictions of separate elements of the technology. Examples include components that are not yet integrated or representative.
4	Technology component and/or basic technology subsystem validation in laboratory environment.	Basic technological components are integrated as sub-systems to establish that they will work together. This is relatively low fidelity compared with the eventual system. Examples include integration of ad-hoc hardware in the laboratory.
5	Technology component and/or basic technology subsystem validation in relevant environment.	Fidelity of technology increases significantly. The basic technological components are integrated with reasonably realistic supporting elements so they can be tested in a simulated environment. Examples include high fidelity laboratory integration of components, and basic field trials to prove capability concepts.
6	Technology system / sub-system model or prototype demonstration in a relevant environment.	Representative model or prototype system, which is well beyond that of TRL 5, is tested in a relevant environment. Represents a major step up in a technology's demonstrated readiness. Examples include field testing a prototype in a high fidelity laboratory environment or in a simulated operational environment operating under proposed protocols.
7	Technology prototype demonstration in an operational environment.	Prototype near or at planned operational system. Represents a major step up from TRL 6 by requiring demonstration of an actual system prototype in an operational environment (e.g., in an aircraft, in a vehicle, or platform in the field).

The results of early experiments on laser welding of titanium alloys by Mazumder and Steen [1977, 1980, 1982] helped raise the TRL to 2-3. TRL 2 is defined as "Technology concept and/or application formulated" [MoD, 2010], and TRL 3 as "Analytical and experimental critical function and/or characteristic proof-of-concept" [MoD, 2010]. It should be noted that all the research performed by Mazumder and Steen [1977, 1980, 1982] was using 10 μm wavelength laser sources, which do not offer the same flexibility as fibre optically delivered

1μm wavelength laser sources. The first results of using 1 μm wavelength laser sources for welding of titanium alloys for aerospace applications were reported by Li et al [1997] and Coste et al [1999]. However, only relatively few studies [Hilton et al, 2007; Mueller et al, 2008] have reported the capability of 1 μm wavelength laser sources to produce the required weld quality in titanium alloy parts for aerospace applications. Furthermore, these studies were limited to use of a directed gas jet, and not the other techniques which have been developed in this project.

In this project, TRL 3 was reached for all the four keyhole laser welding processes examined by performing analytical and experimental studies to determine the effects of key process parameters on the process dynamics, and subsequently the formation of porosity in the weld metal. The production of autogeneous melt runs in relevant thicknesses of titanium alloys with optimised parameter combinations enabled the proof of concept to be performed. The results of these autogeneous melt runs showed that the required weld quality, in terms of subsurface porosity, weld profile and discoloration, could be achieved. The vast majority of work performed in this project was to develop the project up to and within TRL 3.

In addition, TRL 4, defined as "Technology component and/or basic technology subsystem validation in laboratory environment" [MoD, 2010], has been reached but not necessarily completed. The production of butt welds in the laboratory using the techniques developed, incorporating established edge preparation and clamping procedures, have validated that a complete welding procedure gives the desired weld quality in a laboratory environment in a simplistic component, somewhat representative of the joints used in the aerospace industry.

11.5 Advancing the Technology Readiness Level

The TRL *of keyhole laser welding as a process to produce titanium alloy components for the aerospace industry* is currently 4. Since keyhole laser welding is already an established manufacturing process in a number of industry sectors, the actions required to advance this technology to TRL 7 and beyond can be inferred from different industry sectors.

TRL 5 is defined as "Technology system / sub-system model or prototype demonstration in a relevant environment" [MoD, 2010]. In order to reach this level, process parameters would need to be transferred onto actual aerospace components in a laboratory environment, with the produced welds then being characterised using the destructive and non-destructive techniques employed in this research. Components produced using this technology would then need to be tested in a simulated environment.

TRL 6 is defined as "Technology system / sub-system model or prototype demonstration in a relevant environment" [MoD, 2010]. Developing the technology to this level may require substantial effort, depending upon the required level of integration with other sub-systems. For instance, seam tracking and adaptive control systems may be required, and although these are readily available some degree of integration with the existing technology is required. In addition, weld quality sensors and/or post production non-destructive testing procedures may also need to be integrated. This level could be reached in a laboratory operating under the proposed protocols.

TRL 7 is defined as "Technology prototype demonstration in an operational environment" [MoD, 2010]. The system developed to reach TRL 6 would need to be advanced further by producing a prototype system (not necessarily an ad-hoc arrangement of equipment in a laboratory) to be operated in a production environment. Further TRLs could then be reached by validating this technology and leading to full scale production.

11.6 Potential Commercial Benefits

The majority of the potential commercial benefits resulting from this project are related to advancing the TRL of keyhole laser welding titanium alloys for aerospace applications. Since TWI is affectively owned by its Industrial Member companies, and this project has been performed as part of the CRP and the results published to Industrial Member companies, the advancement of the TRL may or may not involve TWI.

For TWI the potential commercial outcome of this project is primarily future project income. This income will come either as a result of a SCP, a GSP or a collaborative project.

- Income from a SCP will primarily be generated by co-ordinating the results of this project with the business development function of TWI, and by presenting the results at relevant conferences and in trade publications. Enquiries, either from member or non-member companies, resulting from these business development activities may then lead to SCP income following further technical discussions and project scope developments. The advancement of the TRL by this method is limited only by the available financial resources of the Industrial Member company.
- The launch of a GSP involving several Industrial Member companies would enable a much larger scope of work to be undertaken; enabling the TRL to be increased for all parties at a price shared equally between the Industrial Member companies.
- Collaborative initiatives, particularly the Seventh Framework Programme run by the European Commission, enable TWI, in conjunction with other companies, to seek

funding for certain technologies that will benefit the wider European Economic Community. The results of this project could be used as the basis for producing a response to a particular funding call, enabling the TRL to be considerably advanced in a medium-long term project.

Furthermore, the results of this project are likely to strengthen TWI's reputation in the field of laser materials processing, which may lead to new Industrial Member companies and project work, either related or unrelated to the aerospace industry.

Part IV

Conclusions and Recommendations for the Future

Chapter 12: Conclusions and Recommendations for the Future

Chapter 12

Conclusions and Recommendations for the Future

12.1 Technical Conclusions

The aim of this research project was to *establish an understanding of the formation of weld metal porosity when keyhole laser welding titanium alloys with 1 μm wavelength laser sources and develop techniques which could prevent its formation*. A detailed review of the background literature revealed that, much of the published research concerning the formation and prevention of porosity when keyhole laser welding was performed using materials other than titanium alloys. Nevertheless, the literature indicated that the most likely sources of porosity when keyhole laser welding titanium alloys were:

1. The entrapment of inert shielding gas as a result of keyhole instability and/or closure.
2. Hydrogen rejection during solidification of the melt pool.

It was anticipated that if appropriate inert gas shielding and material preparation procedures were followed, then the formation of weld metal porosity as a result of hydrogen rejection would only be a minor cause. Consequently, three different techniques for controlling the levels of weld metal porosity when welding titanium alloys with Nd:YAG rod laser have been investigated using systematic experimentation and/or statistical experimental design and analysis techniques. In addition, the potential for welding titanium alloys to the required weld quality criteria with excellent beam quality 1 μm wavelength laser sources has been assessed.

Characterisation of the welding processes using high speed photography and optical spectroscopy, have allowed an original scientific understanding of the effects these methods have on the keyhole, melt pool and vapour plume behaviour to be established. Combining this with a thorough assessment of the weld qualities produced, has enabled the effects of these process behaviours on the formation of weld metal porosity to be determined.

Nd:YAG Laser Welding with a Directed Gas Jet

A jet of inert gas directed towards the laser-material interaction point can be used during Nd:YAG laser welding of titanium alloys to reduce subsurface weld metal porosity. The quality of butt welds produced in 3.25 mm thickness Ti-2.5Cu and Ti-6Al-4V were within the requirements stipulated in company specific aerospace weld quality criteria. Two statistically designed and analysed experiments were used to determine the key process parameters and their working tolerances which allow a high quality weld to be reproducibly achieved. The vapour plume above the keyhole when Nd:YAG laser welding Ti-2.5Cu has been characterised using optical spectroscopy and vapour plume sampling. The plume temperature was calculated to be ~3100 K. The main mechanisms of Nd:YAG laser beam attenuation by the vapour plume have been found to be primarily absorption but also scattering of the incident laser light by a population of 30–60 nm titanium particles. High speed observation of the welding process with and without an optimised directed gas jet has revealed that it disperses the formation of the vapour plume above the keyhole and interacts with the hydrodynamic behaviour of the melt pool. This prevents fluctuations in the keyhole's vaporisation pressure and hence increases keyhole stability, thus reducing weld metal porosity.

Modulated Nd:YAG Laser Welding

Nd:YAG laser welding with a modulated output can be used to produce butt welds in titanium alloys, up to at least 3.25mm in thickness, with an excellent internal quality; provided a square wave modulation, a modulation frequency of ≥125 Hz, a duty cycle of 50%, and a suitable modulation amplitude were used. Undercut present at the weld root can be reduced through the adoption of a defocused laser beam and a decreased modulation amplitude. High speed observation and subsequent Fourier analysis has shown the presence of common periodic behaviours in the vapour plume and keyhole when low porosity welding conditions are used. An oscillating wave was created in the melt pool when low porosity welding conditions were used, which is thought to act in manipulating the ejection angle of the vapour plume and aiding the escape of the gas bubbles in the melt pool.

Dual Focus Nd:YAG Laser Welding

A dual focus configuration can be used to decrease the formation of porosity when welding 3.25 mm thickness Ti-6Al-4V with an Nd:YAG laser. The response surfaces models produced indicate that the weld metal porosity can be reduced to within levels stipulated by stringent aerospace criteria, if a relatively small foci separation (~0.3 mm) and a suitable welding speed (~80 mms^{-1}) are used. Observation and subsequent analysis of the welding process using two high speed cameras has shown that small foci separations (0.15-0.30 mm) increase keyhole stability; and hence reduce the occurrences of keyhole collapse and the formation of weld metal porosity.

Welding with Excellent Beam Quality 1 μm Wavelength Laser Sources

Excellent beam quality 1μm wavelength laser sources were considered for producing high quality welds in titanium alloys. Three different Yb-fibre laser sources, with beam parameter products in the range 0.33-6.0mm.mrad, focused with different optical combinations, have been used to process 2.0-7.0mm thickness Ti-6Al-4V. The results indicate that butt welds which meet the subsurface porosity criteria of company specific aerospace standards can be produced with very different focused beams in the beam parameter product range 1.6-6.0mm.mrad. No special techniques, such as a directed jet of inert gas, were required to produce these high quality welds, as is the case with poorer beam quality Nd:YAG rod laser sources. It is thought that the increased power density available with these laser sources reduces keyhole instability by increasing the radiation pressure within the keyhole.

Porosity Formation

The results of the different keyhole laser welding techniques (concluded above) and a characterisation of weld metal porosity, strongly indicate that the pores are formed as a result of keyhole instability and closure which lead to the presence of shielding gases in the melt pool. These gas bubbles, as a result of the complex molten metal flows present in the melt pool are not able to escape prior to solidification and become entrapped as porosity.

12.2 Commercial Conclusions

This project has been performed as part of the organisational strategy of TWI to maintain and strengthen their reputation as a world leading independent research and development institution in the fields of joining materials, engineering and allied technologies. The research was performed as part of TWI's CRP on behalf of its Industrial Member companies.

The progress made in this project can be quantitatively defined using the TRL metric discussed in Section 10.3, if the technology is considered to be using *keyhole laser welding as a process to produce near-net-shape titanium alloy components for the aerospace industry*. The research has taken the technology from TRL 2-3 and has advanced this to TRL 4, through understanding the formation of porosity and developing procedures to reduce its occurrence. The necessary steps to develop this technology to TRL 7 and above have been outlined and, briefly are:

TRL 5: Transferring process parameters developed in this research onto actual components, which would be characterised and tested in a simulated environment.

TRL 6: Integrating the current system with other sub-systems (e.g a vision system for seam tracking) and operate this in a laboratory operating under proposed protocols.

TRL 7: Production of a prototype system to be operated in a production environment.

TRL 8-9: Validation of the system leading to full scale production.

Reaching the higher TRL levels will enable end-users to take advantage of a technology which has significant advantages over competing joining techniques, specifically in the areas of: automation flexibility, heat input, processing speeds and equipment cost.

The potential commercial outcomes of this project for TWI are related to the advancement of the TRL with Industrial Member companies. This may either be as a confidential SCP, a GSP or a collaborative project. Furthermore, it should not be forgotten that TWI is after all owned by its Industrial Member companies, who may use this research to develop their operations independently of TWI.

12.3 Recommendations for the Future

The majority of this research has been performed using a Nd:YAG rod laser source, and whilst it is has been shown that excellent weld qualities are achievable, it is also acknowledged that this form of laser source has been replaced by other solid-state lasers for beam quality and wall plug efficiency reasons. Nevertheless, 1μm wavelength direct diode lasers with beam qualities approaching that available from Nd:YAG rod lasers and wall plug efficiencies approximately an order of magnitude higher are becoming available [Trumpf, 2010b]. It is envisaged that these laser sources could be utilised for high quality laser welding of titanium alloys using the techniques and nominally identical process parameters to those developed in this thesis. Consequently, the majority of practical research that is recommended for

continuation of this work involves laser sources emitting beams with an excellent quality, specifically; Yb-fibre and Yb:YAG disc lasers. However, the transferability of the welding techniques developed in this project to other high-performance engineering metals, such as nickel alloys, should also be investigated.

In this investigation it has been shown that melt runs with very low levels of subsurface weld metal porosity can be produced using a highly focussed Yb-fibre laser. Transferability of these conditions to industrial joints poses some problems, since the potential for the focussed beam missing the joint line is amplified. Furthermore, in comparison with the company specific weld quality criteria, the thickness of the melt runs at their waist may not be acceptable. Further practical research should be performed to investigate beam oscillating and beam spinning techniques when using highly focussed Yb-fibre and/or Yb-YAG disc laser sources. These techniques have the potential to reduce the effects of poor fit-up and/or beam misalignment, and produce wider welds. Previous research performed using these techniques when welding with CO_2 laser sources may provide pertinent information for the required beam oscillation/spinning frequencies and amplitudes.

The effect of different power densities on the resultant level of weld metal porosity in the weld metal has been highlighted. In order to better understand this effect, further research is required to observe the dynamic behaviours of the melt pool, keyhole and vapour plume when processing with very different focussed beams. This could be performed with the high speed imaging techniques used in this project.

Statistical data analysis techniques have been used in this to project to determine the key process parameters when keyhole laser welding titanium alloys with Nd:YAG rod lasers. Similar statistical techniques should be applied to future welding studies performed with excellent beam quality 1 μm wavelength laser sources. The analyses parameters should include power density, welding speed, focal plane position and Rayleigh length.

It is clear from the results of this project that the high speed observation of the keyhole and the vapour plume can be utilised to predict the porosity content of the resultant weld. Further research should be performed to develop a real-time process control system using the output of the high speed cameras. Such a system could refer to a database of signals known to cause weld metal porosity and apply an appropriate correction factor to the process parameters.

Characterisation of the gases present inside the pores produced, using mass spectroscopy, should give a definitive answer as to whether or not they are caused as a result of hydrogen or shielding gas entrapment.

It was the initial intention of this research project to include a modelling aspect. Specifically, this would have utilised computational fluid dynamics (CFD) to model the keyhole and melt pool behaviour, such as in the research described by Amara and Fabbro [2008] and Geiger et al [2009]. However, such a model would have required the entire attention of this research project, which was not feasible given the aim and objectives of this project. Nevertheless, a CFD model capable of predicting the occurrences of keyhole instability would be very beneficial. Various permutations of parameters could be examined from the outset, leading to a significantly reduced number of experimental trials that must be performed. Initial validation of a CFD model could be performed using the high speed video data generated during this project. Further validation would most likely require use of an X-ray transmission imaging system similar to that used by Matsunawa et al [1998], or the observation of keyhole laser welding of ice or transparent glass.

References

Ahmed, T. & Rack, H.J. (1998) 'Phase transformation during cooling in α+ß titanium alloys', *Mater. Sci. and Eng. A (Struct. Mater.: Prop., Microstruct. and Process.)*, 243(1-2), 206-211.

Amara, E.H. & Fabbro, R. (2008) 'Modelling of gas jet effect on the melt pool movements during deep penetration laser welding', *J. Phys. D: Appl. Phys.*, 41(5), 1-10.

American National Standards Institute (2007) 'ANSI Z136.1-2007 American National Standard for Safe Use of Lasers', American National Standards Institute, Washington DC.

American Welding Society (2001) 'AWS D17.1:2001 Specification for Fusion Welding for Aerospace Applications', American Welding Society, Miami.

Arata, Y., Abe, N. & Oda, T. (1984) 'Beam hole behaviour during laser beam welding', in *Proc. Int. Conf of Appl. of Lasers and Electro-Opt., ICALEO*, *Los Angeles, November 1983,* 38, 59-66.

Arata, Y., Abe, N., Oda, T. & Tsujii, N. (1985) 'Fundamental phenomena during vacuum laser welding', in *Proc. Int. Conf of Appl. of Lasers and Electro-Opt., ICALEO, Boston, November 1984*. 44, 1-7.

Bahun, C.J. & Eng-Quist, R.D. (1962) 'Metallurgical applications of lasers', in *Proc. of the Nat. Electron. Conf.*, 18, 607-619.

Bardin, F., Morgan, S., Williams, S., McBride, R., Moore, A.J., Jones, D.C. & Hand, D.P. (2005) 'Process control of laser conduction welding by thermal imaging measurement with a color camera', *Appl. Opt.*, 44 (32), 6841-6848.

Beck, M.P., Berger, P. & Hügel, H. (1995) 'The effect of plasma formation on beam focussing in deep penetration welding with CO_2 lasers', *J. Phys. D: Appl. Phys.*, 28(12), 2430-2432.

Belforte, D. (2009) 'Economic review and forecast – Keeping the economy in perspective', *Ind. Laser Solut.*, 24 (1), 4-11.

Belforte, D. (2010) 'Economic review and forecast – The worst is over', *Ind. Laser Solut.*, 25 (1), 4-10.

Blackburn, J.E. & Hilton, P.A. (2010) 'Low power laser Surfi-Sculpt®', *in Proc. 3rd Int. Conf. on Power Beam Process. Technol., Beijing, October 2010*, 190-193.

Blackburn, J., Hilton, P., Allen, C. & Li, L. (2010) 'Comparison of high power Yb-fibre and Nd:YAG lasers when welding TI-6AL-4V', *in Proc. Pacific Int. Conf on Appl. of Lasers and Optics*, Wuhan, March 2008, paper 404.

Boyer, R.R. (1996) 'An overview on the use of titanium in the aerospace industry', *Mater. Sci. and Eng. A (Struct. Mater.: Prop., Microstruct. and Process.)*, 213(1-2), 103-114.

British Standards Institution (2007) 'BS EN 60825-1:2007 Safety of laser products – Part 1: Equipment classification and requirements', British Standards Institution, Milton Keynes.

Brückner, M., Schäfer, J.H. & Uhlenbusch, J. (1989) 'Ellipsometric measurement of the optical constants of solid and molten aluminum and copper at λ=10.6 μm', *J. Appl. Phys.*, 66(3), 1326-1332.

Brückner, M., Schäfer, J.H., Schiffer, C. & Uhlenbusch, J. (1991) 'Measurements of the optical constants of solid and molten gold and tin at λ=10.6 μm', *J. Appl. Phys.*, 70(3), 1642-1647.

Caiazzo, F., Curcio, F., Daurelio, G. & Minutolo, F.C.M. (2004) 'Ti6Al4V sheets lap and butt joints carried out by CO_2 laser: mechanical and morphological characterization', *J. Mater. Process. Tech.*, 149(1-3), 546-552.

Canning, J. (2005) 'Fibre lasers and related technologies', *Opt. and Lasers in Eng.*, 44(7), 647-676.

Cho, J-H., & Na, S.-J. (2007) 'Theoretical analysis of keyhole dynamics in polarized laser drilling', *J. Phys. D: Appl. Phys*, 40(24), 7638-7647.

Choudhuri, A.R. (1998) 'The physics of fluids and plasmas: an introduction for astrophysicists', Cambridge University Press: Cambridge.

Clarkson, W.A., Cooper, L.J. Wang, P., Williams, R.B. & Sahu, J.K. (2003) 'Power scaling concepts for fiber lasers', *Trends in Opt. and Photonics Ser.*, 83, 261-267.

Clift, R., Grace, J.R. & Weber, M.E. (1978) 'Bubbles, drops and particles', Academic Press: New York.

Cohen M.I. (1967) 'Melting of half-space subjected to constant heat input', *J. of the Franklin Inst.*, 283(4), 271-285.

Companies House Website (2001) http://wck2.companieshouse.gov.uk (Accessed May 2010).

Costa, A., Miranda, R., Quintino, L. & Yapp, D. (2007) 'Analysis of beam material interaction in welding of titanium with fiber lasers', *Mater. and Manuf. Process.*, 22(7-8), 798-803.

Coste, F., Aubry, P., Hertmanowski, S., Launais, H. Dubois, T. Démure, O. & Fabbro , R. (1999) 'Optimizing the quality of TA6V and Inconel laser welding on airplane part manufacturing', in *Proc. Int. Conf of Appl. of Lasers and Electro-Opt., ICALEO, San Diego, November 1999*, 2, D261-D268.

Dawes, C.J. (1995) 'Introduction to friction stir welding and its development' *Welding and Metal Fabrication*, 63(1).

De, A. and DebRoy, T. (2006) 'Improving reliability of heat and fluid flow calculation during conduction mode laser spot welding by multivariable optimisation', *Sci. and Tech. of Weld. and Join.*, 11(2), 143-153.

Denney, P.E. & Metzbower, E.A. (1989) 'Laser beam welding of titanium', *Weld. J.*, 68(8), 342s-346s.

Donachie, M.J. (2000) 'Titanium: a technical guide', 2nd edition, ASM International, Ohio.

Dowden, J., Davis, M. & Kapadia, P. (1983) 'Some aspects of the fluid dynamics of laser welding', *J. Fluid Mech*., 126, 123-146.

Dowden, J., Postacioglu, N., Davis, M. & Kapadia, P. (1987) 'A keyhole model in penetration welding with a laser', *J. Phys. D: Appl. Phys.*, 20(1), 36-44.

Dowden, J.M., Kapadia, P. & Ducharme, R. (1995) 'Analytical model of deep penetration welding of metals with a continuous CO2 laser', *Intern. J. for the Join. of Mater.*, 7(203), 54-61.

Dowden, J.M. (2009) 'Laser keyhole welding: the vapour phase', in: Dowden, J.M. (ed.) *The theory of laser materials processing: heat and mass transfer in modern technology*, Canopus, Bristol (England), 95-127.

Du, H., Hu, L., Hu, X. & Liu, J. (2003) 'Laser welding of TC-1 titanium alloy', *J. Mater. Sci. Technol.*, 19(5), 475-478.

Duley, W.W. (1999) 'Laser Welding', Wiley: New York.

Earvolino, L.P. & Kennedy, J.R. (1966) 'Laser welding of aerospace structural alloys', *Weld. J.*, 44(3), 127s-134s.

Eberle, H.G. & Richter, K. (1994) 'Welding of aluminium alloys with modulated lasers', in *Proc. Laser Mater. Process.: Ind. and Microelectron. Appl., Vienna, September 1994*,185-191.

Edwards, P. & Ramulu, M. (2010) 'Peak temperatures during friction stir welding of Ti-6Al-4V', *Sci. and Technol. of Weld. and Join.,* 15(6), 468-472.

Einstein, A. (1916) 'Strahlungs-emission und -absorption nach der Quantentheorie', *Dtsch. Phys. Ges.,* 18, 318-323.

Fabbro, R. & Chouf, K. (2000) 'Dynamical description of the keyhole in deep penetration laser welding', *J. Laser Appl.*, 12(4), 142-148.

Fabbro, R., Hamadou, M. & Coste, F. (2004) 'Metallic vapor ejection effect on melt pool dynamics in deep penetration laser welding', *J. Laser Appl.*, 16(1), 16-19.

Fabbro, R., Slimani, S., Doudet, I., Coste, F. & Briand, F. (2006) 'Experimental study of the dynamical coupling between the induced vapour plume and the melt pool for Nd-yag CW laser welding', *J. Phys. D: Appl. Phys.*, 39, 394-400.

Fabbro, R., Slimani, S., Coste, F. & Briand, F. (2007) 'Analysis of the various melt pool hydrodynamic regimes observed during CW Nd-Yag deep penetration laser welding' in *Proc. Int. Conf of Appl. of Lasers and Electro-Opt., ICALEO*, Orlando*, November 2007*, paper 802.

Fan, H.G., Tsai, H.L. & Na, S.J. (2001) 'Heat transfer and fluid flow in a partially or fully penetrated gas tungsten arc welding', *Int. J. Heat and Mass Transf.*, 44(2), 417-428.

Folkes, J., & Pashby, I.R. (2003) 'High power diode laser welding of a titanium alloy', *in Proc. 22nd Int. Cong. on Appl. of Laser and Electro-Optics, Jacksonville, October 2003,* paper 209.

Gapontsev, V., Fomin, V., Ount, A. & Samartsev, I. (1999) '100 kW ytterbium fiber laser source', in *Proc. SPIE Int. Soc. Opt. Eng.*, 3613, 149-54.

Geiger, M. Leitz, K.-H., Kock, H. & Otto, A. (2009) 'A 3D transient model of keyhole and melt pool dynamics in laser beam welding applied to the joining of zinc coated sheets', *Production Eng.*, 3(2), 127-136.

Giesen, A. (2005) 'Thin disk lasers power scalability and beam quality', *Laser Technik J.*, 2, 42-45.

Geusic J.E., Marcos H.M. & Van Vitert L.G. (1964) 'Laser oscillations in Nd-doped yttrium aluminium, yttrium gallium and gadolinium garnets', *Appl. Phys. Lett.*, 4(10), 182-184.

Glowacki, M.H. (1995) 'The effects of the use of different shielding gas mixtures in laser welding of metals', *J. Phys D: Appl. Phys.*, 28(10), 2051-2059.

Gong, S.L., Chen, L., Yao, W. & Tang, Y. (2003) 'Research on Laser Welding of BT20 Titanium Alloy', in *Proc. Int. Conf of Appl. of Lasers and Electro-Opt., ICALEO, Jacksonville, October 2003*, 545-558.

Gorshkov, A.I. & Tret'Yakov, F.E. (1963) 'The effects of hydrogen and alloying elements on the formation of pores in welded joints in titanium', *Autom. Weld.*, 16, 32-37.

Gould, R.G. (1959). 'The LASER, Light Amplification by Stimulated Emission of Radiation', in Franken, P.A. & Sands, R.H. (Eds.)*. The Ann Arbor Conf. on Opt. Pump., Ann Arbor, June 1959,* 128.

Gräf, S., Staupendahl, G., Seiser, C., Meyer, B-J. & Müller. F.A. (2010) 'Generation of a dynamic polarized laser beam for applications in laser welding', *J. Appl. Phys.*, 107(4), 043102-1 – 043102-2.

Gref, W., Russ, A., Leimser, M., Dausinger, F. & Hügel, H. (2003) 'Double focus technique: influence of focal distance and intensity distribution on the welding process', in *Proc. SPIE Int. Soc. Opt. Eng.*, 4831, 289-294.

Greses, J. (2003) 'Plasma effects in CO2 and Nd:YAG laser welding', *Ph.D*. Cambridge: University of Cambridge.

Haboudou, A., Peyre, P., Vannes, A.B. & Peix, G. (2003) 'Reduction of porosity content generated during Nd:YAG laser welding of A356 and AA5083 aluminium alloys', *Mater. Sci. and Eng. A (Struct. Mater.: Prop., Microstruct. and Process.)*, 363 (1-2), 40-52.

Hale, J. (2006) 'Boeing 787 from the ground up', *Boeing Aeromagazine*, Qtr 4.

Hall R.N., Fenner G.E., Kingsley J.D., Soltys T.J. & Carlson R.O. (1962) 'Coherent light emission from GaAs junctions', *Phys. Rev. Lett.*, 9(9), 366-368.

Hall, D. (2009) 'Titanium demand in an uncertain world', conference presentation *European Titanium Conference, Birmingham, June 2009*.

Havrilla, D. & Anthony, P. (2002) 'Process Fundamentals of Industrial Laser Welding and Cutting', Rofin-Sinar Inc.

Hayashi, T., Matsubayashi, K., Katayama, S., Abe, S., Matsunawa, A. & Ohmori, A. (2003) 'Reduction mechanism of porosity in tandem twin-spot laser welding of stainless steel', *Weld. Int.*, 17(1), 12-19.

Hill, B. (2007) 'Titanium use in aerospace applications', *Industrial Heating,* 74(11), 57-61.

Hilton, P.A. (2006-2010) Personal communications, TWI Technology Fellow – Lasers.

Hilton, P., Blackburn, J. & Chong, P. (2007) 'Welding of Ti-6Al-4V with fibre delivered laser beams', in *Proc. Int. Conf of Appl. of Lasers and Electro-Opt., ICALEO, Orlando, November 2007*, 887-895.

Hilton, P.A. & Nguyen, L. (2008) 'A new method of laser beam induced surface modification using the Surfi-Sculpt® process'*, in Proc. Pacific Int. Conf on Appl. of Lasers and* Optics, Beijing, *April 2008*, 61-66.

Hilton, P.A. & Verhaeghe, G. (2009) 'The importance of laser beam brightness on melt run penetration', *TWI Industrial Member Report 918*.

Hilton, P.A. & Blackburn, J. (2010) 'Further studies on the welding performance of high brightness fibre lasers', *TWI Industrial Member Report 959*.

Hochstim, A.R. (1969) 'Kinetic Processes in Gases and Plasmas', New York: Academic.

Hügel, H. & Bohn, W.L. (1998) 'Solid state thin disk laser', in *Proc. SPIE Int. Soc. Opt. Eng.*, 3574, 15 -28.

Hughes, R.V. (1989) 'Plasma arc welding of titanium alloys – new developments', *Join. and Mater.*, 2(7), 333-335.

Iammi, J., Folkes, J., Bi, G. & Pashby, I. (2008) 'Fibre laser welding of Ti-6Al-4V', *in Proc. 3rd Pacific Int. Conf. on Appl. of Lasers and Optics, Beijing, April 2008,* 152-157.

Inoue, H. & Ogawa, T. (1995) Weld Cracking and Solidification Behavior of Titanium Alloys, *Weld. J.*, 74(1), 21s-27s.

International Standards Organisation (2001) 'ISO 13919-2:2001 Welding - Electron and laser beam welded joints - Guidance on quality levels for imperfections' . International Standards Organisation, Geneva.

International Standards Organisation (2005) 'ISO 11146-2:2005 Lasers and laser-related equipment -- Test methods for laser beam widths, divergence angles and beam propagation ratios -- Part 2: General astigmatic beams', International Standards Organisation, Geneva.

IPG Photonics Website (2010) http://www.ipgphotonics.com/apps_materials.htm (Accessed May 2010).

Javan, A. (1959) 'Possibility of production of negative temperature in gas discharges', *Phys. Rev. Lett.*, 3(2), 87-89.

Jarvis, B.L. (2001) 'Keyhole gas tungsten arc welding: a new process variant', *Ph.D.* Wollongong: University of Wollongong.

Jin, X., Li, L. & Zhang, Y. (2002) 'A study on Fresnel absorption and reflections in the keyhole in deep penetration laser welding', *J. Phys. D: Appl. Phys.*, 35(18), 2304–2310.

Kamimuki, K., Inoue, T., Yasuda, K. Muro, M., Nakabayashi, T. & Matsunawa, A. (2002) 'Prevention of welding defect by side gas flow and its monitoring method in continuous wave Nd:YAG laser welding', *J. Laser Appl.*, 14(3), 136-145.

Kaplan, A. (1994) 'Model of deep penetration laser welding based on calculation of the keyhole profile', *J. Phys. D: Appl. Phys.*, 27(9), 1805-1814.

Kaplan, A. (2009) 'Keyhole welding: the solid and liquid phases', in: Dowden, J.M. (ed.) *The theory of laser materials processing: heat and mass transfer in modern technology*, Canopus, Bristol (England), 71-93.

Katayama, S., Seto, N., Jong-Do, K. & Matsunawa, A. (1998) 'Formation mechanism and suppression procedure of porosity in high power laser welding of aluminum alloys', in *Proc. Int. Conf of Appl. of Lasers and Electro-Opt., ICALEO, Orlando, November 1998*, 1, C24-C33.

Katayama, S., Kobayashi, Y. Mizutani, M. & Matsunawa, A. (2001) 'Effect of vacuum on penetration and defects in laser welding', *J.Laser Appl.*, 13(5) 187-192.

Katayama, S., Mizutani, M. & Matsunawa, A. (2003) 'Development of porosity prevention procedures during laser welding', in *Proc. SPIE Int. Soc. Opt. Eng.*, 4831, 281-288.

Kawaguchi, I., Tsukamoto, S., Arakane, G. & Honda, H. (2006) 'Characteristics of high-power CO_2 laser welding and porosity suppression mechanism with nitrogen shielding. Study of high-power laser welding phenomena', *Weld. Int.*, 20(2), 100-105.

Kawahito, Y., Kinoshita, K., Matsumato, N. Mizutani, M. & Katayama, S. (2007) 'High speed observation and spectroscopic analysis of laser-induced plume in high-power fiber laser welding of stainless steel', *Q. J. Jpn Weld. Soc.*, 25(3), 455-460.

Kawahito, Y. Kinoshita, K. Matsumoto, N. & Katayama, S. (2009) 'Visualization of refraction and attenuation of near-infrared laser beam due to laser-induced plume', *J. Laser Appl.*, 21(2), 96-101.

Kern, M., Berger, P. & Hügel, H. (2000) 'Magneto-fluid dynamic control of seam quality in CO2 laser beam welding', *Weld. J.*, 79(3), 72s-78s.

Ki, H. Mohanty, P.S. & Mazumder, J. (2002) 'Multiple reflection and its influence on keyhole evolution', *J. Laser Appl.*, 14(1), 39-45.

Klein, T., Vicanek, M., Kroos, J., Decker, I. & Simon, G. (1994) 'Oscillations of the keyhole in penetration laser beam weld', *J. Phys. D: Appl. Phys.*, 27(10), 2023-2030.

Klein, T., Vicanek, M. & Simon , G. (1996) 'Forced oscillations of the keyhole in penetration laser beam welding', *J. Phys. D: Appl. Phys.*, 29(2), 322-332.

Klemens, P.G. (1976) 'Heat balance and flow conditions for electron beam and laser welding', *J. Appl. Phys.*, 47(5), 2165-2174.

Koechner, W. (1970) 'Thermal lensing in a Nd:YAG laser rod', *Appl. Optics*, 9(11), 2548-2553.

Kroos, J., Gratzke, U. & Simon, G. (1993) 'Towards a Self-Consistent Model of the Keyhole in Penetration Laser Beam Welding', *J. Phys. D: Appl. Phys.*, 26(3), 474-480.

Kuo, T.Y. & Jeng, S.L. (2005) 'Porosity reduction in Nd-YAG laser welding of stainless steel and inconel alloy by using a pulsed wave', *J. Phys. D: Appl. Phys.*, 38(5), 722-728.

Kück, S., Fornasiero L., Mix E. & Huber G. (1998) 'Excited state absorption and stimulated emission of Nd^{3+} in crystals. Part I: $Y_3Al_5O_{12}$, $YAlO_3$, andY_2O_3', *Appl. Phys. B: Lasers and Opt.*, 67(2), 151-156.

Kutsuna, M. & Kurokawa, T. (2004) 'Study of porosity formation in CO_2 laser welding of magnesium alloy', in *Proc. Int. Conf of Appl. of Lasers and Electro-Opt., ICALEO, San Francisco, October 2004*, xxx-xxx.

Kutsuna, M. & Yan, Q. (1998) 'Study on porosity formation in laser welds of aluminium alloys (Report 1): Effects of hydrogen and alloying elements', *Weld. Res. Abroad, 45(2)*, 20-32.

Lacroix, D. Jeandel, G. & Boudot, C. (1997) 'Spectroscopic characterisation of laser induced plasma created during welding with a pulsed Nd:YAG laser', *J. Appl. Phys.*, 81, 10, 6599-6606.

Ladenburg, R.W. (1928) 'Untersuchungen ber die Anomale Dispersion Angeregter Gase', *Z. fur Phys.*, 48, 15-50.

Lakomski, V.I. & Kalinyuk, N.N. (1963) 'The solubility of hydrogen in liquid titanium', *Autom. Weld.*, 16, 28-32.

Lampa, C. Kaplan, A.F.H., Resch, M. & Magnusson, C. (1998) 'Fluid flow and resolidification in deep penetration laser welding', *Lasers in Eng.*, 7, 241-253.

Li, C., Muneharua, K., Takao, S. & Kouji, H. (2009) 'Fiber laser-GMA hybrid welding of commercially pure titanium', *Mater. and Des.*, 30(1), 109-114.

Li, X., Xie, J. & Zhou, Y. (2005) 'Effects of oxygen contamination in the argon shielding gas in laser welding of commercially pure titanium thin sheet', *J. Mater. Sci.*, 40(13), 3437-3443.

Li, Z., Gobbi, S.L., Norris, I., Zolotovsky, S. & Richter, K.H. (1997) 'Laser welding techniques for titanium alloy sheet', *J. Mater. Process. Tech.*, 65(1-3), 203-208.

Lide, D.R., Ed. (1997) 'Handbook of Chemistry and Physics', 78th ed. CRC, Boca Raton, Fl.

Lindh, D.V. & Peshak, G.M. (1969) 'The influence of weld defects on performance', *Weld. J.*, 48(2), 45s-56s.

Lütjering, G.D. & Williams, J.C. (2007) 'Titanium', 2nd edition, Springer, Berlin.

Maiman, T.H. (1960) 'Stimulated optical radiation in ruby', *Nature*, 187, 493-494.

Mankins, J. (1995) ' Technology Readiness Levels', A White Paper, Office of Space Access and Technology, NASA.

Matsunawa, A. & Ohnawa, T. (1991) 'Beam-plume interaction in laser materials processing', *Trans. of Join. and Weld. Res. Inst.*, JWRI, 20(1), 9-15.

Matsunawa, A. & Semak, V. (1997) 'The simulation of front keyhole wall dynamics during laser welding', *J. Phys. D: Appl. Phys.*, 30(5), 798-809.

Matsunawa, A., Kim, J.D., Seto, N., Mizutani, M. & Katayama, S. (1998) 'Dynamics of keyhole and molten pool in laser welding', *J. Laser Appl.*, 10(6), 247-254.

Matsunawa, A. (2001) 'Problems and solutions in deep penetration laser welding', *Sci. and Technol. of Weld. and Join,* 6(6), 351-354.

Matsunawa, A., Mizutani, M., Katayama, S. & Seto, N. (2003) 'Porosity formation mechanism and its prevention in laser welding', *Weld. Int.*, 17(6), 431-437.

Mazumder, J. & Steen, W.M. (1977) 'Laser welding of titanium 6Al-4V', *IPC Sci. and Technol. Press*, 307-315.

Mazumder, J. & Steen, W.M. (1980) 'Welding of Ti-6Al-4V by a continuous wave CO2 laser', *Metal construc.*, 12(9), 423-427.

Mazumder, J. & Steen, W.M. (1982) 'Microstructure and mechanical properties of laser welded titanium 6Al-4V', *Metall. trans. A, Phys. metall. and mater. sci.*, 13(5), 865-871.

Mears, R.J., Reekie, L., Juancey, M. & Payne, D.N. (1987) 'Low-noise erbium-doped fiber amplifier operating at 1.54μm', *Electron. Lett.*, 23(19), 1026-1028.

Mitchell, D.R. (1965) 'Porosity in titanium welds', *Weld. J.*, 44(4), 57s-167s.

Mitchener, M. & Kruger, C.H. (1973) 'Partially Ionized Gases', Wiley, New York.

Miyamoto, I., Maruo, H. & Arata, Y. (1984) 'Role of assist gas in CO2 laser welding', in *Proc. Int. Conf of Appl. of Lasers and Electro-Opt., ICALEO, Boston, November 1984*. 44, 68-75.

Ministry of Defence Website (2010) http://www.aof.mod.uk/aofcontent/tactical/techman/downloads/trl_definitions.pdf (Accessed November 2010).

Mueller, S., Stiles, E. & Dienemann, R. (2006) 'Study of porosity formation during laser welding of Ti6Al4V', in *Proc. Int. Conf of Appl. of Lasers and Electro-Opt., ICALEO, Scottsdale, November 2006,* 133-138.

Mueller, S., Bratt, C., Mueller, P., Cuddy, J. & Shankar, K. (2008) 'Laser beam welding of titanium – a comparison of CO_2 and fiber laser for potential aerospace applications', in *Proc. Int. Conf of Appl. of Lasers and Electro-Opt., ICALEO, Temecula, October 2008*, 846-854.

NASA Website (2010) http://www.hq.nasa.gov/office/codeq/trl/trlchrt.pdf [Accessed November 2010].

Oiwa, S. Kawahito, Y. & Katayma, S. (2009) 'Optical properties of laser-induced plume during high power laser welding', in *Proc. Int. Conf of Appl. of Lasers and Electro-Opt., ICALEO*, *Orlando, November 2009*, 359-365.

Pastor, M., Zhao, H., Martukanitz, R.P. & DebRoy, T. (1999) 'Porosity, underfill and magnesium loss during continuous wave Nd:YAG laser welding of thin plates of aluminium alloys 5182 and 5754', *Weld. J.*, 78(6) 207s–216s.

Patel C.K.N. (1964) 'Continuous-Wave Laser Action on Vibrational-Rotational Transitions of CO_2' *Phys. Rev. Lett.*, 136, 1187-1193.

Platonov, N.S., Gapontsev, D.V., Gapontsev, V.P. & Shumilin, V. (2002) '135W cw fiber laser with perfect single mode output', in *Proc. Conf. on Lasers and Electro-Optic., CLEO 2002,Long Beach, May 2002,* CPDC31-CPDC34.

Poueyo-Verwaerde, A., Fabbro, R., Deshors, G., de Fruttos, A.M. & Orza, J.M. (1993) 'Experimental study of laser induced plasma in welding conditions with continuous CO_2 laser', *J. Appl. Phys.*, 74(9), 5773-5780.

Qin, G., Qi, X. & Lin, S. (2007) '*Critical power of keyhole formation in CW Nd:YAG laser'*, *China Weld.*, 16(1), 36-40.

Ready, J.F. (1997) 'Industrial Applications of Lasers', 2nd edition, Academic, San Diego.

Richter, K., Reisgen, U., Behr, W, & Holtz, R (2007) 'Welding of titanium and other refractory metals with a free pulse shaping laser', *J. Laser Appl.,* 19(2), 116-123.

Russell, M.J. & Freeman, R. (2007), 'FSW for titanium [friction stir welding]', *Metalworking Production*, 151(3), 30.

Sadin, S.R., Povinelli, F.P. & Rosen, R. (1989) 'The NASA technology push towards future space mission systems', *Acta Astronautica*, 20, 73-77.

Sanderson, A. (2006) 'Four decades of electron beam development at TWI', *IIW Assembly, Quebec, August 2006*, IIW Doc. IV-913-06.

Sato, S., Takahashi, K. & Mehmetli, B. (1996) .Polarization effects of a high-power CO_2 laser beam on aluminum alloy weldability', *J. Appl. Phys.*, 79(12), 8917–8919.

Schawlow, A.L. & Townes, C.H. (1958) 'Infrared and Optical Masers'. *Phys. Rev.*, 112(6), 1940-1949.

Schulz, W., Simon, G. & Vicanek, M. (1986) 'Ablation of opaque surfaces due to laser irradiation', *J. Phys. D: Appl. Phys.*, 19(9), 173-177.

Schwarz, H. & DeMaria, A.J. (1962) 'Electron, ion, and light beams as present and future material working tools'. in *Proc. of the Nat. Electron. Conf.*, 18, 351-365.

Semak, V.V., Hopkins, J.A., McCay, M.H. & McCay, T.D. (1995) Melt pool dynamics during laser welding, J. Phys. D: Appl. Phys., 28(12), 2443-2450.

Semak, V. & Matsunawa, A. (1997) The role of recoil pressure in energy balance during laser materials processing, J. Phys. D: Appl. Phys., 30, 2541–2552.

Seto, N., Katayama, S. & Matsunawa, A. (1999) 'High-speed simultaneous observation of plasma and keyhole behavior during high power CO2 laser welding: Effect of shielding gas on porosity formation', *J. Laser Appl.*, 12(6), 245-250.

Short, A.B. (2009) 'Gas tungsten arc welding of α+β titanium alloys: a review', *Materials Science and Technology*, 25(3), 309-324.

Smith, L.S., Threadgill, P. & Gittos, M. (1999) 'Welding titanium – a designers and users handbook', Titanium Information Group.

Snitzer, E. (1961a) 'Proposed fiber cavities for optical masers', *J. Appl. Phys.*, 32(1), 36-39.

Snitzer, E. (1961b) 'Optical maser action of Nd3+ in a barium crown glass', *Phys. Rev. Lett.*, 7(12), 444-446.

Sokolowski, W.G., Herziger, G. & Beyer, E. (1988) 'Spectral Plasma Diagnostics in Welding with CO_2 lasers', in *Proc. SPIE Int. Soc. Opt. Eng.*, 96-102.

Solana, P. & Negro, G. (1997) 'A study of the effect of multiple reflections on the shape of the keyhole in the laser processing of materials', *J. Phys. D: Appl. Phys.*, 30(23), 3216–3222.

Steen, W.M. (1998) 'Laser Material Processing', 2nd edition, Springer-Verlag, London.

Stratton, J.A. (1941) 'Electromagnetic Theory', McGraw-Hill, New York.

Sullivan, A.B.J. & Houldcroft, P.T. (1967) 'Gas-jet laser cutting', British Weld. J., 14(8), 443-445.

Szymański, Z. & Kurzyna, J. (1994) 'Spectroscopic measurements of laser induced plasma during welding with CO_2 laser', *J. Phys. D: Appl. Phys.*, 76(12), 7750-7756.

Szymański, Z., Kurzyna, J. & Kalita, W. (1997) 'The spectroscopy of the plasma plume induced during laser welding of stainless steel and titanium', *J. Phys. D: Appl. Phys.*, 30(22) 3153–3162.

Talkington, J., Harwig, D., Castner, H. & Mitchell, G. (2000) 'Development of *Titanium* Weld Color Inspection Tools', *Weld. J.*, March, 79(3), 35-39.

Tang, H. (2010) 'Latest advances in joining technologies for automotive body manufacturing', *International Journal of Vehicle Design*, 54(1), 1-25.

Threadgill, P., Wynne, B., Russell, M. & Davies, P. (2008) 'Prefabricated materials preforms in titanium alloys using stationary shoulder friction stir welding', in *Proc. The Minerals, Metals and Materials Society 137th Annual Meeting and Exhibition. New Orleans, March 2008*, 333-338.

Threadgill, P.L., Leonard, A.J., Shercliff, H.R. & Withers, P.J. (2009) 'Friction stir welding of aluminium alloys', *International Materials Reviews*, 54(2), 49-93.

Trumpf Website (2010a) http://www.trumpf-laser.com/en/products/solid-state-lasers/disk-lasers/trudisk.html (Accessed May 2010).

Trumpf Website (2010b) http://www.trumpf-laser.com/en/products/solid-state-lasers/diode-lasers/trudiode.html (Accessed September 2010).

TWI Website (2010a) http://www.twi.co.uk/content/companies_act.pdf (Accessed May 2010).

TWI Website (2010b) http://www.twi.co.uk/content/main_about_us_index.html (accessed December 2010).

TWI Website (2010c) http://www.twi.co.uk/content/ar_annualreview.pdf (accessed December 2010).

Tu, J.F., Inoue, T. & Miyamoto, I. (2003) 'Quantitative characterization of keyhole absorption mechanisms in 20kW-class CO2 laser welding processes', *J. Phys. D: Appl. Phys.*, 36(2), 192-203.

Verhaeghe, G. & Hilton, P. (2005) 'The effect of spot size and laser beam quality on welding performance when using high-power continuous wave solid-state lasers', in *Proc. Int. Conf of Appl. of Lasers and Electro-Opt., ICALEO, Miami, November 2005*, 264-271.

Verhaeghe, G. & Dance, B. (2008) 'An assessment of the welding performance of high-brightness lasers and a comparison with in-vacuum electron beams', in *Proc. Int. Conf of Appl. of Lasers and Electro-Opt., ICALEO, Temecula, October 2008*, 406-414.

Vollertsen, F. & Thomy, C. (2006) 'Magnetic Stirring during laser welding of aluminum', *J. Laser Appl.*, 18(1), 28-34.

Vollertsen, F. (2009) 'Properties and Prospects of High Brightness Solid State Lasers', *Laser Technik J.*, 5, 27-31.

Wang, H. Shi, Y. & Gong, S. (2006) 'Numerical simulation of laser keyhole welding processes based on control volume methods', *J. Phys. D: Appl. Phys.*, 39(21), 4722–4730.

Weberpals, J., Russ, A., Dausinger, F. & Hügel, H. (2005) 'Influence of the focus diameter in laser welding with thin disk laser', in *Proc. of the 3rd Int. Conf. on Lasers in Manufacturing. LIM, Munich, June 2005*, 39-42.

Willgoss, R.A. (1981) 'A practical future for EM stirring of the weldpool', *Weld. Met. Fabr.*, 49(4), 189-197.

Williams, S.W., Scott, G. & Calder, N.J. (2001) 'Direct diode laser welding of aerospace alloys', *LaserOpto*, 33(4), 50-54.

Xiang, Z., Hu, M., Ge, J.H., Zhao, Z.G., Wang, S. Liu, C. & Chen, J. (2009) 'Influence of spherical aberrations on fundamental mode beam quality under different laser resonators', *Chinese Phys. B*, 18(7), 2806-2810.

Xie, J. (1999) 'Plasma Fluctuation and Keyhole Instability in Laser Welding', in *Proc. Int. Conf of Appl. of Lasers and Electro-Opt., ICALEO, San Diego, November 1999*, 2, D11-D20.

Xie, J. (2002) 'Dual Beam Laser Welding', *Weld. J.*, 81(10), 223s-230s.

Yunlian, Q., Hu, D., Quan, H. & Liying, Z. (2000) 'Electron beam welding, laser beam welding and gas tungsten arc welding of titanium sheet', *Mater. Sci. and Eng. A (Struct. Mater.: Prop., Microstruct. and Process.),* 280(1), 177-181.

Zhang, Y., Sato, Y.S., Kokawa, H., Park, S.H.C. & Hirano, S. (2010) 'Grain structure and microtexture in friction stir welded commercial purity titanium', *Sci. and Technol. of Weld. and Join.*, 15(6), 500-505.